Electrical Signature Analysis for Induction Motor Driven Thruster Assemblies

Koen W. Kruimer

Delft University of Technology

TU Delft

Allseas

Electrical Signature Analysis for Induction Motor Driven Thruster Assemblies

by

Koen W. Kruimer

to obtain the degree of Master of Science
at the Delft University of Technology,
to be defended publicly on Thursday February 2, 2023 at 13:00.

Student number:	4469887	
Report number:	2022.MME.8757	
Project duration:	March 1, 2022 – February 2, 2023	
Thesis committee:	Dr. Ir. H. Polinder,	TU Delft, supervisor
	Dr. A. Coraddu,	TU Delft, supervisor
	Ir. J. Dong,	TU Delft
	Dr. Ir. D. Boskos	TU Delft
	Dr. Ir. A. Veltman,	Piak Electronic Design BV.
	Ir. M. Langelaar,	Allseas Engineering BV.

Cover: Pioneering Spirit decommissioning Gyda platform jacket - July 2022 - North Sea - Allseas Engineering BV.

An electronic version of this thesis is available at `http://repository.tudelft.nl/`.

TU Delft

Preface

When I look back to when I first started this graduation assignment in March 2022, I am thrilled with what this journey has become. I walked into the Allseas office on the first day just like all of my colleagues: with a dream to work on the biggest boat with the biggest machinery and no knowledge of Electrical Signature Analysis whatsoever. Eventually, this turned out to be of no concern, since the project started to take shape rather quickly. I think the biggest reason for this was the great enthusiasm that everyone seems to have for this project. And even after 10 months of working with current and voltage sensors, I am still excited by the topic of ESA. Because, to me, it still feels like something straight out of a science-fiction movie. Now coming to the end of this ride, I am not only content with the thesis that you're currently looking into, but I cannot be happier with the adventure that it entailed.

The biggest challenge over the last few months has been trying to squeeze everything I have learned during my research into a thesis. The last feedback I received boiled down to two things. Firstly, that I "see the apples, but haven't picked them yet." And secondly, that I should think about "how to sell it." I struggled with addressing this. On the one hand, I want to take my readers through the research and clearly explain how one would set up an ESA strategy, including how I have come to all individual conclusions. But on the other hand, showing every single plot that I'm excited about and that made me learn something new will inevitably make a reader "unable to see the forest through all the trees," as one would say in Dutch. Reflecting on this now, I think walking this fine line proved hard for me, but definitely made me learn a great deal about conveying my message. So, I hope you enjoy reading it!

It goes without saying that this research would not have been possible without the help of many people. First and foremost I would like to thank everybody at Allseas Engineering BV for providing me with the opportunity to perform this research on the boat of my dreams. In particular, I would like to thank my supervisors at Allseas, Maarten Langelaar and Nicolas Chasiotis, as I sincerely felt great comfort in the faith you seemed to have in me and the project. Secondly, I want to thank my TU Delft supervisors Henk Polinder and Andrea Coraddu. Their feedback on the earlier versions of this thesis is greatly appreciated, and even if I haven't succeeded in "picking the apples" this time around, I still see myself using that great metaphor a lot in the future. But most importantly, I want to thank Deesje, Bassie, Jelm and Jels, because I can't thank them enough.

Koen W. Kruimer
Delft, January 2023

Summary

Electrical Signature Analysis (ESA) is a technique in which the voltage and current of a three-phase Induction Motor (IM) are measured and analysed to assess the health of the machine. The use of ESA for detecting mechanical defects in IM assemblies has been a popular topic in scientific research since the 1970's. However, this research is limited to laboratory test setups for small motors and ESA has never been widely implemented in the industry. Therefore, in this thesis the possibilities for ESA as a CM method for marine thruster assemblies are explored by implementing a current and voltage measurement setup on three thrusters of the Pioneering Spirit (PS).

The current and voltage of the three phases of the three thrusters will be recorded during ramp-up tests, in which the motor speed is increased in increments of 5%. During such an interval, the motor speed is maintained constant. Out of these measurements, the demodulated current, voltage, torque and power are calculated, after which their spectra are plotted. These spectra are then analysed for the presence of frequencies with a mechanical origin and thus the mechanical behaviour of the machines is identified. Finally, the identification of the mechanical behaviour might be used in assessing the health of the machine and making a machine health diagnosis.

Out of the three thrusters that are subject to the test, the first is suspected to be healthy, the second is suspected to have bearing wear inside the thruster and the third is suspected to have bearing wear inside the IM. Therefore, these three thrusters serve as a diverse population for testing the potential of ESA in identifying different states of mechanical machine health. Furthermore, in order to validate and compare the results of the ESA measurements with different monitoring techniques, the thrusters will be subject to mechanical vibration measurements and mechanical shaft torque measurements during the same ramp-up tests. Also, historical vibration data from accelerometers mounted inside the thruster is available for this purpose.

The results of the tests validate that the mechanical behaviour of the machines can be identified in the spectra of the electrical measurements, and is most easily detected in the demodulated current, torque and power spectra. Furthermore, there are two possibilities to detect unhealthy machine behaviour through these spectra. Firstly, this can be done by the detection of mechanical frequencies that only occur in the case of a damaged component, such as bearing frequencies. Or this can be done by monitoring the mechanical vibrations that are considered healthy over time. When a trend or sudden increase in amplitude is detected, this might also indicate faulty behaviour. Examples of these healthy vibrations are the motor shaft frequency or Blade Pass Frequency (BPF). The monitoring of these healthy vibrations can only be done per individual thruster and at the same motor speed. Since, the three thrusters showed different amplitudes in their mechanical vibrations that were still considered healthy, and there was no linear relation between the amplitude of the vibrations and the motor speed.

Once faulty machine behaviour is detected, the final step in a machine health diagnosis is to assess the severity of the damage. Currently, this is still complex for ESA, as the measured amplitude of a mechanical vibration in the electrical spectra is dependent on many mechanical and electrical machine parameters, as well as the location of the fault inside the thruster. This suggests that a large amount of labeled ESA failure data for specific machines must be gathered to make a reliable fault severity assessment. However, a fault severity assessment through ESA might be simplified by using vibration analysis ISO standards. Since, in some cases the results of an ESA analysis show overlap with the patterns described for certain stages of damage in these ISO standards.

When comparing the ESA-based method for mechanical health monitoring with the currently implemented CM campaign, based on vibration analysis, for the thruster assemblies of the PS, it can be concluded that at this point the ESA-based method cannot replace the vibration analysis campaign. The two main reasons for this are the previously stated point on the complexity of fault severity assessment through ESA and secondly, the fact that it has not yet been proven (or disproved) that ESA can detect mechanical failure behaviour originating from deep down in the underwater part of the thruster. However, ESA can be implemented as an additional autonomous CM system to detect mechanical and electrical failures. A step-by-step approach for the implementation of such a system is presented in Chapter 6 of this thesis and an overview of this approach is shown in Figure 1.

Finally, the baseline load (0 Hz-component) of the electrically deduced torque showed great resemblance to the baseline load measured with the mechanical shaft torque measuring device, as the baseline load measured with the two different techniques consistently had an accuracy of 0 - 3%, when compared to each other. However, this same accuracy was not found for the torsional vibrations measured at any other frequency. Still, the ESA measurement show potential to replace the mechanical shaft torque measurements in cases that only the baseline load is of interest.

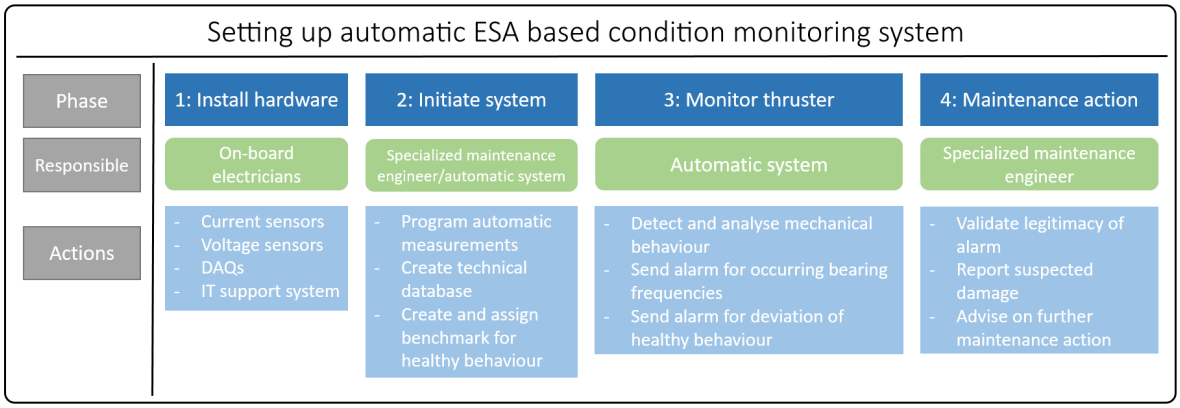

Figure 1: Proposed implementation of an ESA based condition monitoring method

Contents

Nomenclature

Abbreviations

Abbreviation	Definition
AC	Alternating Current
BPF	Blade Pass Frequency
BPFI	Ball Pass Frequency Inner
BPFO	Ball Pass Frequency Outer
BSF	Ball Spin Frequency
CM	Condition Monitoring
DAQ	Data Acquisition
DP	Dynamic Positioning
EPVA	Extended Park Vector Approach
ESA	Electrical Signature Analysis
FFT	Fast Fourier Transform
FMECA	Failure Mode, Effects and Criticality Analysis
FTF	Fundamental Train Frequency
HV	High Voltage
IM	Induction Motor
ISO	International Organization for Standardization
MCSA	Motor Current Signature Analysis
MV	Medium Voltage
NDS	Non-Drive Side
PdM	Predictive Maintenance
PS	Pioneering Spirit
PWM	Pulse Width Modulation
RUL	Remaining Useful Life
T1,T3,T6	Thruster 1, 3 and 6
VA	Vibration Analysis
VFD	Variable Frequency Drive

1 Introduction

The Induction Motor (IM) is often seen as the workhorse of the industry, since it is responsible of over 60% of the global industrial electrical power consumption and more than 85% of motors used in industrial appliances are IMs. The main reasons for this are the low cost, robustness, low maintenance requirements and capability to operate in extreme working conditions of IMs [1]–[3]. Considering this crucial role the IM has in almost every industry, e.g. production plants, wind energy, and the rail, maritime and automotive industry, the reliability of these machines is of high importance in both safety and economical perspectives. Especially in the case of large and costly Medium Voltage (MV) machines, unexpected downtime of an IM could lead to an entire production process shutting down, often resulting in high revenue loss [4].

Logically, a proper maintenance strategy should be implemented in IM applications to prevent unnecessary downtime and its consequences. Currently, the maintenance strategy that is seen as most advanced is Predictive Maintenance (PdM), in which the conditions of the operating equipment are monitored in order to predict possible failures and correct this at an optimal time. The reasoning for this is that in 99% of the cases of equipment failure, the failure is preceded by certain signs, conditions or indications that a failure is going to occur [5]. However, a correct implementation of a PdM strategy can be much more than using vibration analysis or thermal imaging to catch possible signs of failure beforehand. PdM is sometimes seen as a philosophy that can improve productivity, product quality, and overall effectiveness of a manufacturing plant by using the operating condition of the plants' equipment to optimize the total operation of the plant [6].

In the maritime industry seagoing vessels will often have hundreds of IMs running simultaneously, most noticeably a ship's thrusters in the case of diesel-electric propulsion systems. These assemblies of MV IMs and thrusters are tailor-made and highly expensive. Also, performing maintenance on them would halt the operations of the entire ship, causing a considerable revenue loss. Therefore, the implementation of a proper condition based PdM strategy for these thruster assemblies will likely increase a vessel's overall efficiency. However, the current industry standard for these machines is a planned maintenance strategy combined with Vibration Analysis (VA) [7]. One of the main downsides of this type of monitoring for thruster assemblies is its intrusiveness: Vibration sensors located in the underwater part of a thruster often can't be reached without removing the thruster assembly from the vessel. This makes the question arise whether other condition monitoring techniques might be better suited for designing a PdM strategy for these types of machines.

Another type of Condition Monitoring (CM) much similar to VA is Electrical Signature Analysis (ESA), a technique specially developed for the unintrusive monitoring of IMs [8], but not widely implemented in the maritime industry. This technique could potentially be more effective in setting up a PdM strategy for IMs in the maritime industry. Therefore, investigating how this technique can best be implemented in order to reach this goal and how ESA weighs up to VA in this industry can be useful research. However, a literature review on the topic of ESA, which is presented in Appendix H, makes clear that the current state of the art of this technique is only to detect and classify mechanical machine failures. A lack of labeled failure data is the primary cause that making predictions on the course of machine failures, which is the goal of PdM, is considered to be too complex at this point. Furthermore, the technique of ESA for mechanical failure detection has proven to be successful in small laboratory test-bench setups many times, but is not widely implemented in the industry.

For this reason, a gap in the scientific literature can be recognized when considering the implementation of ESA as a PdM strategy in the maritime industry. This gap concerns testing the potential of ESA as a CM technique on actual MV and multi-megawatt IM assemblies on a marine vessel. Performing research on this subject would further progress the state of the art of ESA and would be the first step in testing the potential of ESA as a PdM strategy for mechanical failures in the maritime industry.

1.1. Research questions

To test the potential of ESA as a CM technique for mechanical failures in the maritime industry, the main research question and subsequent subquestions of this graduation assignment are:

Main question:

- *'How can Electrical Signature Analysis successfully be implemented as a Condition Monitoring technique for mechanical failures in induction motor driven thruster assemblies in the maritime industry?'*

Subquestions:

1. *'Which mechanically induced vibrations can be detected in the induction motor current and voltage measurements?'*
2. *'How can these mechanically induced vibrations be most effectively detected in the induction motor current and voltage measurements?'*
3. *'How can the detection of these mechanically induced vibrations be used for mechanical fault detection and a machine health assessment?'*
4. *'How does this method compare to Condition Monitoring based on mechanical vibration measurements?'*
5. *Perform a machine health diagnosis of thruster 1, 3 and 6 of the Pioneering Spirit based on the researched method.*

These research questions were set up following a literature review on the topic of ESA and PdM. A short description of this literature review including its conclusions is shown in Chapter 2. Also, the entire literature review is added to this thesis as Appendix H. The research questions will be answered by performing and analysing measurements on three identical thruster assemblies of a marine vessel. Firstly, the methodology and analysis steps for these measurements are presented in Chapter 3. Next, the results of the measurements will be shown in Chapter 4. Hereafter, the ESA measurements of the thrusters will be validated by separately collected mechanical vibration measurements and torsional vibration measurements, as shown in Chapter 5. Then, the results of all measurements, both electrical and mechanical, will be further discussed in Chapter 6, including a comparison between the different methods. Finally, a conclusion is presented in Chapter 7 followed by a list of recommendations in Chapter 8. A further elaboration on the structure of this thesis and its design to eventually answer the main research question is presented in Figure 1.1.

Furthermore, as these research questions will be answered by measuring a marine vessel's thruster assemblies, a second objective of this research is to create a machine health diagnosis of these thrusters using the knowledge gained in the research, which is highlighted as subquestion 5. This machine health diagnosis for the thrusters is presented as a separate scientific paper in the form of a case study, which is included in Appendix A. The results of this diagnosis will also be added into the conclusion in Chapter 7.

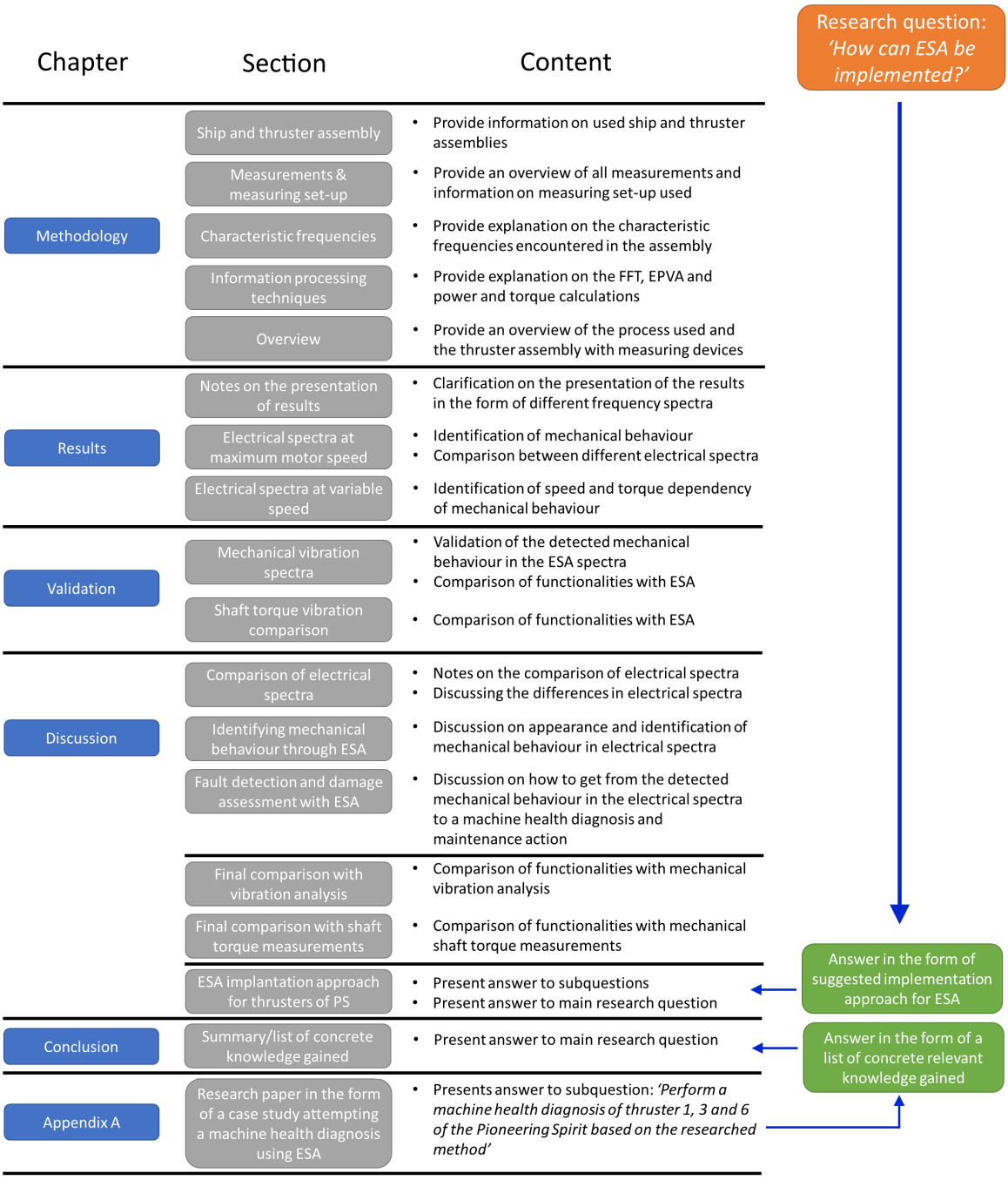

Figure 1.1: Explanation of the structure of this research

2 Literature Review

As stated in the Introduction, the first step of investigating the potential of ESA for a PdM strategy in the maritime industry is to analyse the available scientific literature. In this chapter, the setup of the performed literature review is shortly introduced, after which its conclusions are presented. In addition, the entire literature is added in Appendix H.

The use of the literature review is to identify a gap in the scientific literature regarding ESA and PdM and to set up the research questions for this thesis, as was also stated in the Introduction. For this reason, it should be noted that the conclusions of the literature review have been used to shape the remainder of the research. Therefore, the research questions used for the literature review, as shown in Section 2.1, slightly deviate from the research questions of this thesis, which are shown in Section 1.1.

2.1. Structure and research questions

The literature review focuses on Motor Current Signature Analysis (MCSA). This CM technique for IMs originates from the 1970's and has been been a popular research topic in scientific literature ever since it was first contrived [8]–[12]. The objective of the literature review is to investigate the different possibilities in creating a PdM strategy for IM driven thruster assemblies used in the maritime industry based on MCSA. Therefore, the main research question and subquestions of this literature review are:

Main question:

- *'How can Motor Current Signature Analysis be best implemented to create a predictive maintenance strategy for mechanical failures in induction motor assemblies in the maritime industry?'*

Subquestions:

1. *'How is a predictive maintenance strategy ideally set up?'*
2. *'What are the common mechanical failures of an induction motor?'*
3. *'What sets the maritime industry, its maintenance strategies and its use of induction motors apart?'*
4. *'How are current maintenance strategies that make use of Vibration Analysis set up?'*
5. *'What different methods exist to use Motor Current Signature Analysis as a means for condition monitoring in induction motors?'*

As can be seen in the questions above, each subquestion concerns a different research topic. To answer these research questions, the literature review is divided into five chapters, all concerning a single topic. This way, each chapter answers one subquestion, in order to finally answer the main research question. The conclusions of the literature review are presented in the next section.

2.2. Conclusions

Out of the information presented in the literature review, multiple conclusions can be drawn. These conclusions are listed below.

A - Firstly, MCSA is proven to have functionalities that other CM techniques, such as VA, do not have and is proven to be able to detect mechanical failures in IM assemblies. Therefore, it would be interesting further research to try and develop this method in the maritime industry on an actual marine IM assembly, instead of solely researching the method in a test-bench setup.

B - Secondly, when setting up this type of research, it is of added value to include voltage measurements next to stator current measurements. This way, more information is gathered for analysis. The method would then be more accurately called ESA instead of MCSA.

C - Continuing, one of the most appealing assets in the maritime industry on which a PdM strategy based on ESA might be interesting to develop would be the IM driven thruster assemblies of marine vessels. These heavy and costly machines with complex maintenance requirements offer the most possible gain of a successful PdM strategy in terms of overall expenses and preventing unexpected maintenance. Also, these partially submerged assemblies are a good subject for unintrusive CM techniques.

D - The first attempts at information processing should be the easiest and most conventional ones, such as manually analysing the frequency spectrum and the demodulated spectrum. Depending on the effectiveness of this, more complex techniques can be implemented to: improve the fault diagnostics process, work towards a prognostics approach or enable fault detection in the first place, in the case that the Fast Fourier Tranform (FFT) is not able to distinctly show fault behaviour. These more complex techniques can be both physical model-based or data-driven. It depends on the type of data obtained to judge what will be most useful, but there are plenty of data processing tools that have proven successful.

E - Ultimately, a Wavelet Transform approach might be best suited for an actual PdM strategy based on ESA for DP thruster assemblies. This is because a vessel on Dynamic Positioning (DP) will constantly change its motor torque and speed to remain in the same geographical position. Therefore, the motor speed and load will always be transient, for which the WT offers the best analysis.

F - Also, some techniques that show promise to be used for MCSA, but have not been widely implemented are: Cepstrum analysis, as it is effective in the analysis of sidebands, and the Convolutional Neural Network, as it required no data pre-processing and feature evaluation for it to be successfully used for diagnostics.

G - Finally, to be able to set up a PdM strategy based on MCSA, the prognostics will be the most difficult part to set up. This is because either an extensive amount of machine data including failure data has to be available or a novel prognostics technique has to be used, which are currently being researched, but cannot yet be called proven concepts.

3 Methodology

As stated in Chapter 1.1, in order to answer the research questions, a multitude of measurements are performed on the MV IMs of a marine vessel's thruster assemblies. In this Chapter, firstly, the ship and thruster assemblies that are to be analysed are introduced. Secondly, the specific approach for taking the measurements is discussed, as well as the measuring setup that is used. Thereafter, the frequencies of interest are highlighted in terms of mechanically induced vibrations or electrical oscillations that are critical for the analysis. Then, the information processing techniques used to extract useful information from the raw data are discussed. Finally, an overview of the entire process and analysis is presented, as well as an overview of the thruster assemblies containing all used measuring devices.

3.1. Ship and thruster assembly

The marine vessel on which the research will take place is the Pioneering Spirit (PS) of the Dutch engineering company Allseas Engineering BV, located in Delft. The PS is an offshore construction vessel with a diesel-electric propulsion system specialized in both subsea pipelay, as well as heavy-lift operations. For this, it uses 12 Rolls-Royce azimuth thrusters, each driven by a 6.5 MW 3 kV IM. A 3D-model of the specific thruster as used on the PS is shown in Figure 3.1. More specific technical information on the ship and thruster assemblies can be found in Appendix B.

The three thrusters on which the measurements will take place are T1, T3 and T6. These specific thrusters are chosen for analysis because T1 shows no signs of mechanical wear, T3 shows early signs mechanical wear in the double spherical input shaft bearing, as shown in Figure B.3, and T6 shows early signs of bearing in the NDS IM bearing. This means that measuring these three thrusters gives the most diverse baseline of mechanical behaviour, consisting of both a healthy thruster that can serve as a baseline of measurements and two thrusters showing different signs of faulty machine behaviour. Therefore, this set of thrusters will provide the measurements most suited to answer the research questions.

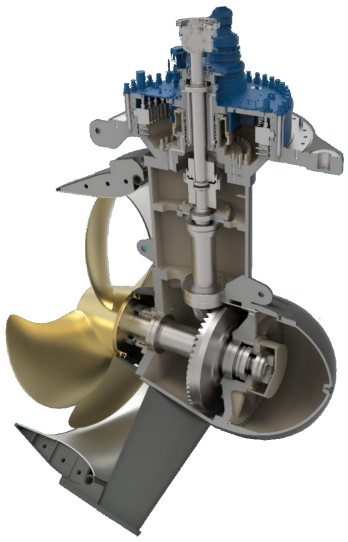

Figure 3.1: Section view of specific Rolls-Royce Ulstein UUC-455 assembly as used on the PS [13]

3.2. Measurements

The approach for taking the ESA measurements is as follows: Firstly, ramp-up tests are performed for all three thrusters, in which the motor speed is increased with increments of 5% until the maximum torque is reached. During these intervals the motor speed is constant and the current and voltage are recorded for intervals of 90 seconds. These measurements are the main focus of this research project and for the deduction of mechanical machine behaviour through ESA.

For means of comparison and validation, there are additional measurements taken next to the ESA measurements and there is historical data made available. The includes the measurements and data as explained below. Also, an overview of the available data is shown in Table 3.1.

- For T1 and T6 there are additional mechanical vibration measurements taken on the NDS of the IM during the same intervals of the ramp-up tests. This is done in three directions: radially in a 0 degree and a 90 degree orientation, as well as axially. These measurements are performed in order to validate and compare the ESA measurements, especially focused on the early stage NDS bearing wear. Contrary to the ESA measurements, these vibration measurements are only sampled in intervals of 10 seconds.
- For T3 and T6 there is historical data available from vibration sensors located at different positions in the thruster assemblies. This data can also be used to validate and compare the machine health through different measuring methods.
- For T1 there are shaft torque measurements available taken at the same time as some ESA measurements. These are used in order to validate and compare the shaft torque deduced from the electrical measurements.
- For T1 there is an additional set of current and voltage measurements available taken two months in advance of all other measurements. These measurements might be used in order to check the degradation of the machine and changing of its mechanical behaviour over a period of two months.
- For all three thrusters there is an extensive amount of current and voltage measurements taken during DP operations of the ship, as this is the most common operational mode for the thrusters. Therefore, it might be useful to try and analyse the 'regular' operations of the thrusters for their mechanical behaviour instead of initiating a ramp-up test.

Thruster and damage → Measurements ↓	Thruster 1 (No damage)	Thruster 3 (Thruster bearing)	Thruster 6 (NDS bearing)
3 Phase current and voltage (40 – 100% speed)	✓	✓	✓
3 Phase current and voltage (on DP)	✓	✓	✓
3 Phase current and voltage (two months apart)	✓		
Shaft torque (40 – 70% speed)	✓		
NDS Vibration (40 – 100% speed)	✓		✓
Historical vibration data (7 sensors in thruster)		✓	✓

Table 3.1: Overview of all measurements

3.3. Measuring setup

In this section the measuring setup and approach is introduced for the ESA measurements, mechanical vibration measurements and torque measurements. More detailed information on the individual components used can be found in Appendix C.

Current and voltage measurements

The current and voltage of all three phases are measured between the Variable Frequency Drive (VFD) and the IM. These measurements are sampled at 20kHz by a Data Acquisition (DAQ) system, which is set up outside the VFD. An 8th order low pass pre-filter is used for these measurements. The voltage is measured using High Voltage (HV) voltage probes mounted on the output bus bar of each phase and grounded inside the VFD. The current is measured using zero-flux type current transducers, which are each mounted on one of the cables connected to the output bus bars of the VFD. Each phase has 7 individual of these connection cables, which bundle up and connect the VFD to the IM. This means that only 1/7th of the current is measured of each phase. The reasoning for this is purely practical: The 7 individual output cables of each phase don't bundle up into the same cable. So, there is no single cable that can be used to measure the entire current between the VFD and IM. To work around this, the current measurements are multiplied by a factor of 7 later in the analysis. The assumption is made that the differences in dampening and transducing of the individual cables are negligible.

Mechanical vibration measurements

The mechanical vibrations are measured using two different methods. Firstly, for the measurements on the IM NDS bearing, a magnetically mounted accelerometer [14] in combination with a Fluke VIBXpert II is used, which is a handheld vibration scanning DAQ [15]. These mechanical vibration measurements are sampled at 8 kHz.

Secondly, there is a total of six additional vibration sensors mounted inside each thruster. These are monitored by a 3rd party (Pruftechnik NV), that performs a monthly CM analysis for the thrusters of the PS based on this vibrational data. The location of these sensors inside the thruster is shown in C. Unfortunately, it was not possible to use these sensors in the same ramp-up intervals as both the ESA and the handheld measurements, so only historical data of these sensors is available.

Shaft torque measurements

On T1 an additional sensor setup has been installed. This is a shaft torque and power measurement system named MetaPower Quad [16], which is fabricated and installed by Kongsberg Maritime. This device consists of two slotted discs mounted on two ends of the shaft. By detecting the passing of these slots, two optical sensors can measure the speed and position of the two ends of the shaft. Out of these measurements the shaft torque, speed and power can be calculated. Unfortunately, at the time it was not possible to use this device simultaneously with the ESA measurements during the 70-100% motor speed ramp up intervals. Therefore, the available measurements only reach up to 70% motor speed. A 3D model of this sensor setup can be seen in Figure C.3.

3.4. Characteristic frequencies

In order to identify mechanical machine behaviour in ESA measurements, it is crucial to calculate the characteristic machine frequencies in which vibrations might be generated and transduced throughout the assembly. Firstly, this concerns the mechanically induced vibration frequencies, as these are the frequencies that can directly identify mechanical behaviour. Secondly, it is practical to calculate and identify the electrical frequencies, as by excluding vibrations that are definitely not mechanical, the mechanical machine behaviour can be determined more accurately. More importantly however, some electrical frequencies will serve as a carrier frequency on top of which mechanically induced frequencies might be modulated.

In this section the most important mechanical and electrical frequencies, as well as their origin, are presented. A complete overview of these frequencies in the thruster assemblies of the PS and their order of the shaft speed, e.i. the scalar factor with which they are related to the shaft speed, are shown in Appendix D.

3.4.1. Mechanical frequencies

Mechanical characteristic frequencies in rotating equipment are almost always determined by the motor shaft speed of a machine. Mechanical vibrations in these characteristic frequencies can always be present in a system, i.e. a machine is not necessarily faulty when vibrations in these frequencies exist in the machine. Only when the vibrations are abnormally, high a machine fault is the suspected cause. In the case of a thruster assembly the most important mechanical characteristic frequencies are listed below:

- **Motor Shaft Frequency** - The motor shaft speed or motor shaft frequency is the frequency at which the motor shaft is rotating. Therefore, this is the same frequency as the mechanical rotation frequency of the rotor. It will be denoted as f_{motor}. Usually, the motor shaft speed is considered in RPM. However, in this research the motor shaft speed is considered in Hz, like all other frequencies. The method used to identify the motor shaft speed in the electrical spectra is explained in Appendix D.
- **Propeller Shaft Frequency** - This is the frequency at which the propeller shaft is rotating. It can be deduced from the motor shaft speed by the following equation, in which i is the gear ratio between the motor shaft and propeller shaft. In the thruster assemblies of the PS i = 62/13, as can be seen in Table B.2.
$$f_{prop} = f_{motor} i \tag{3.1}$$
- **Blade Pass Frequency** - This is the frequency at which a propeller blade passes by the base of the thruster. It can be deduced from the propeller shaft frequency by the following equation, in which n denotes the amount of blades on the propeller. In the case of the thruster assemblies of the PS, $n = 4$, as can be seen in Table B.2.
$$f_{BPF} = f_{prop} n \tag{3.2}$$
- **Gear Mesh Frequency** - This is the frequency at which the teeth of two gears mesh with each other. In the case of the thruster assemblies of the PS, this would be the meshing of the teeth of the pinion gear, which is connected to the motor shaft, and the crown wheel, which is connected to the propeller shaft. The gear mesh frequency can be deduced from both the motor shaft speed and the propeller shaft speed by the following equation, in which n is the number of teeth on the pinion gear, and N is the number of teeth on the crown wheel. For the PS; $n = 13$ and $N = 62$, as can be seen in Table B.2.
$$f_{GM} = f_{motor} n = f_{prop} N \tag{3.3}$$

3.4.2. Bearing frequencies

Bearing frequencies are, similar to the previously mentioned frequencies, of a mechanical nature. However, as these frequencies all originate from a roller type bearing and have some specific characteristics, they are discussed separately. Bearing frequencies are determined by the shaft speed and the geometry of the bearing. Usually, bearing frequencies will only be induced once a fault is present in a bearing or it is nearing the end of its lifetime and is starting to show wear. Since, the surfaces of a healthy bearing are so smooth that they won't induce any noticeable mechanic vibrations. Assuming that the outer raceway of the bearing is stationary, the four main characteristic frequencies of any roller type bearing and their geometric deductions are listed below [17], in which f is the shaft speed at the location of the bearing, n is the amount of rolling elements in a bearing and the remaining geometric parameters are shown in Figure 3.2.

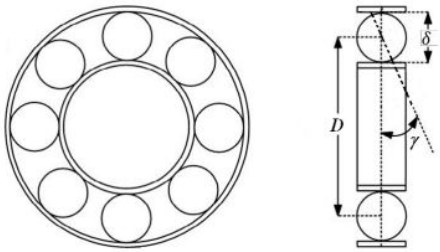

Figure 3.2: Geometric parameters of a roller bearing [18]

- **Ball Pass Frequency Inner Raceway (BPFI)** - This frequency is related to faults on the inner raceway of a bearing. It can be interpreted as the frequency at which a rolling element passes over a single specific point on the inner raceway of the bearing.

$$f_{BPFI} = f * \frac{n}{2}[1 + \frac{\delta}{D}cos(\gamma)] \tag{3.4}$$

- **Ball Pass Frequency Outer Raceway (BPFO)** - This frequency is related to faults on the outer raceway of a bearing. It can be interpreted as the frequency at which a rolling element passes over a single specific point on the outer raceway of the bearing.

$$f_{BPFO} = f * \frac{n}{2}[1 - \frac{\delta}{D}cos(\gamma)] \tag{3.5}$$

- **Ball Spin Frequency (BSF)** - This is the frequency at which a single rolling element spins around its own axis inside a bearing. Also, the second harmonic of this frequency is known as the Ring Pass Frequency on Ball (RPFB), which depicts each time a single point on the surface of a rolling element passes either the inner or outer raceway.

$$f_{BPF} = f * \frac{D}{\delta}[1 - (\frac{\delta}{D}cos(\gamma))^2] \tag{3.6}$$

- **Fundamental Train Frequency (FTF)** - This is the frequency at which the cage or train of a bearing will spin around its own axis.

$$f_{FTF} = f * \frac{1}{2}[1 - \frac{\delta}{D}cos(\gamma)] \tag{3.7}$$

3.4.3. Electrical frequencies

In an electrical powertrain, many different types of electrically induced oscillations might exist. The frequencies at which these will occur can be related to the functioning of the VFD or motor, but can also be caused by machine faults, such as stator winding insulation faults. For the mechanical analysis presented in this research, the electrical frequencies that were analysed are listed below. However, it should be noted that this is just a small selection of the electrical frequencies that can occur in an IM.

- **Drive Frequency** - The drive frequency is the frequency of the AC at which the IM is driven and will be denoted as f_1. In the case of a VFD driven IM, this means that this frequency will vary depending on the speed of the machine. For the thruster assemblies of the PS this frequency will vary between 0 and 50 Hz for rotor standstill and maximum rotor speed. As the drive frequency is the frequency in which all electrical power is transferred to the machine, this frequency is always the single most powerful frequency occurring in the electrical signature of a machine and many of its harmonic frequencies will be present in the signature as well. Also, all identifiable mechanical frequencies in the machine will be modulated on top of the drive frequency and will appear as sidebands around the drive frequency. A further explanation of this can be found in the literature review in Appendix H.
- **Switching Frequency** - The switching frequency is an electrical frequency that originates in the VFD and will therefore only occur in VFD driven IMs. A VFD works by means of Pulse Width Modulation (PWM). This technique is used to excite an alternating current by creating short varying voltage pulses. The frequency at which these voltage pulses are created is a set frequency for a specific machine and is usually in the range of multiple kHz for LV machines. For large MV machines the switching frequency is often lower. The VFDs of the thruster assemblies of the PS work with a switching frequency of 333.4 Hz for speeds of 0 up to 50% of the maximum motor speed and a switching frequency of 666.9 Hz for speeds from 50% up to 100% of the maximum motor speed.
- **Ship AC Frequency** - For VFD driven machines it is a possibility that the electrical signature of the IM gets contaminated with the AC frequency of the power grid of the ship. In normal circumstances this shouldn't happen, since the IM is powered by the variable AC originating from the VFD. However, the VFD itself is powered by the 60 Hz AC frequency of the ships power grid, and thus the IM is indirectly powered by this as well. This means it is not uncommon that the 60 Hz line frequency of the ship can be visible in the electrical signature of the IMs.
- **Slip** - In short, the slip can be considered as the difference in the actual rotating speed of the rotor (and motor shaft) and the synchronous speed of the rotor. It can be calculated as a ratio or percentage of the synchronous speed, or in Hz. The synchronous rotor speed is deduced from the drive frequency and can be considered as the rotor speed in the case that the rotational speeds of the magnetic fields of both the stator and rotor would exactly match. When an IM is in a 'motoring' operating condition, which means that the IM is used to drive a load, the actual rotor speed will be lower than the synchronous speed and the slip will be between 0 and 1. The equations for determining the slip as a fraction of synchronous speed are shown below, in which n_s denotes the synchronous rotor speed in Hz, f_1 denotes the drive frequency, n denotes the actual rotor speed (equal to f_{motor}) in Hz, p is the number of poles of the IM and s denotes the slip [19]. When analysing the slip in Hz, it is also referred to as slip speed and it is calculated as shown in Equation 3.10.

$$n_s = f_1 \frac{2}{p} \tag{3.8}$$

$$s = \frac{n_s - n}{n_s} \tag{3.9}$$

$$f_s = \frac{p}{2}(n_s - n) = s f_1 \tag{3.10}$$

3.5. Information processing techniques

To be able to extract useful information out of the raw data obtained in the measurements, a variety of information processing techniques is used. The most important of these techniques are shortly introduced in this section.

3.5.1. FFT and frequency spectra

The Fast Fourier Transform (FFT) is one of the best known and most used algorithms in signal processing. The FFT can be used to map a time-based signal into the frequency domain by means of a discrete Fourier transform, which creates a frequency spectrum of the time-based signal. When identifying mechanical behaviour of rotating equipment, the frequency spectrum of a time-based vibration signal can be used to establish the presence and magnitude of vibrations in the characteristic frequencies of a mechanical assembly. With this purpose, the FFT is used in all types of measurements as described in Section 3.2. Some further properties of an FFT are explained below.

Frequency range

The frequency range of the spectrum is determined by the sampling frequency (f_s) of the time signal. The highest frequency portrayed in a frequency spectrum is equal to $f_s/2$, as stated by the Nyquist theorem [20]. However, for the highest accuracy it is usually recommended to use an f_s that is at least 10 times higher than the highest frequency of interest in a measurement. For the frequency spectrum this means that the highest accuracy will be between 0 Hz and $f_s/10$ Hz.

Furthermore, frequencies outside of the 0 - $f_s/2$ range can also appear in the FFT due to aliasing. This is an effect in which frequencies that are higher than the Nyquist frequency 'fold' back over the Nyquist frequency into the spectrum. For example, a frequency of 10001 Hz will now appear as 9999 Hz in a spectrum with a Nyquist frequency of 10 kHz. For a proper analysis it is critical to prevent aliasing, as it will irreversibly contaminate the measurement. This can be done by using a pre-filter in the form of a low-pass filter, which will filter out higher frequencies and prevents them from folding back into the spectrum.

Complex and real spectra

It possible to distinguish between 'negative' and 'positive' frequencies when using an FFT for creating a spectrum. When this 'directional' information is critical for an analysis and needs to be retained, a two-sided 'complex' spectrum can be created, ranging from $-f_s/2$ Hz to $f_s/2$ Hz. In this case, a distinction can be made between positive and negative frequencies. However, most commonly the choice is made to create a real spectrum using the absolute value of the output of an FFT algorith, as is done in this research and can be seen in Appendix E. This causes the negative frequencies to be folded over the positive frequencies, which means that the negative and positive amplitudes of a frequency will add up and show as a single frequency. This phenomenon is important to keep in mind when considering the modulation of frequencies on a carrier frequency. For example, a hypothetical negative sideband frequency of 60 Hz modulated on a 40 Hz carrier frequency, will appear at $|40-60| = 20$ Hz in a regular spectrum.

Resolution

The resolution of the frequency spectrum is acquired by dividing the sampling frequency by the amount of samples analysed in a measurement, as can be seen in the formula below. In practice this means that the resolution is entirely determined by duration or length of a measurement.

$$f_{resolution} = \frac{f_s}{N_{samples}} \tag{3.11}$$

An FFT will be most useful in the case of steady-state machine and vibrational behaviour. As long as the vibrations in a machine remain constant during a measurement, a long sample time can be taken, resulting in a high resolution. However, when the machine behaviour is transient and thus the presence and magnitude of vibrations in certain frequencies change over time, the individual peaks in a frequency spectrum will either disappear or start to overlap. In this case, no clear peaks can be deduced [10]. Therefore, either a shorter time period should be analysed for the measurement, which will cause a lower resolution, but a higher certainty in what point in time a frequency was present in the spectrum. Or, another type of information processing technique should be adopted.

Window function

A final note on the use of an FFT is that the input signal is often multiplied by a window function before applying the FFT algorithm. A window function is a mathematical function that is zero everywhere, except around a chosen interval. Conceptually, this means that the FFT is calculated in data segments, which produces a tapering effect for the resulting output. In practice this means that the spectrum created out of the output will have narrower and better distinguishable peaks. In all FFT spectra used in this research, a Hanning-type window function was implemented.

3.5.2. Extended Park Vector Approach

The Extended Park Vector Approach (EPVA) [8] is a technique in ESA that is especially useful in identifying mechanical behaviour. The reason for this is that EPVA demodulates a 3-phase current or voltage measurement around the drive frequency. This means that it takes information out of all three phase measurements and creates a spectrum in which the 0 Hz component is now the drive frequency. All sidebands of the drive frequency are now stacked on top of each other to appear in the spectrum at their own original frequency. This makes mechanical characteristic frequencies often much easier to identify than by analysing the spectrum obtained from an individual current or voltage measurement.

The first step in the EPVA is to transform the three phase current or voltage into a two dimensional current or voltage. This transformation is called the Clarke transform or $\alpha\beta0$-transform. The formulas used in this transform are shown below, in which i_R, i_S and i_T represent the current measurements of the three phases of the IM. Note that all equations containing currents presented in this section hold true for voltages as well.

$$\begin{bmatrix} i_\alpha \\ i_\beta \\ i_0 \end{bmatrix} = \frac{2}{3} \begin{bmatrix} 1 & -\frac{1}{2} & -\frac{1}{2} \\ 0 & \sqrt{\frac{3}{2}} & -\sqrt{\frac{3}{2}} \\ \frac{1}{2} & \frac{1}{2} & \frac{1}{2} \end{bmatrix} \begin{bmatrix} i_R \\ i_S \\ i_T \end{bmatrix} \tag{3.12}$$

When the phases of an IM are balanced, i_0 will become 0 for the entire duration of the signal. This means that the three-dimensional dataset is now reduced to two dimensions containing the same information. The Clarke transform shown in Equation 3.12 is amplitude-invariant, meaning it preserves the amplitude of the three-dimensional signal into the two-dimensional signal. However, this transform is also power-variant, which means that the power of the signal is not preserved. When the power of the signal must be preserved, a Concordia transform can be used [21] or a correction term can be introduced.

The remaining two variables i_α and i_β together represent a current that rotates with the same speed as the drive frequency. This can be visualized by plotting i_α and i_β together, showing the orbit of the current. In literature, this is also sometimes referred to as a Park Vector [22], [23]. An example of this for the IM of T1 can be seen in Figure 3.3. When analysing this rotating representation of the current, it can be useful to consider i_α and i_β together as a complex value. The complex representation of the current then becomes:

$$i_c = i_\alpha + j * i_\beta \tag{3.13}$$

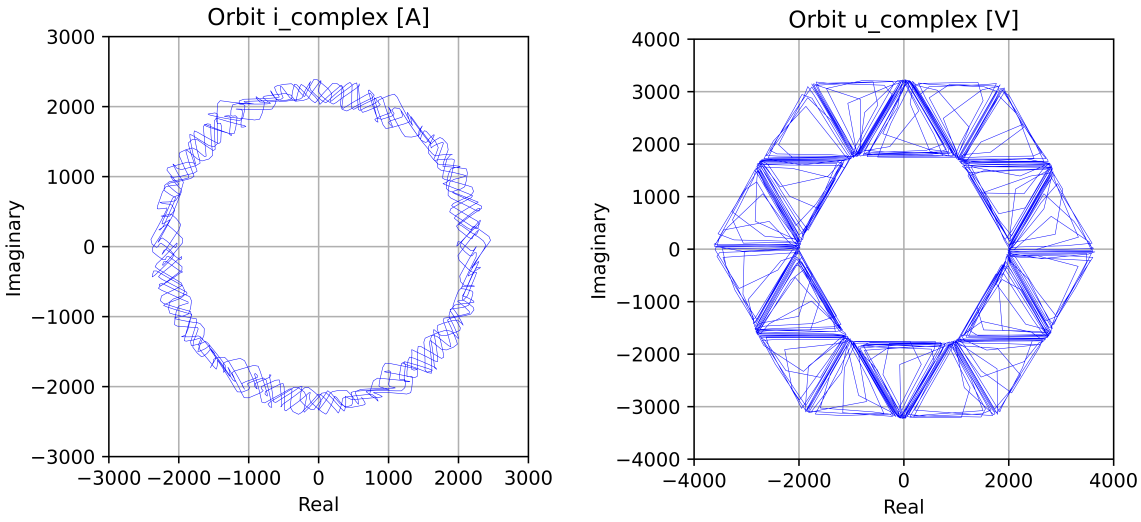

Figure 3.3: Orbit of i_c (left) and u_c (right) in T1 at 85% motor speed with t = 0.11s (4 periods)

The complex current and voltage can now be used as input for an FFT. This approach automatically demodulates the spectrum around the drive frequency, which means that the mechanically induced sidebands now appear in their original frequency. This can be done with multiple approaches, as shown in the equations below, in which y denotes the input of the FFT. Firstly, a common approach in literature is to use the squared magnitude of the complex current, as can be seen in Equation 3.14 [24]. However, in practice, plotting the squared magnitude did not improve the visibility of mechanical behaviour over plotting the magnitude itself. Also, plotting the magnitude has more physical meaning than plotting the squared magnitude. Therefore, the approach used in this research is to use the magnitude of the complex current or voltage as input for the FFT, as can be seen in Equation 3.15.

$$y = |i_c|^2 = |i_\alpha + (j * i_\beta)|^2 \tag{3.14}$$

$$y = |i_c| = \sqrt{i_\alpha^2 + i_\beta^2} \tag{3.15}$$

A third approach is to plot the complex current and voltage in a complex spectrum, containing both negative and positive frequencies. As explained earlier in this chapter, the advantage of this is that the directional information is retained in the spectrum. In practice, this information turns out to be mostly interesting for some electrical frequencies. An example of this is shown in Figure F.1 in Appendix F. In this complex spectrum of i_c, it can be seen that there is a large discrepancy in the occurrence of some positive and negative harmonics of the drive frequency. The difference in amplitude between the positive and negative counterparts of some of these harmonics is of several orders of magnitude. However, in the case of mechanical frequencies appearing as sidebands of the drive frequency, the amplitude of the positive and negative sideband of the same frequency tend to differ very little. Therefore, the choice was made to focus on the demodulated real spectra that are created using the input shown in Equation 3.15. This is because the positive and negative sidebands adding up to appear as a single, larger peak at the original mechanical frequency proved to be more beneficial than retaining the directional information for mechanical frequencies.

3.5.3. Calculating and plotting power and torque

Up until this point, the suggested methods of analysis have focused on using either the current or voltage. However, the mechanical and electrical behaviour of a machine is always determined by both the current and voltage, so analysing these values together might bring added value. This might be done by analysing the power spectrum of the machine, which is in literature sometimes referred to as its instantaneous power spectrum [25], or analysing the electrical torque of the machine. Both these parameters can be deduced using the current measurements as well as the voltage measurements, as shown in the following equations. Note that both the power and torque are calculated from measurements of all six sensors combined, which means these parameters must intuitively contain the maximum amount of relevant vibration and oscillation information present in any single parameter.

Firstly, the power can be calculated by multiplying the complex voltage with the conjugated complex current, as shown in Equation 3.16. From this complex power, the active power can be obtained with $P = Real(S)$, the reactive power is $Q = Imag(S)$ and the apparent power is $|S|$. Note that the Clarke transform used in Equation 3.12 conserved the amplitude of the signal and thus reduced the power, as was explained before. This is simply rectified by a factor 1.5 in the power calculation.

$$S = 1.5(u_c \bar{i_c}) \tag{3.16}$$

In order to calculate the torque in the machine, first the magnetic flux needs to be determined. This is done by a discrete time integration over the voltage and is performed in Matlab as shown in Appendix E. The mathematical equation for this process to obtain the stator flux is shown below, in which Φ is the stator flux and R_s is the estimated stator resistance.

$$\Phi = \int u_c - i_c R_s \, dt \tag{3.17}$$

The stator flux can now be used for a torque calculation, as shown in Equation 3.18, in which p denotes the number of pole-pairs in the IM. Similarly to the calculated power, the calculated torque will also be in the form of a complex number, which is denoted as T_c. In this case, however, the actual torque is obtained by $T = Imag(T_c)$. The 'reactive torque' can be seen as the attraction between stator and rotor and is obtained by $A = Real(T_c)$. Under normal or ideal operating circumstances this attraction will perform no work in the machine, as the air gap between the stator and rotor should remain constant and thus there will be no movement in the direction of this 'torque'. Finally, the 'apparent torque' can be denoted as $|T_c|$, although there is no scientific documentation available on the mechanical interpretation of this parameter.

$$T_c = 1.5(i_c \bar{\Phi}) \frac{p}{2} \tag{3.18}$$

3.6. Overview

In this section a visual overview of this research project is presented. Firstly, in Figure 3.4 the process for detecting the mechanical health of the thrusters is presented, together with the validation methods for this process. Secondly, in Figure 3.5 the entire thruster assembly is shown, including the VFD, IM, thruster and hull of the ship. The assembly is accompanied by the measurement setup, consisting of all three current and voltage sensors, the handheld vibration sensor, the shaft torque sensor and al DAQ's. Furthermore, an overview of the thruster assembly before adding the measuring equipment is shown in Figure B.5, along with more visualisations and drawings of the thruster assembly. Also, a model of the Kongsberg MetaPower device is shown in Figure C.3. Finally, an overview of all mechanical vibration sensors that are built-in to the thruster is shown in Figure C.2.

3.6.1. Flow charts of the measurements and analysis

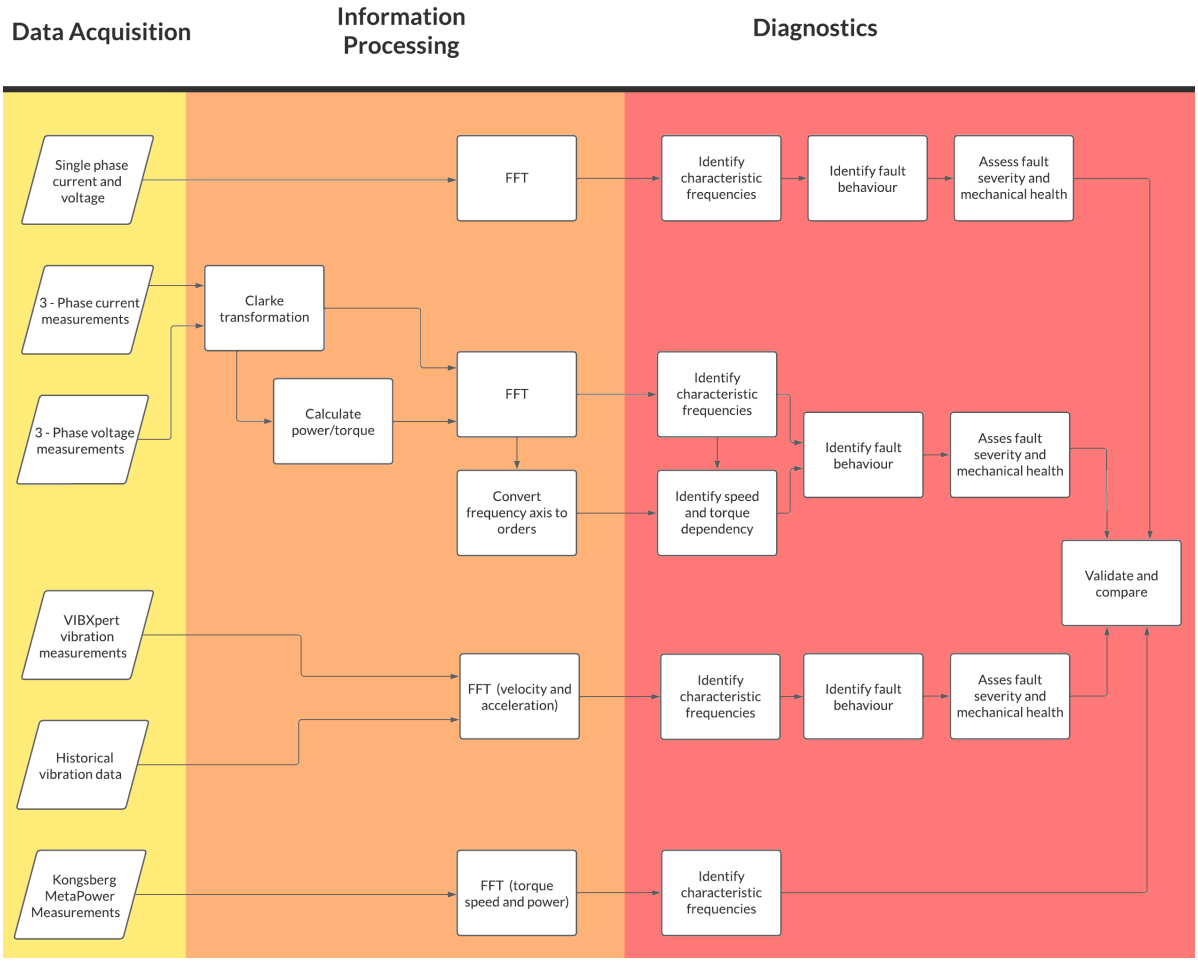

Figure 3.4: Flow chart of the measurement and analysis process for fault detection

3.6.2. Assembly overview

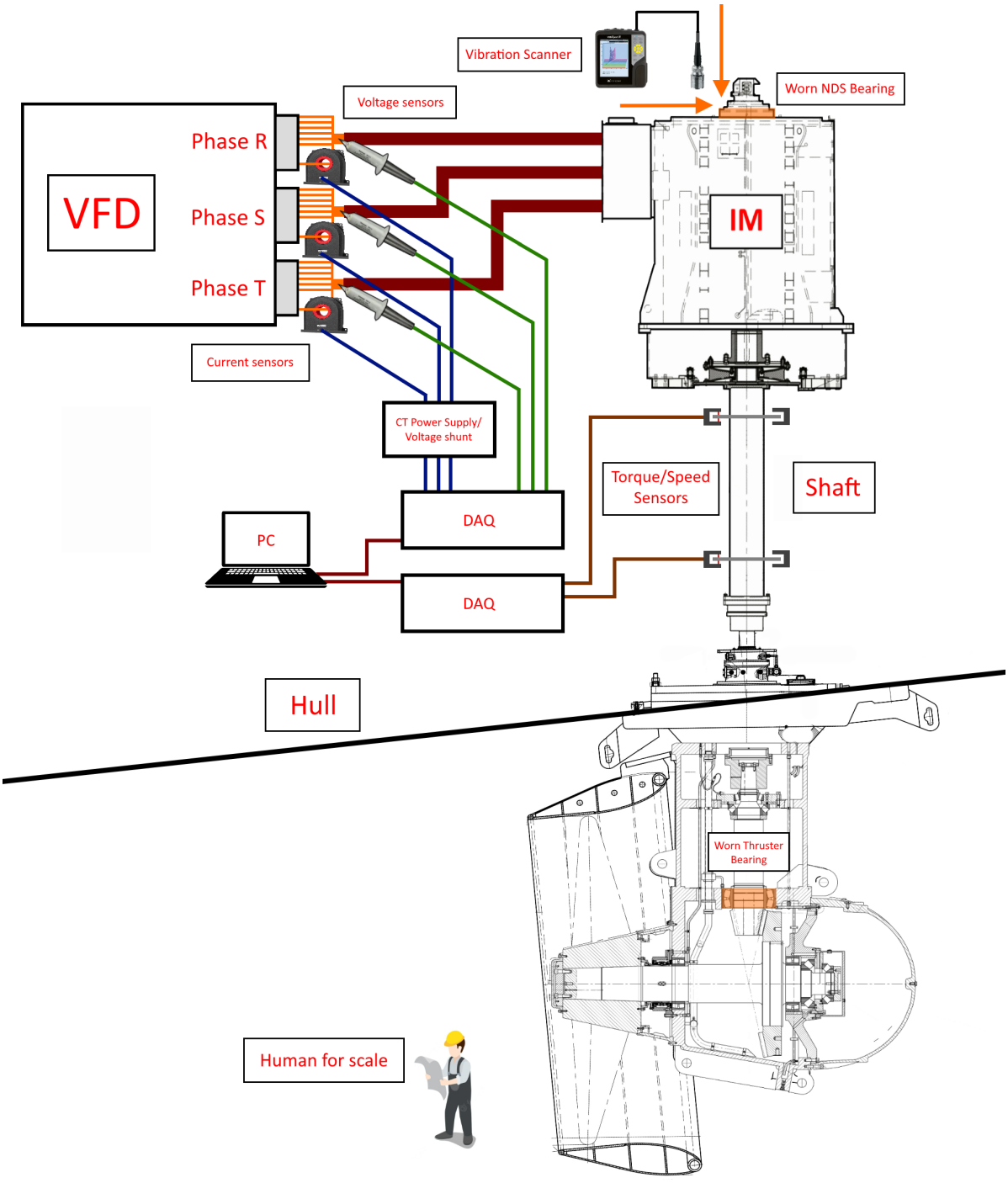

Figure 3.5: Overview of the assembly including measuring devices [26], [27]

4 Results

In this chapter the results of the ESA measurements are presented. These consist of an analysis at 85% motor speed for all different measured or calculated parameters, followed by an analysis of T6 at different motor speeds. Also, as this Chapter includes many different plots with lengthy explanations on their contents, a summary of the most important findings is included as the last section. The results of the mechanical vibration measurements and shaft torque vibration measurements are presented in Chapter 5, as they serve the purpose of validating the ESA measurements, as well as comparing the functionalities of the different measuring methods.

4.1. Notes on the presentation of the results

Plotting results

The results are summarized in an extensive amount of frequency spectrum plots. As the amount of images resulting from all measurements is high, only the most important plots are shown in this chapter. All other plots can be found in Appendix F.

Usually, frequency spectra are plotted on semi-logarithmic axes in scientific literature. One of the reasons for this is that the semi-logarithmic scale can present a more complete image of a signal, as it can show frequencies in a much larger range of amplitudes. This way, all frequency dependent information of a signal can be presented in a single image. However, in this thesis most spectra are presented on a linear scale with a frequency range of 0 - 200 Hz and an amplitude range that is adjusted to highlight all relevant mechanical vibrations. The reasoning for this is the following:

- The scope of this research is to detect mechanical vibrations in the electrical measurements. In practice, these mechanical vibrations are most easily detected in the lower frequency ranges (0 - 200 Hz).
- High frequency electrical oscillations that might be detectable at a much lower or higher amplitude than the mechanical vibrations are not of interest. Therefore, the axes of the plots are not adjusted to include them.
- In the presented plots, the amplitude of the drive frequency harmonics and 0 Hz components of the signals will sometimes fall outside the chosen amplitude range. Since, the baseline loads of the parameters are often much higher than the strength of the oscillations. However, these values are most often not of interest for this research, so the axes will not be adjusted to include them.
- When using this proposed method of linear axes adjusted to include the amplitudes of all frequencies of interest in the 0 - 200 Hz range, it becomes easier to denote and present the different mechanical vibrations to a reader. Since, this method makes the individual peaks visually stand out better above the noise floor of the signal. In the end, due to this benefit the choice was made to use the proposed method, as it outweighs the argument of including all frequency dependent information of the signal.

Highlighting frequencies of interest

All results are presented in a similar manner: The specific spectrum is shortly introduced, followed by a qualitative analysis of the spectrum and an image of the spectrum itself, to which information on the appearing frequencies is added. In all spectra, the identified frequencies will be highlighted in the image. This will be done in the manner that is listed below. Finally, as was also stated in Chapter 3, the method used for deducing the origin of all peaks represented in the plots can be found in Appendix D.

- The specific frequency will be highlighted by a part of its name or an abbreviation. For example: 'Motor' denotes the motor shaft frequency and 'NDS BPFI' denotes the Ball Pass Frequency Inner of the bearing at the Non-Drive Side of the IM.
- When an oscillation can't be identified, it will be assigned an abbreviation in the form of 'E1', meaning 'unidentified electrical frequency 1' or simply 'U1' for 'unidentified frequency 1'.
- Harmonics of a certain frequency are indicated by an integer multiplication in front of the name or abbreviation. For example: The third harmonic of the motor shaft frequency will be denoted as '3x Motor'.
- When modulation occurs, positive and negative sidebands of a frequency will be denoted by a + or - symbol. In this case, the carrier frequency will have an assigned number to which the sideband frequencies refer. For example: The carrier frequency will be denoted as 'NDS BPFI (1)' and its negative sideband of the second harmonic of the motor shaft frequency will be denoted as '1 - 2x Motor'.

4.2. Electrical Signature Analysis: 85% motor speed

Firstly, the current and voltage spectra are shown and compared of the three thrusters at the highest possible speed and torque available in the measurements. Since, in these measurements the most vibration and oscillation behaviour will likely be present. The highest possible speed for all three thrusters was 85% motor speed, which was accomplished in a ramp-up test during sailing intervals. However, the sailing speed was not completely identical for the three instances and thus the load on the three thrusters varies by a margin for the three sets of thruster data. In the analysed measurements in this section, the average torque on T1 was roughly 65.5 kNm, the average torque on T3 was 64.8 kNm and the average torque on T6 was 62.8 kNm. This was determined from the calculated torque of these measurements and can be seen in Figure F.2.

The maximum speed was 85%, since the ship wasn't sailing at full speed during the ramp-up tests. This means that the torque limit of the IM was reached during tests with a higher speed setpoint. This can be seen in Figure F.3, in which the drive frequency over time is analysed for both 85% motor speed and 95% motor speed. The figure shows that the drive frequency is kept constant at 85% motor speed, but is heavily oscillating at 95% motor speed due to the torque limit. Therefore, much frequency dependent information is lost in the FFT of higher speeds than 85%, as the vibrations are spread over a range of frequencies instead of appearing as a single frequency.

4.2.1. Single phase spectrum

Current

The single phase spectra of the R-phase current of T1, T3 and T6 can be seen in Figure 4.1. When analysing this graph, these are the first things that stand out:

- The frequencies determined to be of a mechanical nature appear as sidebands in the form of narrow peaks on the drive frequency. These narrow peaks represent a vibration or oscillation that exist only at a certain specific frequency, that can be pinpointed with an accuracy of $\pm f_{res}/2$. Also, these narrow peaks assumed to be of a mechanical nature overlap for all three thrusters, which further validates that they are only dependent on the drive and motor shaft frequency, as these values were almost identical for the three thrusters during this test.
- There is a second type of peak visible in the spectrum that does not appear as a sharp peak at a specific frequency, but rather as a hill spread out over a small range of frequencies. Therefore, this type of oscillation in a spectrum will also be referred to as 'haystack'. Examples of these haystacks can be seen in Figure 4.1 denoted with $1 - E1$ and $1 + E1$. These phenomena closely resemble a pattern that can also be expected for mechanical resonance [28]. However, they are determined to be of an electrical nature, which is further explained in Appendix G.
- T1 and T3 show very similar behaviour, while T6 shows many narrow peaks at more mechanical frequencies related to the NDS bearing. However, it proves hard to perform a proper mechanical analysis with the mechanical frequencies modulated as sidebands on the drive frequency. Therefore, a further mechanical analysis will be performed in the following subsections.

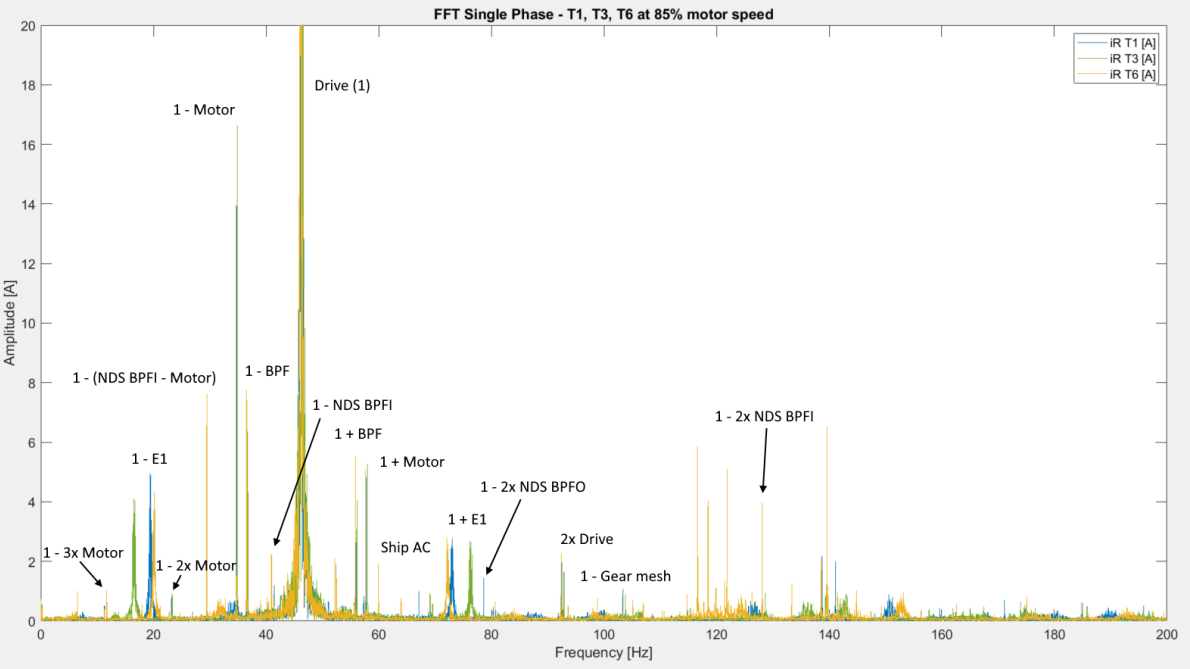

Figure 4.1: Single phase current FFT of T1, T3, T6. Fs = 20 kHz, sample time = 50 s

Current and voltage

Next to comparing the phase currents of the three thrusters, this same analysis can be made for the phase voltages (Figure 4.2). It is also interesting to compare the difference in frequency components between the voltage and current in general. This is done by plotting the spectra of the voltage and current in the same graph. A plot with linear axes ranging from 0 - 400 Hz containing the single phase current and voltage of T6 is shown in Figure F.4. A plot on a semi-logarithmic scale ranging 0 - 1000Hz is shown in Figure F.5. The first points becoming clear in these images are:

- The harmonic frequencies of the drive frequency are better represented in the voltage spectrum.
- As can be seen in Figure F.5, the oscillations in voltage seem to gain in strength for higher frequencies, while the oscillations in current seem to slightly decrease in strength.
- As can be seen in Figure F.4 and Figure 4.2, the frequencies that are mechanically induced are better visible in the lower frequency ranges (0 - 200 Hz). This gives the impression that for a mechanical analysis, it might be best to analyse these lower frequency ranges.
- Also, these mechanical frequencies appearing in the lower frequency ranges (0 - 200 Hz), such as the motor shaft frequency and the BPF, seem to be better represented in the current spectra than in the voltage spectra.
- As expected, there are more frequencies than just the drive frequency on which other frequencies are modulated as sidebands. This can be seen in Figure F.5 in which the switching frequency can be clearly seen in the voltage spectrum, including many sideband frequencies. These frequencies are mostly related to electrical phenomena and are therefore further discussed in Appendix G. However, this shows that it is a possibility that higher harmonic sideband frequencies on the switching frequency might be able to pop up in the lower frequency ranges at which mechanical frequencies are expected to be better represented.
- There also appear to be sideband frequencies for harmonics of the drive frequency, as can be seen in Figure F.4. It even seems like there are frequencies modulated on top of the 6th harmonic of the drive frequency, which is interesting because this frequency itself is not present in the signal.

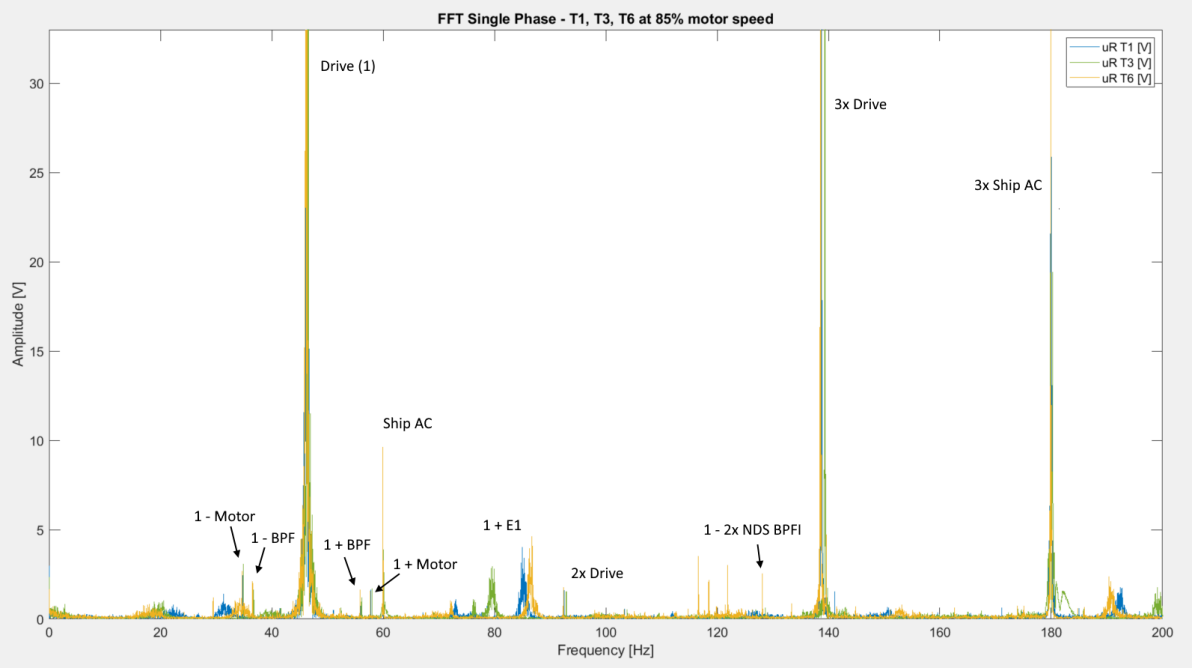

Figure 4.2: Single phase voltage FFT of T1, T3 and T6. Fs = 20 kHz, sample time = 50 s

4.2.2. EPVA Method

Current

The spectra of the magnitude of the complex currents following the EPVA method and Equation 3.15 of T1, T3 and T6 are shown in Figure 4.3. The first things that stand out are the following:

- The mechanical frequencies have become much better identifiable than in the single phase FFT, due to their appearance in their original frequencies instead of sidebands.
- There is a large peak present at the 2x Drive frequency. According to [24], the cause of this is an unbalance in the phase currents. Small phase unbalances are not considered unhealthy machine behaviour. Also, the fact that the current of only one out of each 7 phase cables is measured, might increase the measured unbalance.
- The motor shaft harmonics, BPF and its harmonics, as well as the gear mesh frequency all appear exactly at their predicted frequency, i.e. within $\pm f_{res}/2$ of the predicted frequency as shown in Appendix D.
- The mechanical frequencies related to the NDS BPFI of T6 all appear with an offset related to their harmonic of the NDS BPFI. This offset can be calculated as $\Delta = n * 0.1Hz$, in which Δ denotes the offset and n denotes the harmonic. For example, the NDS BPFI itself appears at 87.16 Hz, while it is predicted to be 87.06 Hz according to the motor shaft frequency and shaft speed order obtained from the bearing manufacturer. This difference in the measured and expected frequencies is further discussed in Chapter 6.
- For T1 there appears to be an NDS BPFO vibration present in the system, as a peak shows at its 2nd harmonic. This could indicate early stage bearing wear, but this needs to be further evaluated. Since, there is no prior knowledge available on damage to this specific bearing.
- Next to the haystack of E1, new haystacks appear in E2 and E3. These seem to be modulated around the 3rd harmonic of the drive frequency, as they show symmetry around this frequency. Also, at 6.0 Hz an unidentifiable frequency has appeared. All these frequencies will be discussed in Appendix G.

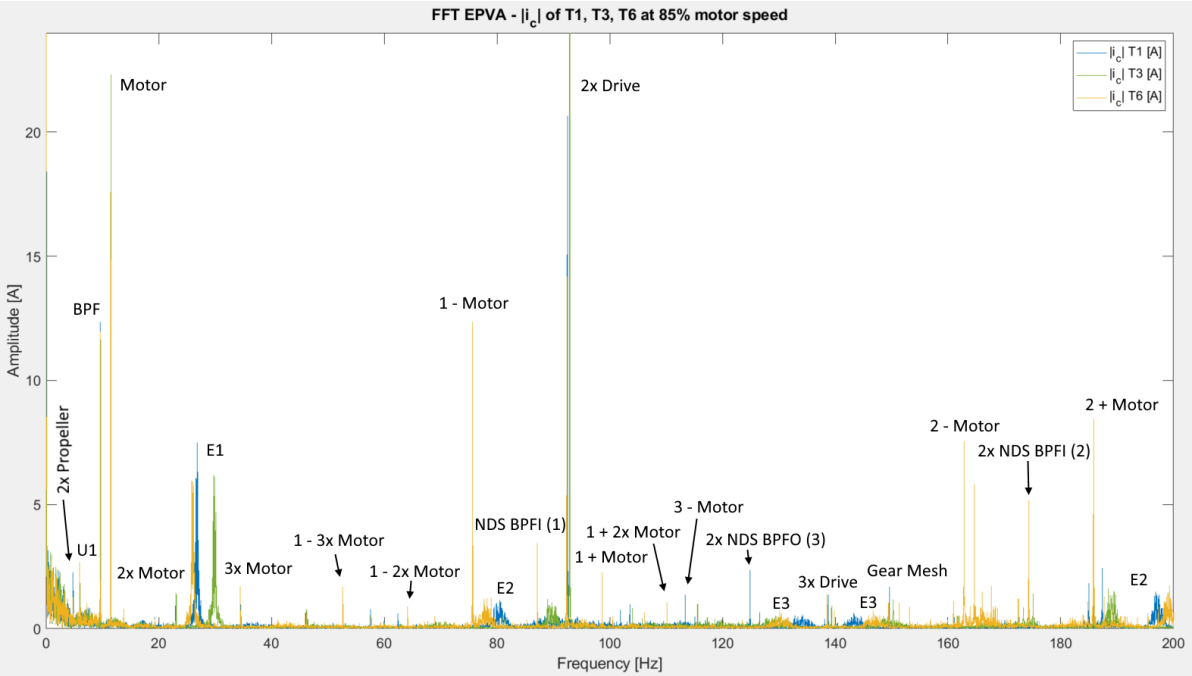

Figure 4.3: EPVA $|i_c|$ FFT of T1, T3 and T6. Fs = 20 kHz, sample time = 50 s, f_{res} = 0.02 Hz.

Current and voltage

The same EPVA spectrum has been made for the complex voltages and is shown in Figure 4.4. Also, the two spectra of T6 are compared in Figure 4.5. Finally, the two spectra of T6 are plotted in a semi-logarithmic scale in Figure F.6. From these graphs the following points stand out:

- The voltage is much less sensitive in the low frequency ranges. This can be seen in all images, but is most obvious in Figure F.6, as the noise floor decreases in amplitude close to 0 Hz. Therefore, the mechanical behaviour is somewhat more easily identifiable in the EPVA current. In these graphs the low frequencies represent the frequencies that were originally close to the drive frequency.

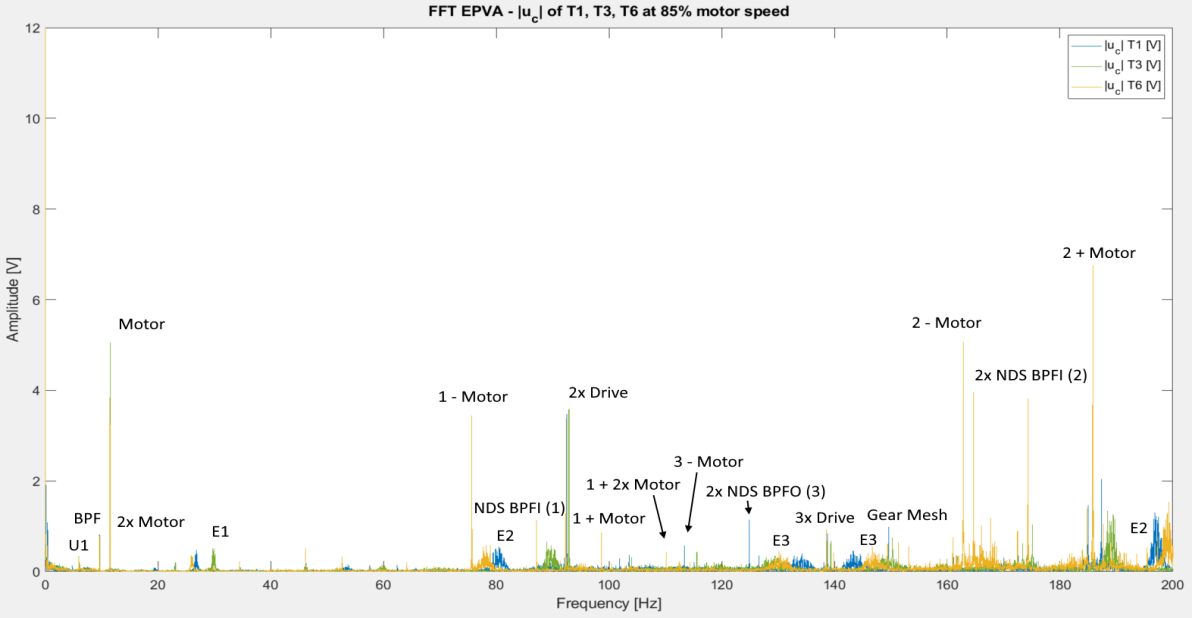

Figure 4.4: EPVA $|u_c|$ FFT of T1, T3 and T6. Fs = 20 kHz, sample time = 50 s, f_{res} = 0.02 Hz.

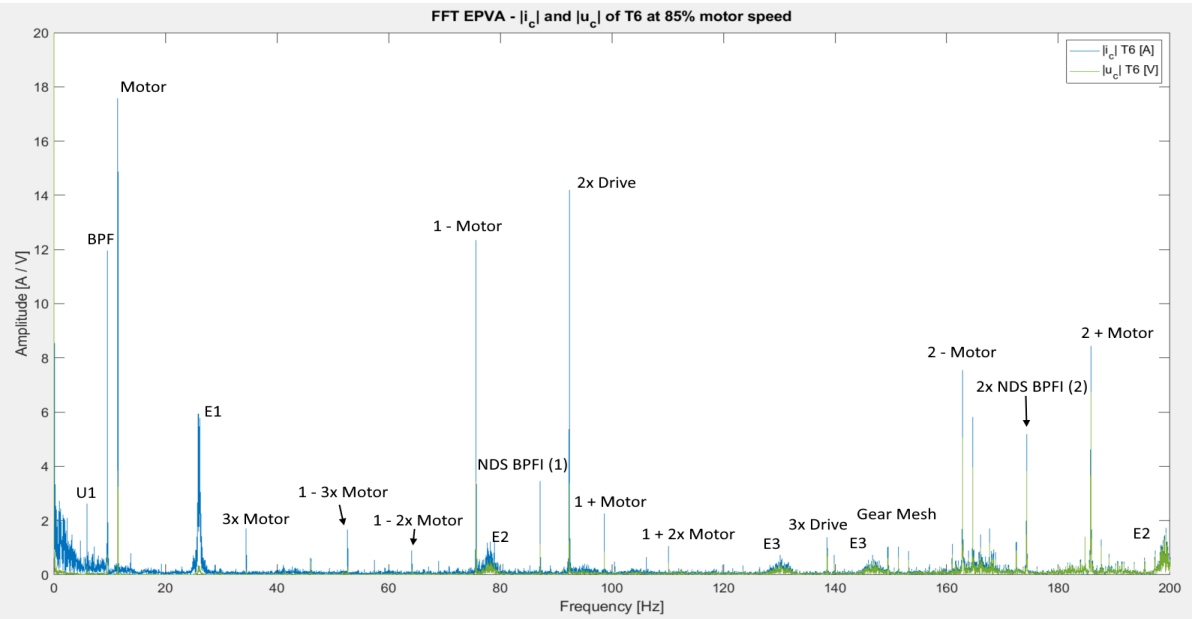

Figure 4.5: EPVA $|i_c|$ and $|u_c|$ FFT of T6. Fs = 20 kHz, sample time = 50 s, f_{res} = 0.02 Hz.

4.2.3. Power spectrum

The results of both the active power spectrum and reactive power spectrum are shown in Figure 4.6 and Figure F.7. A comparison of the active power spectrum and reactive power spectrum for T6 is shown in Figure 4.7. The following points stand out from these graphs:

- The identified mechanical vibration frequencies are similarly visible as in the current EPVA spectrum showed in Figure 4.3.
- The active power and reactive power show similar behaviour, also considering that the baseline active power (4.7 MW) is roughly twice as high as the baseline reactive power (2.1 MVar). However, for some frequencies, such as the motor shaft frequency, the vibration is much stronger represented in the reactive power.

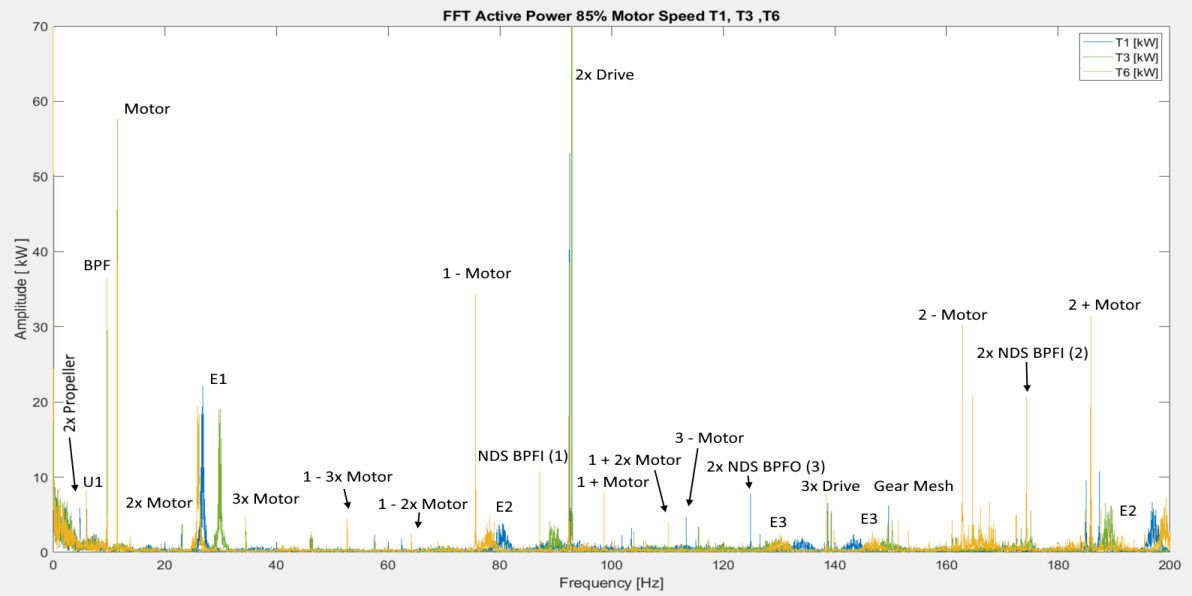

Figure 4.6: Active Power FFT of T1, T3 and T6. Fs = 20 kHz, sample time = 50 s, f_{res} = 0.02 Hz.

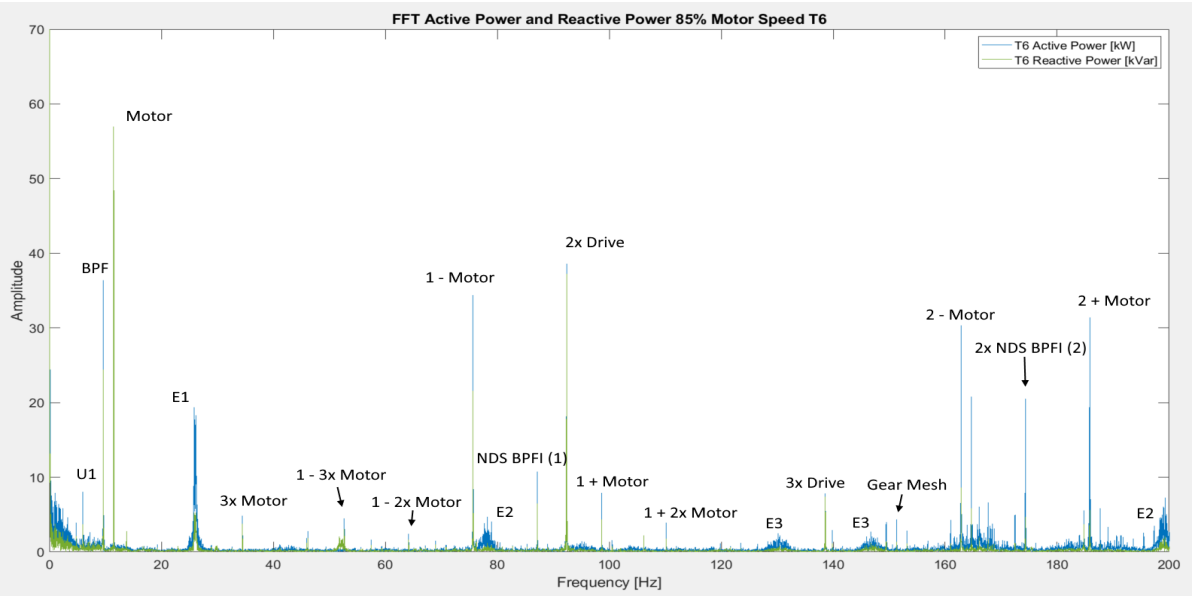

Figure 4.7: Active Power and Reactive Power FFT of T6. Fs = 20 kHz, sample time = 50 s, f_{res} = 0.02 Hz.

4.2.4. Torque spectrum

The results of both the torque spectrum and attraction spectrum are shown in Figure 4.8 and Figure F.8 respectively. A comparison of the torque spectrum and attraction spectrum for T6 is shown in Figure 4.9. Qualitatively, these spectra show much similarity with the different power spectra shown in the previous subsection:

- The torque and attraction show similar behaviour, also considering that the baseline torque (63.0 kNm) is roughly twice as high as the baseline attraction (32.4 kNm). However, for some frequencies, such as the motor shaft frequency, the vibration is much stronger represented in the attraction. Note that the unit for the attraction is presented as kNm. This is only used as a means of comparison, as the attraction is physically not the same as a torque in kNm. This is because in the case of attraction the force vector is parallel to the lever arm and will thus not enforce a rotation, nor do work.

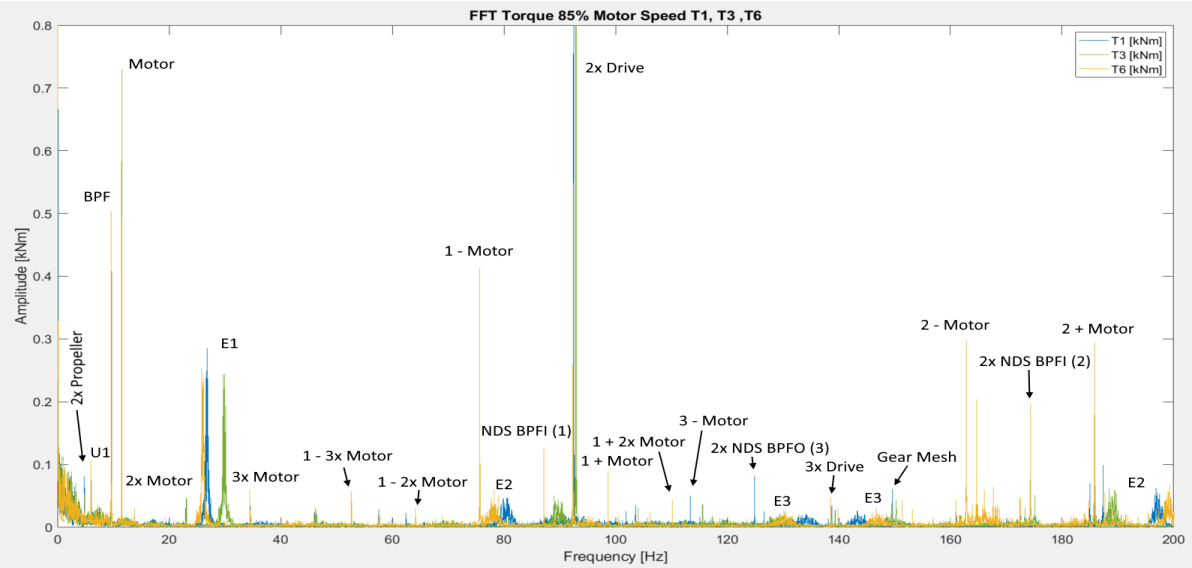

Figure 4.8: Torque FFT of T1, T3 and T6. Fs = 20 kHz, sample time = 50 s, f_{res} = 0.02 Hz.

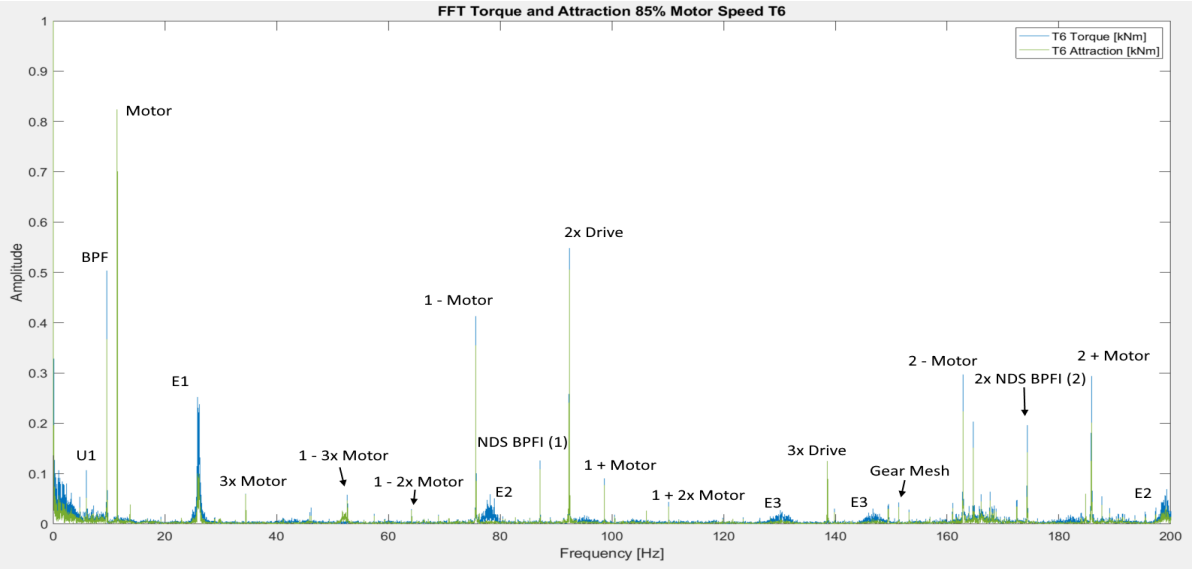

Figure 4.9: Torque and Attraction FFT of T6. Fs = 20 kHz, sample time = 50 s, f_{res} = 0.02 Hz.

4.3. Electrical Signature Analysis: Variable motor speed

In this section, the effects of motor speed on the oscillation behaviour in the different spectra is analysed. This analysis will be performed on the measurements of T6, as this is the thruster showing most mechanical vibrations in its spectra. Firstly, an analysis is performed in the high motor speed range, which ranges from 70% to 85% of the maximum motor speed. Secondly, the low speed range of 40% to 70% of the maximum motor speed is analysed. This split is made, since the high speed measurements were performed during a sailing interval and the low speed measurements were performed on a different, day while on DP. The high speed range is analysed as it is expected to show the most mechanical vibrations, while the low speed range is analysed to examine down to what motor speed and torque the mechanical behaviour of the machine is still detectable.

Furthermore, the spectra used are the EPVA current spectrum and torque spectrum, as these were amongst the spectra that qualitatively gave the best identification of mechanical frequencies. Also, using these spectra will include both a spectrum comprised of three measurements (current) and a spectrum comprised of six measurements (torque).

4.3.1. High speed range

The spectra are analysed in two ways. Firstly, the spectra at different speeds are plotted over each other without any modifications. Secondly, the spectra are normalised through dividing the frequency axis by the shaft speed, before plotting them over each other. This modification causes all peaks in the spectrum that are solely related to the motor speed to fall over each other for different speeds, making them appear as an 'order' of the motor speed on the X-axis, instead of at a specific frequency.

The torque spectra at different speeds before and after normalization are shown in Figure 4.10 and Figure 4.11 respectively. The EPVA current spectra at different speeds before and after normalization are shown in Appendix F in Figure F.9 and Figure F.10 respectively. Also, some close ups of these spectra to point out specific frequencies have been made. These can be found in Appendix F as well. Out of these images, the following information can be gathered:

- The frequencies related to mechanical behaviour all exactly overlap in their order when viewed in the normalized spectra. This is a further validation that these vibrations are indeed of a mechanical nature and thus originate from the bearings, since they match these expected frequencies. This holds true for both the NDS BPFI in T6, as well as the NDS BPFO of T1, of which an image is added in Appendix F (Figure F.14).
- The current and torque spectra qualitatively show almost identical behaviour in terms of relative amplitudes of the mechanical vibrations (compared to each other).
- For most mechanical frequencies the amplitude steadily increases for a higher speed and torque setting. An example of this is the torque of the motor shaft frequency, which is highlighted in Figure F.13. However, this is not always the case, as the BPF in this same graph does not show the same behaviour. This could be caused by local resonance or hydromechanical factors for the blades of the propeller. A more detailed explanation for this is investigated in Chapter 6.
- Another explanation for the fact that some mechanical frequencies show stronger oscillations at lower speeds, can be the fact that these mechanical frequencies coincide with a much stronger electric oscillation. This can be seen in the case of the '2x NDS BPFI + Motor' peak (in all images), which seems to show the strongest amplitude at 75% motor speed. However, this high peak is actually caused by the fourth harmonic of the drive frequency.
- The haystacks introduced as E1, E2. etc. don't appear to be caused by mechanical resonance, as it can be seen in Figure 4.10 and Figure F.9 that these vibrations do not occur in the same frequency range for the different motor speeds. This is further explained in Appendix G.
- The oscillation identified as U1 appears to be unrelated to motor speed, but increases in amplitude for each higher speed and torque setting. This can be clearly in Figure F.13.

Torque spectrum before normalization

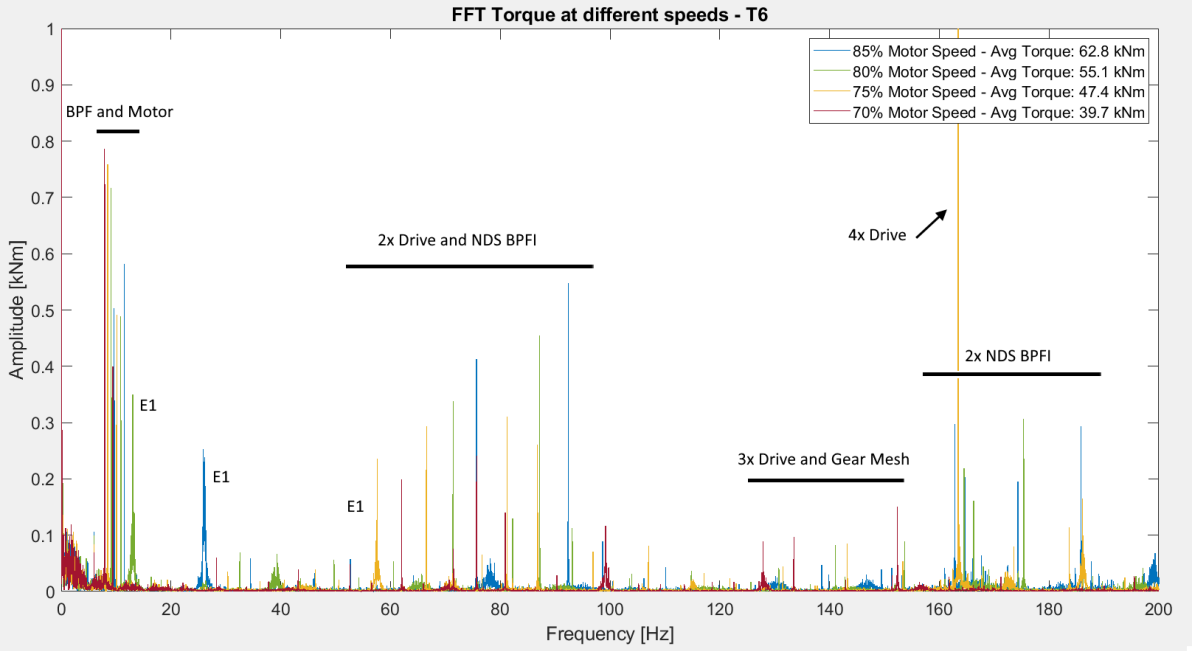

Figure 4.10: Torque FFT of T6 at variable speed. Fs = 20 kHz, sample time = 50 s, f_{res} = 0.02 Hz.

Torque spectrum normalized

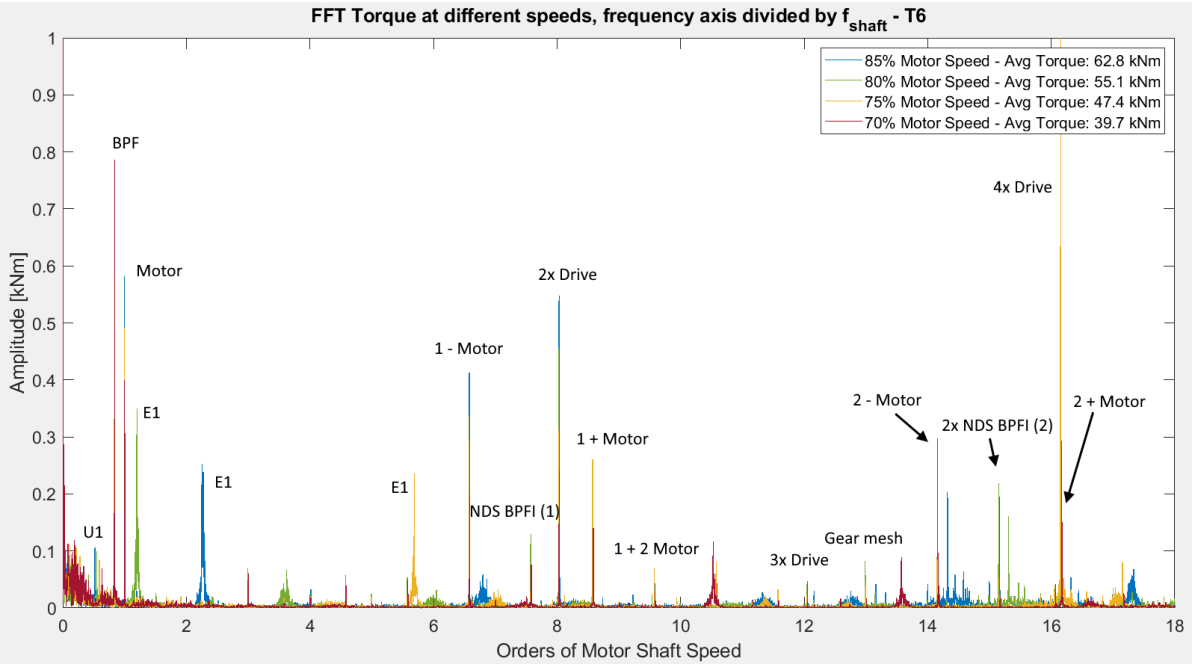

Figure 4.11: Torque FFT of T6 at variable speed, frequency axis divided by motor shaft frequency. Fs = 20 kHz, sample time = 50 s, f_{res} = 0.02 Hz.

4.3.2. Low speed range

As stated before, the low speed range is analysed to examine down to what motor speed and baseline torque the mechanical behaviour of the machine can still be detected. Secondly, since both the high speed and low speed ramp-up tests contain a measurement at 70% motor speed, the mechanical behaviour at the same motor speed but at a different baseline torque can be analysed. The reason for this different torque at the same speed, is the fact that a higher vessel speed will cause a higher flow speed of water on to the propeller of the thruster, which lowers the torque needed to maintain the same motor speed. Therefore, the baseline torque at 70% motor speed on DP was 47.3 kNm, while the baseline torque at 70% motor speed during sailing was 39.7 kNm. It should be noted that there is a slight discrepancy in actual motor speed during these two measurements. The motor speed on DP was 568.8 RPM, while the motor speed during sailing was 565.4 RPM.

The normalized torque spectrum and normalized EPVA current spectrum for the low speed range are shown in Figure 4.12 and Figure F.11. The torque spectrum and EPVA current spectrum (before normalization) at 70% motor speed, but different sailing conditions are shown in Figure 4.13 and F.12 respectively. Out of these spectra, the following points become apparent:

- Some of the mechanical frequencies, such as the BPF and motor shaft frequency, are still easily detectable down to 40% motor speed. However, the gear mesh frequency is hardly detectable even at 70% speed.
- The vibrations related to the NDS BPFI are easily detectable down to 50% motor speed. However, at 40% motor speed these vibrations have mostly drowned in electrical noise. Furthermore, the vibrations related to the second harmonic of the NDS BPFI are hardly detectable at these lower motor speeds.
- At 60% and 70% motor speed the motor shaft frequency sidebands of the NDS BPFI have a remarkably high amplitude. Some sidebands at 60% motor speed are even more strongly represented than at 70% motor speed.
- When analysing the torque vibrations at 70% motor speed but varying baseline torques (Figure 4.13), it becomes apparent that a higher baseline torque doesn't necessarily correspond with a higher amplitude in torque vibrations. The amplitudes of the same vibrations are comparable for all detectable mechanical frequencies. Some of these frequencies have a slightly higher amplitude in the ramp-up test during sailing, while others have a slightly higher amplitude in the ramp-up test on DP.

Torque spectrum normalized 40% - 70% motor speed

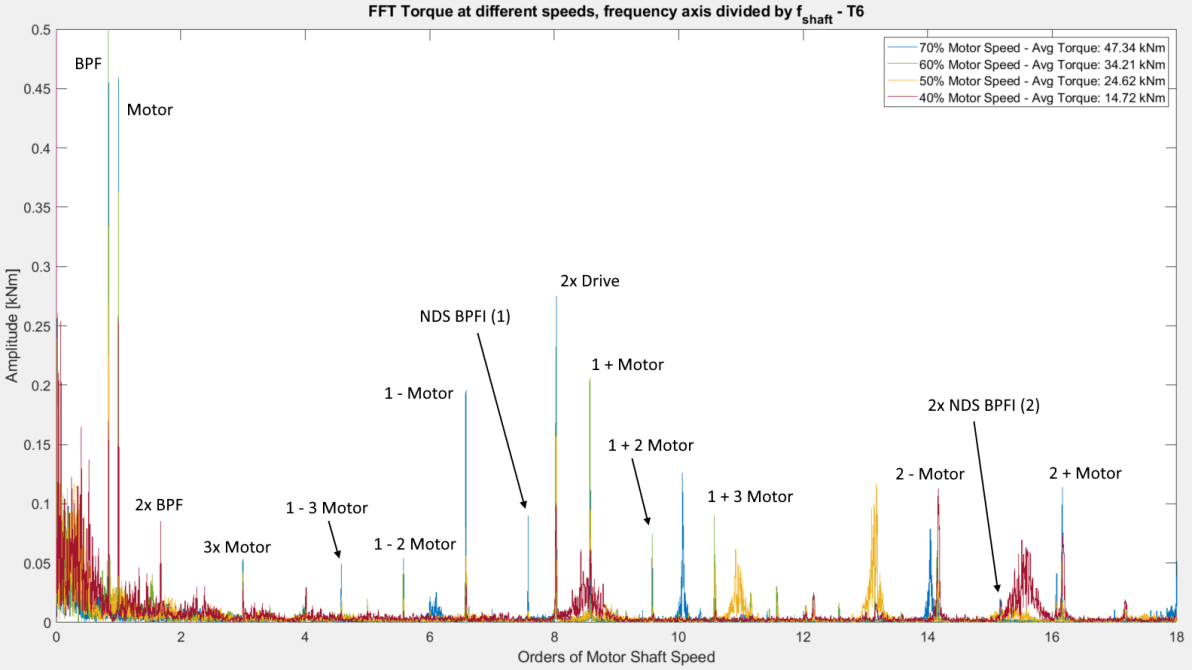

Figure 4.12: Torque FFT of T6 at variable speed, frequency axis divided by motor shaft frequency. Fs = 20 kHz, sample time = 50 s, f_{res} = 0.02 Hz.

Torque spectrum at 70% motor speed and varying baseline torque

As this chapter shows many different

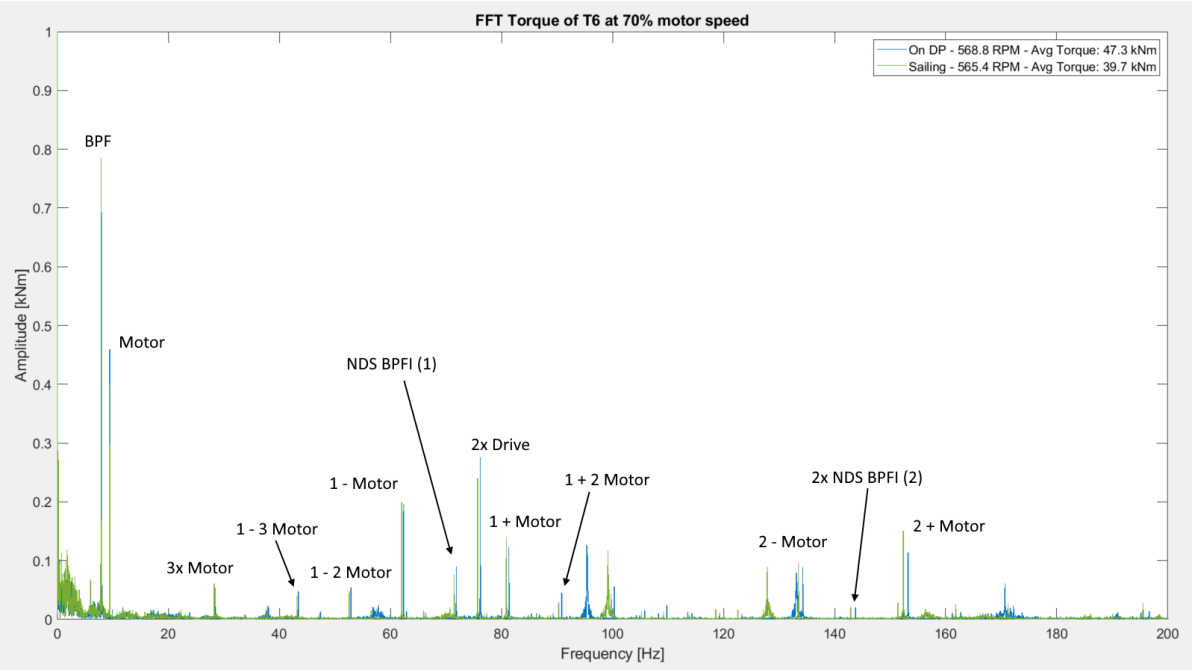

Figure 4.13: Torque FFT of T6 at 70% motor speed and varying torque. Fs = 20 kHz, sample time = 50 s, f_{res} = 0.02 Hz.

4.4. Summary of results

As this chapter presents many different spectra with lengthy explanations on their contents, this section presents a summary of the most important findings in terms of answering the research questions. This is done in the following manner:

- Tables 4.2 and 4.3 provide an answer to subquestion: *'Which mechanically induced vibrations can be detected in the induction motor current and voltage measurements'*.
- Table 4.1 provides an answer to subquestion *'How can these mechanically induced vibrations be most effectively detected in the induction motor current and voltage measurements'*.
- Table 4.2 provided the start of answering subquestion *'Perform a machine health diagnosis of thruster 1, 3 and 6 of the Pioneering Spirit based on the researched method.'* The full machine health diagnosis is performed in the corresponding paper, which is presented in Appendix A.

Also, more notes and details on the use of the different spectra and the identification of mechanical behaviour are presented in Section 6.1 and Section 6.2 respectively.

	Identifiability of mechanical behaviour	Limitations	Other use
Single phase current	Poor	Mechanical frequencies appear as sidebands instead of their original frequency.	Identify electrical behaviour. Pinpoint drive frequency
Single phase voltage	Poor	Mechanical frequencies appear as sidebands instead of their original frequency. Oscillations are somewhat weaker in low frequency range.	Identify electrical behaviour. Pinpoint drive frequency
EPVA Current	Clear		
EPVA Voltage	Clear	Oscillations are somewhat weaker in low frequency range.	
Active Power	Clear		
Reactive Power	Clear	Less mechanical context/interpretation compared to active power	
Torque	Clear		
Attraction	Clear	Less mechanical context/interpretation compared to torque	
Variable speed (EPVA current and torque)	Very clear	More measurements (at variable speeds) needed	

Table 4.1: Overview of different spectra

	Motor	Propeller	BPF	Gear mesh	NDS Bearing	DS Bearing	Thruster Bearings
T1	Fundamental and harmonics	2nd harmonic	Fundamental and harmonics	Fundamental	2x BPFO and 3x BPFO	None	None
T3	Fundamental and harmonics	2nd harmonic	Fundamental and harmonics	Fundamental	None	None	None
T6	Fundamental and harmonics	2nd harmonic	Fundamental and harmonics	Fundamental	BPFI fundamental and harmonics, including motor shaft sidebands	None	None

Table 4.2: Overview of detected mechanical vibrations in T1, T3 and T6

	Motor	Propeller	BPF	Gear mesh	NDS Bearing	DS Bearing	Thruster Bearings
Lowest detection speed	40%	40%	40%	70%	40~50%	None	None

Table 4.3: Overview oflowest speed for the detection of specific mechanical frequencies.

5 Validation

This chapter presents the results of the mechanical vibration measurements and shaft torque measurements. As stated in Chapter 3, this is done in order to validate the results of the ESA measurements, as well as to compare the functionalities of ESA with other CM techniques. Firstly, the results of the mechanical vibration measurements are presented. Hereafter, the results of the shaft torque measurements are shown, including a comparison with the electrically deduced torque.

5.1. Mechanical vibration

First of all, to validate the occurrence of mechanical vibrations in the ESA spectra, the mechanical vibration measurements obtained with the handheld vibration scanner during the ramp-ups test at 85% motor speed are shown for T1 and T6. Secondly, to compare the sensitivity of the measurement techniques, the same measurements at 40% motor speed for T6 are presented. Finally, as the ramp-up tests for T3 did not include measurements with the handheld vibration scanner, some historical data originating from the sensors down in the thruster is highlighted.

5.1.1. Analysis at 85% motor speed

The velocity spectra originating from the 0°, 90° and axial vibration measurement are shown in Figure 5.1, Figure F.15 and Figure 5.2 respectively. In all velocity spectra, the unit of [mm/s] denotes the peak of the speed measured of a vibration at a certain frequency. The following points can be deduced from these spectra:

- The same mechanical vibrations are visible for T1 and T6 as in the ESA measurements, but without the added electrical noise and harmonics.
- T1 and T6 show much similar vibration behaviour compared to each other, except for the NDS BPFI related vibrations of T6 and the NDS BPFO vibrations for T1.
- The 0° and 90° spectra show similar behaviour: almost all peaks show up in both spectra. However, there are some discrepancies in the amplitudes of the peaks.
- In the axial measurements, all NDS related vibrations have a much higher (up to 30 times) amplitude than in the radial measurements. This is likely caused by the fact the NDS is an angular contact bearing on which a portion of the weight of the rotor and motor shaft is suspended. Therefore, there is a high axial load on this bearing.

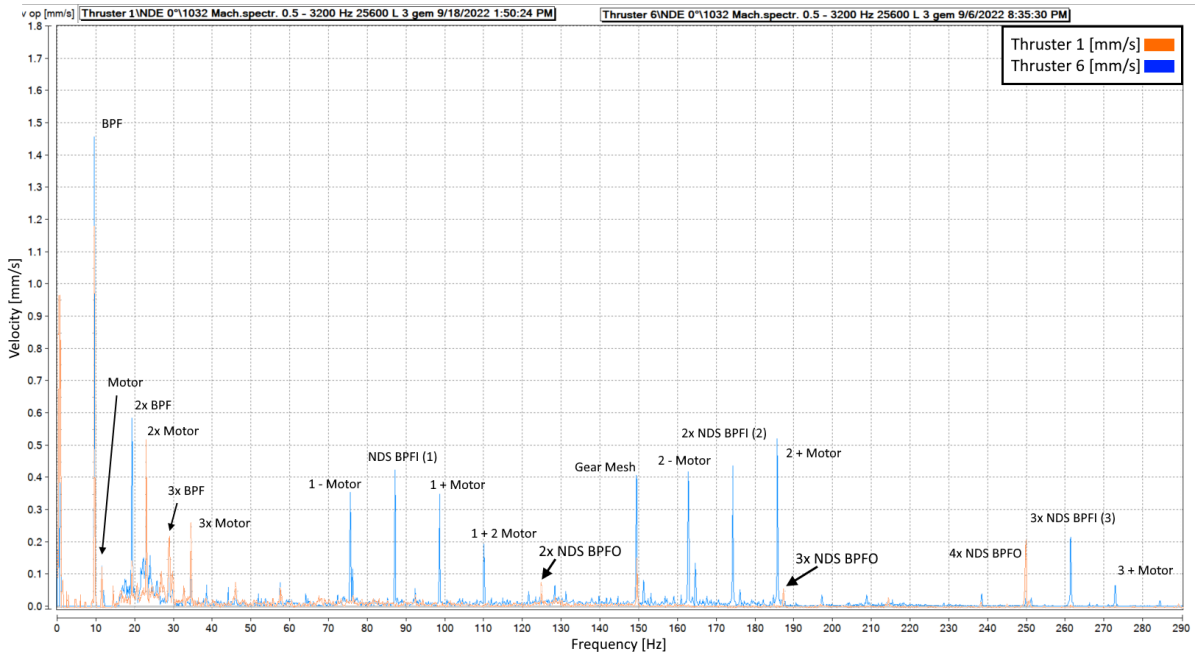

Figure 5.1: Mechanical Vibration Velocity Spectrum of T1 and T6 at 0°. f_s = 25.6 kHz, sample time = 8 s, f_{res} = 0.125 Hz.

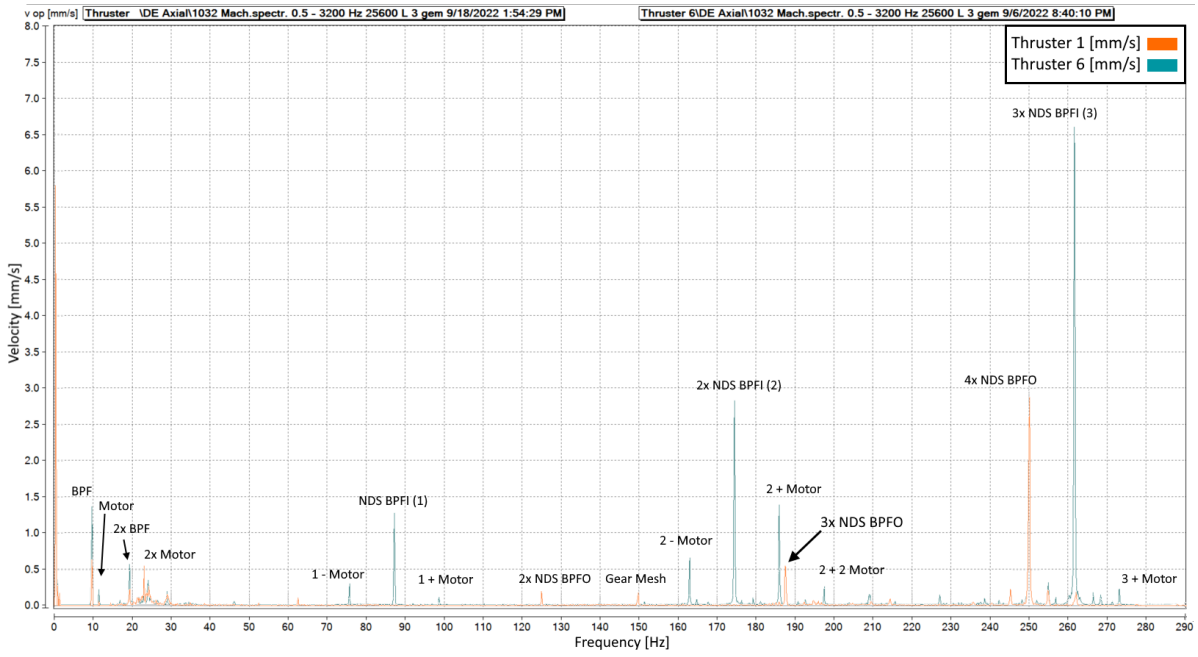

Figure 5.2: Mechanical Vibration Velocity Spectrum of T1 and T6 axial. f_s = 25.6 kHz, sample time = 8 s, f_{res} = 0.125 Hz.

5.1.2. Analysis at 40% motor speed

The velocity spectra originating from the 0°, 90° and axial vibration measurement are shown in Figure 5.3, Figure F.17 and Figure F.18 respectively. The following points can be deduced from these spectra:

- The only noticeable vibrations at this speed are all related to the NDS BPFI. This frequency is present up to its fifth harmonic, including sidebands of the motor shaft frequency at all harmonics.
- These measurements indicate that the mechanical vibrations related to the NDS bearing are slightly better detectable at this low speed in the mechanical velocity spectra, compared to the ESA spectra. Since, these same vibrations start to drown in electrical noise in the ESA spectra at 40% speed. Also, it should be noted that the ESA measurements had a considerably longer sample time: 50 seconds for the ESA measurements, compared to 8 seconds for the mechanical vibration measurements.

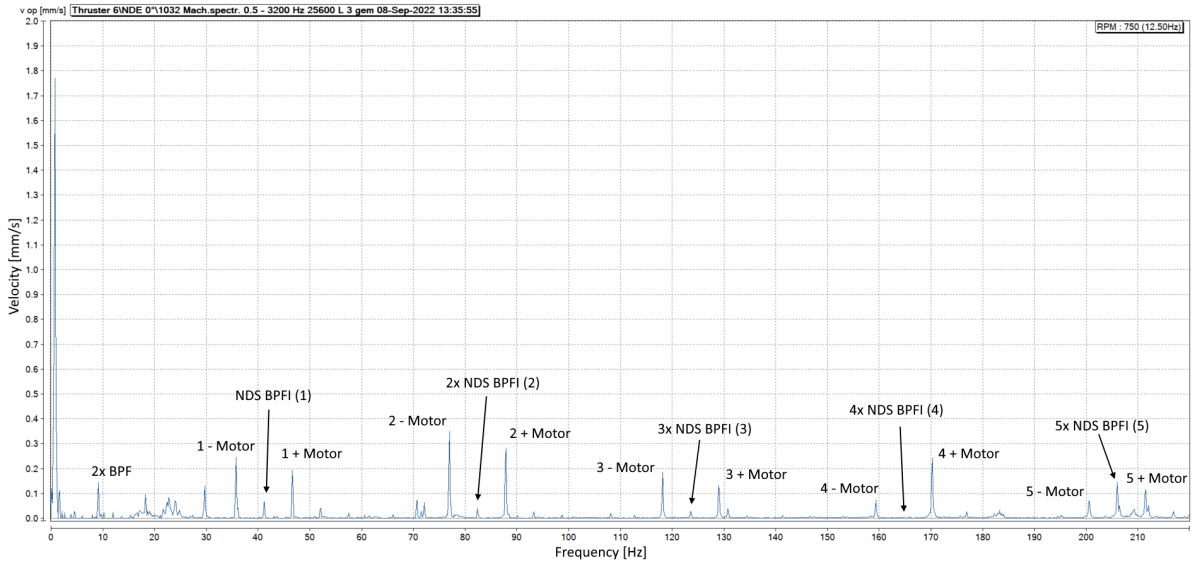

Figure 5.3: Mechanical Vibration Velocity Spectrum of T6 at 0°- 40% motor speed. f_s = 25.6 kHz, sample time = 8 s, f_{res} = 0.125 Hz.

5.1.3. Historical vibration data

As explained in Chapter 3, T3 has suspected early stage wear in one of the bearings inside the thruster. This knowledge was gained through a measuring report of Pruftechnik NV, of which a screenshot is shown in Figure 5.4 (with added notations in red for clarification purposes). This analysis states that in the time-waveform of the acceleration measured by thruster sensor 3 (see Figure C.2), a frequency can be found that closely resembles the BPFI of the input shaft double spherical bearing of the thruster. In order to validate this, the velocity spectrum taken at the same instance as the measurement from the report is shown in Figure 5.5. Also, a more recent velocity spectrum at a slightly higher motor speed is shown in Figure F.16. Both these measurements originate from sensor 3 as well and were retrieved from the database of historical vibration measurements of the PS. When analysing the report and two spectra, the following points become apparent:

- The suspected BPFI vibration seems to have a frequency of 55 Hz when analysing the velocity spectrum in Figure 5.5. Also, the second and third harmonic of this frequency seem to be present in the spectrum.
- When identifying the motor shaft speed as 4.25 Hz from this same spectrum, the order of the peak at 55 Hz is 12.96X. This value resembles the gear mesh frequency (order of 13X) more closely than it resembles the input shaft double spherical bearing BPFI (order of 10.84X).

- The same orders of vibration can be seen in Figure F.16 at a slightly higher speed, also more closely resembling the gear mesh frequency than the suspected BPFI.
- Sensor 3 is located next to the pinion gear. Meaning, it would be logical that the gear mesh frequency is found in these measurements. Nevertheless, when analysing the velocity spectra of measurements of the other sensors spread through the assembly, the same vibrations at roughly 13X show up as well. This further validates that this frequency is most likely the gear mesh frequency.
- All in all, it seems unlikely that there are actually vibrations present in the BPFI of the input shaft double spherical bearing. This means that is also most probably not experiencing any wear.

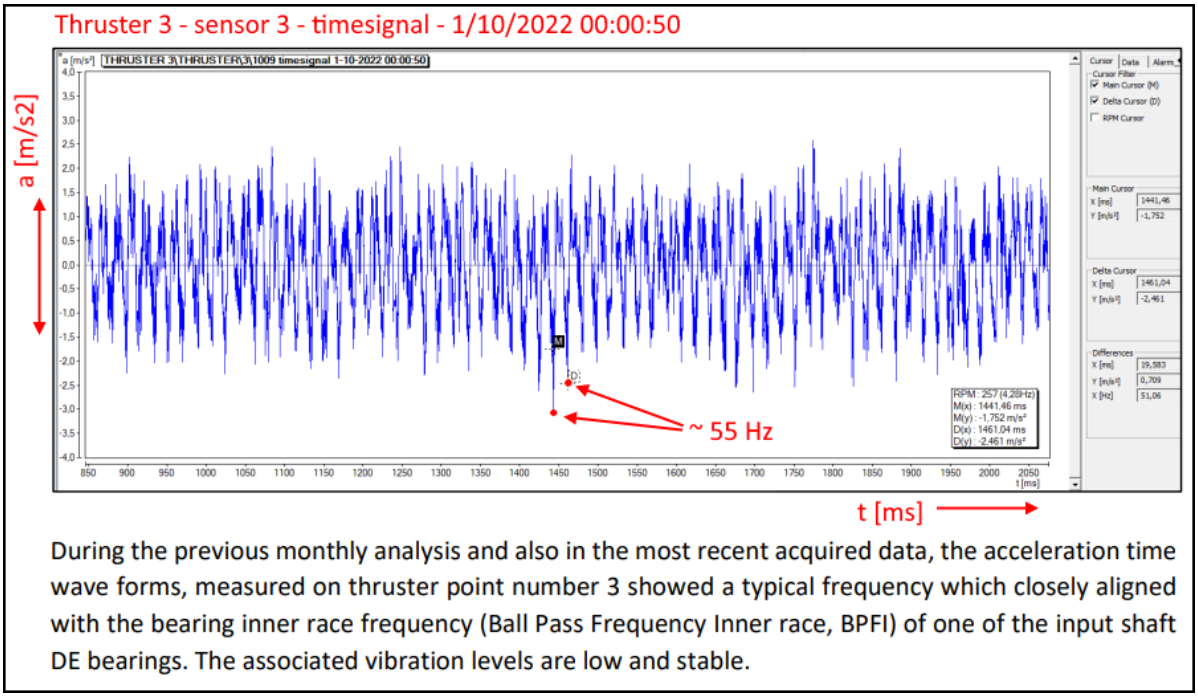

Figure 5.4: Section of a measuring report from Pruftechnik NV for T3 in August 2022. [29]

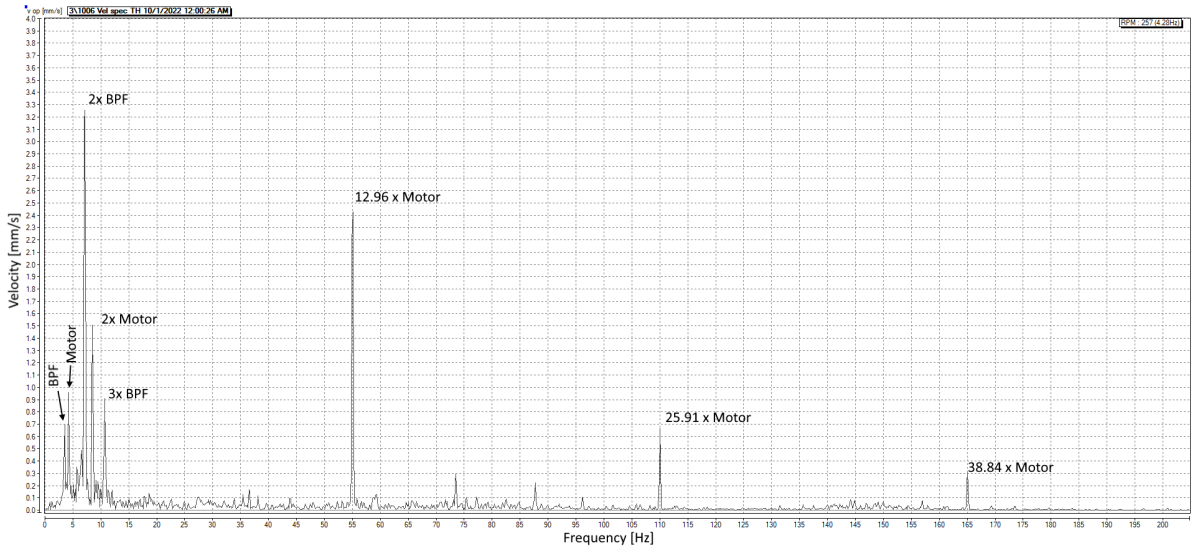

Figure 5.5: Velocity spectrum of sensor 3 taken at the same time as the measurement in Figure 5.4. Motor speed: 257 RPM (34%)

5.2. Kongsberg MetaPower

In this section, the results of the Kongsberg MetaPower measurements will be discussed. As these measurements only concern T1, the mechanical behaviour will be identified, but this will not include any faulty machine behaviour. Therefore, only the presence of the general mechanical characteristic frequencies might be identified for comparison and validation with the ESA measurements. Firstly, this comparison will be performed for the results at 70% motor speed, as this was the highest speed in which the Kongsberg MetaPower system was run. Secondly, an analysis is done over the entire range of speeds at which a measurement took place in the ramp-up tests.

5.2.1. Results at 70% Motor Speed

The comparison of electrically deduced torque and shaft torque measured by the Kongsberg MetaPower system is shown in Figure 5.6. The comparison of electrical active power and shaft power is shown in Figure F.21. The first things that stand out in these graphs are:

- There is a slight difference in amplitude for the 0 Hz component for the electrical torque (47.72 kNm) and the shaft torque (46.67 kNm).
- The amplitude of the BPF vibration in the motor shaft is remarkably high (2.81 kNm).
- Almost all measured vibrations in the motor shaft originate from the propeller speed, motor shaft speed and BPF.
- Apart from the 1x motor shaft frequency, all mechanical vibrations are much stronger represented in the motor shaft torque than in the electrical torque.
- The 2nd harmonic of the NDS BPFO seems to be well represented in the shaft torque. However, there appears to be no oscillation in the 1x NDS BPFO frequency.
- The gear mesh frequency is strongly represented in the shaft torque vibrations. It also appears to have sidebands of the motor shaft speed.

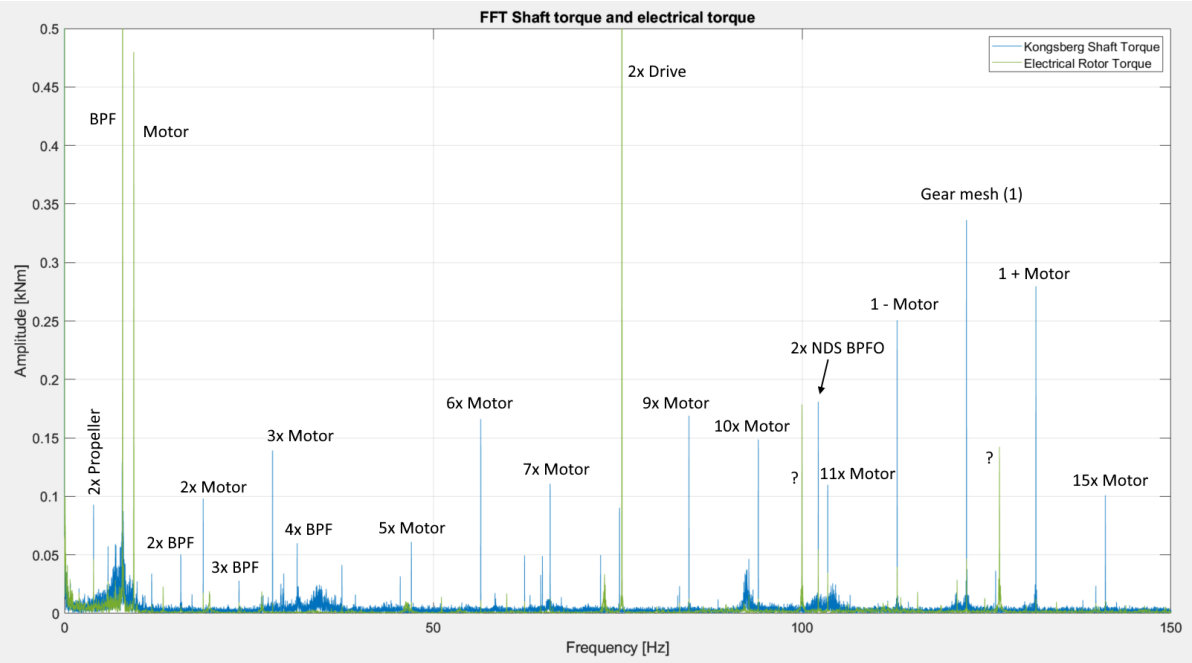

Figure 5.6: Torque FFT of T1 at 70% speed of Kongsberg MetaPower: Fs = 1600 Hz, sample time = 50s. And electrically deduced torque: Fs = 20 kHz, sample time = 50 s

5.2.2. Results at variable speed: shaft torque only

In this subsection the variable speed results of only the Kongsberg MetaPower system will be examined. In the next subsection some variable speed results of the electrical torque are included as well. Firstly, the torque spectrum normalized by shaft speed is shown in Figure 5.7. Secondly, the torque spectrum before normalization in a semilogarithmic scale is shown in Figure F.19. Finally, a close up of the torque spectrum between 0 and 20 Hz for 40% and 70% motor speed can be seen in Figure F.20. When analysing these results the following things become apparent:

- For lower motor speeds, a vibration of 3x NDS BPFO starts to become visible in the shaft torque.
- At lower speeds, the gear mesh frequency appears to have sideband frequencies of the BPF and propeller shaft frequency as well.
- There appears to be a region around 8 to 9 Hz in which vibrations seem strongest. This is logical, as in this region the BPF and motor shaft speed will mostly occur. However, at 40% motor speed the 2x BPF (around 9 Hz) peak is considerably higher than the 1x BPF peak (Figure F.20), which is the case for no other speed. One explanation for this could be the presence of a resonance frequency around this frequency range. This, or another possible explanation will be further analysed in Chapter 6.
- There appear to be more of these resonance regions detectable in the shaft torque. This becomes visible in Figure F.19, in which the torque spectra of different motor speeds are shown to have similar regions of heightened amplitude at the same frequencies.

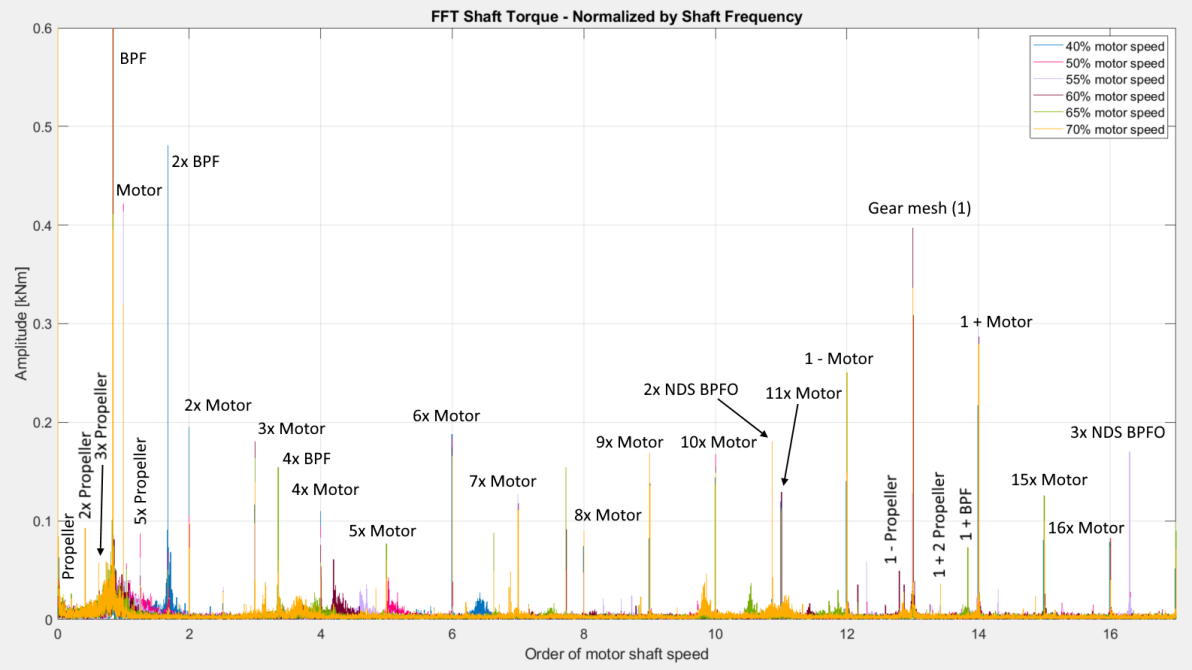

Figure 5.7: Torque FFT of T1 at different speeds of Kongsberg MetaPower, sample time = 25s.

5.2.3. Results at variable speed: shaft torque and electrical torque

When analysing the shaft torque and electrical torque simultaneously, it becomes possible to determine how well the amplitudes of certain vibrations match for the two different measurements at different speeds. This is firstly done by comparing the amplitude of the 0 Hz-component for both techniques at all speeds. In this case, the 0 Hz component represents the baseline torque produced by the IM for the electrical measurements, and represents the baseline torque measured in the motor shaft for the shaft torque measurements. Secondly, the amplitudes of the vibrations measured at the BPF, motor shaft frequency and the gear mesh frequency are compared. A table containing all measurements is shown in Table 5.1. This also includes the ratio between the two measurements, which is calculated according to Equation 5.1, and the variation in % of the measurements, which is calculated according to Equation 5.2. In these equations, T_s represents the shaft torque and T_e represents the electrical torque. The baseline electrical and shaft torque measurements for the different speeds are plotted in Figure F.22. The ratio of the two types of measurement at different speeds and different mechanical frequencies is plotted in Figure 5.8. What becomes apparent from these measurements is the following:

- As can be seen in Figure F.22, the measured baseline shaft torque and baseline electrical torque show much similarity. Table 5.1 shows the two measurements only vary in a range of 0 - 3%. This inaccuracy seems to rise with the motor speed and torque level.
- At 40% speed, the measured baseline shaft torque seems to be higher than the measured baseline electrical torque. Normally, this behaviour should not occur, as the torque is created inside the IM. However, this could be caused by the fact that at 40% speed the propeller of T1 might be influenced by the water flow created by the propeller of the two thrusters next to it, as these were powered at a similar speed at that time. This could have caused the torque at the propeller end to be higher than in the motor. Another explanation of this would be the inaccuracy of the measurements.
- The measured amplitudes of the mechanical vibrations (other than the 0 Hz-component) are less compatible for the two measuring approaches. As can also be seen in Figure 5.6, the shaft torque shows much stronger vibrations in most mechanical frequencies.
- The BPF has a considerably higher amplitude in all shaft torque measurements compared to the electrical measurements. One explanation of this could be the fact that this vibration is caused at the propeller end and will therefore have dampened by the time it reaches the IM.
- The motor shaft frequency shows the least consistent ratio and variation for both measuring methods at different speeds. At some speeds, oscillations show strongest in the electrically deduced spectrum. At other speeds, the shaft torque shows a slightly stronger oscillation for the same mechanical vibration. An explanation for the fact that this vibration is measured comparably stronger in the electrical measurements than the BPF and gear mesh frequency, could be because this vibration originates in the motor shaft and rotor itself.
- Vibrations in the gear mesh frequency are much better represented in the shaft torque measurement. This can also be seen in Figure 5.6, in which many motor shaft frequency sidebands on the gear mesh frequency appear. None of these sidebands are represented in the electrical torque. Moreover, the amplitude of the vibrations in the gear mesh frequency itself is only a small fraction in the electrical torque compared to the shaft torque, as can be seen in Table 5.1.

$$Ratio = \frac{T_e}{T_s} \tag{5.1}$$

$$Variation = \frac{T_e - T_s}{T_s} \tag{5.2}$$

	Motor Speed [%]	T_e [kNm]	T_s [kNm]	Ratio	Variation [%]
Baseline torque	40	15.45	15.78	0.98	- 2.10
	50	25.28	25.09	1.01	+ 0.78
	55	30.47	30.15	1.01	+ 1.04
	60	35.42	35.02	1.01	+ 1.15
	65	41.55	40.86	1.02	+ 1.69
	70	47.72	46.68	1.02	+ 2.24
BPF	40	0.106	0.282	0.38	- 62.4
	50	0.336	0.992	0.34	- 66.1
	55	0.450	1.231	0.37	- 63.4
	60	0.716	2.170	0.33	- 67.0
	65	0.729	2.786	0.26	- 73.8
	70	0.750	2.810	0.27	- 73.3
F_{motor}	40	0.349	0.176	1.98	+ 98.3
	50	0.367	0.422	0.87	- 13.0
	55	0.364	0.414	0.88	- 12.1
	60	0.417	0.320	1.30	+ 30.3
	65	0.468	0.305	1.53	+ 53.4
	70	0.530	0.320	1.66	+ 65.6
Gear Mesh	40	0.003	0.218	0.01	- 98.6
	50	0.020	0.104	0.19	- 80.8
	55	0.060	0.236	0.25	- 74.6
	60	0.009	0.398	0.02	- 97.7
	65	0.013	0.224	0.06	- 94.2
	70	0.046	0.336	0.14	- 86.3

Table 5.1: Torque difference of 0Hz component at variable speed

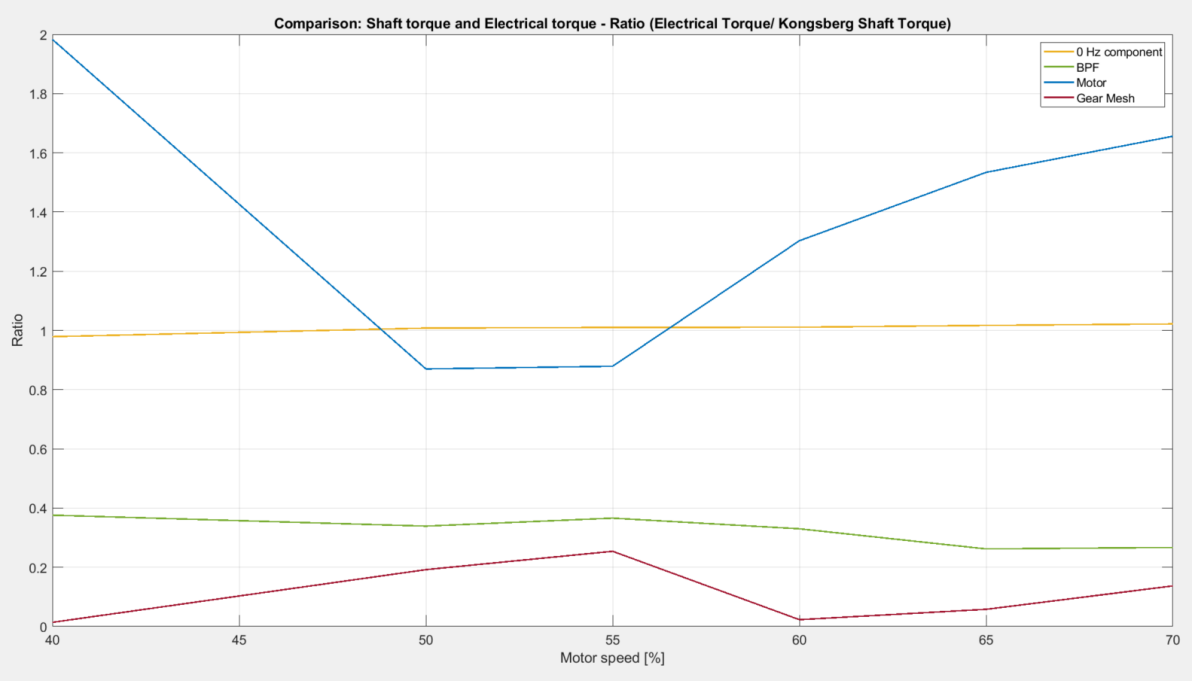

Figure 5.8: Ratio between electrical torque and shaft torque measurement for different mechanical frequencies

6 Discussion

In this Chapter, the results presented in Chapter 4 are further discussed in order to answer the research questions. Firstly, the different electrically deduced parameters and their spectra of the IM are compared. Then, the identification of the mechanical behaviour itself is further examined, after which the potential of fault detection and damage assessment is discussed. Hereafter, all the different methods of measurement presented in this paper are compared for the last time. Finally, in order to answer the main research question of this thesis, an approach for the successful implementation of ESA for the CM of the thrusters of the Pioneering Spirit is suggested.

6.1. Comparison of electrical spectra

Notes on the methods of comparison

First of all, it should again be stated that the comparison between the different electrical spectra in this research is only of a qualitative nature. As explained in Chapter 4, the spectra were plotted in such a way to make the mechanical behaviour easily visually identifiable. This means all statements regarding the comparison between the individual spectra are based on this. In the end, there were multiple spectra identified that were able to clearly highlight the mechanical behaviour. Researching which of the parameters quantifiably created the best spectrum for identifying mechanical behaviour did not have the highest priority. However, for future research this could be attempted. Some examples of methods to make the differences in the spectra quantifiable are by calculating the signal to noise ratio of the peaks at mechanical frequencies, or by calculating the relative amplitude of a mechanical vibration with respect to their baseline value (0 Hz-component).

Moreover, in some spectra two different parameter are plotted in the same figure, such as current and voltage in Figure F.4. It should be noted that the baseline values, noise floor and measured unit of these parameters are not the same. Therefore, these spectra are only meant to show the differences or similarities in the presence of vibrations or oscillations at specific frequencies, but not to 1:1 compare the amplitudes of the two parameters.

Qualitative comparison of electrical spectra

First of all, the single phase spectra for both voltage and current seem to be better suited to identify the electrical behaviour of the machine. This is because the electrical frequencies, such as the drive, switching and ship AC frequency, can be easily identified in their original frequency. The opposite is true for mechanical frequencies, as these will all show up modulated on the drive frequency, making them harder to identify.

The spectrum of $|i_c|$, created using the EPVA method, is the first method in which the mechanical behaviour of the machine becomes easily visible, as all mechanical frequencies modulated on the drive frequency now appear in their own frequency. When comparing the spectra of $|i_c|$ and $|u_c|$, it becomes apparent that the mechanical behaviour is better identifiable in the $|i_c|$ spectrum, as the mechanical frequencies are all relatively low (< 200 Hz) and the voltage spectrum is more susceptible to higher frequencies. This becomes visible when analysing the switching frequency and higher harmonics of the drive frequency, which are all much better represented in the voltage than in the current.

Continuing, the spectra containing most information of the different sensors are the torque and power spectrum. Normally, the torque spectrum would be expected to give the best mechanical impression of a machine, as it represent the torsional vibration, but in this case the power and torque

spectrum qualitatively show much similarities. A reason for this could simply be the fact that both parameters originate from the same 6 sensors. The only difference is an integration step for transforming the voltage into flux, as shown in Equation 3.17, after which the torque is calculated using the current and flux. In other words, any mechanical vibrations will likely show in both the torque and power spectra.

Finally, when comparing $|i_c|$ and the electrically deduced torque of the machine, the $|i_c|$ spectrum can be regarded as the spectrum showing radial vibrations of the motor shaft, while the torque spectrum shows torsional vibrations. This is because the mechanical vibrations showing in the $|i_c|$ spectrum are caused by variations of the air gap, which indicates a relative movement between the rotor and stator. On the other hand, the torque spectrum will contain variations in motor torque and thus in torsion of the motor shaft. However, these two parameters will show much more similarity then the (radial) mechanical vibration measurements of the motor and the mechanical torque measurements of the motor shaft. This is only logical, as both the $|i_c|$ and electrically deduced torque still originate from the same electrical measurements.

6.2. Identifying mechanical behaviour with ESA

Normal mechanical vibrations

The primary mechanical characteristic frequencies that become apparent in any of the thruster assemblies are the motor shaft frequency and the BPF. The presence of vibrations in these frequencies is considered normal machine behaviour, since any slight asymmetry or unbalance in the motor shaft will cause a vibration in this frequency, which is inevitable. The vibrations at the BPF are caused by a hydrodynamic effect occurring each time a propeller blade passes by the base of the propeller. In other words, the spinning of the propeller through a uniform and unstationary wake creates load variations that excite the torsional vibrations in the BPF [30]. This BPF torque fluctuation is especially visible in the 70% motor speed MetaPower torque measurement, in which the peak to peak amplitude of this torque variation is 5.62 kNm, equal to 12 % of the base torque at this time.

Continuing, the propeller shaft frequency is hard to identify in both the electrical and mechanical spectra. The second and third harmonics of the propeller shaft frequency can in some cases be seen. In the shaft torque spectra, multiple harmonics and sidebands of the propeller shaft frequency can be spotted as well. However, some of these vibrations can also be subharmonics of the BPF or sidebands of the propeller shaft frequency on the BPF. There are multiple possible explanations for this. Firstly, the propeller shaft is located far away from the electrical and mechanical vibrations measurements. Vibration due unbalance, for example, might be dampened too much by the system before reaching the sensors. Or, these lateral vibrations in the propeller shaft might not be able to properly transfer to the motor shaft in the gearbox. Also, the frequency of these vibrations would be so low that sidebands on the drive frequency might be drowned in electrical noise. Finally, the low frequency of the propeller shaft might also mean that any vibrations due to unbalance are just too weak to detect in the electrical measurements or the velocity spectrum.

The final identifiable mechanical frequency that was encountered in the thrusters and that doesn't necessarily indicate faulty machine behaviour, is the gear mesh frequency. As explained in Chapter 3, this frequency indicates the meshing of the teeth of the pinion gear and crown wheel. The discrete meshing of all individual teeth is responsible for the transfer of torque between the propeller shaft and the motor shaft. Therefore, an oscillation in this frequency will always be present in the system, which is especially visible in the MetaPower shaft torque measurements.

Lastly, the motor shaft frequency an BPF were detectable all the way down to 40% motor speed. These frequencies might even be detectable at lower speeds, but this was not tested. The gear mesh frequency and propeller shaft frequencies start to drown more in electrical noise in these low speed ranges, making them more difficult to detect.

Bearing related mechanical vibrations

The last type of mechanical frequency encountered in the thruster assemblies are bearing related frequencies. The presence of these frequencies in the electrical spectra is considered faulty machine behaviour, as these must be caused by a relative movement (in any but the rotational motion of the machine) between the stator and rotor, which should never occur in the case of a healthy and smooth machine bearing. These lateral vibrations for the NDS bearing in T6 can clearly be detected. Also, for T1 some bearing vibrations might have been detected. In both these cases, the specific bearing presumed to cause these vibrations was the NDS IM bearing.

In T3, which supposedly contained early stage bearing wear for input shaft double spherical bearing of the thruster, no bearing vibrations were found in the ESA measurements. However, upon further analysing the mechanical vibration measurements, the conclusion was made that there was likely no wear in this bearing. Therefore, none of the three thrusters that were measured were showing any signs of wear in the bearings located inside the thruster. This means that it can't be validated that ESA would or would not be able to detect bearing related vibrations originating from outside the IM for this use case. As explained in Chapter 2, ESA tends to be less accurate for large assemblies, as the mechanical vibrations occurring far away from the IM can be dampened throughout the load path. On top of that, these thruster assemblies have a flexible Vulkan coupling (Figure B.4)in the motor shaft, which might also have a high dampening effect on bearing related vibrations originating down the shaft. Still, this does not validate that ESA would entirely be unable to detect these vibrations.

Furthermore, as stated in Chapter 4, the NDS BPFI related oscillation that was found in almost all spectra of T6 did not exactly occur in the predicted frequency. This offset could not be explained by the accuracy of the deduced motor shaft frequency, as explained in Appendix D, and the resolution of the spectrum. However, the predictions of these bearing frequencies is based on an order of the shaft speed that is calculated using only the geometry of the bearing, which is explained in Chapter 3, but is effectively obtained in the bearing specifications provided by the manufacturer. Therefore, any deviation in the geometry of the bearing, for example due to differences in temperature or tolerance, can be the cause of this offset. Ultimately, the order of the NDS BPFI measured during the ramp-up tests was determined to be 7.579 instead of 7.570, as predicted by the manufacturer. This was further demonstrated in the variable speed spectra in Figure 4.11, in which the order of the NDS BPFI remained the same for different speeds.

Finally, the ESA spectra of the low speed ranges showed that the bearing frequencies in T6 were easily detectable down to 50% motor speed. Some of these bearing frequencies still showed at 40% motor speed, but most bearing frequencies started to drown in electrical noise at this point.

Sidebands on mechanical frequencies

Some mechanical frequencies encountered in the thrusters have sideband frequencies of the motor shaft frequency modulated on them. The best example of this is the NDS BPFI frequency found in T6, which has sidebands of multiple motor shaft frequency harmonics, as can be seen in all demodulated spectra of T6. The reason for this is the fact that the thruster has a loaded zone, i.e. there is an area in the circumference of the stator in which the reaction force on the rotor is highest. Therefore, a defect that is stationary with respect to the rotor, such as an inner race defect of the NDS bearing, will experience a variation in load of exactly the motor shaft frequency. This causes an amplitude modulation of the motor shaft frequency on the NDS BPFI. This same phenomenon would not occur with a defect on the outer race of this thruster setup, since the outer race is stationary with respect to the stator. Therefore, this type of defect would not experience a load variation caused by spinning in and out of the loaded zone [17].

The same modulation effect occurs at the gear mesh frequency, which can be clearly seen in the mechanical shaft torque measurements in Figure 5.6. By its definition, the gear mesh frequency will coincide with a harmonic of the motor shaft frequency. For the thrusters of the PS this is the 13th harmonic, since the pinion gear on the motor shaft has 13 teeth. Consequently, this means that sideband frequencies of the motor shaft frequency on the gear mesh frequency will coincide with the $13 \pm n$

harmonics of the motor shaft frequency. The spectrum shows that the motor shaft frequency harmonics around the gear mesh frequency have a much higher amplitude than the harmonics further away from the gear mesh frequency. Therefore, it is likely that the vibrations in these frequencies are mostly caused by sideband effects of the gear mesh frequency than by harmonics of the motor shaft frequency.

Amplitude of vibrations

When analysing the ESA spectra of variable speed measurements in Figure 4.10 and Figure 4.13, as well as the shaft torque spectrum of both 40% and 70% motor speed in Figure F.20, some relations concerning the amplitude of the mechanical vibrations at different speeds can be found. First of all, the amplitude of the mechanical vibrations seems to mostly increase for an increasing motor speed and torque, as is shown in Figure 4.10 and Figure F.20. However, the comparison of the torque spectra at 70% motor speed but at varying baseline torques in Figure 4.13 shows that the amplitude of vibrations is not necessarily higher for a higher baseline torque, but a similar motor speed.

Continuing, it can be clearly seen in Figure F.20 that the previously stated relation of 'an increasing vibration amplitude for an increasing motor speed' does not always hold true. Since, in this figure, the BPF and motor shaft frequency show higher vibration amplitudes at lower speeds. One explanation for this is that this effect is caused by the presence of a resonance frequency somewhere in this range, which is further highlighted in Figure F.19. It is likely that any mechanical vibration in these frequency ranges will experience an increased amplitude due to the resonance behaviour. However, another explanation for this heightened vibration amplitude at the BPF at lower frequencies could be the effect of non-linear hydrodynamic drag, in which the hydrodynamic drag increases in a transition region from laminar to turbulent flow. In order to further reach a conclusion regarding this, a more detailed analysis of the flow of the propeller blades could be performed. Also, it should be noted that when analysing an ESA spectrum for the presence of mechanical vibrations, in some cases the strong oscillations in a suspected mechanical frequency might be caused by the presence of an electrical oscillation in the same frequency. This can clearly be seen in Figure 4.11, in which the '2x NDS BPFI + Motor' frequency coincides with the 4th harmonic of the drive frequency.

Regardless of the actual cause of these stronger vibrations, this means that the amplitude of a mechanical vibration can not be solely predicted by the torque and motor speed. This in turn means that comparing the mechanical vibration behaviour of a specific machine should always be done at the same speed to account for the effect of resonance on the individual vibration frequencies. Furthermore, as the resonance behaviour or the presence of a vibration in some particular frequency might even originate from a different piece of equipment in the vicinity of the machine, it should even remain in the same environment for a 1:1 comparison.

A final note on the identification of machine behaviour in the ESA spectra is the influence of the VFD. If the (torsional) vibrations in the machine become large enough, the controller of the VFD will likely actively counter them in order to try and prevent any torque ripple in the machine and maintain a constant torque and speed. It might be the case that this behaviour of the VFD can be detected in the measurements, for example by comparing the relative amplitudes of the current and voltage oscillations in the cases that the VFD does or does not try to counter a torque vibration. Another method this influence of the VFD might be tested, is by measuring the phase difference for the oscillations in current and voltage. Since, when the VFD measures a ripple in the current and acts on it by adjusting the voltage, there could in theory be a phase difference between the current and voltage oscillation of the same frequency. However, these analysis steps were not performed in this research and therefore no conclusive statements regarding their use or outcome can be made. The statements should merely be interpreted as an hypothesis that could be tested in future research.

6.3. Fault detection and damage assessment for ESA

When the mechanical behaviour of a machine can be detected, a next step is to make a diagnosis of the machine health based on the detected mechanical behaviour. This is done by detecting any failures that might occur, followed by assessing the damage based on the measurements. In other words: This section tries to describe how to get from a Fourier analysis (spectrum) to a health assessment and maintenance action and thus to answer the subquestion: *.How can the detection of these mechanically induced vibrations be used for mechanical fault detection and a machine health assessment'.* The important steps for doing this are explained below.

Fault detection for bearing failures

Bearing fault detection through ESA consists of multiple steps in order to ensure the validity of the diagnosis. As explained before, the presence of mechanical vibrations in the characteristic bearing frequencies means that the specific bearing is damaged. Since, a healthy bearing will create no noticeable vibrations. However, the spectra originating from the electrical measurements will be full of electrical noise, so when a demodulated spectrum is analysed and oscillations in these bearing frequencies are detected, it must first be validated that these vibrations are indeed of a mechanical nature. When measurements at multiple motor speeds are available, the spectra can be normalized by the shaft speed to ensure that the vibration frequency of interest is of the same order for all motor speeds. When this is the case, the oscillation is likely to be of a mechanical nature, as almost all mechanical vibrations created by the machine itself will scale with the motor shaft speed. A second validation is to analyse the single phase spectra of the machine and manually search for the individual sideband frequencies of the bearings modulated on the motor shaft. When these can be found it, can be checked whether these sideband frequencies are not in fact oscillations of other frequencies modulated on a different electrical frequency. Since, the appearance of the bearing frequency in a demodulated spectrum could also actually be an entirely different (electrical) frequency that has shifted into the region of a mechanical frequency of interest due to demodulation effects.

Fault detection for other mechanical failures

Fault detection for non-bearing failures works slightly different. Since, the other mechanical frequencies, as discussed in Chapter 3, are easily detectable in the ESA spectra, even for healthy machines. This is visible in all ESA spectra in Chapter 4. Therefore, when mechanical failures related to these frequencies must be detected, such as a loose coupling or a broken tooth, the only way of doing this is by monitoring the vibrations in the machine over a longer period of time. In that case, a threshold can be created for what strength of vibrations in all frequencies is deemed healthy behaviour or the strength of vibrations can be plotted over time to analyse a possible increasing trend. This analysis must be performed at the same motor speed, as the amplitude of vibrations does not scale linearly with the motor speed, which was explained in Section 6.2. Also, as explained in the literature review in Appendix H, a promising way of approaching this is by training some sort of ML algorithm to learn the healthy behaviour of a machine over time to be able to detect deviant or unhealthy behaviour when it would occur.

When an increase of vibrations over time is then detected, for example in the motor shaft frequency, this could indicate a loose coupling or unbalance. Or, when the gear mesh frequency and its sidebands start to increase, this could indicate a broken gear tooth. Furthermore, it should be stressed that amplitude of vibrations in two machines of the same type shouldn't be directly compared, since they can have vibrations of different amplitudes that is considered normal. This can be seen from the fact that many frequencies, such as the motor shaft frequency, have different amplitudes in all spectra for T1, T3 and T6 at the same speed, but there is no damage related to this.

Damage assessment

The hardest step in diagnostics for ESA measurements will be the mechanical damage assessment. For comparison, damage severity assessment in vibration analysis is mostly performed by the use of ISO standards. There are many standards available describing the entire process and diagnostics of vibration analysis for specific types of machines, such as ISO 13373 [17]. For example, in the case of an

inner race bearing fault this standard divides the faults in 5 severity classes based on the appearance of certain vibrations in different kinds of measurements. Also, in ISO 20816 [31] the allowable amplitudes of vibrations in specific types of machines are categorized bases on their size, power, speed and even more parameters. This can also be used to assess the severity of faults in a machine.

In contrast, there are multiple reasons why severity assessment is currently more complex in ESA. First of all, ESA is not common practice for the analysis of mechanical vibrations in a machine, so these same standards do not exist for ESA. Secondly, there is no straightforward relation between the strength of a mechanical vibration and the measured electrical oscillation that it causes, as this depends on many factors: There are essentially three systems through which a mechanical vibration needs to travel before being detected in ESA. Firstly, a mechanical variation in the form of a velocity or acceleration needs to travel through the mechanical system of the thruster, consisting of all mechanical components, their inertia and dampening ratios. Consequently, it becomes a variation in magnetic flux, which is then transformed into a variation in current or voltage. In other words, there is no general or simple relation between the original variation in velocity [mm/s] or acceleration [m/s2] originating from somewhere in the machine into a detectable variation in voltage [V] or current [A]. Therefore, for any mechanical vibration originating from a different position in the machine or for any different machine in general, there will be a unique response in the current or voltage.

However, this does not mean that severity assessment in ESA is entirely impossible. In some cases the same, standards as used for vibration analysis can offer some help. For example, the appearance of the motor speed sidebands on the BPFI peak in T6 suggests that a bearing fault is considered to be of stage 2 (medium bearing degradation) in ISO 13373. These same sidebands appear in the ESA spectra as well, so they might offer a similar classification. Furthermore, the vibration analysis standards were for a large part created empirically, i.e. out of practice and experience. If ESA would become a widely adopted strategy for mechanical fault diagnostics, a start could be made in creating similar standards, even though transducing of vibrations in ESA is more complex. To be able to set this up, large amounts of information are required, such as: labeled data on measured electrical oscillations on corresponding mechanical damage, electrical and mechanical information on the specific assemblies and operational parameters at the time of the measurements. Or, a same type of standard could be set up without the use of labeled data containing the severity of actual mechanical damage, but by using vibration analysis in parallel with ESA, as the same classification for vibration analysis already exists.

6.4. Final comparison with vibration analysis

Some final remarks can be made on the comparison between the use of ESA and mechanical vibration analysis. As also stated in the conclusions of the literature review in Chapter 2, both methods serve their own purpose and one cannot replace the other. First of all, ESA might be able to make multiple accelerometers obsolete, as it can cover the detection of the same mechanical vibrations as for which multiple acceloremeters in the IM are now used. However, a more complete image of the state of the machine can be gathered by simply implementing more vibration sensors throughout the machine, including at locations of which the vibrations might not be detectable by ESA. Also, the damage severity assessment is more straightforward in vibration analysis, partially due to the large amount of empirical data available. However, ESA still offers an unintrusive monitoring technique that is sensitive enough to identify changes in mechanical machine behaviour and might be used in places unsuitable for accelerometers.

When comparing the sensitivity of the two methods, it can be stated that the bearing damage in T6 was more easily detected at lower speeds through the mechanical vibration measurements than through the ESA measurements. However, at higher speeds these vibrations were easily detectable through both methods. Also, when only considering the higher speeds, another opportunity has now presented itself to compare the sensitivity of the current CM campaign based on mechanical vibration measurements and ESA. Since, the NDS BPFO vibrations in T1 can be more clearly detected in the ESA spectra than in the mechanical vibration measurements. This means that if a visual inspection of this bearing would be performed, the state of the bearing could be validated. Depending on the

outcome of this inspection, it could prove that ESA was more sensitive to the fault detection in this case.

Finally, in the case of the thrusters of the PS, the ESA method currently cannot fully replace the VA provided by Pruftechnik NV This is because it has not yet been proven that ESA can detect all the same failures as VA, at all different locations throughout the machine and correctly assess their severity. However, the implementation of ESA can serve as a reliable extra CM method that can learn the normal mechanical vibration behaviour of each machine over time and send an alarm once the mechanical vibrations in the ESA spectra start showing aberrant behaviour. This is either by detecting heightened amplitudes of normal vibrations, or detecting the presence of bearing frequencies. At that point, a further analysis (for example by VA) can be performed to identify the true damage. This would be of added value, as it would be a continuous and self-controlled type of monitoring. In contrast, the mechanical VA of Pruftechnik NV collects only a few samples per week and has proven to not be fully reliable in the past.

6.5. Final comparison with Kongsberg MetaPower

When analysing the measurements of the mechanical shaft torque and the electrically deduced torque, it becomes evident that the shaft torque measurement is much more sensitive for the detection of most torsional vibrations. A possible explanation could be the fact that some of these vibrations originate closer to the Kongsberg MetaPower system than to the IM. For example, the only mechanical vibration that appears in a similar magnitude in the electrical measurements is the vibration at the motor shaft frequency. This is also the only measured mechanical vibration that can originate from inside the IM. The torsional vibrations originating from the gearbox or propeller could be substantially dampened before being detected in the IM at the other end of the assembly. This dampening effect could be increased by the flexible Vulkan coupling mounted in the assembly (Figure C.2).

However, there seems to be a close relation between the measured baseline torque for both the electrical torque and the shaft torque. In cases where the baseline torque is considered the most important information in these measurements, it might be possible to replace the expensive MetaPower device by current and voltage sensors, depending on the needed accuracy of the measurements. An example for which this application might work is determining the Remaining Useful Life (RUL) of certain components in the drive shaft by continuously monitoring its remaining fatigue life. For these kind of calculations, only a baseline torque needs to be measured continuously for all running hours of a machine [13].

6.6. Implementation approach of ESA for thruster assemblies

The previous sections of this chapter have discussed the results of all performed ESA tests in detail, as well as some nuances in the process of mechanical fault diagnostics through ESA. Furthermore, the advantages, disadvantages and current limitations of ESA have been highlighted. Finally, a comparison between the used ESA method and mechanical vibration and torque measurements was made. Using all this knowledge, a final answer to the main question, *'How can Electrical Signature Analysis successfully be implemented as a Condition Monitoring technique for mechanical failures in induction motor driven thruster assemblies in the maritime industry?'*, can be presented. Therefore, in this section a step-by-step implementation approach for ESA on the thruster assemblies of the Pioneering Spirit is suggested. This approach is summarized in the overview shown in Figure 6.1.

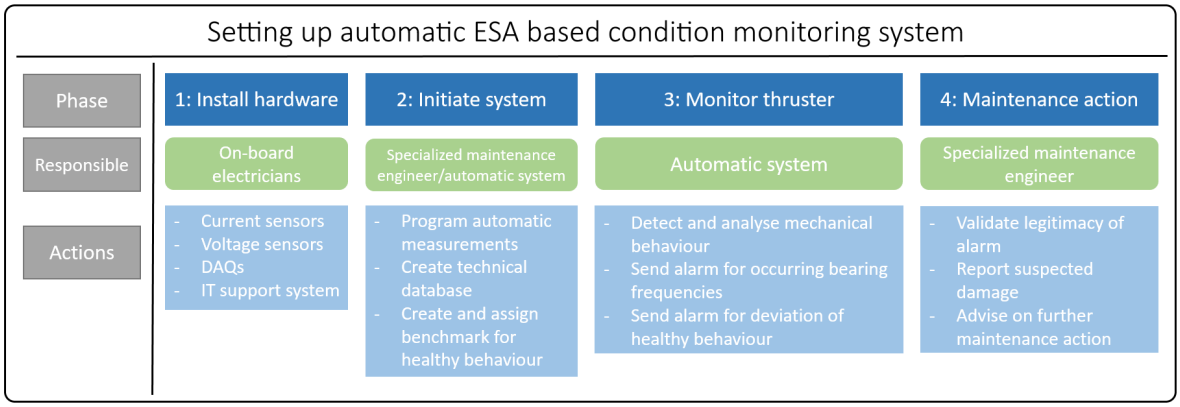

Figure 6.1: Proposed implementation of an ESA based condition monitoring method

Setting up measuring devices

The first step in setting up a CM campaign for the thrusters by ESA is to install all necessary measuring devices. The devices used in this research have proven to be suitable for the purpose of ESA. So, a first option of an ESA setup for all thrusters of the PS is to implement the same current and voltage sensors inside the VFD of each thruster, along with their own power supplies and DAQs. This would require an investment of roughly €35000 per thruster. However, since the thrusters are grouped together (Figure B.1), it could also be a possibility to use bigger DAQs for groups of thrusters, instead of for individual thrusters. For example, one DAQ per three thrusters: One DAQ would be placed in both bows of the ship and two would be placed in the aft. This DAQ would need at least 18 inputs (3 voltage and 3 current per thruster). An advantage of such a system would be that it requires less work to maintain and set up than 12 individual DAQs. However, the cable lengths for all sensors would be significantly longer in this case. So, it should be tested whether this influences the results in terms of added noise or decreased signal strength.

Furthermore, some modern types of VFD have built-in functions to export accurate measurements of the phase currents and voltages of the system. Since, this type of information is also needed by the VFD itself for controlling the IM. At this point, the VFDs of the PS can't provide these measurements at a sufficient sample rate. However, there is a chance that future updates of the current VFDs on board the PS might enable the continuous export of current and voltage measurements of sufficient quality for the purpose of ESA. If this would be the case, this would mean that almost no extra hardware would be necessary in order to set up a CM campaign using ESA, reducing the cost of such a campaign.

Setting up IT system

When running an ESA based CM campaign, a large amount of data will be gathered daily for each thruster. This information needs to be stored on hard-drives or servers readily available for the responsible engineers. In other words, there needs to be an IT system controlling the measuring devices and storing their information. As such an IT system was not included in the scope of this research, no specific advice regarding such a system can be presented. Nevertheless, it should be noted that an IT system capable of transmitting the machine data from ship to shore would have a preference. Since, in that case an engineer on shore could have oversight of the possible ESA systems aboard different ships simultaneously. Currently, this would likely not be a viable option, as the transmitting of large amounts of data between ship and shore through an internet connection is a slow and unreliable process when at sea [32]. This means that a local system with a responsible engineer on board would the only other choice. However, Allseas Engineering BV is currently running tests for a ship to shore internet connection through the recently developed Starlink satellite system [33]. These early tests have shown an increase of over 10 times in data transfer capacity. So, if this system would be enabled for all vessels in the future, an overseeing engineer on-shore would be a possibility.

Programming measurements

When all hardware is in place, the ESA measurements can be started. For an accurate analysis, a relatively long measurement is needed at a constant and high motor speed. When looking at the different modes of operation of the thrusters of the PS in Appendix B, it becomes clear that the only time these measurements can be taken is during a sailing interval. Also, the measurements of a single thruster can only be compared at the same motor speed. This means that the ideal approach for collecting measurements would be to let the motors run at one or more specific motor speeds for a certain amount of time at each sailing interval, for example exactly 70% or 80% of the maximum speed. The ESA systems can then be programmed to detect the specific constant motor speed and start their measurements.

However, the motor speeds of the vessel during a sailing interval are determined by the desired vessel speed, the water current and the wind speed. Therefore, even for a same vessel speed the motor speeds might be different for two different sailing intervals. Therefore, either the vessel must be controlled to sail at completely similar motor speeds for brief times during sailing intervals, or the ESA systems must be programmed to start measuring when a constant motor speed is detected in a small range of possible motor speeds, for example any constant motor speed between 75% and 80% of the maximum speed. The second option would require no different sailing strategy for the mates responsible for the sailing of the ship, but it would likely also complicate the machine diagnostics through ESA.

Also, most mechanical frequencies were detectable at motor speeds as low as 50% of the maximum speed. The ship does not need to sail to reach these speeds. Instead, it can be controlled to reach these speeds while on DP. This enables the possibility to also collect data while the vessel is on DP, which is the most common operational mode of the vessel. However, it should be noted that these tests would cause a larger fuel consumption, as the motor speeds while on DP are commonly lower than this (between 20% and 40%).

Monitoring system design and initiation

In order to run a continuous CM campaign based on ESA, a tool for automatically detecting machine failures can be used in order to save man-hours in manually analysing data. Such a tool will consist of an automatic 'system' in terms of an application or software that can automatically alert a responsible engineer when machine failures occur. The automatic capturing of data as discussed in the previous sections can be seen as the first part of such a system. The conceptual approach for designing the second part of such a system, capable of the automatic monitoring of the mechanical behaviour of the thrusters, is discussed in the following paragraphs and the next section.

Firstly, an extensive amount of technical information of the thrusters is required. This information includes the mechanical and electrical frequencies of interest for the thruster assemblies, as was presented in Chapter 3. As most of this information was already used for the purpose of this thesis, it is

readily available in the form of the Excel sheets that are presented in Appendix D. However, there are more frequencies of interest that can be added to this in order to create a more extensive database for both mechanical and electrical fault diagnostics. Two examples of this are the oil whirl frequency or rotor bar frequency.

Secondly, a benchmark for healthy vibration for all individual thrusters needs to be created. Therefore, the ESA campaign has a 'warm-up' period in which machine data for all thrusters is collected, but no fault detection based on increasing vibration trends is possible. Instead, the system builds a database of vibration behaviour in mechanical frequencies per thruster that is considered healthy. However, fault diagnostics based on the detection of bearing frequencies will be possible in this period, as the presence of these frequencies will always indicate a failure.

Monitor thrusters

When a database of healthy machine vibrations per thruster is created, the CM campaign can start. There are multiple possible methods for monitoring of the mechanical behaviour of the thrusters through ESA, but a general approach should include the following steps:

- A new measurement at a certain constant speed is captured.
- The 3 voltage and 3 current measurements per thruster can be transformed to either the EPVA current spectrum or the torque spectrum.
- The ESA system automatically identifies the relevant mechanical frequencies and logs their amplitudes. This identification works as presented in Appendix D: The exact motor shaft frequency is deduced from the spectrum by firstly identifying the drive frequency and then finding the peak that occurs roughly at $f_{drive}/4$. From the motor shaft frequency all other mechanical frequencies can be calculated and detected.
- The amplitudes of these mechanical frequencies are then stored over time at the same speed for the same thruster.
- If a mechanical frequency related to a bearing starts to show in the spectra, the system should automatically alarm a responsible engineer.
- If an increasing trend or a sudden increase in one of the common mechanical frequencies starts to show, the system should recognise this as well automatically alarm a responsible engineer.

There are many different data processing tools that can be used to look for these increasing trends or sudden increases. Some examples of this could be simply creating a threshold around the mean of an amplitude of certain mechanical vibration over time. If this threshold is crossed, the system could send an alarm. Also, a system can be designed to approximate a (linear) coefficient with which a certain vibration increases in amplitude over time. If the actual amplitude of a certain frequency is then much higher than the approximation, the system could send an alarm. One method to do this would be through a linear regression model based on supervised learning. In general, many more ML based models might be implemented for this monitoring purpose. More specific information on these methods can be found in the literature review in Appendix H.

A final, slightly different ML based method that might help to monitor the mechanical behaviour is to use certain parameters out of the measurements as inputs for a ML model, such as a neural network, which can give a health indication as output. These inputs can be the amplitudes at certain mechanical frequencies, the trends or mean of these amplitudes over time, the raw current and voltage data, the correlation between current voltage and many more standard features.

All in all, the implementation of these methods were not part of the scope of this research. This means a conclusion regarding what types of data processing tools will give the best results cannot be presented, but might be interesting for future research.

Fault alarms and corrective actions

As explained in the previous step, the proposed way of monitoring the thrusters is by designing an automatic system that can send alarms to a responsible engineer when it detects a fault or another kind of deviant behaviour. In that case, the first action should be to have the responsible engineer manually look at the data in order to judge whether there actually might be something wrong with the machine, or the alarm was false. This is because the interpretation of the mechanical behaviour of a machine over time can only be done by an experienced engineer.

Depending on the results of the analysis and suspected damage, there are multiple actions the engineer can initiate. For example, the choice can be made to monitor a certain thruster or component more closely for a period of time, a component can be replaced or a visual inspection can be executed. However, it is also possible to perform a more thorough mechanical vibration analysis to the component with suspected damage. Since, once damage is suspected, an easier assessment of the damage severity can be obtained by mechanical vibration analysis.

7 Conclusion

In light of answering the research questions introduced in Chapter 1.1, a multitude of conclusions can be made. These conclusions are categorized by which subquestion they present an answer to, with the exception of Conclusion A, which serves as a validation of the ESA method for this specific case. Also, the results of the performed diagnostics for T1, T3 and T6 from the paper in Appendix A are included. Finally, an answer to the main question is presented:

Validation

A - Electrical Signature Analysis can successfully be implemented for Condition Monitoring of a marine vessel's thruster assemblies, as it is sensitive enough to detect differences in mechanical vibrations from which the health of a machine can be deduced.

Subquestions

'Which mechanically induced vibrations can be detected in the induction motor current and voltage measurements?'

B - Bearing related frequencies originating from inside the IM can be detected by ESA. There was no proof of bearing related frequencies originating from down in the thruster for any of the thrusters. So, it cannot be concluded whether the vibrations of these bearings could also be detected or not.

C - Torsional vibrations can be detected by ESA, even if they originate from deep down in the thruster. This can be seen in the detection of the BPF and the gear mesh frequency.

D - In the case of the thruster assemblies of the Pioneering Spirit, all healthy mechanical frequencies or their harmonics were detectable. This includes: the motor shaft frequency, propeller shaft frequency, blade pass frequency and gear mesh frequency. Also, the characteristic bearing frequencies were detectable for worn bearings inside the IM.

'How can these mechanically induced vibrations be most effectively detected in the induction motor current and voltage measurements?'

E - Qualitatively, the mechanical behaviour of a machine is most easily visually distinguishable in the demodulated current, torque and active power spectra. The demodulated voltage spectrum is less sensitive in the low frequency ranges in which the mechanical vibrations occur.

F - In case measurements at multiple motor speeds are taken, the mechanical behaviour of a machine can be detected by normalizing the frequency axis of the different measurements by the shaft speeds and checking for the presence of vibrations solely dependent on the shaft speed.

G - The single phase spectra are less suited for visually distinguishing mechanical behaviour, but can be an important validation once mechanical vibrations are found in the demodulated spectra.

H - The mechanical behaviour of the machine is most easily detected in measurements at a high motor speed and torque. However, some mechanical frequencies are detectable at speeds as low as 40% of the maximum speed.

'How can the detection of these mechanically induced vibrations be used for mechanical fault detection and a machine health assessment?'

I - Mechanical fault detection through ESA can be performed either by the detection of a mechanical frequency that should not be present in a healthy machine, such as bearing frequencies, or by analysing the trend of normally occurring mechanical vibrations.

J - For mechanical fault severity assessment through ESA, in some cases, for example in bearing health assessment, a start can be made by analysing ISO standards for vibration analysis. However, in general more empirical failure data on fault detection labeled with the actual damage is needed to accurately assess the damage through ESA measurements.

K - The mechanical behaviour of a machine can only be compared for a single specific machine. Since, two machines of the same type in the same conditions might still show different mechanical vibration characteristics due to tiny differences in the assembly or environment.

L - The mechanical behaviour or a machine can only be compared in similar speed and torque settings. Since, for most mechanical vibrations no straightforward linear relation between the strength of a mechanical vibration and the motor speed and torque exist.

'How does this method compare to Condition Monitoring based on mechanical vibration measurements?'

M - Both ESA and mechanical VA have their strengths and weaknesses. These are listed in Table 7.1. All in all, at this point it is not possible to entirely replace vibration analysis for the thrusters of the Pioneering Spirit, but it could serve as a reliable added CM method for the thrusters.

Electrical Signature Analysis	Mechanical Vibration Analysis
Less intrusive	Easier severity assessment
Less sensors needed for same information	Ability to use more sensors enables analysis
Also enables electrical diagnosis	of larger machines

Table 7.1: Comparison of ESA and vibration analysis

N - It is hard to compare the sensitivity of ESA and vibrations analysis for the detected faults in this case. However, upon visually inspecting the NDS bearing of T1 and validating its health it can either be concluded that ESA was more sensitive to the fault in this case, or that vibration analysis was more reliable method in this case. But, the bearing related vibrations in T6 seemed to be more easily detectable in the velocity spectra than in the ESA spectra at the lowest measured motor speed (40%).

O - The electrically measured baseline torque has consistently shown an accuracy between 0 and 2.5 % compared to the baseline shaft torque measured at speeds of 40% to 70% of the maximum motor speed. However, the electrically measured amplitudes of the torque vibrations at the motor shaft frequency, BPF and gear mesh frequency are not comparable with the measured shaft torque vibrations at the same frequencies.

Performed machine diagnostics of T1, T3 and T6

T1 - Thruster 1 shows some aberrant behaviour in the form of oscillations present in the first four harmonics of the NDS BPFO. This is unusual, as there is no prior knowledge available on a worn NDS bearing in thruster 1 and the detection of any bearing frequency would imply damage. Furthermore, the performed mechanical vibration measurements, using both the vibration scanner and shaft torque measuring device, show some vibration in these frequencies, but not as strong as in the ESA measurements. All in all, a further investigation into the health of this bearing is advised, such as a visual

inspection.

T3 - Thruster 3 shows no sign of any mechanical wear in the performed ESA measurements. Also, the historical velocity spectra of the sensors throughout the thruster showed little reason to believe that there currently is (premature) damage in the machine. Therefore, no further maintenance action is required.

T6 - Thruster 6 clearly shows aberrant vibrations in the NDS BPFI frequency (as well as its harmonics) with motor shaft frequency sidebands. This is validated in the mechanical vibration analysis, in which these same vibrations are strongly present. The pattern categorises stage 2 bearing wear (medium wear), indicating the presence of spalling or cavitations in the inner race. As this type of failure will get progresively worse, immediate visual inspection or replacement of the bearing is advised.

Main question

'How can Electrical Signature Analysis successfully be implemented as a Condition Monitoring technique for mechanical failures in induction motor driven thruster assemblies in the maritime industry?'

The case presented in this thesis suggests that ESA can be successfully implemented for CM of mechanical failures by measuring all three phase current and voltages of an IM at different, constant speeds. From these measurements the demodulated current, power and torque will provide the best spectra for visually distinguishing the mechanical behaviour. This mechanical behaviour can be validated by examining the single phase current and voltage spectra before demodulation or by normalizing the spectra by the shaft speeds for different speed measurements. Fault detection is then performed either by analysing the trend of normally occurring mechanical vibrations, or by the appearance of vibrations that directly indicate a failure, such as bearing failures. In some cases, such as bearing faults, the health assessment shows some similarity with ISO standards for vibration analysis. However, in order to reliably assess the severity of multiple types of failures in mechanical assemblies through ESA, more failure data labeled with actual damage should be obtained. Finally, a more detailed step-by-step approach for an implementation of ESA in the PS is presented in Section 6.6.

8 Recommendations

Considering the discussion and conclusions in Chapter 6 and Chapter 7, multiple recommendations can be made. Firstly, the recommendations for Allseas Engineering BV are presented. Secondly, some recommendations are made for future scientific research regarding the presented methods.

Allseas Engineering BV

A - The damage in thruster 6 is reaching levels of severity that can no longer be ignored. A visual inspection or replacement is advised at the first possibility.

B - There is enough reason to believe that the NDS BPFO vibrations in thruster 1 are indeed of a mechanical nature and the bearing is showing early signs of wear. This is not as certain as for thruster 6, but a visual inspection could be performed in order to validate this. This validation would also be interesting from a scientific standpoint, as it would prove or disprove the potential of this ESA method in performing better than the mechanical vibration measurements for this purpose. In any case, a further investigation into these vibrations is advised.

C - As it has not yet been proven that ESA can or cannot detect bearing related vibrations originating down in the thruster, this might be interesting for future research. In this case, it would be recommended to wait until one of the twelve thrusters is showing early signs of bearing wear down in the thruster, according to the CM campaign of Pruftechnik NV At that point, the ESA method presented in this research could be implemented for this specific thruster as well, in order to investigate whether the same fault detection can be performed by ESA.

D - As ESA has proven to be able to detect the mechanical behaviour and early damage of the thruster assemblies, it has the potential to be implemented as a CM method. The recommended implementation approach for this is presented in Section 6.6.

E - This thesis is focused on how ESA can best be implemented for the PS. Regarding the question whether it should be implemented or not, it might be best to first quantify what gain this implementation could bring. For example, a Failure Mode, Effects and Criticality Analysis (FMECA) can be performed to find out what the most occurring, critical and costly failures of the machines are and if the implementation of ESA would be effective in addressing these problems.

F - For baseline torque measurements the electrical torque showed much similarity with the shaft torque. Therefore, in cases where only the baseline shaft torque is needed, it might be interesting to further investigate a relation between the two measurements. Since, the use of current and voltage sensor could present a cheaper alternative for the expensive Kongsberg MetaPower shaft torque measuring devices.

Recommendations for future research

G - This research has only focused on the magnitude of electrical and mechanical oscillations. However, the phase of these vibrations might also contain information on the potential defects in a mechanical system. For example, according to the ISO guidelines for vibration diagnosis, a phase shift in the motor shaft frequency might be able to distinguish unbalance from misalignment [17]. Therefore, for future research it might be interesting to analyse the phase behaviour or certain vibrations and their information on the health of the machine as well.

H - The analyses of different electrical parameters and spectra in this research were solely qualitative. In future research a more quantitative approach for comparison might be attempted. For example, including relative amplitudes of vibrations compared to their baseline load or signal to noise ratios.

I - All different analyses presented in this research were based on constant motor speeds. However, when analysing transient machine behaviour, more information on the health of the machine might be obtained. There were different types of methods presented for this in the literature review in Appendix H, which could be subject for future research.

J - The VFD controls the thrusters to maintain a constant speed, which means it will likely sense certain vibrations in torque and try to counter these. This behaviour might be detectable in the measurements obtained in this research, but was not analysed. In future research, this influence of the VFD on torque oscillations could be examined. For example, this might be attempted by comparing the ratios of amplitude of certain current and voltage vibrations at the same frequency or by analysing the phase differences in current and voltage oscillations at the same frequency.

Acknowledgements

I want to thank Dr. Ir. André Veltman (Piak Electronic Design BV) for the many useful discussions on electric drives and measurements that helped me navigate the world of electrical engineering as a mechanical engineer. In addition, I want to thank Dr. Veltman for making his Matlab scripts for torque calculation available for this research. Finally, I want to thank Allseas Engineering BV for providing me with the opportunity and resources to perform this research.

References

[1] C. Reza, D. Islam, and S. Mekhilef, “A review of reliable and energy efficient direct torque controlled induction motor drives,” *Elsevier Renewable and Sustainable Energy Reviews*, vol. 37, pp. 919–932, 2014.

[2] S. Kumar, D. Mukherjee, P. K. Gucchait, *et al.*, “A comprehensive review of condition based prognostic maintenance (cbpm) for induction motor,” *IEEEAccess*, vol. 7, pp. 90 690–90 704, 2019.

[3] I. Alsofyani and N. Idris, “A review on sensorless techniques for sustainable reliablity and efficient variable frequency drives of induction motors,” *Elsevier Renewable and Sustainable Energy Reviews*, vol. 24, pp. 111–121, 2013.

[4] P. Zhang, Y. Du, T. G. Habetler, and B. Lu, “A survey of condition monitoring and protection methods for medium-voltage induction motors,” *IEEE Transactions on Industry Applications*, vol. 47, no. 1, pp. 34–46, 2011.

[5] H. Bloch and F. Geitner, *Machinery Failure Analysis and Troubleshooting - Volume 2* (Practical Machinery Management for Process Plants), 3th ed. Houston, TX: Gulf Prosessional Publishing, 1999, ISBN: 978-0-88415-662-8.

[6] R. K. Mobley, *An Introduction to Predictive Maintenance* (Plant Engineering), 2nd ed. Woburn, MA: Butterworth-Heinemann, 2002, ISBN: 978-0-88415-662-8.

[7] “Rules and Regulations for the Classification of Ships”, Maritime industry regulations/standard, Lloyd’s Register, London, July 2022.

[8] D. Miljkovic, “Brief review of motor current signature analysis,” *CrSNDT Journal*, vol. 5, pp. 14–26, 2015.

[9] A. Korde, “On-line condition monitoring of motors using electrical signature analysis,” *Recent Advances in Condition Based Plant Maintenance*, Mumbay, 17-18 may 2002.

[10] M. E. H. Benbouzid, “A review of induction motors signature analysis as a medium for faults detection,” *IEEE Transactions on Industrial Electronics*, vol. 47, no. 5, pp. 984–993, 2000.

[11] R. Schoen, T. Habetler, F. Kamran, and R. Bartheld, “Motor bearing damage detection using stator current monitoring,” *IEEE Transactions on Industrial Electronics*, vol. 31, no. 6, pp. 1274–1279, 1995.

[12] G. Kliman and J. Stein, “Methods of motor current signature analysis,” *Electric Machines and Power Systems*, vol. 20, no. 5, pp. 463–474, 1992.

[13] J. Keski-Rahkonen, ”Thruster Digital Twin Handout”, Technical Presentation, Kongsberg Maritime Oy, March 2020.

[14] Pruftechnik, “Accelerometer (industrial) VIB 6.12x, 6.14x installation and operation”, Technical Datasheet, Fluke Deutschland GmbH, Germany, 2018.

[15] Fluke, ”VIBXPERT® II: The versatile, long-lasting tool for data collection, data analysis, field balancing ”, Technical Datasheet, Fluke Deutschland GmbH, Germany, 2011.

[16] Kongsberg, “Torque and Power monitoring KONGSBERG MetaPower Quad”, Technical Description, Kongsberg Maritime, Norway, March 2022.

[17] “Condition monitoring and diagnostics of machines — vibration condition monitoring — part 3: Guidelines for vibration diagnosis,” *ISO standard 13373-3:2015(E)*, 2015.

[18] F. Cipollini, L. Oneto, A. Coraddu, and S. Savio, “Unsupervised deep learning for induction motor bearings monitoring,” *Data-Enabled Discovery and Applications*, vol. 3, no. 1, 2019.

[19] H. Polinder, ”Drive and Energy Systems - Lecture 9: Induction Machines”, Lecture [PowerPoint slides], Delft University of Technology, MSc Mechanical Engineering, 2022.

[20] H. J. Landau, “Sampling, data transmission, and the nyquist rate,” *Proceedings of the IEEE*, vol. 55, no. 10, pp. 1701–1706, October 1967.

[21] I. Y. Onel and M. E. H. Benbouzid, “Induction motor bearing failure detection and diagnosis: Park and concordia transform approaches comparative study,” *IEEE/ASME Transactions on mechatronics*, vol. 13, no. 2, pp. 257–262, April 2008.

[22] A. J. M. Cardoso and E. S. Saraiva, “Computer-aided detection of airgap eccentricity in operating three-phase induction motors by park’s vector approach,” *IEEE Transactions on industry applications*, vol. 29, no. 5, pp. 897–901, 1993.

[23] N. Mehala and R. Dahiya, “Detection of bearing faults of induction motor using park’s vector approach,” *International Journal of Engineering and Technology*, vol. 2, no. 4, pp. 263–266, 2010.

[24] E. L. Bonaldi, L. E. de Lacerda de Oliveira, J. G. B. da Silva, G. Lambert-Torres, and L. E. B. da Silva, “Predictive maintenance by electrical signature analysis to induction motors,” in *Induction Motors - Modelling and Control*. R. Araujo, Intech: Rijeka, Croatia, 2012, ch. 20, pp. 487–520.

[25] S. F. Legowski, A. H. M. S. Ula, and A. M. Trzynadlowsh, “Instantaneous power as a medium for the signature analysis of induction motor,” *IEEE Transactions on industry applications*, vol. 32, no. 4, pp. 904–909, August 1996.

[26] Rolls-Royce, ”Service manual mechanical and hydraulical part - UUC 455 Azimuth Thruster”, Technical Specification PI-635S0-101-M-X-001, Rolls-Royce Oy Ab, Rauma, Finland, 2012.

[27] Hyundai, ”Technical Specification for Induction Motor (6200k@, 8P, 3kV, 12 sets)”, Technical Specification PI-635S0-212-E-F-001, Hyundai Heavy Industries Co. Ltd. 2010.

[28] Mobius Institute, “Vibration Analysis Training Manual Category II”, Chapter 17, Training Course Material, Mobius Institute, 2016.

[29] W. Jansen, ”Allseas B.V. Pioneering Spirit (IMO9593505) Online Thruster Monitoring - August 2022”, Pruftechnik N.V., Antwerpen, August 2022.

[30] N. Abbas, N. Kornev, I. Shevchuk, and P. Anschau, “Cfd prediction of unsteady forces on marine propellers caused by the wake nonuniformity and nonstationarity,” *Ocean Engineering*, vol. 104, pp. 659–672, 2015.

[31] “Mechanical vibration — measurement and evaluation of machine vibration — part 3: Industrial machinery with a power rating above 15 kw and operating speeds between 120 r/min and 30 000 r/min,” *ISO standard 13586-3:2022(E)*, 2022.

[32] T. Wei, W. Feng, Y. Chen, C.-X. Wang, N. Ge, and J. Lu, “Hybrid satellite-terrestrial communication networks for the maritime internet of things: Key technologies, opportunities, and challenges,” *IEEE Internet of Things Journal*, vol. 8, no. 11, pp. 8910–8934, June 2021.

[33] D. Stevenson. “Starlink maritime: Everything you need to know [2022].” (December 2022), [Online]. Available: `https://blinqblinq.com/starlink-maritime/` (visited on 01/23/2023).

[34] Ansaldo, ”Silcovert GN medium voltage PWM-VSI Drive user maintenance manual”, Technical Specification SVGN E 2776, Ansaldo Sistemi Industriali S.p.A. 2011.

A Corresponding Paper

Mechanical Fault Diagnosis of a Marine Vessel's Thruster Assemblies through Electrical Signature Analysis: A Case Study

K. Kruimer
Delft University of Technology, Netherlands

ABSTRACT: This paper presents a case study of fault detection and diagnosis of three induction motor driven thruster assemblies currently in use aboard the offshore construction vessel "Pioneering Spirit." This diagnosis is performed by measuring the three-phase current and voltage of the induction motor driving the thrusters, which is done at a constant motor speed for different speed settings. These measurements are used to calculate the complex current using the EPVA method and the stator torque of the machine. The spectra of these parameters are plotted using an FFT algorithm to analyse the mechanical vibration behaviour. In addition, the spectra at different speeds for each thruster will be normalized to analyse the speed dependent behaviour of the measured vibrations. The measurements are validated by mechanical vibration measurements captured on the Non-Drive Side of the induction motor, as well as by historical vibration data originating from sensors throughout the thruster assemblies. Finally, a health diagnosis along with recommended maintenance actions is presented for the three individual thrusters.

1 INTRODUCTION

The thruster assemblies are some of the most critical assets aboard every marine vessel. Since the introduction of diesel-electric propulsion, the main choice of propulsion for construction vessels has become Induction Motor (IM) driven thruster assemblies, as these electric motors offer excellent direct speed and torque adjustability for the Dynamic Positioning (DP) of a vessel [1]. In order to monitor the health of these assets and prevent downtime of an entire vessel, the industry standard of Condition Monitoring (CM) for these assets is by mechanical vibration analysis [2,3]. However, such a CM campaign often requires many sensors spread out through the entire thruster, most of which are located in the enclosed underwater part of the assembly. Maintaining these sensors is impossible without removing the thruster from the vessel, which is such an expensive operation that it will not be performed without it being absolutely necessary for the health of the thruster, or to meet the overhauling requirements set by Lloyds Register [2]. Therefore, the question arises whether another less intrusive CM technique could be implemented for continuously monitoring the mechanical health of these thruster assemblies.

The use of an IM for propulsion offers a second type of CM for the thrusters, much similar to mechanical vibration analysis, which is commonly referred to as Electrical Signature Analysis (ESA). This CM method can be used for the monitoring of both mechanical and electrical failures in a machine and has been a popular research topic since it was first developed in the 1970's in the form of Motor Current Signature Analysis (MCSA) [4-7]. One of the reasons for this is the low intrusiveness of this method, as the only measurements it requires are the voltage and current measurements of the IM. However, the use of ESA for the monitoring of the mechanical health of equipment has never been widely implemented in the industry.

This paper, in the form of a case study, will investigate the potential of using ESA for the mechanical health of a marine vessel's thruster assemblies by performing a machine health diagnosis for three thrusters that are currently in use on a construction vessel. This will be validated by comparing it with the measurements of a mechanical vibration analysis of the same three thrusters. The paper will be structured accordingly: Firstly, the specific ship and thruster assemblies are presented in Chapter 2, along with the measuring setup used. Then, the methodology for acquiring the measurements, information processing and performing the diagnostics are discussed in Chapter 3. Hereafter, the results of the measurements are highlighted in Chapter 4 and will be discussed in Chapter 5. Finally, the conclusion and recommendations for maintenance actions for the three thrusters are presented in Chapter 6.

2 TECHNICAL SET-UP

2.1 *Thruster Assemblies*

The thruster assemblies subject to the fault diagnosis are thruster 1 (T1), thruster 3 (T3) and thruster 6 (T6) of the Pioneering Spirit (PS), which is an offshore construction vessel operated by Allseas Engineering BV. The vessel is capable of lifting both topsides and jackets of offshore platforms, as well as subsea pipelaying. The three identical thrusters are powered by a Variable Frequency Drive (VFD) driven IM. More information on the thruster, IM and VFD can be found in Table 1, Table 2 and Table 3 respectively. A technical drawing of the thruster and IM is shown in Figure 1.

The three specific thrusters were chosen for their different health conditions. According to prior knowledge, T1 has no suspected wear of any kind and is thus in pristine condition, T3 has suspected early stage bearing wear in the input shaft double spherical bearing and T6 has suspected early stage bearing wear in the Non-Drive Side (NDS) bearing of the IM. These bearings are highlighted in Figure 1 as well. The prior knowledge on the conditions of the thrusters is based on a vibration monitoring program overseen by Pruftechnik NV, that is being run since the commissioning of the PS [8].

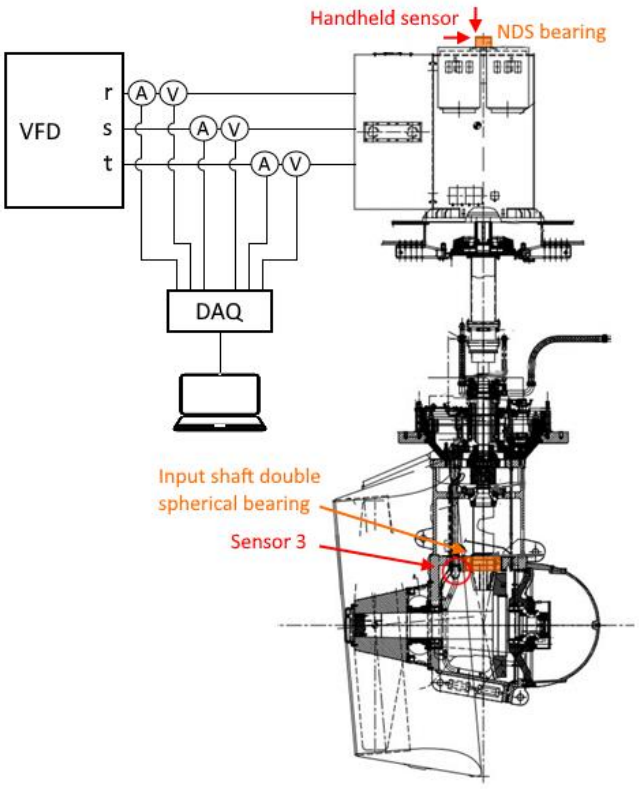

Figure 1: Assembly overview and sensor locations

Table 1. Thruster specifications [9]

Brand	Rolls-Royce
Type	Ulstein Aquamaster UUC 455 FP
Function	Main propulsion and DP
Max. power	5.5 MW
Max. shaft torque	70.0 kNm
Nominal speed in/out	750 RPM/157.3 RPM
Gears	13/62 (ratio = 4.769)
Propeller	Fixed pitch, right-handed
Number of blades	4

Table 2. Induction motor specifications [10]

Brand	Hyundai Heavy Industries
Type	HRN7 1005-88Y, 3-phase
Number of poles	8
Rated/peak power	6.1 MW/6.5 MW
In-/output at 750 RPM	3kV; 1200A; 54.2 Hz; 5.5 MW
Max. torque	Limited at 70.0 kNm
Power factor at 750 RPM	0.9
Efficiency at 750 RPM	97.6%

Table 3. VFD specifications [11]

Brand	Ansaldo
Type	Silcovert GN PWM Voltage Source Inverter Active Front End 24 Pulse
Output frequency	0 – 60 Hz
Switching frequency	666.9 Hz

2.2 *Measuring devices*

The measuring setup for the ESA measurements consists of three zero-flux current transformers, combined with a separate power supply and built-in voltage shunt [12], three HV voltage probes [13] and a DAQ to which all these sensors are connected. The voltage probes are connected inside the VFD, directly to the bus bar of each output phase of the VFD. The current transformers are connected inside the VFD to one out of seven cables connecting each phase of the VFD and IM. This means they measure $1/7^{th}$ of current running between the VFD and IM.

The mechanical vibration sensors used for the validation by vibration analysis are Integrated Circuit-Piezoelectric accelerometers [14]. Most of these sensors are built into the thruster assemblies. For these sensors historical vibration data is available. In Figure 1, sensor 3 is highlighted, as this sensor is closest to the input shaft double spherical bearing and therefore the measurements of this sensor will be analysed in this research. Also, a sensor connected to a handheld data acquisition device is available, which can be connected close to the Non-Drive Side (NDS) bearing of the IM in radial 0° and 90° direction, as well as in axial direction of the motor shaft. This is highlighted in Figure 1 as well.

3 METHODOLOGY

3.1 *Measuring process*

The measurements on the thrusters will be performed during ramp-up tests when the ship is sailing. In these tests, the motor speed is increased from 70% of the maximum motor speed up to 85%, in increments of 5%. At these intervals, the motor speed will be kept constant, and the 3-phase current and voltage will be measured at 20 kHz for 60 seconds. Simultaneously, the mechanical vibration measurements are performed on the non-drive side bearing of the IM for T1 and T6. For T3 this extra mechanical measurement was not performed. Historical vibration data is available from the sensors mounted throughout the assembly for all three thrusters.

Note that the tests for the three thrusters were performed on three different days, each time with a slightly different cruising speed of the vessel. Therefore, the experienced torque of the three thrusters is not identical at the same motor speeds. Also, no speeds higher than 85% motor speed were possible since the torque limit of the IM was reached just above this speed for all three ramp-up tests.

3.2 *Analysis and diagnosis process*

Firstly, the measurements at the highest speed and torque (85% speed) for all three thrusters will be analysed. This is done by calculating the complex current or orbit of the machine out of the ESA measurements using a Clarke transform, according to the EPVA method. Also, the motor torque is calculated out of these measurements. Both these calculations are further explained in Section 3.3. The positive spectra of the complex current and motor torque will then be plotted using the Fast-Fourier-Transform. Out of these, spectra the information regarding the mechanical vibrations of the machine will be interpreted. This process is further explained in Section 3.4.

Secondly, the complex current and motor torque for the thrusters at all different speeds will be calculated. For each thruster, the spectra are created at the different motor speeds, after which they are normalized by the shaft speed during each measurement and plotted over each other. This way, the mechanical vibrations of the machine can be observed at different motor speeds.

Out of these two types of analysis, a diagnosis of the mechanical behaviour of each machine is created, which will be validated using the mechanical vibration measurements captured at the same time, as well as the historical vibration data that is available.

3.3 *EPVA method and torque calculation*

As stated before, the complex current or orbit will be calculated according to the Extended Park Vector Approach (EPVA) [15,16]. This is done by transforming the 3 – phase current (and voltage) into an alpha, beta and zero component using an amplitude invariant Clarke transform. This is shown in the following equation:

$$\begin{bmatrix} i_\alpha \\ i_\beta \\ i_0 \end{bmatrix} = \frac{2}{3} \begin{bmatrix} 1 & -\frac{1}{2} & -\frac{1}{2} \\ 0 & \sqrt{\frac{2}{3}} & -\sqrt{\frac{2}{3}} \\ \frac{1}{2} & \frac{1}{2} & \frac{1}{2} \end{bmatrix} \begin{bmatrix} i_R \\ i_S \\ i_T \end{bmatrix}$$

The complex current, and similarly the complex voltage, is then created according to:

$$y = i_c = i_\alpha + j * i_\beta$$

The magnitude of this complex current vector is then used as input for the FFT algorithm creating the spectra.

The torque is calculated by first integrating the complex voltage into the magnetic flux. This is done according to the following equations, in which n_p denotes the number of pole-pairs and the factor 1.5 is added since the Clarke transform conserved the amplitude and not the power of the signal:

$$\Phi_{stator} = \int u_c - i_c R_s \, dt$$

$$T_c = n_p * 1.5 * (i_c \bar{\Phi})$$

The torque of the machine is then defined as the imaginary value of the complex vector T_c, which will also be used as input for the FFT creating the spectra.

3.4 *Frequencies*

The created spectra will be analysed for the presence of frequencies of a mechanical nature. In order to do this, the most important mechanical and electrical frequencies are listed below:

Drive frequency – This is the frequency of alternating current in the IM, supplied by the VFD. Most mechanical frequencies will be modulated as sidebands on this frequency. However, by using the EPVA method, the spectra are demodulated with respect to the drive frequency. Meaning, these modulated frequencies will appear as their original frequency in the spectra.

Switching frequency – This is the frequency of voltage pulses created by the VFD in order to simulate an alternating current. Some frequencies will be modulated on this frequency as well.

Motor shaft frequency – The mechanical spinning frequency of the rotor and motor shaft.

Propeller shaft frequency – Equal to the motor shaft frequency divided by the gear ratio.

Blade pass frequency – Equal to the number of propeller blades times the propeller shaft frequency.

Gear mesh frequency – Equal to the number of teeth on the motor shaft times the motor shaft frequency, or the number of teeth on the propeller shaft times the propeller shaft frequency.

Bearing frequencies – Bearing related frequencies are determined by the shaft speed and geometry of the bearing. Generally, there are four relevant mechanical frequencies of vibration that might be induced in bearings. These are:

Ball Pass Frequency Inner (BPFI) – Related to a fault on the inner raceway of the bearing.
Ball Pass Frequency Outer (BPFO) – Related to a fault on the outer raceway of the bearing.
Ball Spin Frequency (BSF) – The spinning frequency of the rolling elements around their own axis and related to a fault on a rolling element of the bearing.
Fundamental Train Frequency (FTF) – The spinning frequency of the train or cage of the bearing.

All relevant mechanical frequencies are calculated for the thruster assemblies and are shown both in their order of the shaft speed and their frequency at 85% motor speed (in the T1 measurement) in Table 4. The bearing related frequencies are obtained from the original equipment manufacturer.

Table 4. First harmonics of mechanical frequencies

Motor shaft speed	1.00X	11.50 Hz
Propeller shaft speed	0.21X	2.411 Hz
Blade Pass Frequency	0.84X	9.645 Hz
Gear Mesh Frequency	13.0X	149.5 Hz
NDS BPFO	5.43X	62.45 Hz
NDS BPFI	7.57X	87.06 Hz
NDS BSF	2.26X	26.02 Hz
NDS FTF	0.44X	4.807 Hz
DS BPFO	6.62X	76.08 Hz
DS BPFI	8.38X	96.42 Hz
DS BSF	4.18X	48.08 Hz
DS FTF	0.44X	5.072 Hz

4 RESULTS

The resulting spectra for the three thrusters at 85% motor speed are shown in Figure 2 and Figure 3. It becomes apparent that no aberrant mechanical vibration is visible in the spectra for T3. Therefore, only the variable speed spectra for the torque of T1 and T6 are presented in Figure 4 and Figure 5. Furthermore, the mechanical vibration measurements of T1 and T6 are shown in Figure 6 and Figure 7 to serve as a validation.

As stated in Chapter 3, no mechanical vibration measurements were performed with the handheld scanning device during the ramp up tests for T3. Therefore, the mechanical vibration measurements captured by all sensors mounted inside the thruster were obtained from the historical database in order to validate the ESA measurements. Out of all these measurements, a recent velocity spectrum of sensor 3 was selected and is shown in Figure 8. This choice was made, since this sensor is closest to the input shaft double spherical bearing, in which early stage bearing wear was suspected according to prior knowledge.

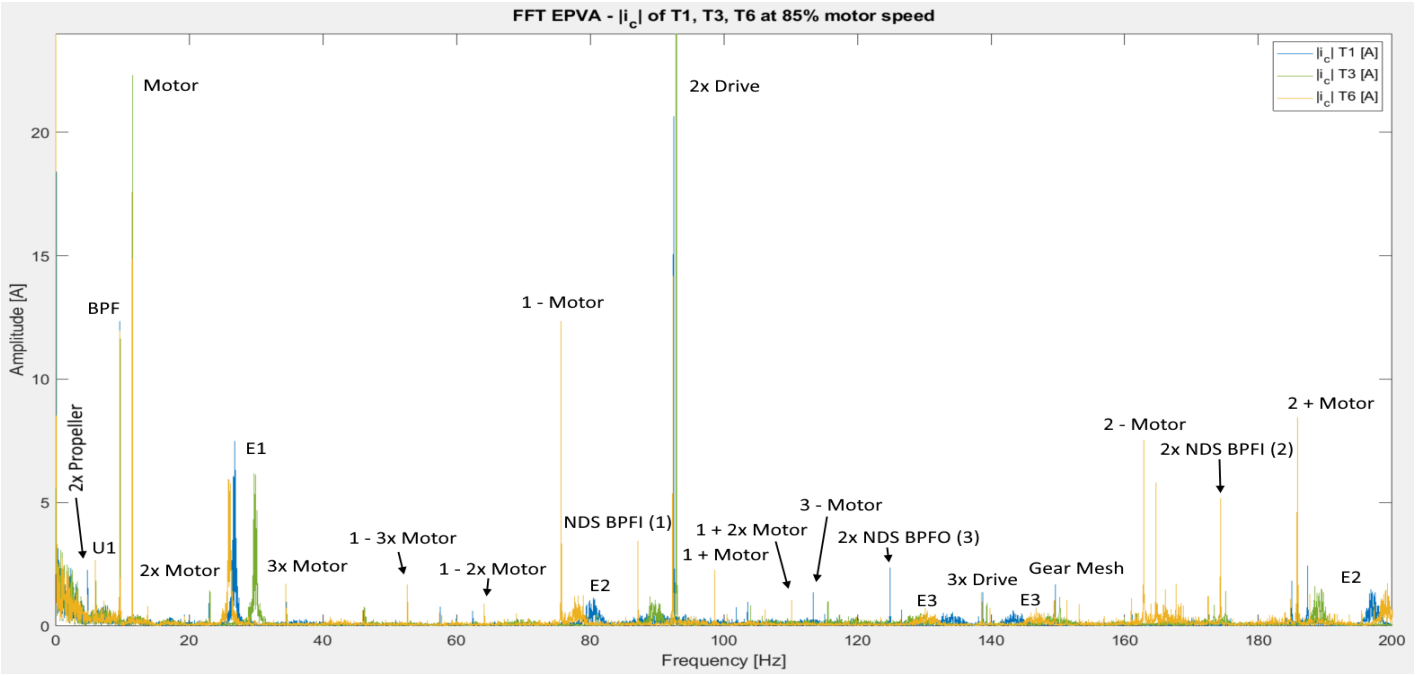

Figure 2: EPVA spectrum of T1, T3 and T6. Fs = 20 kHz, t = 50 s

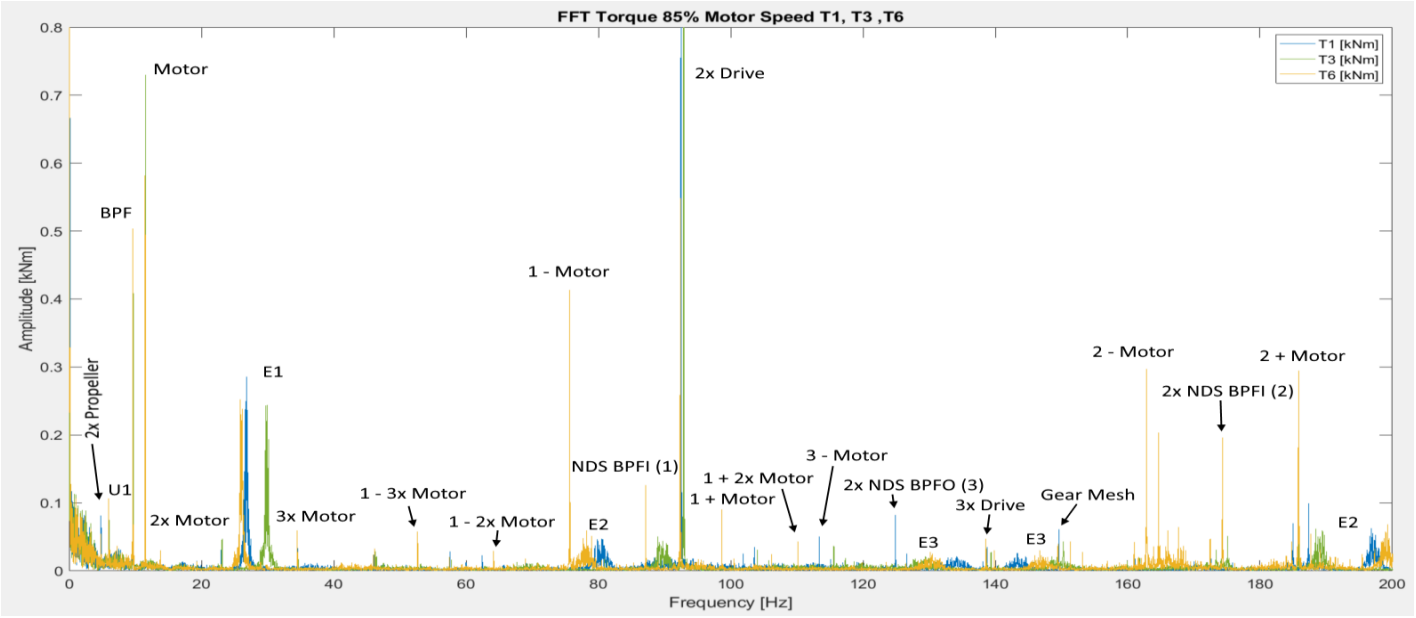

Figure 3: Torque spectrum of T1, T3 and T6. Fs = 20kHz, t = 50 s

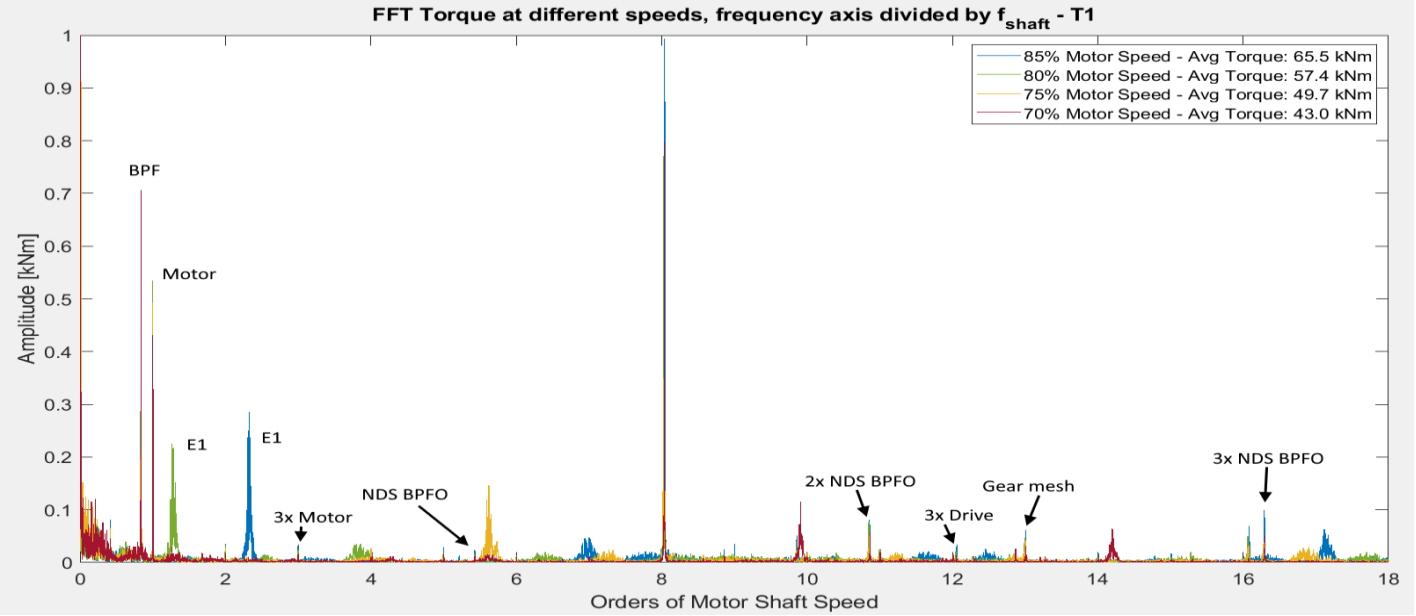

Figure 4: Torque spectrum of T1 at all motor speeds, normalized by shaft speed. Fs = 20kHz, t = 50s

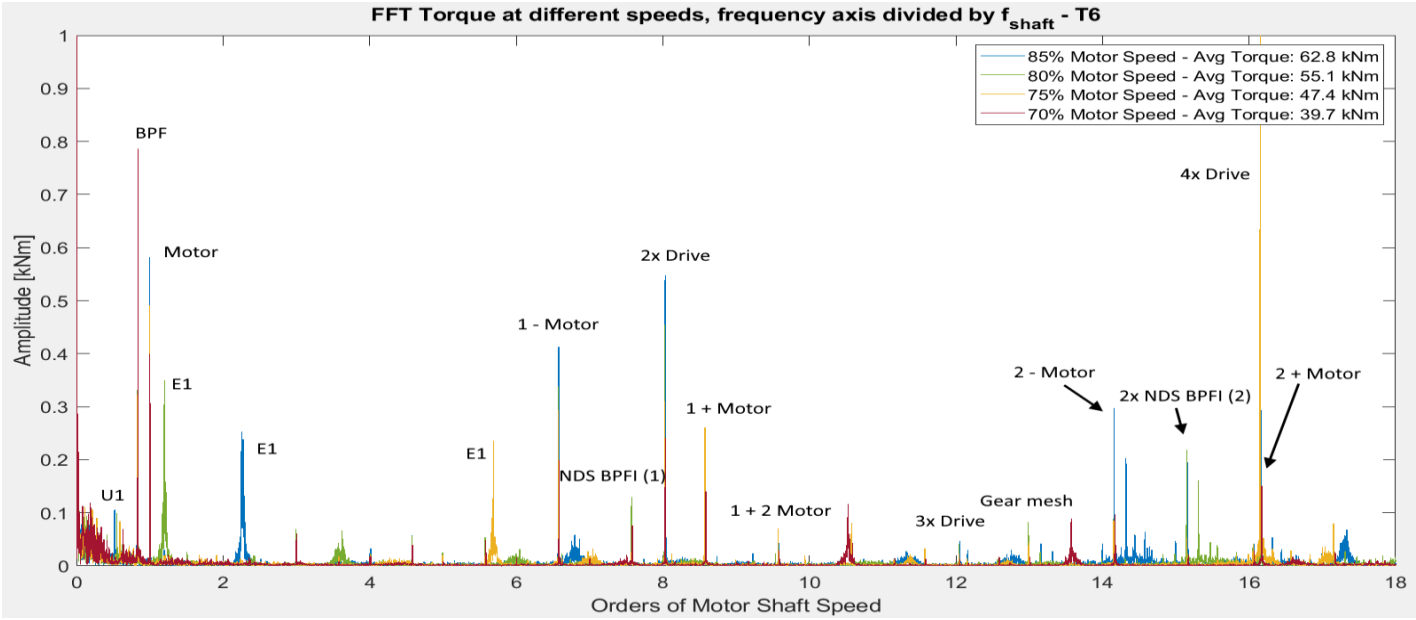

Figure 5: Torque spectrum of T6 at all motor speeds. Normalized by shaft speed. Fs = 20 kHz, t = 50 s

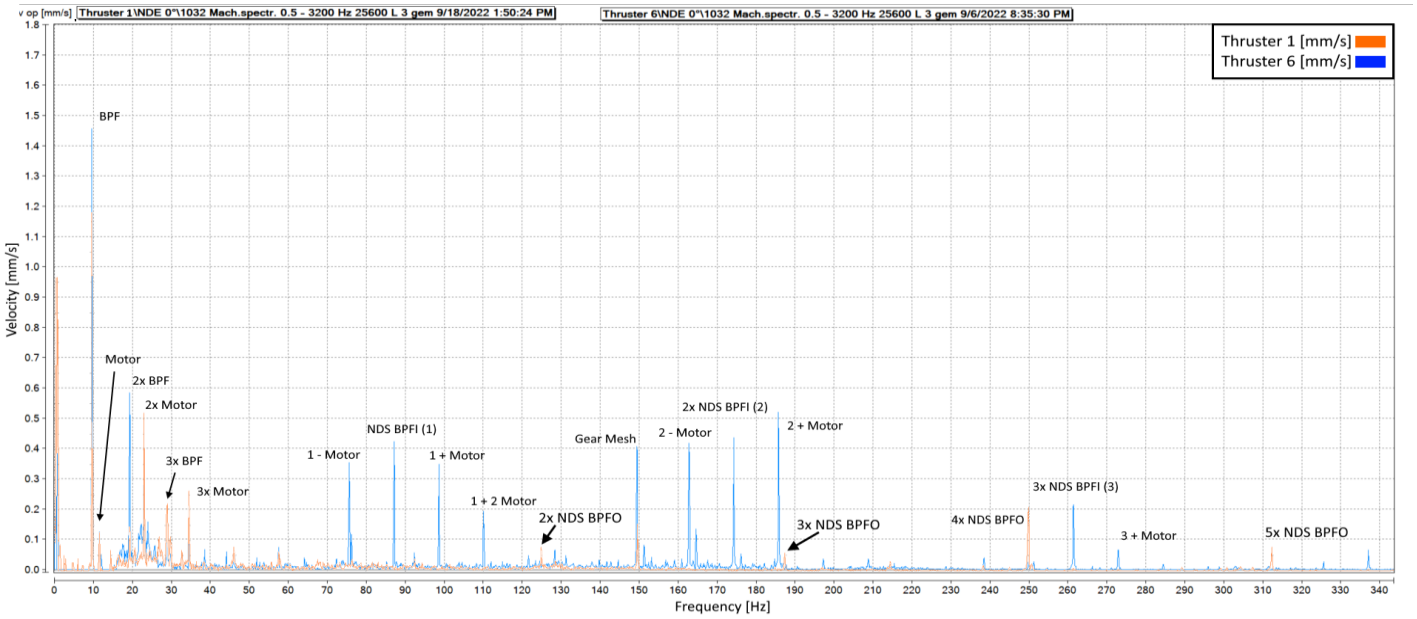

Figure 6: Velocity spectrum of radial 0° vibration measurement T1 and T6. Fs = 8192 Hz, t = 8 s.

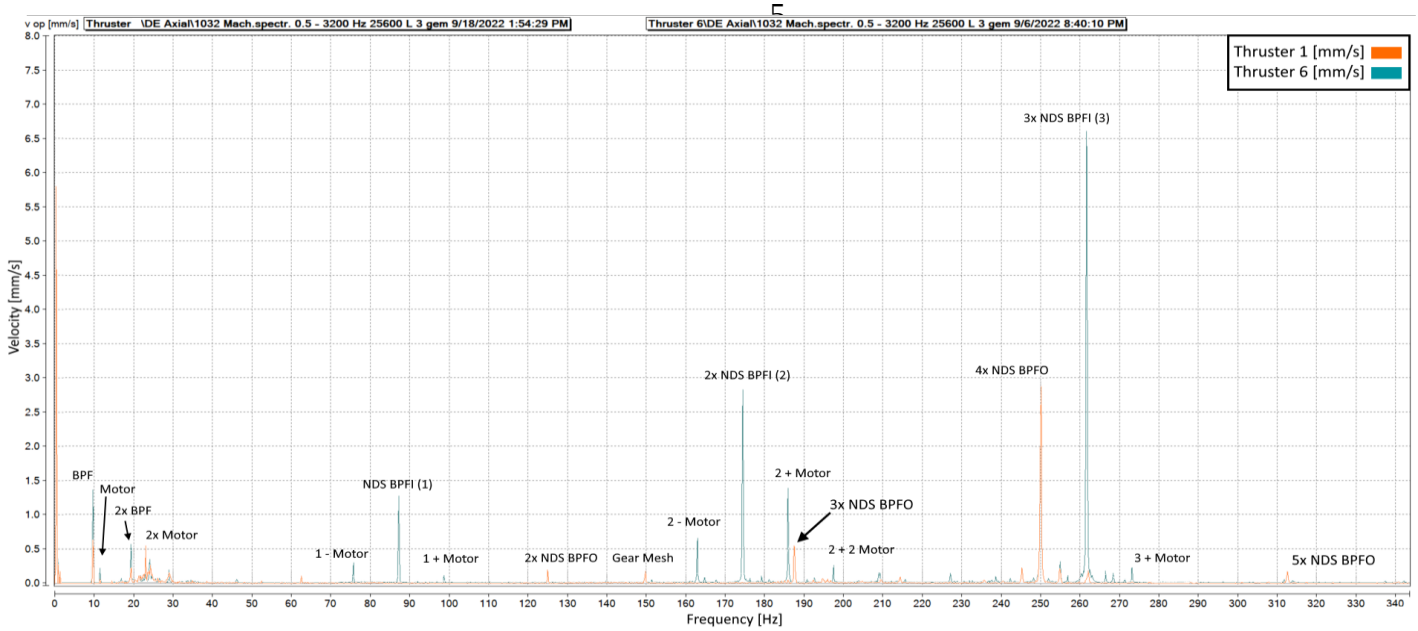

Figure 7: Velocity spectrum of axial vibration measurement T1 and T6. Fs = 8192 Hz, t = 8s.

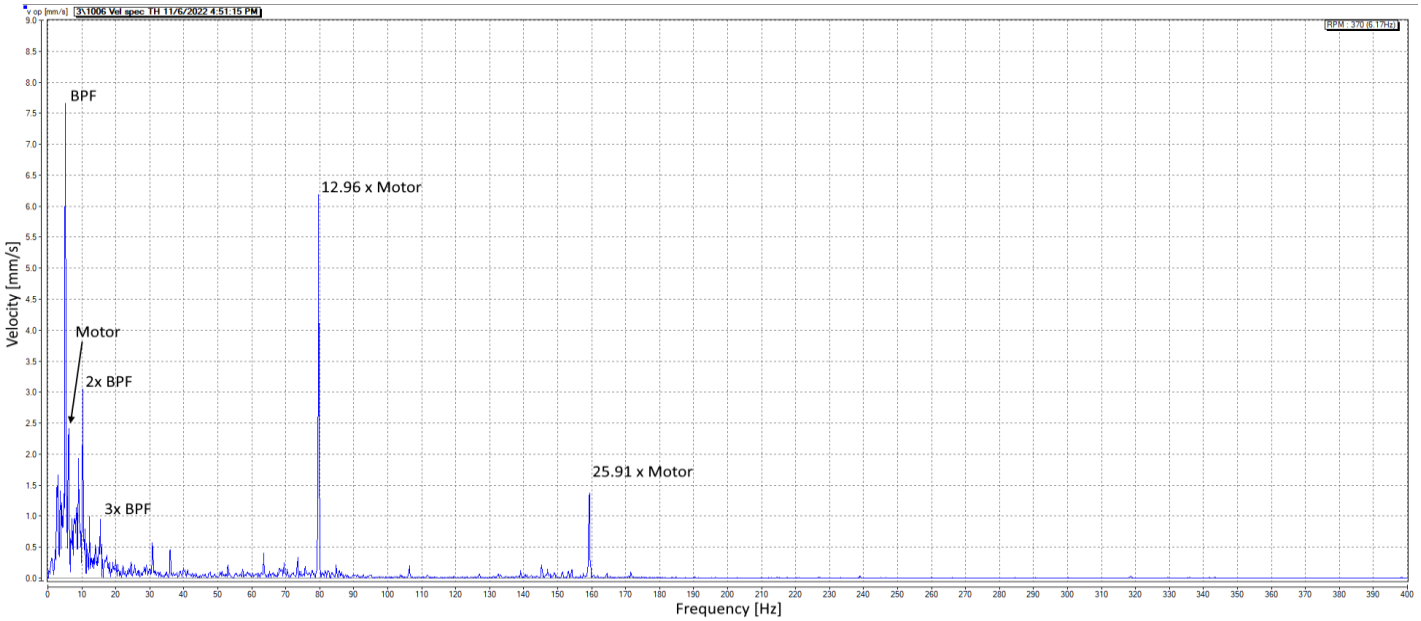

Figure 8: Velocity spectrum of sensor 3 on T3. Fs = 8192 Hz, t = 8s.

5 DISCUSSION

5.1 *Healthy oscillations*

Evidently, in all ESA based spectra the oscillations originating by mechanical behaviour of the machine are accompanied by many oscillations of an electrical nature. Firstly, this is noticed in the much higher noise level in the ESA spectra. Secondly, harmonics of the drive frequency are well represented in all ESA spectra. Especially the second harmonic of the drive frequency, which occurs due to unbalance of the three phase currents and voltages [15]. A slight unbalance, which is the case for all three thrusters, is not considered unhealthy machine behaviour. Finally, different haystack shaped peaks, denoted with E1 – E3, occur in the ESA spectra, which slightly resemble resonance behaviour of the machine [17]. However, the fact that these peaks don't fall in the same frequency region for the different measurements and thrusters indicates that resonance cannot be the cause. Also, the ESA spectra normalized by speed show that these haystacks are not dependent on the motor shaft speed. This indicates that the haystacks are likely not of a mechanical nature, which is further validated by their absence in the velocity spectra. Therefore, it is suspected that these frequencies are healthy electrical oscillations.

Furthermore, the motor shaft frequency and its harmonics, as well as the BPF and gear mesh frequency, are clearly present in all ESA spectra and the mechanical vibration spectra. These vibrations are considered healthy, as they will be present in any thruster assembly. Detecting faulty behaviour through these frequencies is ideally done by monitoring the vibrations for a longer time period and detecting an increasing trend.

5.2 *Thruster 1*

Thruster 1 appears to show oscillations in the ESA spectra at 85% motor speed (Figure 2 and Figure 3), which coincide with the BPFO of the Non-Drive Side (NDS) IM bearing and its 2nd and 3rd harmonic. When analysing the torque spectrum normalized by the motor speed in Figure 4, these same vibrations occur in the same order of the motor shaft speed for all motor speeds. This indicates that it is highly likely that these oscillations are indeed of a mechanical nature. This would indicate the presence of early stage bearing wear, as the order they appear in is exactly the order of the NDS BPFO, which should not be present in the case of healthy bearing. Furthermore, when analysing the mechanical vibration measurements at 85% motor speed, there is some indication of light vibrations at 2x NDS BPFO. An unusually strong vibration is detected at 4x NDS BPFO in the mechanical vibration spectra, but in the ESA spectrum the only small oscillation visible in this order is at 70% motor speed. Since these mechanical vibrations are so low, it can't be conclusively stated that there is indeed early stage bearing wear in this bearing.

5.3 *Thruster 3*

The spectra of EPVA and torque in Figures 2 and 3 do not show any aberrant vibrations of a mechanical nature. When analysing the mechanical vibration measurements from the historical database for all vibration sensor throughout T3, no faulty machine behaviour and no increasing trend of vibrations is detected. This means that the suspected bearing damage according to prior knowledge based on the vibration monitoring program of Pruftechnik NV could not be validated.

The velocity spectrum in Figure 8 shows harmonics of the BPF and motor shaft frequency. The suspected wear is related to the BPFI of the input shaft double spherical bearing, which has an order of 10.84X motor speed [8]. However, the only found frequency close to this order is at 12.96X motor speed (and its 2nd harmonic at 25.91X motor speed). This means that this frequency actually represents the gear mesh frequency.

It should be noted that all this data was collected at motor speeds of 60% or lower, which possibly could be too low to detect any vibrations indicating faulty behaviour. Still, it is likely that T3 is operating in pristine conditions.

5.4 *Thruster 6*

The EPVA and torque spectra in Figures 2 and 3 show a clear presence of the NDS BPFI and its 2nd and 3rd harmonic. Furthermore, there appear to be multiple sidebands of the motor shaft frequency modulated on these vibrations. It also shows that these vibrations occur at all different speed settings and in the exact same order of the motor shaft speed in Figure 5. The presence of these mechanical vibrations is validated in the 0° velocity spectrum in Figure 6, and these vibrations are represented even stronger in the axial velocity spectrum in Figure 7. This is likely caused by the fact that the NDS BPFI is an angular contact bearing of the vertical motor shaft. Therefore, a portion of the weight of the rotor and motor shaft is suspended on this bearing.

According to the ISO standards for vibration-based condition monitoring, this pattern of shaft frequency sidebands on the BPFI indicates stage 2 bearing wear or medium bearing wear [18]. This means that the inner raceway of the bearing is showing spalling or cavitations, which will progressively get worse while the machine is continued to be operated.

6 CONCLUSION

6.1 *Thruster 1*

The only aberrant behaviour detected in the ESA spectra of T1 points towards possible early-stage wear in the NDS bearing. However, the measured mechanical vibrations in these frequencies were so low that it can't be conclusively stated that the NDS bearing is indeed showing wear. At this point, only a visual inspection would be able to validate the presence of early-stage wear in this bearing. Nevertheless, from a reliability and maintenance engineering standpoint, a visual inspection of this bearing currently does not have the highest priority. Since, if the bearing has any wear at all, it will probably be very little, and it can likely continue to be used in the near future. However, it is advised to keep closely monitoring the health of this bearing.

6.2 *Thruster 3*

As stated in Chapter 5, no aberrant vibrations were detected in any of the spectra of T3. Also, the historical velocity spectra of the sensors throughout the thruster showed little reason to believe that there currently is (premature) damage in the machine. This means that the early stage bearing wear suspected by the vibration monitoring program can't be validated and the thruster is likely in pristine condition. Therefore, no further maintenance action is required.

6.3 *Thruster 6*

The ESA spectra of T6 clearly show aberrant vibrations indicating medium bearing wear. This is further validated in the spectra of mechanical vibrations. Wear of this type will progressively get worse up until the point that it can cause a machine failure. Therefore, it is advised to visually inspect or replace this bearing at the earliest opportunity.

ACKNOWLEDGMENTS

I want to thank Dr. Ir. André Veltman (Piak Electronic Design BV) for the many useful discussions on electric drives and measurements that helped me navigate the world of electrical engineering as a mechanical engineer. In addition, I want to thank Dr. Veltman for making his Matlab scripts for torque calculation available for this research.

Finally, I want to thank Allseas Engineering BV for providing me with the opportunity and resources to perform this research.

REFERENCES

[1] A.F. Adnanes, "Maritime Electrical Installations And Diesel Electric Propulsion" ABB AS Marine, Oslo, 2013.

[2] "Rules and Regulations for the Classification of Ships", Maritime industry regulations/standard, Lloyd's Register, London, July 2022.

[3] "Condition monitoring and diagnostics of machines - Vibration condition monitoring - Part 9: Diagnostic techniques for electric motors" ISO 13373-9, 1st ed. 2017.

[4] D. Miljkovic, "Brief review of motor current signature analysis", *CrSNDT Journal*, vol 5, pp. 14-26, 2015.

[5] G.B. Kliman and J. Stein, 'Methods of Motor Current Signature Analysis", *Electric Machines and Power Systems*, vol. 20, no. 5, pp. 463 – 474, 1992.

[6] R.R. Schoen, T. G. Habetler, F. Kamran and R. G. Bartheld, "Motor Bearing Damage Detection Using Stator Current Monitoring", *IEEE Transactions on Industry Applications*, vol. 31, no. 6, pp. 1274 – 1279, 1995.

[7] M.E. H. Benbouzid, "A Review of Induction Motors Signature Analysis as a Medium for Faults Detection", *IEEE Transactions on Industrial Electronics*, vol. 47, no. 5, October 2000.

[8] W. Jansen, "Allseas B.V. Pioneering Spirit (IMO9593505) Online Thruster Monitoring – August 2022", Pruftechnik N.V. Antwerpen, 10-2022.

[9] Rolls-Royce, "Service manual mechanical and hydraulical part - UUC 455 Azimuth Thruster", Technical Specification PI-635S0-101-M-X-001, Rolls-Royce Oy Ab, Rauma, Finland, 2012.

[10] Hyundai, "Technical Specification for Induction Motor (6200k@, 8P, 3kV, 12 sets)", Technical Specification PI-635S0-212-E-F-001, Hyundai Heavy Industries Co. Ltd. 2010.

[11] Ansaldo, "Silcovert GN medium voltage PWM-VSI Drive user & maintenance manual", Technical Specification SVGN E 2776, Ansaldo Sistemi Industriali S.p.A., Milano, 2011

[12] Danisense, "DM1200ID", Technical Datasheet, 3-2022.

[13] Tektronix, "Passive High Voltage Probes - P6015A", Technical Datasheet, Tekronix Inc., 1-2016.

[14] Pruftechnik, "Accelerometer (industrial) VIB 6.12x, 6.14x installation and operation", Technical Datasheet, Fluke Deutschland GmbH, 2018.

[15] E. L. Bonaldi, L. E. de Lacerda de Oliveira, J. G. B. da Silva, G. Lambert-Torresm, and L. E. B. da Silva, "Predictive maintenance by electrical signature analysis to induction motors," in Induction Motors - Modelling and Control. R. Araujo, Intech: Rijeka, Croatia, 2012, ch. 20, pp. 487–520.

[16] N. Mehala and R. Dahiya, "Detection of bearing faults of induction motor using park's vector approach", *International Journal of Engineering and Technology*, vol. 2, no. 4, pp. 263 – 266, 2010.

[17] Mobius Institute, 'Vibration Analysis Training Manual Category II", Chapter 17, 2016.

[18] "Condition monitoring and diagnostics of machines - Vibration condition monitoring - Part 3: Guidelines for vibration diagnosis" ISO 13373-3, 1st ed. 2015.

B Ship and Thruster Assemblies

B.1. Ship

B.1.1. General overview

The PS is an offshore construction vessel with a diesel-electric propulsion system, specialized in both subsea pipelay, as well as heavy-lift operations. The entire ship is powered by 8 MAN diesel engines, each driving an 11 MW Hyundai generator providing 11 kV 60 Hz AC to the ships' power grid. Also, one smaller, spare MAN diesel engine and generator are available for use in the harbor. Furthermore, the ship is propelled by twelve Rolls-Royce azimuth thrusters [26], each powered by a 6.1 MW Hyundai IM [27] in combination with an Ansaldo Variable Frequency Drive (VFD) [34]. More information on the thrusters and their electrical powertrains can be found in the following subsections. The location of the thrusters on board the PS can be seen in Figure B.1.

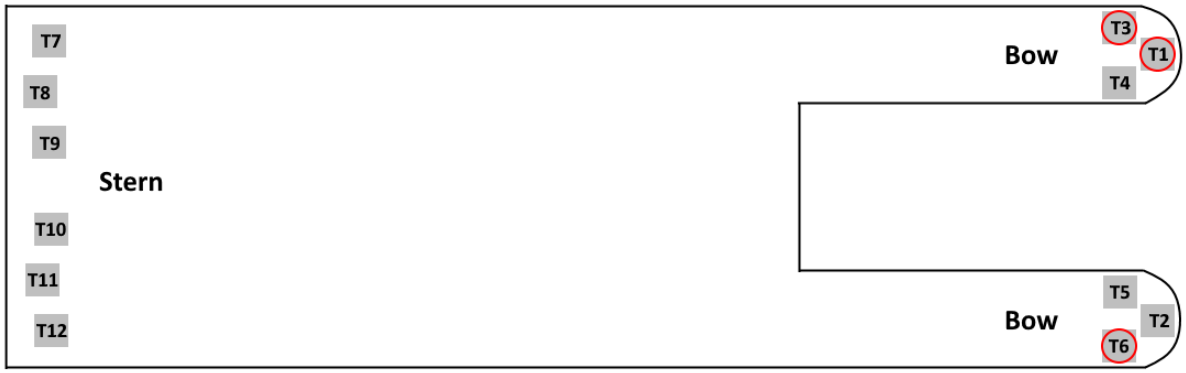

Figure B.1: Location of thrusters on board the PS

B.1.2. Operations

For the pipelay and heavy-lift operations, the most common operational mode for the thrusters is DP. In this case, all twelve thrusters of the ship are actively steered and powered to keep the ship in a set position or follow a specific trajectory. This means that the torque and speed of the thrusters is constantly being changed and the machines will rarely maintain a constant speed for more than a few seconds. Next to DP operations, the thrusters will either be switched off entirely, when the ship is docked, or the thrusters will be set to a constant speed and heading when the ship is sailing.

B.2. Thruster assembly

B.2.1. Powertrain

The powertrain of each thruster consists of the following components: A double HTT transformer set-up that transforms the 11 kV electrical power from the ships' power grid to 2 x 2 x 1850 V AC. This is fed into the Ansaldo VFD, which in turn provides a 3-Phase variable frequency AC to the Hyundai IM, which can provide a power of up to 6.1 MW. An overview of this powertrain can be seen in Figure B.1.

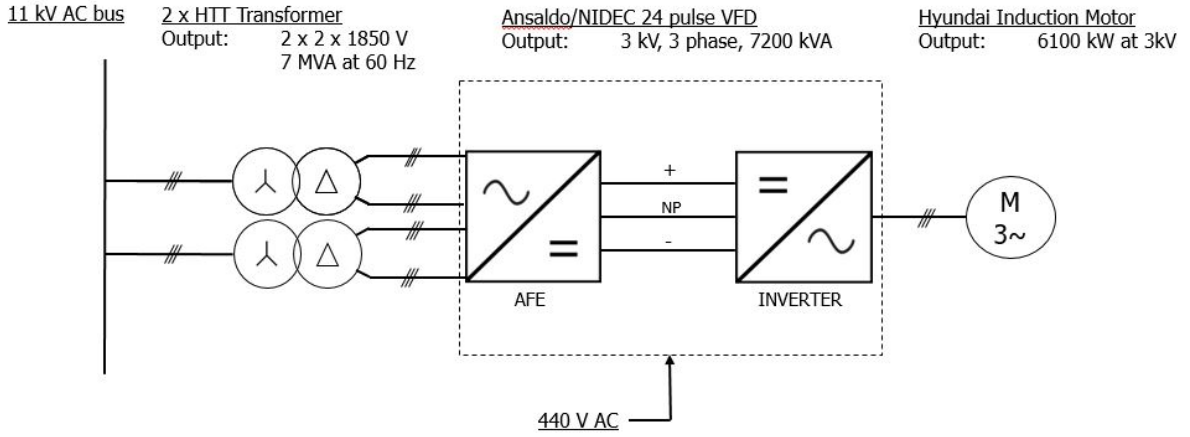

Table B.1: Overview of the electric powertrain of each thruster assembly [34]

B.2.2. Thruster

The thrusters themselves are fabricated by Rolls-Royce Maritime, which has since the fabrication been taken over by Kongsberg Maritime. More information on the thruster and the IM can be found in Table B.2 and Table B.3 respectively. Furthermore, a sectional view of the thruster can be seen in Figure B.2, an overview of the entire mechanical side of the thruster assembly can be seen in Figure B.4 and an overview of the underwater part of the thruster can be seen in Figure B.3. Finally, an overview of the entire assembly including thruster, IM and VFD can be seen in Figure B.5.

Brand	Rolls-Royce
Type	Ulstein Aquamaster UUC 455 FP
Max. power	5.5 MW
Nominal speed in/out	750 RPM/157.3 RPM
Gears	13/62 (ratio = 4.769)
Propeller	Fixed pitch, right handed
Number of blades	4
Function	Main propulsion and DP
Max shaft torque	70.0 kNm

Table B.2: Specifications of a thruster [26]

Brand	Hyundai Heavy Industries
Type	HRN7 1005-88Y, 3 phase
Number of poles	8
Rated power	6.1 MW
Peak power	6.5 MW
In-/output at 750 RPM	5.5 MW; 3 kV; 1200 A; 54.2 Hz
Power factor at 750 RPM	0.9
Efficiency at 750 RPM	97.6 %
Max torque	limited at 70.0 kNm

Table B.3: Specifications of an IM [27]

Thruster assembly overview images

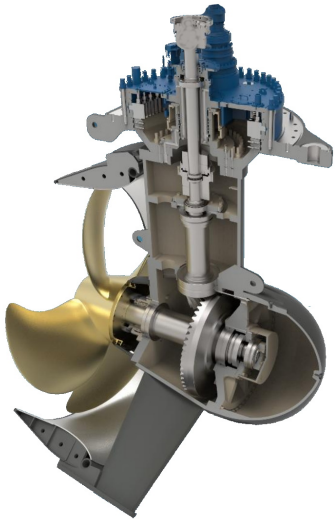

Figure B.2: Inside view of a similar Rolls Royce Ulstein UUC-455 assembly as used on the PS [13]

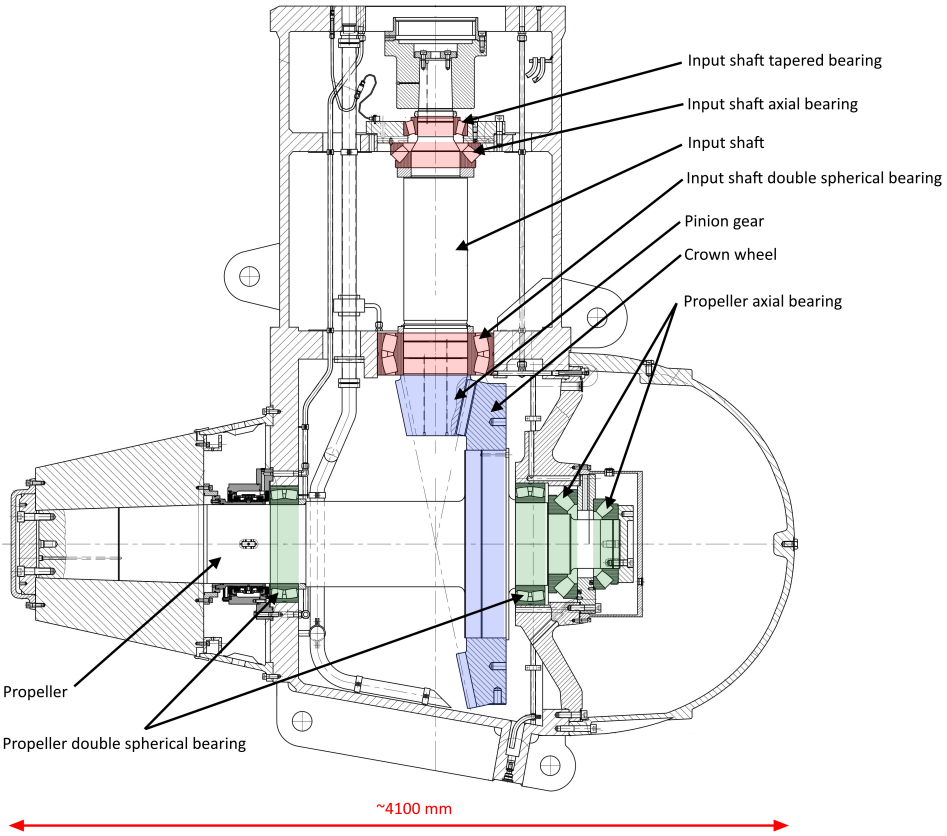

Figure B.3: Overview of the underwater part of the thruster assemblies on the PS [26]

Thruster assembly overview images

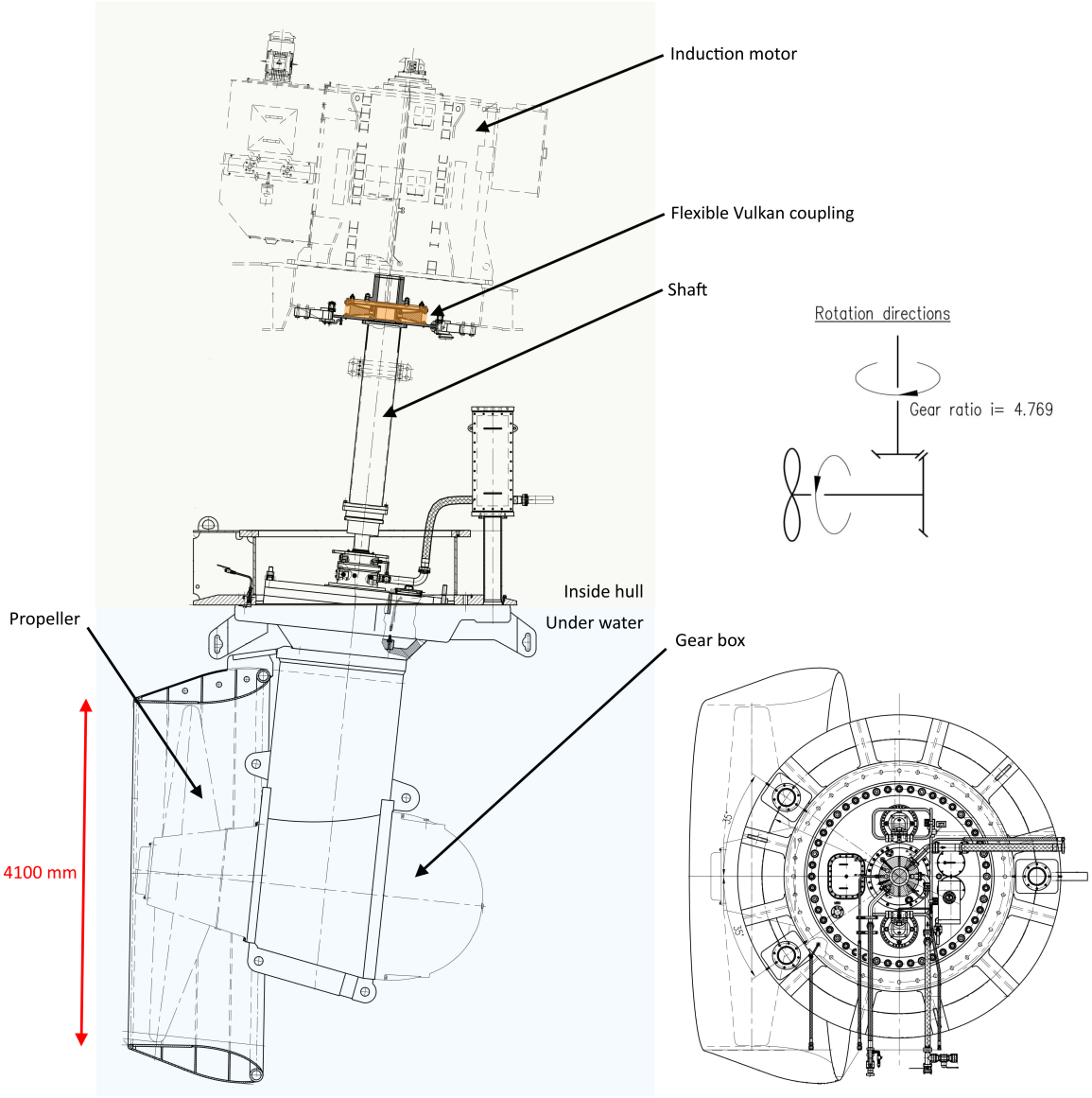

Figure B.4: Overview of the thruster assembly as used on the PS [26], [27]

Thruster assembly overview images

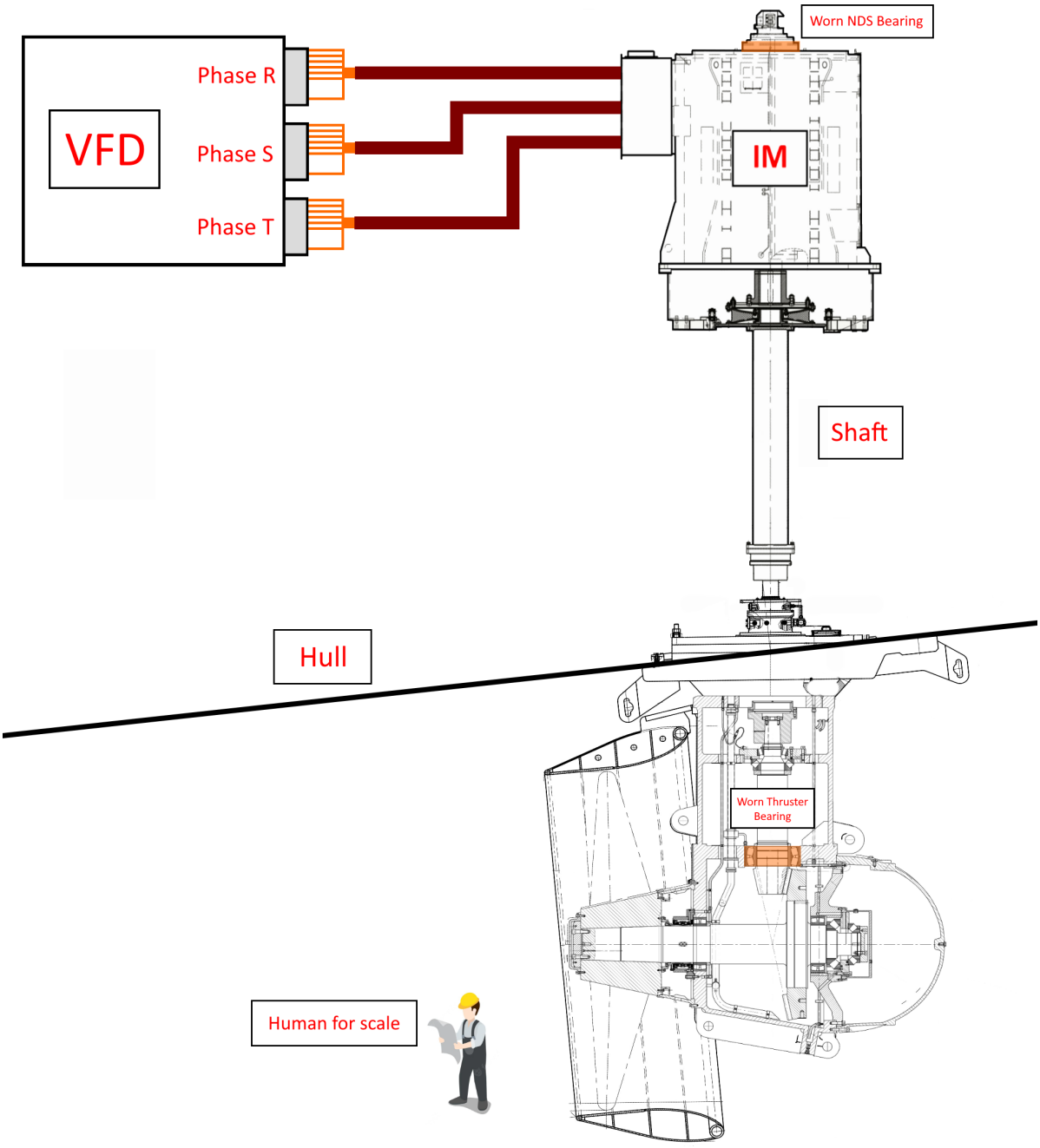

Figure B.5: Overview of the entire thruster assembly [26], [27]

C Measuring setup

ESA Measurements	DAQ	Dewetron Trionet + Trion-1620-LV-6-BNC Measuring card
	Voltage Sensor	Tektronix P6015A High Voltage Probe
	Current Sensor	Danisense DM1200ID + power supply and voltage shunt
	Power Supply	Danisense DSSIU-6-1U-V
	Voltage Shunt	Danisense VOM0800-10 built-in to power supply
Vibration Measurements	Handheld Scanner	VIBExpert II
	DAQ	VIBGuard
	Sensors	VIB 6.142R Integrated Piezo Electric accelerometers
Torque Measurements	Sensor System	Kongsberg MetaPower

Table C.1: Components of the measurement setup

Figure C.1: Sensor setup inside the VFD. The HV probes are connected on top of the bus bars. The Current Transformers are connected around 1 of 7 phase cables.

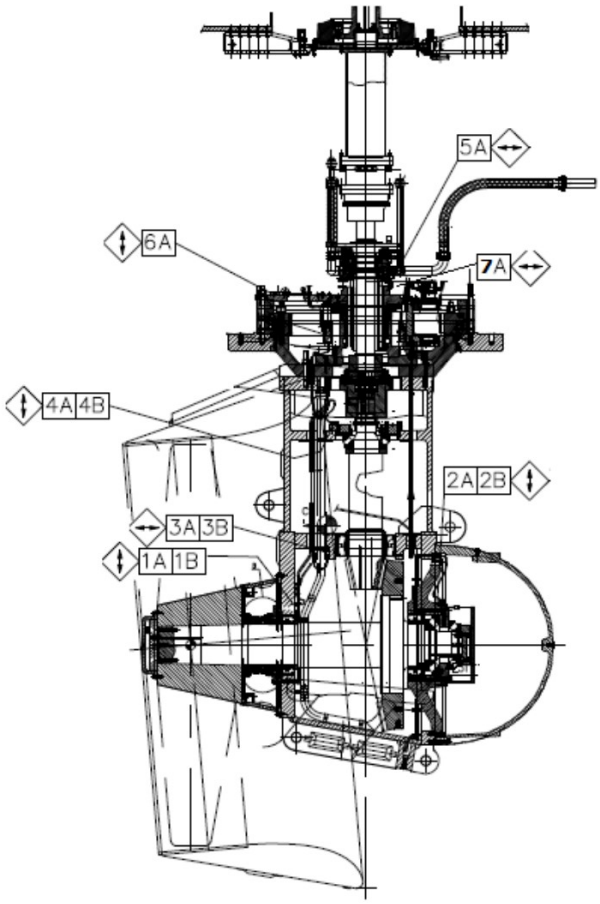

Figure C.2: Vibration sensor locations on the thruster assemblies of the PS [29]

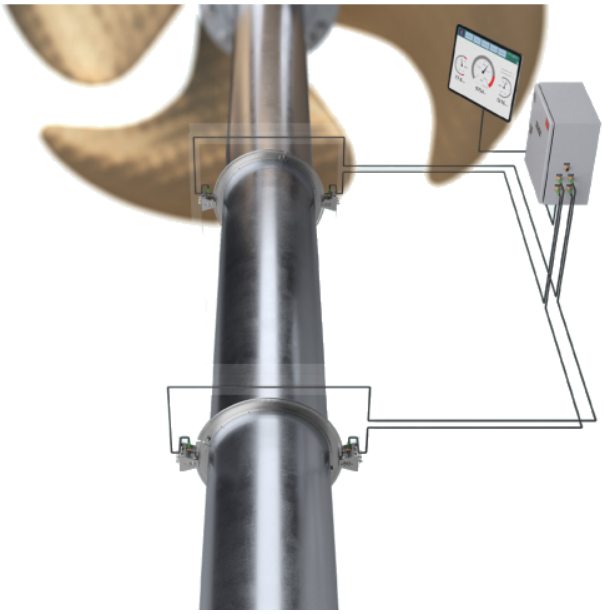

Figure C.3: 3D model of the MetaPower Quad torque measuring system as installed on T1 [16]

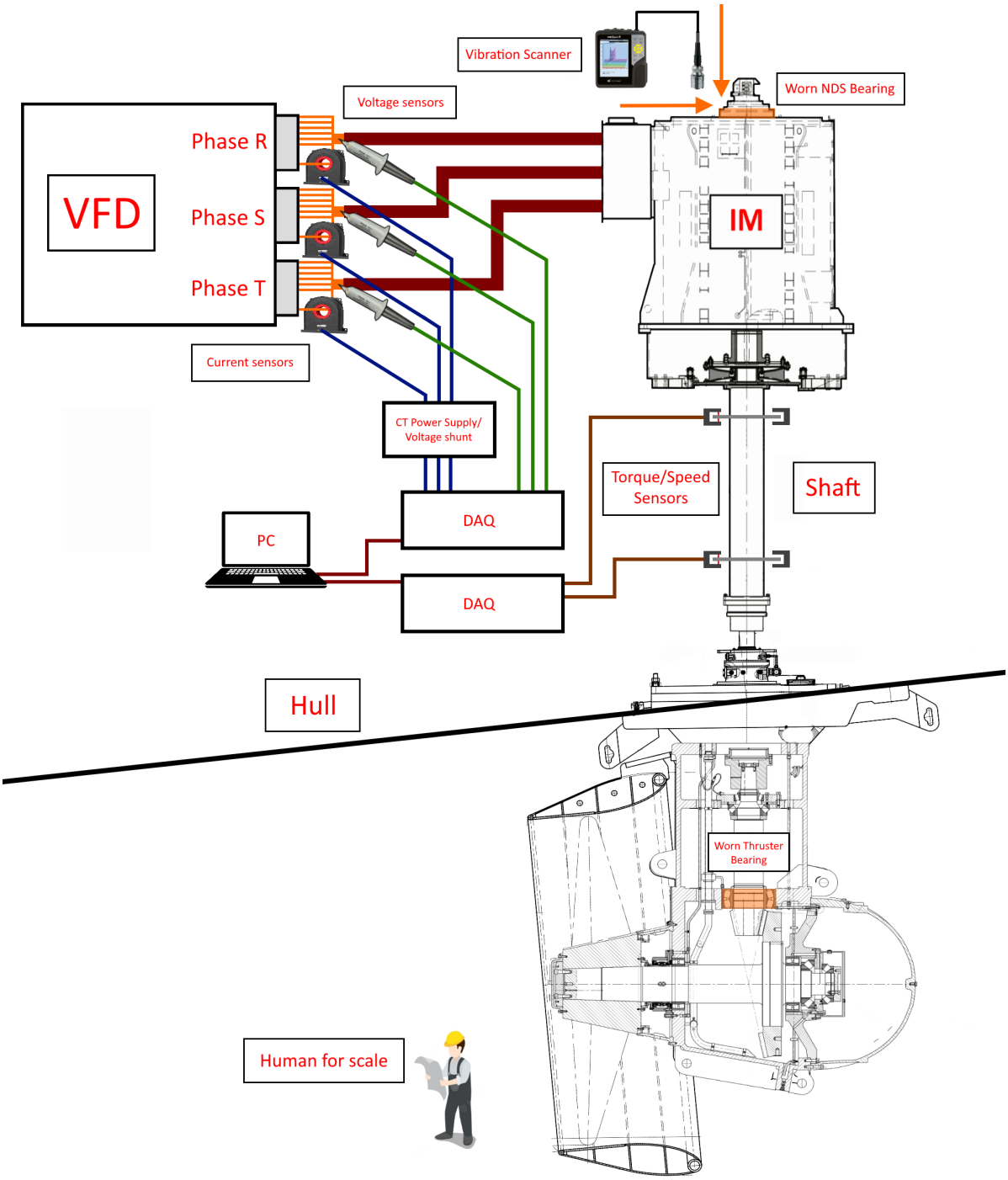

Figure C.4: Overview of the assembly including measuring devices [26], [27]

D Frequency overview

D.0.1. Induction motor and thruster assembly frequencies

This appendix contains the overview of characteristic frequencies as presented in Chapter 3 and calculated for the thruster assemblies of the PS. The excel file shown in Figure D.1 and Figure D.2 contains the mechanical and electrical frequencies, as well as their harmonics, calculated for a certain shaft frequency and drive frequency. These calculated frequencies can then be identified in the spectra created by EPVA or originating from mechanical vibration or torque vibration sensors. For the current and voltage spectra created by EPVA this approach works as follows:

- First, the drive frequency needs to be determined. This preferably done by using the single phase current spectrum and detecting its highest peak, which can be done using a simple Matlab script. This value is filled into the 'Fdrive' cell. After this step, it is best to switch to the EPVA spectrum.
- The 'Fshaft estimate' cell takes 'Fdrive' and divides it by 4 (number of pole pairs). This value will give an estimate of the shaft frequency if the slip were to be 0.
- Now, the EPVA spectrum is analysed to find the closest peak to 'Fshaft estimate'. This peak will be the actual shaft frequency and its value will be filled into the 'Fshaft' cell. In order to find an even more accurate value for the motor shaft frequency it is also possible to search for the gear mesh frequency in the spectrum and divide this value by 13, which is the order of the gear mesh frequency. When using this method in a spectrum with a resolution of 0.2 Hz, the motor shaft frequency can be determined with an accuracy of $\pm$ 0.008 Hz.
- All remaining mechanical frequencies are related to the actual shaft frequency and are now calculated.
- The slip frequency is calculated using both the shaft frequency and drive frequency.

Take from spectrum:	**Fdrive:**	**4.05**	**Fshaft estimate:**	**1.0125**	**Fshaft:**	**1.00**			
	1st	**Harmonics**							
F_	**[Hz]**	**2 [Hz]**	**3 [Hz]**	**4 [Hz]**	**5 [Hz]**	**6 [Hz]**	**7 [Hz]**	**8 [Hz]**	**9 [Hz]**	**10 [Hz]**
Electrical Frequencies										
Drive	4.05	8.1	12.15	16.2	20.25	24.3	28.35	32.4	36.45	40.5
Slip	0.013	0.025	0.037	0.050	0.062	0.075	0.087	0.100	0.113	0.125
Mechanical Frequencies										
Motor shaft	1.00	2.00	3.00	4.00	5.00	6.00	7.00	8.00	9.00	10.00
Propeller Shaft	0.21	0.42	0.63	0.84	1.05	1.26	1.47	1.68	1.89	2.10
BPF	0.84	1.68	2.52	3.35	4.19	5.03	5.87	6.71	7.55	8.39
Gear mesh	13.0	26.00	39.00	52.00	65.00	78.00	91.00	104.00	117.00	130.00
Bearing IM DS										
BPFO	6.62	13.23	19.85	26.46	33.08	39.70	46.31	52.93	59.54	66.16
BPFI	8.38	16.77	25.15	33.54	41.92	50.30	58.69	67.07	75.46	83.84
BSF	4.18	8.36	12.54	16.72	20.91	25.09	29.27	33.45	37.63	41.81
FTF	0.44	0.88	1.32	1.76	2.21	2.65	3.09	3.53	3.97	4.41
Bearing IM NDS										
BPFO	5.43	10.86	16.29	21.72	27.15	32.58	38.01	43.44	48.87	54.30
BPFI	7.57	15.14	22.71	30.28	37.85	45.42	52.99	60.56	68.13	75.70
BSF	2.26	4.53	6.79	9.05	11.32	13.58	15.84	18.10	20.37	22.63
FTF	0.42	0.84	1.25	1.67	2.09	2.51	2.93	3.34	3.76	4.18

Figure D.1: Overview of characteristic frequencies and their harmonics. The shaft speed is purposefully set to 1 Hz, as this means that all other mechanical frequencies now appear as their order of the shaft speed.

D.0.2. Thruster bearing frequencies

Take from spectrum:	Fdrive:	4.05	Fshaft estimate:	1.0125	Fshaft:	1.00			
	1st	Harmonics							
F_	[Hz]	2 [Hz]	3 [Hz]	4 [Hz]	5 [Hz]	6 [Hz]	7 [Hz]	8 [Hz]	9 [Hz]	10 [Hz]
Thruster bearing 1										
BPFO	8.62	17.23	25.85	34.47	43.09	51.70	60.32	68.94	77.55	86.17
BPFI	11.38	22.77	34.15	45.53	56.91	68.30	79.68	91.06	102.45	113.83
BSF	3.44	6.88	10.32	13.75	17.19	20.63	24.07	27.51	30.95	34.39
FTF	0.43	0.86	1.29	1.72	2.15	2.59	3.02	3.45	3.88	4.31
Thruster bearing 2										
BPFO	7.94	15.89	23.83	31.78	39.72	47.67	55.61	63.55	71.50	79.44
BPFI	10.06	20.11	30.17	40.22	50.28	60.33	70.39	80.45	90.50	100.56
BSF	2.98	5.97	8.95	11.93	14.92	17.90	20.88	23.86	26.85	29.83
FTF	0.44	0.8826	1.32	1.77	2.21	2.65	3.09	3.53	3.97	4.41
Thruster bearing 3										
BPFO	8.16	16.31	24.47	32.63	40.78	48.94	57.10	65.25	73.41	81.57
BPFI	10.84	21.69	32.53	43.37	54.22	65.06	75.90	86.75	97.59	108.44
BSF	3.37	6.73	10.10	13.47	16.83	20.20	23.57	26.93	30.30	33.67
FTF	0.43	0.86	1.29	1.72	2.15	2.58	3.01	3.43	3.86	4.29
Thruster bearing 4										
BPFO	1.67	3.33	5.00	6.66	8.33	9.99	11.66	13.33	14.99	16.66
BPFI	2.11	4.22	6.33	8.43	10.54	12.65	14.76	16.87	18.98	21.08
BSF	0.63	1.25	1.88	2.50	3.13	3.75	4.38	5.00	5.63	6.25
FTF	0.09	0.19	0.28	0.37	0.46	0.56	0.65	0.74	0.83	0.93
Thruster bearing 5										
BPFO	1.77	3.55	5.32	7.09	8.86	10.64	12.41	14.18	15.96	17.73
BPFI	2.21	4.42	6.63	8.84	11.06	13.27	15.48	17.69	19.90	22.11
BSF	0.67	1.33	2.00	2.67	3.33	4.00	4.67	5.34	6.00	6.67
FTF	0.09	0.19	0.28	0.37	0.47	0.56	0.65	0.75	0.84	0.93
Thruster bearing 6										
BPFO	2.75	5.50	8.26	11.01	13.76	16.51	19.26	22.02	24.77	27.52
BPFI	3.33	6.66	9.99	13.31	16.64	19.97	23.30	26.63	29.96	33.29
BSF	1.08	2.17	3.25	4.34	5.42	6.51	7.59	8.68	9.76	10.85
FTF	0.09	0.19	0.28	0.38	0.47	0.57	0.66	0.76	0.85	0.95
Thruster bearing 7										
BPFO	2.75	5.50	8.26	11.01	13.76	16.51	19.26	22.01	24.77	27.52
BPFI	3.33	6.66	9.99	13.32	16.64	19.97	23.30	26.63	29.96	33.29
BSF	1.08	2.17	3.25	4.34	5.42	6.51	7.59	8.67	9.76	10.84
FTF	0.09	0.19	0.28	0.38	0.47	0.57	0.66	0.76	0.85	0.95

Figure D.2: Similar overview as in Figure D.1 containing the bearing frequencies from all bearings in the thruster. The bearings are numbered from top to bottom and right to left. Bearing 3 is the bearing showing wear in T3.

D.0.3. Sideband frequencies

In the analysis of the single phase spectra directly created from the stator current or voltage, the mechanical frequencies will appear as sidebands of the drive frequency. An overview of some mechanical frequencies and their sideband frequencies is shown in Figure D.3. This excel file continues for all other frequencies as shown in Figure D.1 and Figure D.2.

Also, this file contains the ship AC frequency and switching frequencies as these would not appear as sideband frequencies of the drive frequency. These will thus only be visible at their original frequency in the stator and voltage spectra before the Clarke transform. Note that the ship AC frequency and the switching frequencies are set values and are unrelated to any other frequency. The switching frequencies are actually 325 Hz and 650 Hz, according to the technical datasheet of the IM. However, in the current spectra they are measured to be 666.9 Hz and 333.4 Hz.

The process of identifying the different frequencies works similar to process shown in Section D.0.1. However, the motor shaft frequency is now determined by searching in the spectrum for the first positive sideband of the motorshaft frequency on the drive frequency, with roughlyt the value of 'Fshaft estimate'. To get the actual motor shaft frequency, the frequency of this peaks is substracted from the drive frequency.

Taken from spectrum:	Fdrive: 46.20			Fshaft estimate: 11.55		Fshaft: 11.5			
	1st Harmonics								
F_	[Hz]	2 [Hz]	3 [Hz]	4 [Hz]	5 [Hz]	6 [Hz]	7 [Hz]	8 [Hz]	9 [Hz]	10 [Hz]
Electrical Frequencies										
Drive	46.20	92.4	138.6	184.8	231	277.2	323.4	369.6	415.8	462
Slip	0.050	0.1	0.15	0.2	0.25	0.3	0.35	0.4	0.45	0.5
Ship AC	60.00	120	180	240	300	360	420	480	540	600
Switch High	667.00	1334	2001	2668	3335	4002	4669	5336	6003	6670
Switch Low	333.50	667	1000.5	1334	1667.5	2001	2334.5	2668	3001.5	3335
Mechanical Frequencies										
Motor shaft	11.50	23.00	34.50	46.00	57.50	69.00	80.50	92.00	103.50	115.00
Sideband -1	34.70	23.20	11.70	0.20	11.30	22.80	34.30	45.80	57.30	68.80
Sideband +1	57.70	69.20	80.70	92.20	103.70	115.20	126.70	138.20	149.70	161.20
Propeller Shaft	2.41	4.82	7.23	9.65	12.06	14.47	16.88	19.29	21.70	24.11
Sideband -1	43.79	41.38	38.97	36.55	34.14	31.73	29.32	26.91	24.50	22.09
Sideband +1	48.61	51.02	53.43	55.85	58.26	60.67	63.08	65.49	67.90	70.31
BPF	9.65	19.29	28.94	38.58	48.23	57.87	67.52	77.16	86.81	96.45
Sideband -1	36.55	26.91	17.26	7.62	2.03	11.67	21.32	30.96	40.61	50.25
Sideband +1	55.85	65.49	75.14	84.78	94.43	104.07	113.72	123.36	133.01	142.65
Gear mesh	149.50	299.00	448.50	598.00	747.50	897.00	1046.50	1196.00	1345.50	1495.00
Sideband -1	103.30	252.80	402.30	551.80	701.30	850.80	1000.30	1149.80	1299.30	1448.80
Sideband +1	195.70	345.20	494.70	644.20	793.70	943.20	1092.70	1242.20	1391.70	1541.20

Figure D.3: Sideband frequencies of mechanical frequencies modulated on the drive frequency.

E Matlab script

System constants, torque and power calculation

This code represents the torque and power calculation, as introduced in Chapter 3 by first loading and estimating the system constants. This code was provided by Dr. A. Veltman (Piak Electronics BV).

```
1
2  %% System constants, torque calculation, power calculation
3
4  % System constants:
5  Ncoils = 7;                                                    %number of parallel coils
       in machine
6  np = 4;                                                        %polepairs
7
8  % Estimated from data:
9  Ls = 0.735e-3;                                                 %0.638e-3;
10 Lm = 0.012814;                                                 %will tend to get bigger at
       lower flux levels (magnetic saturation).
11
12 % PU analysis
13 Pn   = 6e6;
14 UnLL = 3000/sqrt(2);
15 UnLN = UnLL/sqrt(3);                                           %Vrms LN
16 In   = Pn/3/UnLN;                                             %Arms L
17 Zn   = UnLN/In;                                               %ohms LN
18 Rs   = 0.01*Zn;                                               %Rough guess: about 1%
19 Rr   = (2/3)*Rs;                                              %Zoals later aangepast
20 Tr   = Lm/Rr                                                  %check rotor time constant
       approximate value....
21
22 % Integration constants
23 t = t1;
24 t   = t-t(1);
25 dt  = t(2)-t(1);
26 fs  = 1/dt;
27 fnyq = 0.5*fs;
28
29 % Flux
30 whp = 2*pi*1;
31 s=tf('s');
32 D = 0.5*sqrt(3);                                              %Bessel tuning
33 Hhp = s/whp^2 /(s^2/whp^2 + 2*D*s/whp + 1);                   %second order bandpass:
       pure integrator above whp.
34 Heq = s^2/whp^2 /(s^2/whp^2 + 2*D*s/whp + 1);                 %second order hipass
35
36 FC0 = lsim(Hhp,UC,t);                                         %Stator-Flux
37 FC = lsim(Hhp,UC-Rs*IC,t);                                    %Stator-Flux
38 FR = FC-IC*Ls;                                               %Rotor-Flux (roundest
       solution)
39
40 % Complex torque and power
41
42 TC1  = np* 1.5*(IC1.* conj(FC1));                             %Imag = torque, Real =
       attraction
43 PC1 =  1.5*(UC1.*conj(IC1));                                  %Imag = Reactive power,
       Real = Active power
```

Creating frequency spectra through FFT algorithm

This code presents the creation of all frequency spectra, including the spectra normalized by the motor shaft speed. However, for the Kongsberg MetaPower torque spectra the sampling frequency and motor shaft frequency were calculated manually per data set.

```
1
2  %% Frequency spectrum through FFT
3
4  % Setting up FFT
5
6  N = length(IC);
7  T = 1/samplefreq;
8  xf = samplefreq*(0:(N/2))/N;                                    %Set frequency axis
9  w = hann(N);                                                    %Hanning window
10 wb = w./mean(w);
11 fres = (samplefreq/2)/(length(xf)-1);                          %Frequency resolution
12
13 Y = abs(IC);
14 f = fft(Y.*wb);                                                 %FFT algorithm
15
16 P2 = abs(f/N);                                                  %Create real spectrum
17 P1 = P2(1:floor(N/2+1));
18 P1(2:end-1) = 2*P1(2:end-1);
19
20 % Calculate drive frequency and motor shaft frequency
21
22 m1=max(P1(10:end));
23 [a1 b1] = find(P1==m1);
24 ff = xf(a1);                                                   %Fundamental frequency
25
26 m2=max(P1((1/fres*floor(ff/4))-20:floor(1/fres*ff/4)+20));
27 [a2 b2] = find(P2==m2);
28 sf = xf(a2);                                                   %Motor shaft frequency
29
30 % Plot EPVA complex current spectrum
31
32 figure
33 plot(xf, P1)                                                   %Plot frequency spectrum
       complex current
34 plot(xf/sf, P1)                                               %Plot frequency spectrum
       normalized by shaft speed
```

F Results: Extra Graphs

Complex spectrum of i_c

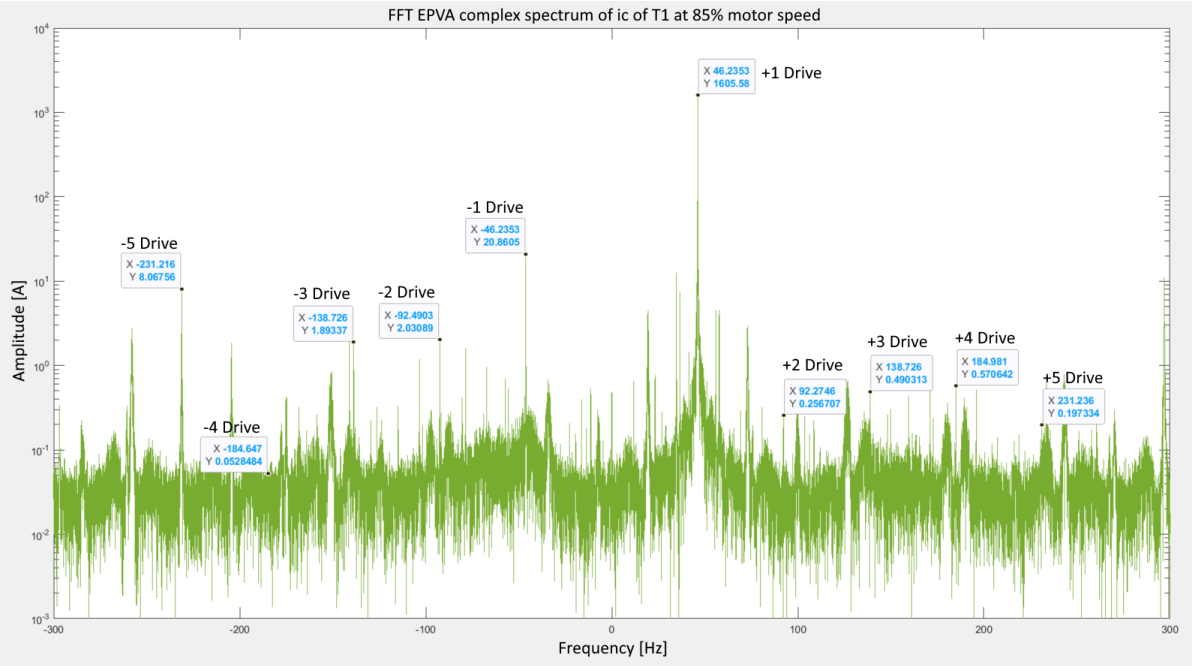

Figure F.1: Complex spectrum of i_c in T1 at 85% motor speed.

Torque during 85% motor speed tests

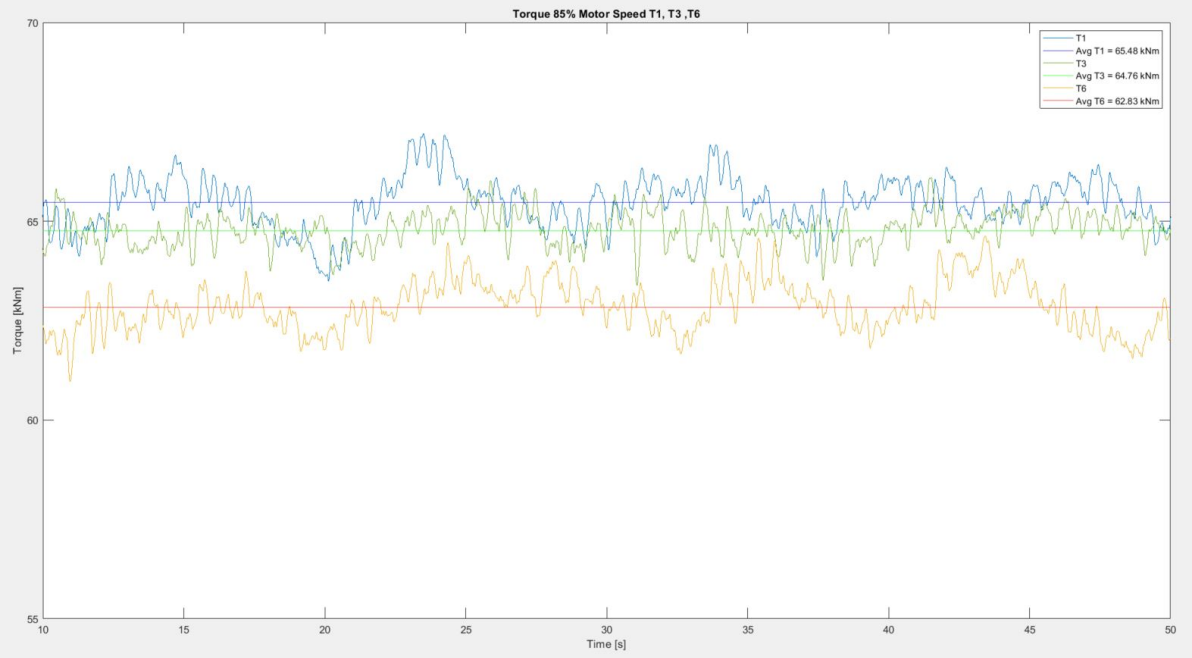

Figure F.2: Calculated torque over time for T1, T3 and T6 during the 85% motor speed measurements. The results are filtered with a 5 Hz LP butterworth filter

Drive frequency during 85% motor speed tests

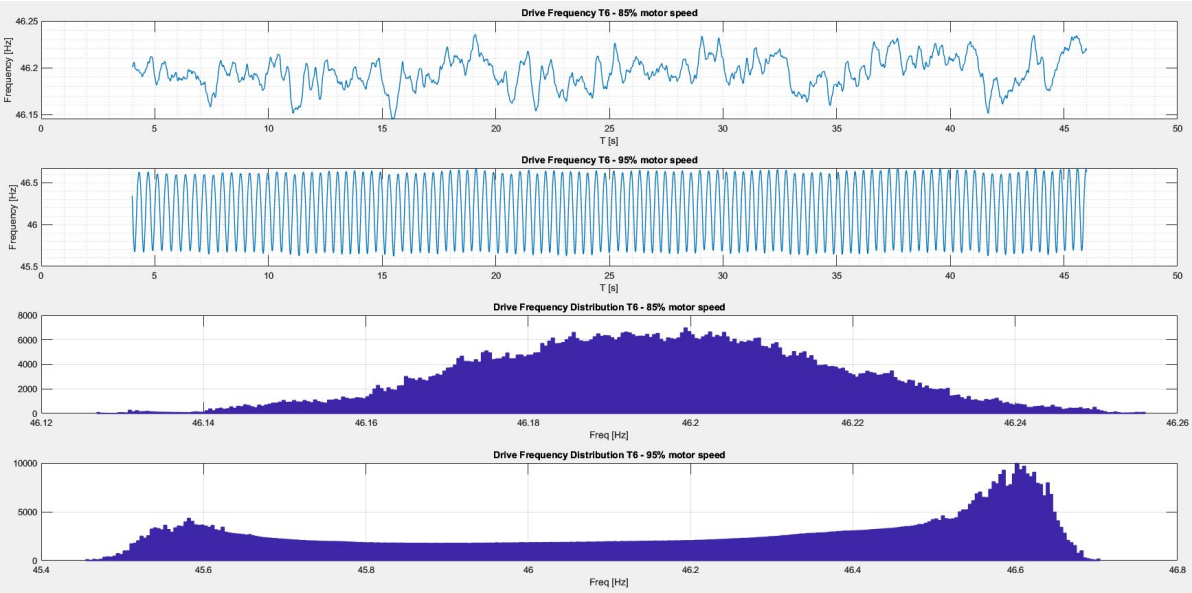

Figure F.3: Drive frequency over time for a measurement at 85% motor speed and 95% motor speed for T6

Single phase current and voltage spectrum

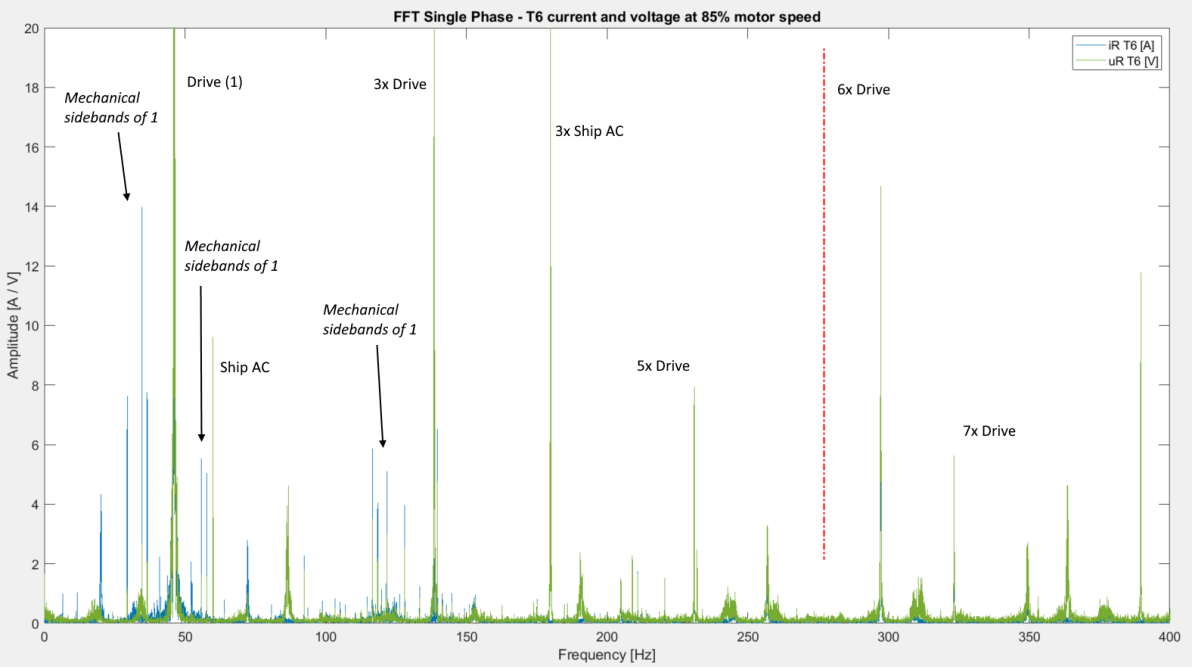

Figure F.4: Single phase current and voltage FFT of T6. Fs = 20 kHz, sample time = 50 s

Single phase current and voltage spectrum

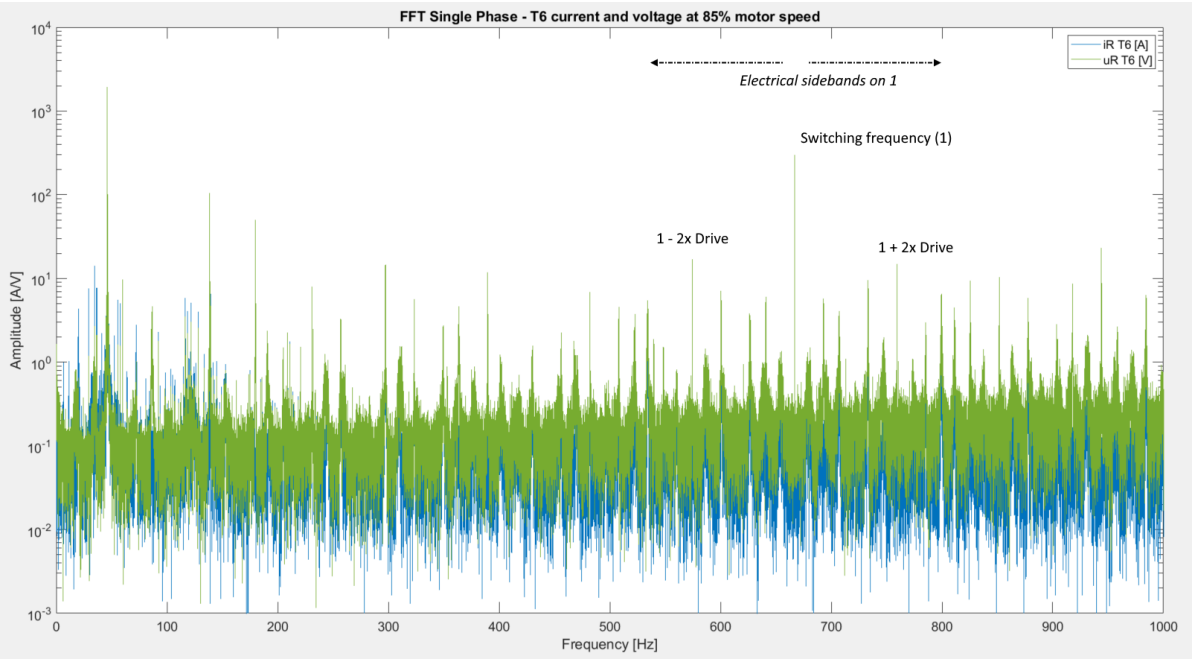

Figure F.5: Single phase current and voltage FFT T6. Fs = 20 kHz, sample time = 50 s

EPVA $|i_c|$ and $|u_c|$ spectrum

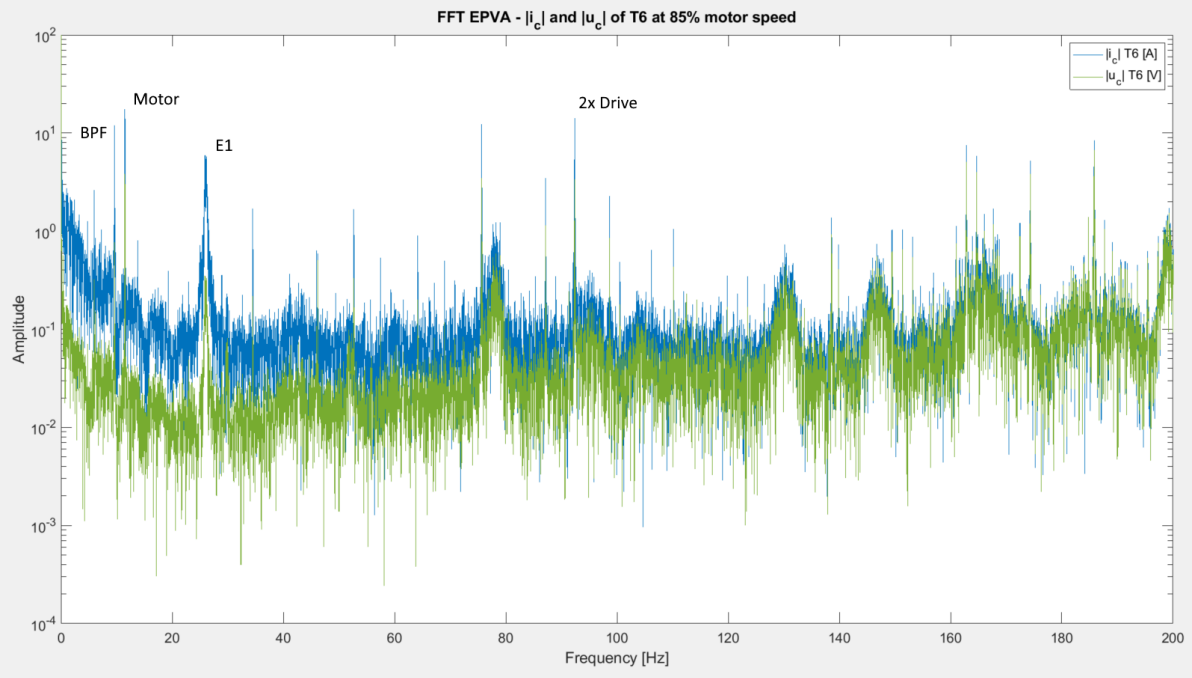

Figure F.6: EPVA $|u_c|$ and $|i_c|$ FFT of T6. Fs = 20 kHz, sample time = 50 s, f_{res} = 0.02 Hz.

Reactive power spectrum

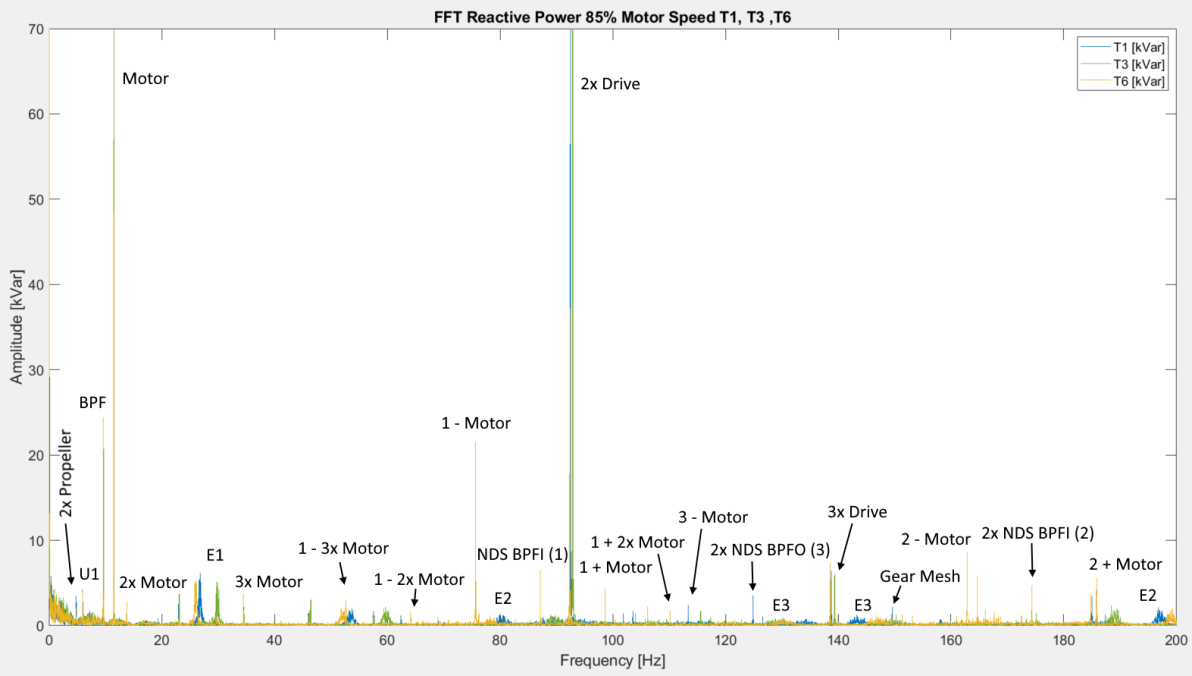

Figure F.7: Reactive power FFT of T1, T3 and T6. Fs = 20 kHz, sample time = 50 s, f_{res} = 0.02 Hz.

Attraction spectrum

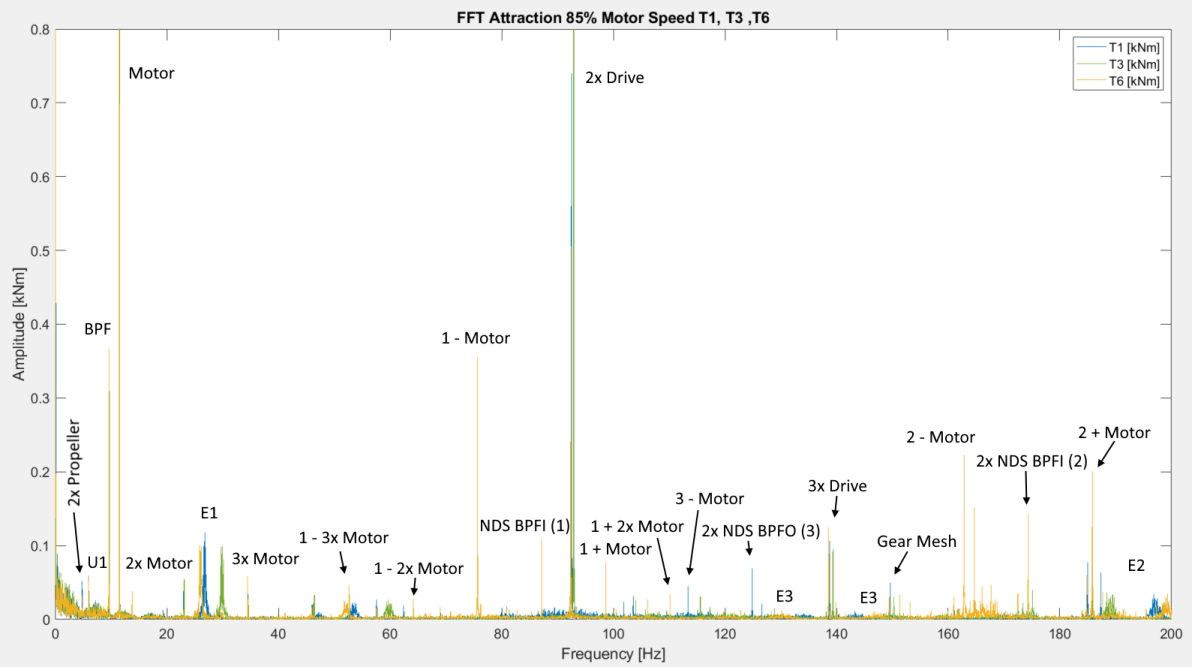

Figure F.8: Attraction FFT of T1, T3 and T6. Fs = 20 kHz, sample time = 50 s, f_{res} = 0.02 Hz.

EPVA Current spectrum of T6 before normalization at 70% - 85% motor speed

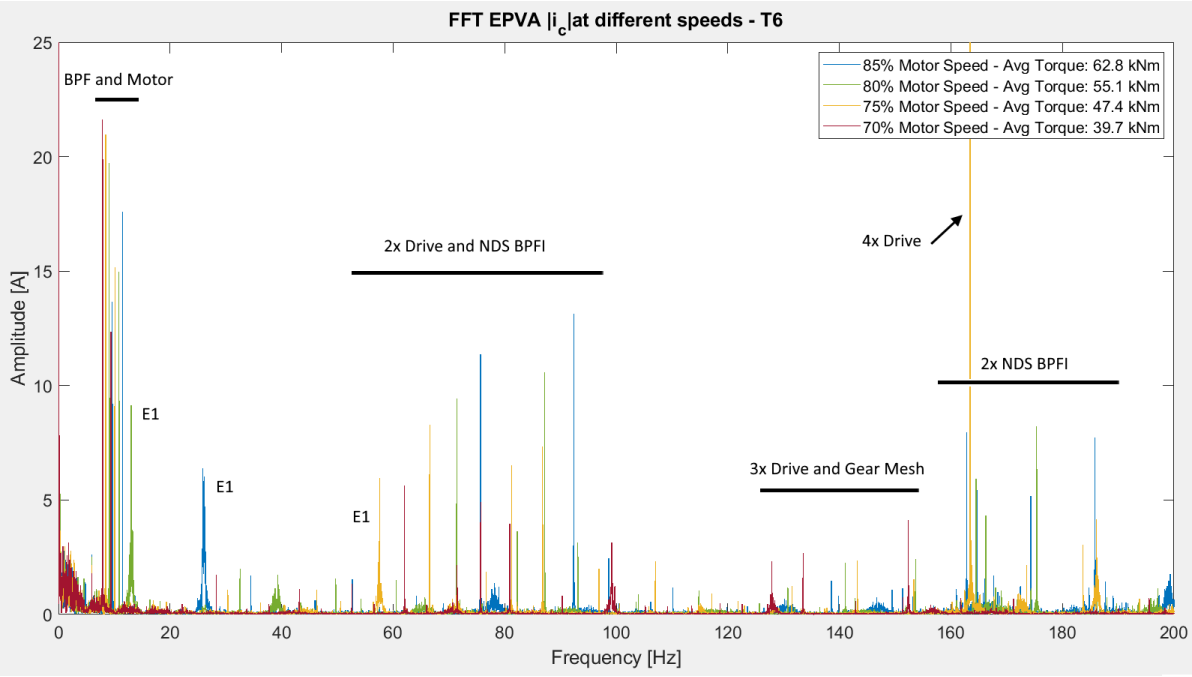

Figure F.9: EPVA $|i_c|$ FFT of T6 at variable speed. Fs = 20 kHz, sample time = 50 s, f_{res} = 0.02 Hz.

EPVA Current spectrum of T6 normalized at 70% - 85% motor speed

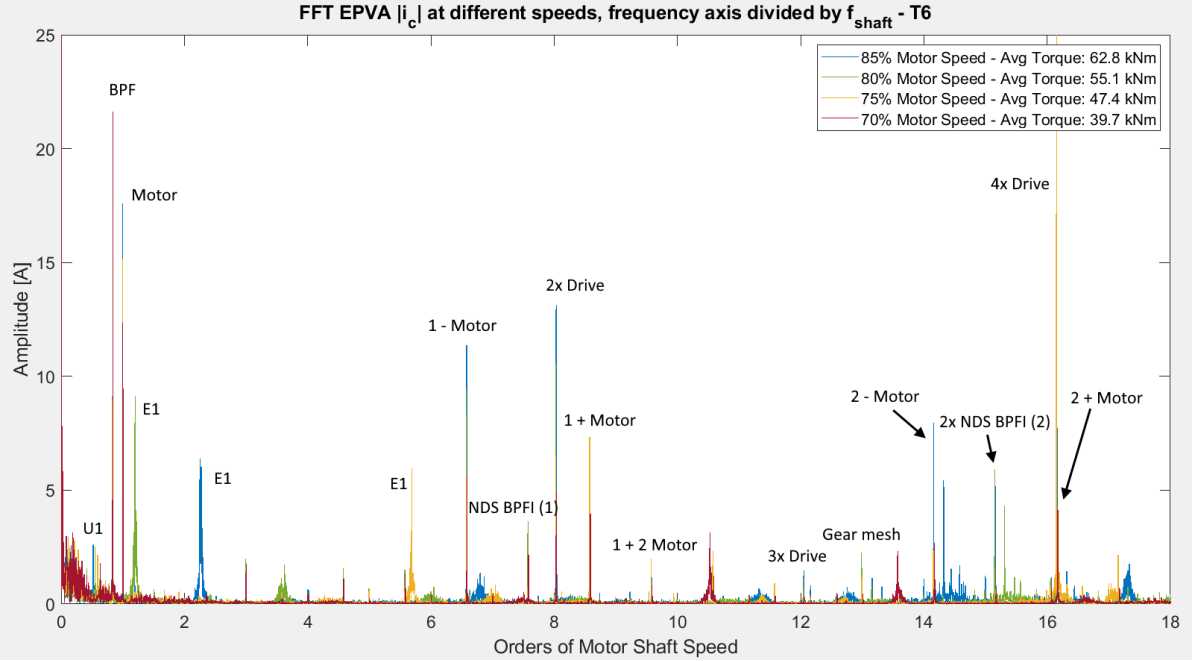

Figure F.10: EPVA $|i_c|$ FFT of T6 at variable speed, frequency axis divided by motor shaft frequency. Fs = 20 kHz, sample time = 50 s, f_{res} = 0.02 Hz.

Torque spectrum of T6 normalized at 40% - 70% motor speed

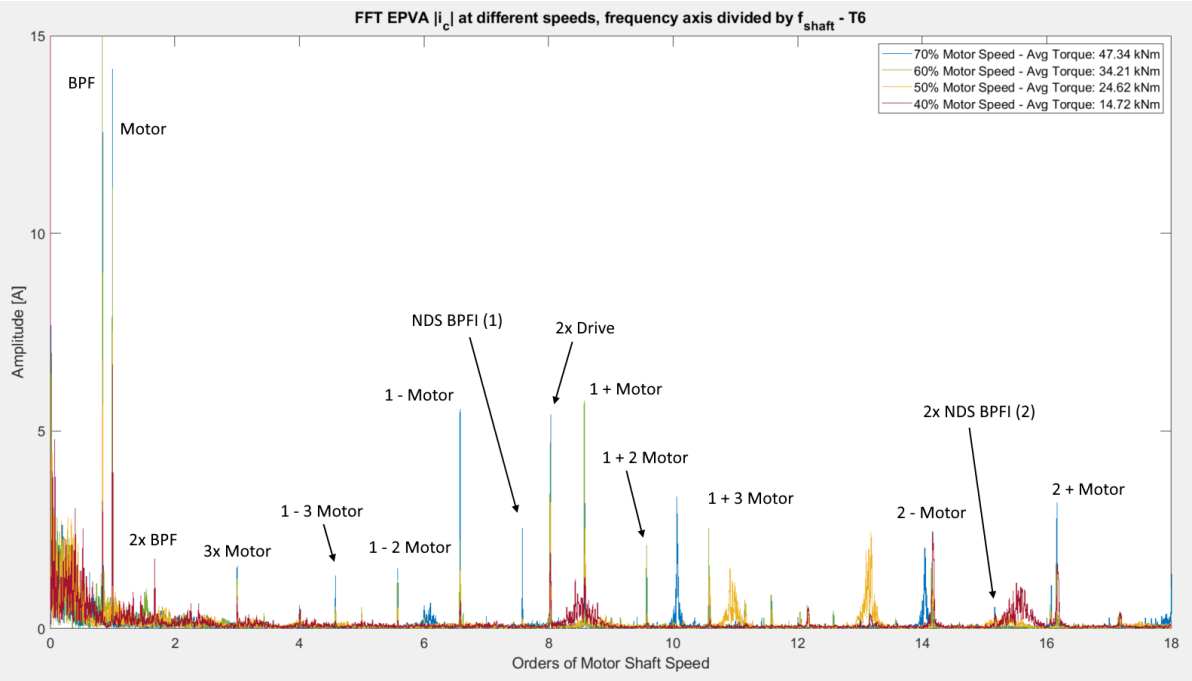

Figure F.11: EPVA $|i_c|$ FFT of T6 at variable speed, frequency axis divided by motor shaft frequency. Fs = 20 kHz, sample time = 50 s, f_{res} = 0.02 Hz.

Torque Spectrum of T6 at 70% motor speed and varying baseline torque

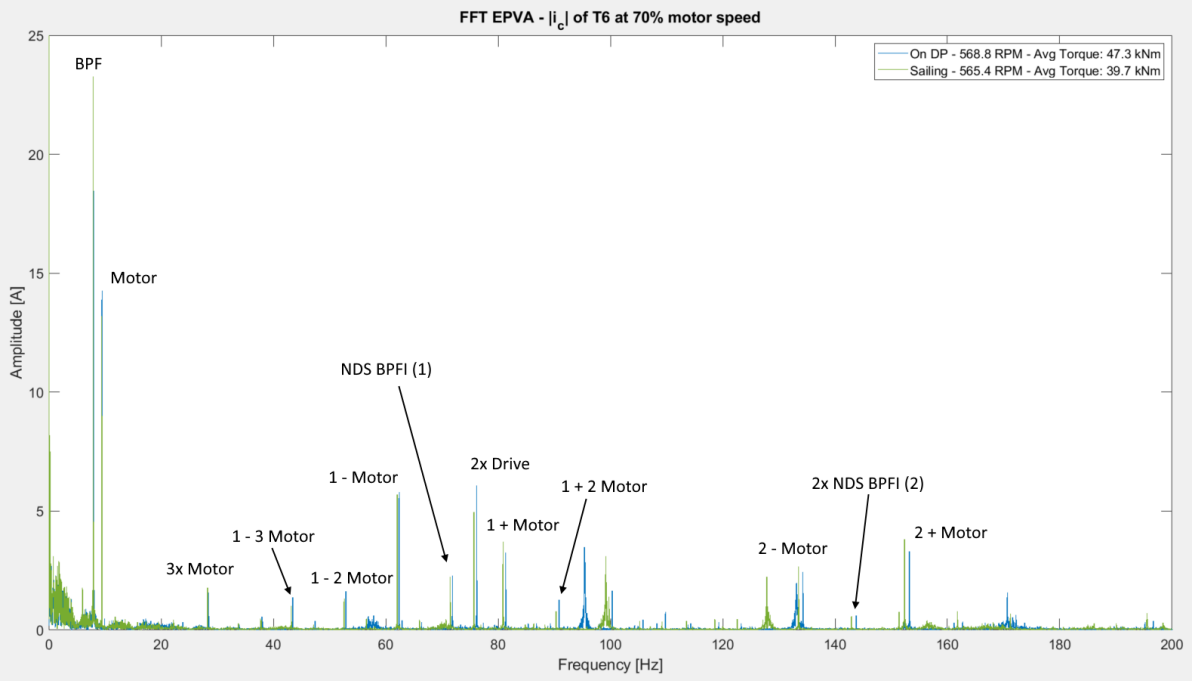

Figure F.12: EPVA $|i_c|$ FFT of T6 at 70% motor speed and varying torque. Fs = 20 kHz, sample time = 50 s, f_{res} = 0.02 Hz.

Close-up of torque spectrum of T6 before normalization at 70% to 85% motor speed

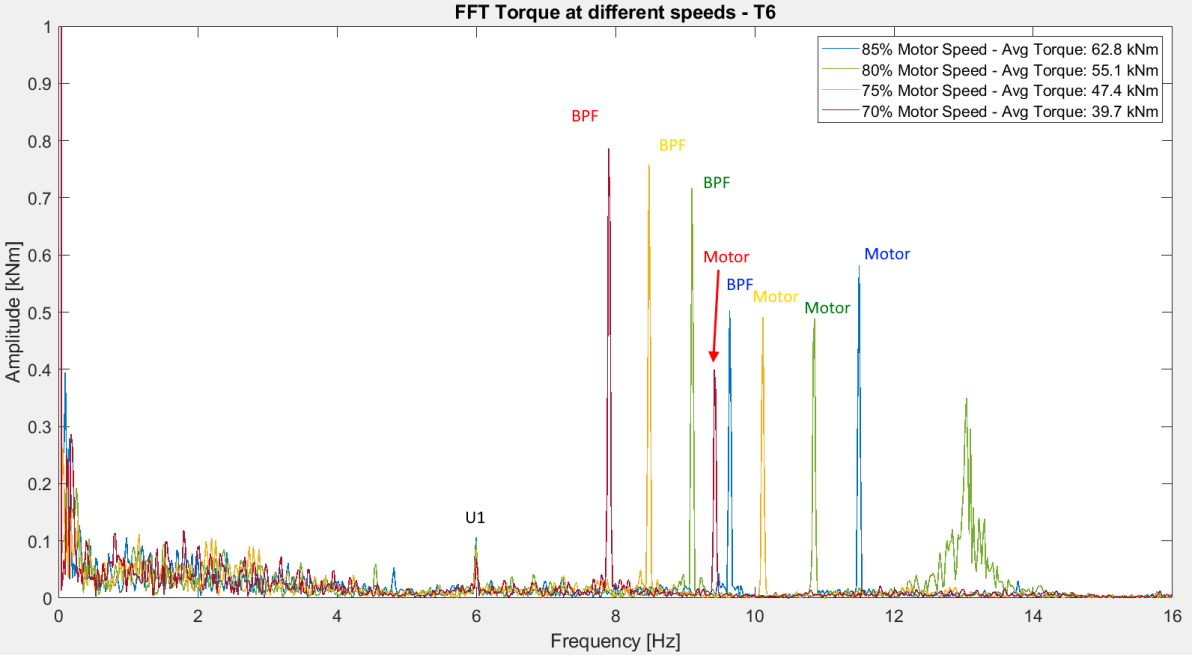

Figure F.13: Torque FFT at different speeds before normalization. Fs = 20 kHz, sample time = 50 s

Torque spectrum of T1 normalized at 70% - 85% speed

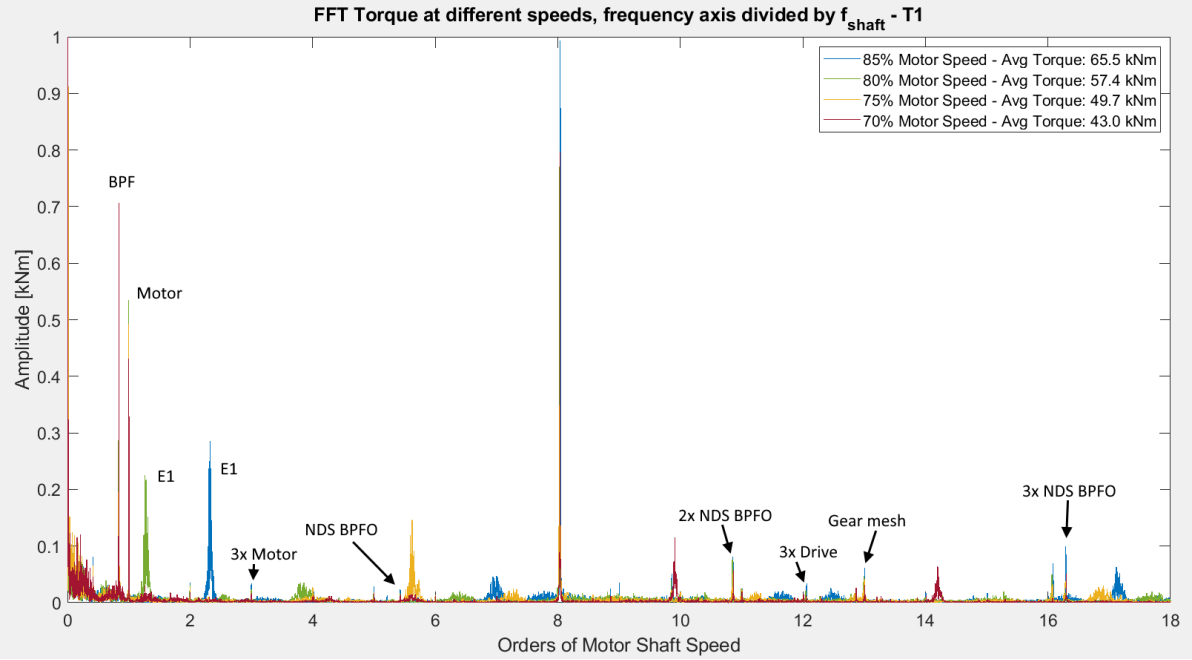

Figure F.14: Torque FFT of T1 at variable speed. Fs = 20 kHz, sample time = 50 s, f_{res} = 0.02 Hz

Mechanical vibration 90° direction, high speed

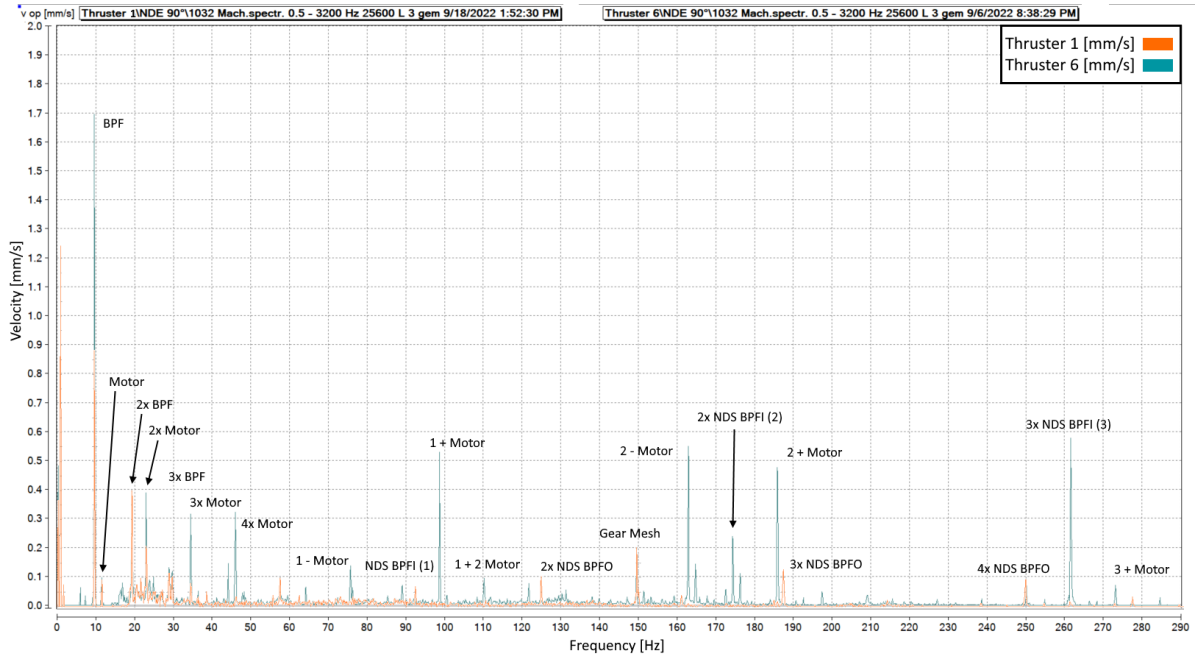

Figure F.15: Mechanical Vibration Velocity Spectrum of T1 and T6 at 90°. f_s = 25.6 kHz, sample time = 8 s, f_{res} = 0.125 Hz.

Mechanical vibration of sensor 3 of T3 at the highest available speed

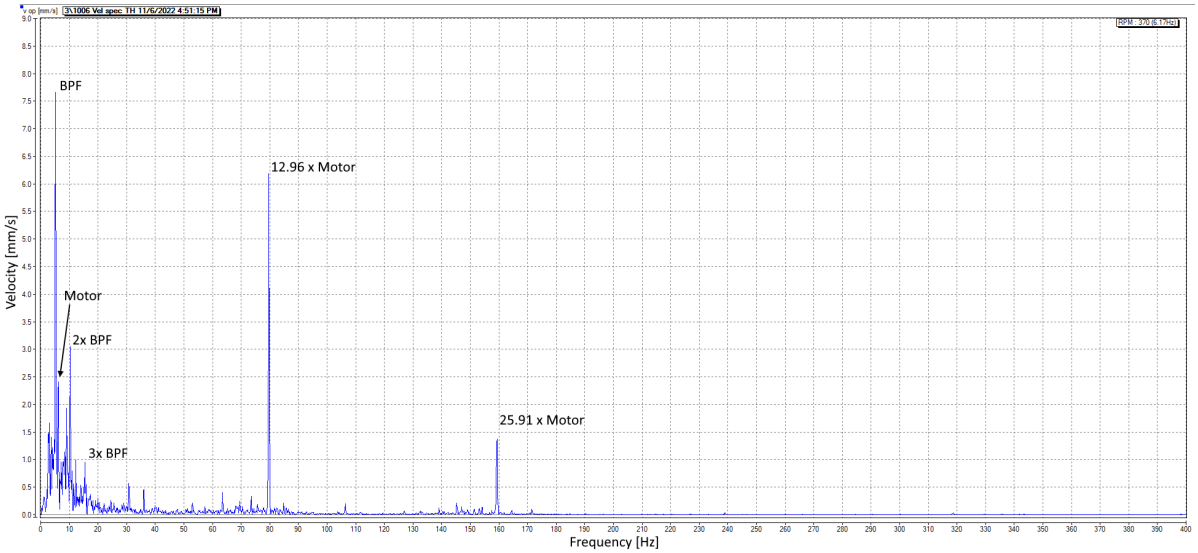

Figure F.16: Velocity spectrum of sensor 3 at 370 RPM (49%)

Mechanical vibration 90° direction of T6, low speed

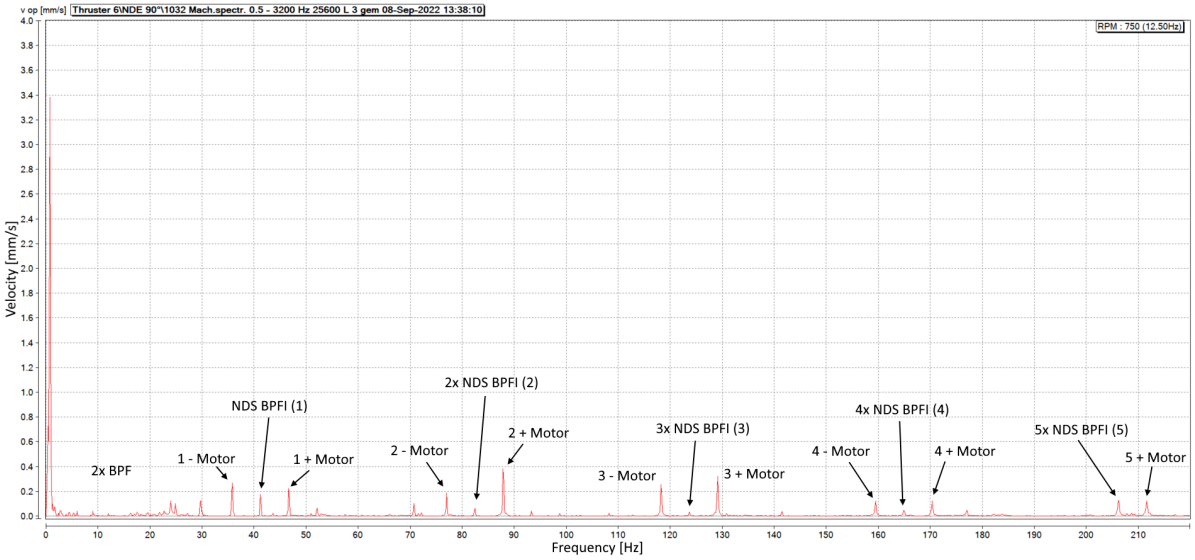

Figure F.17: Mechanical Vibration Velocity Spectrum of T6 at 90°- 40% motor speed. f_s = 25.6 kHz, sample time = 8 s, f_{res} = 0.125 Hz.

Mechanical vibration axial direction of T6, low speed

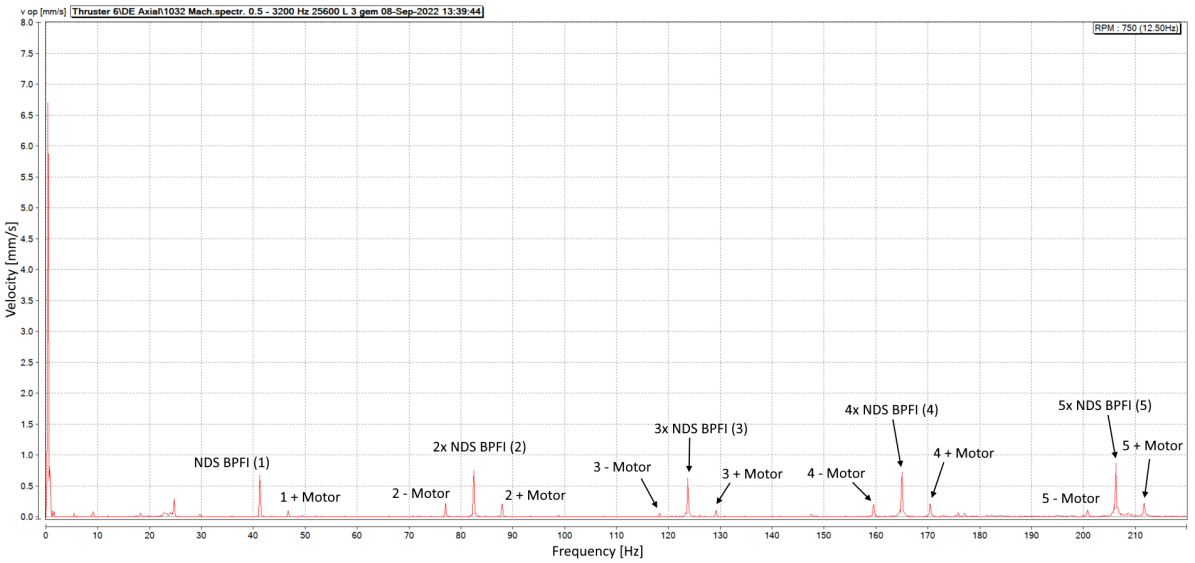

Figure F.18: Mechanical Vibration Velocity Spectrum of T6 axial. - 40% motor speed. f_s = 25.6 kHz, sample time = 8 s, f_{res} = 0.125 Hz.

Shaft torque spectrum of T1 at 40% - 70% speed

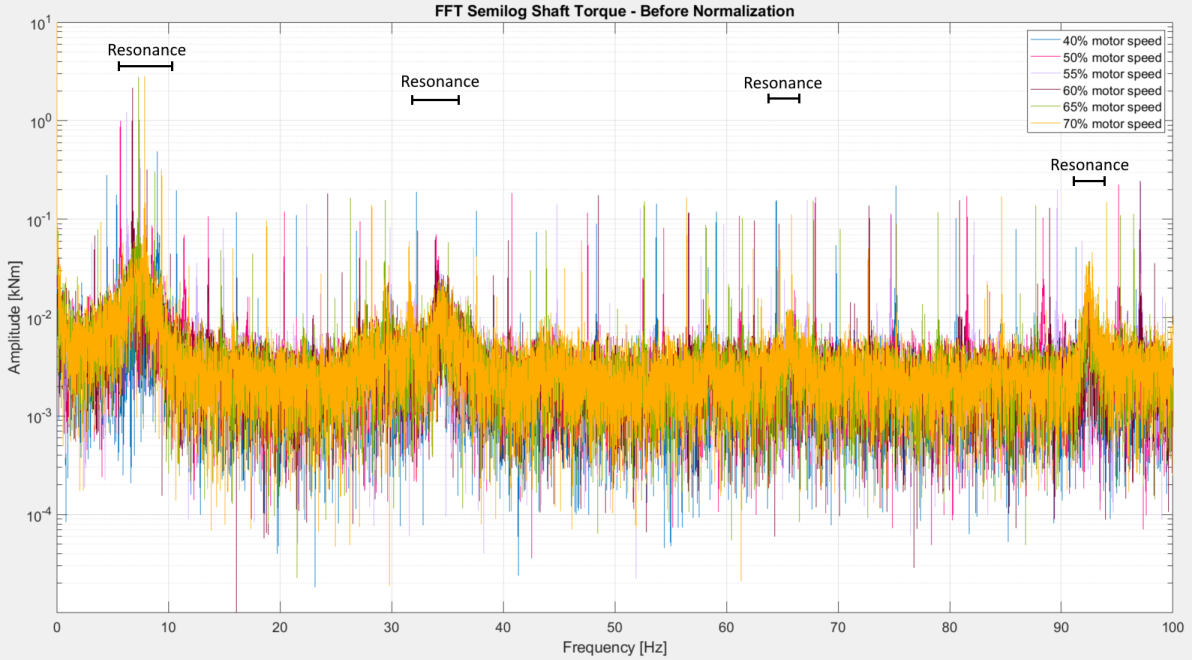

Figure F.19: Torque FFT of T1 at different speeds of Kongsberg MetaPower, sample time = 25s.

Shaft torque spectrum of T1 at 40% and 70% speed

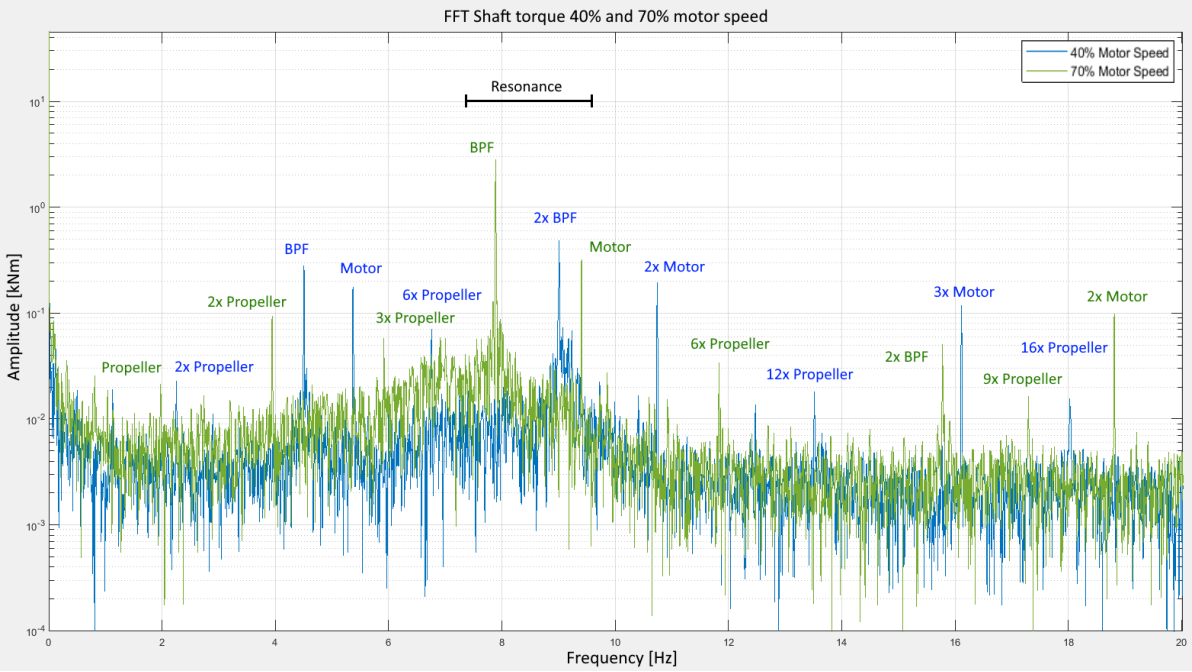

Figure F.20: Torque FFT of T1 at 40% speed (800 Hz) and 70% speed (1600 Hz) of Kongsberg MetaPower, sample time = 25s.

Shaft power spectrum of T1 at 70% speed

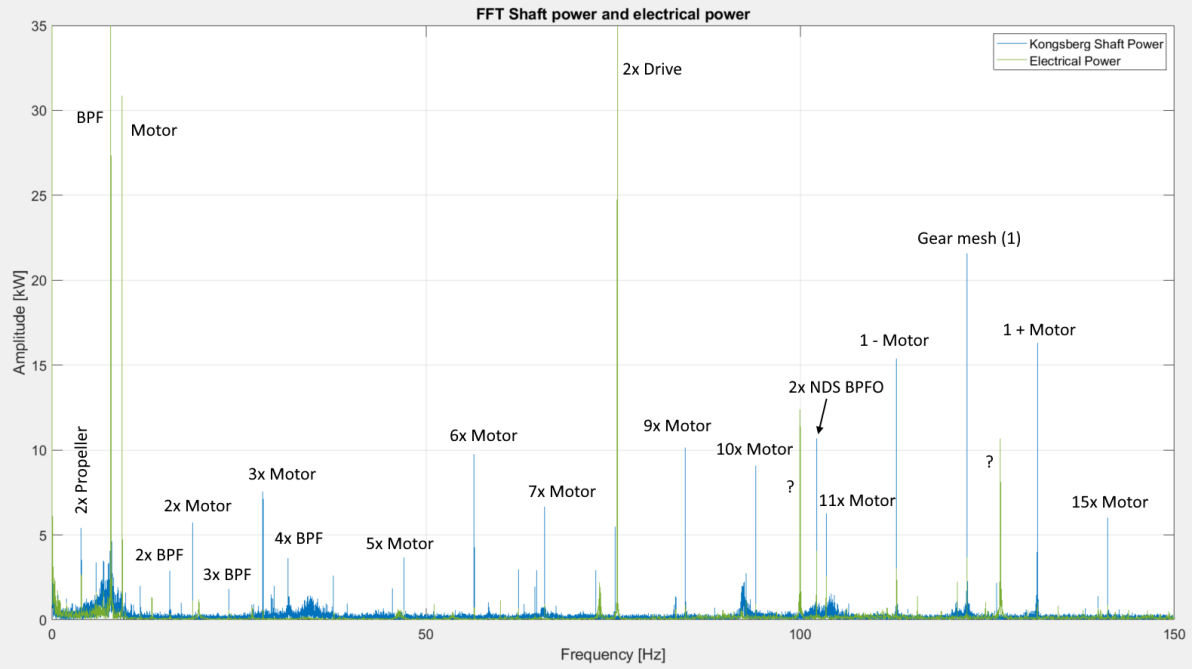

Figure F.21: Power FFT of T1 at 70% speed of Kongsberg MetaPower: Fs = 1600 Hz, sample time = 50s. And electrically deduced torque: Fs = 20 kHz, sample time = 50 s

Shaft torque and electrical torque comparison

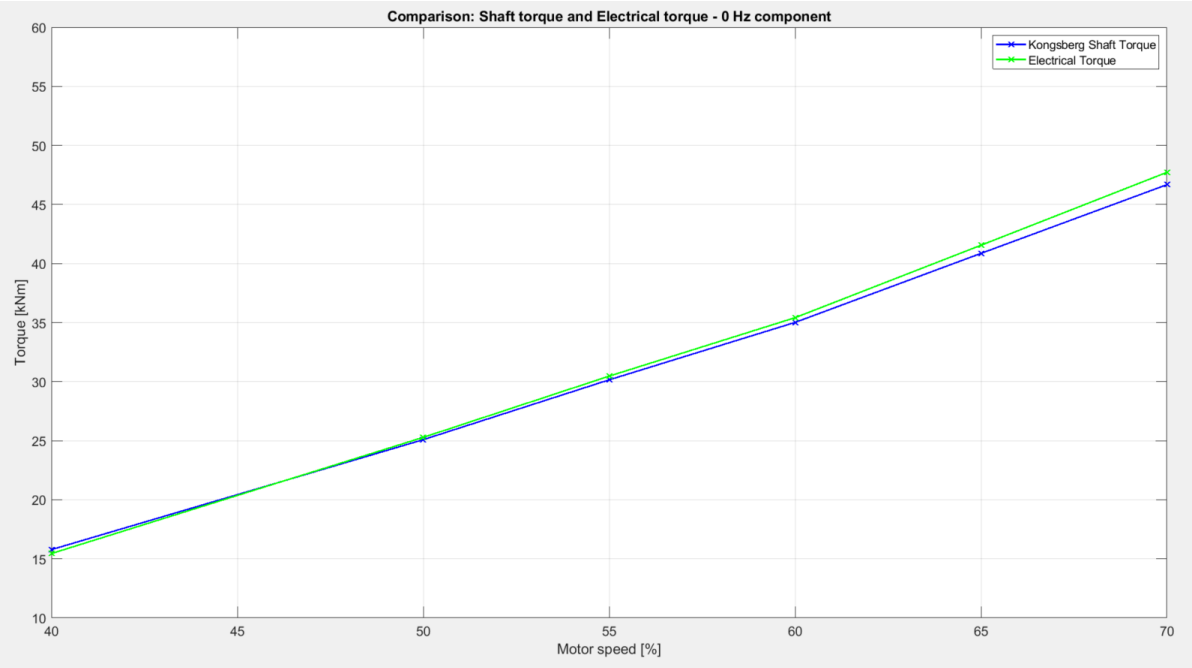

Figure F.22: Baseline electrical torque and shaft torque measured at different speeds

G Results: Unidentified Oscillations

After identifying most oscillations found in the different spectra throughout this paper, a few interesting unidentified oscillations remain. As introduced in Chapter 4, this includes the peaks identified as E1, E2, E3 and D1. In this Chapter, a further exploration on the origin of these oscillations is provided.

E1, E2, E3 peaks

As can be seen in every ESA based spectrum shown in Chapter 4, there appear to be haystack shaped sideband frequencies on the drive frequency and some of its harmonics. These were denoted with E1, E2 and E3. Interestingly, these frequencies actually appear throughout the entire frequency range in the spectrum as sidebands on multiple harmonics of the drive frequency and the switching frequency. This is easily spotted, since symmetrical patterns clearly start to appear when the spectra are viewed at a large frequency range. It also helps that the data for three different thrusters with the E1 peaks at slightly different frequencies are plotted in the same image, as this only increases the detectability of the sideband behaviour. A clear example of this symmetrical behaviour is visualized in Figure G.1 and Figure G.2. In these images the different peaks that are actually identical sidebands around different carrier frequencies have been tried to be identified, solely by visually inspecting symmetry. This process has narrowed all these peaks down to a suspected six or less (denoted as E1 to E6) original frequencies that create all these sidebands.

When further analysing these oscillations, a few more things become apparent: Firstly, the haystack shaped pattern might indicate mechanical resonance. However, the frequencies are not found in any of the mechanical measurements. Also, they do not consistently appear in the same frequency regions for different speeds, which can be seen in Figure 4.10. Continuing, there appears to be no clear relation between the frequencies of these peaks and the motor speed and motor torque, as the tiny differences in these values for these parameters can't explain the larger differences of the E1 - E6 peaks.

Nevertheless, when narrowing down solely on the E1 peak, a suspected cause or hypothesis has been found. The E1 sideband peaks appear to be caused by interference between (harmonics of) the two strongest carrier signals in the measurements. This could be the case, since the switching frequency is so low in this application that it falls in the range of the higher harmonics of the drive frequency. The suspected cause of the E1 peaks is described as follows:

- In thruster 1 the drive frequency is 46.23 Hz. Its 15th harmonic is then 693.45 Hz. The difference of this with the switching frequency is 693.45 - 666.9 = 26.55 Hz. This frequency can explain the E1 sidebands on the drive in Figure G.3.
- This works similarly for thruster 3. The drive frequency is 46.43 Hz, its 15th harmonic is 696.45. This makes the difference with the switching frequency 25.8 Hz, which explains the E1 sidebands in Figure G.3.
- Finally, for thruster 6 the drive frequency is 46.18 Hz and its 15th harmonic is 692.7 Hz. The difference with the switching frequency is 25.8 Hz, also explaining the E1 sidebands in Figure G.3.

As mentioned before, this explanation only covers the E1 peak. However, as the E2 - E6 are only characterized by their visual symmetry in the spectrum, it can still be the case that these other peaks are somehow also related to E1 or can have a similar origin as E1.

Also, this explanation is just a hypothesis, but the remaining arguments in this section have clearly indicated that these peaks are not of a mechanical nature. Therefore, no proof for this hypothesis will be searched.

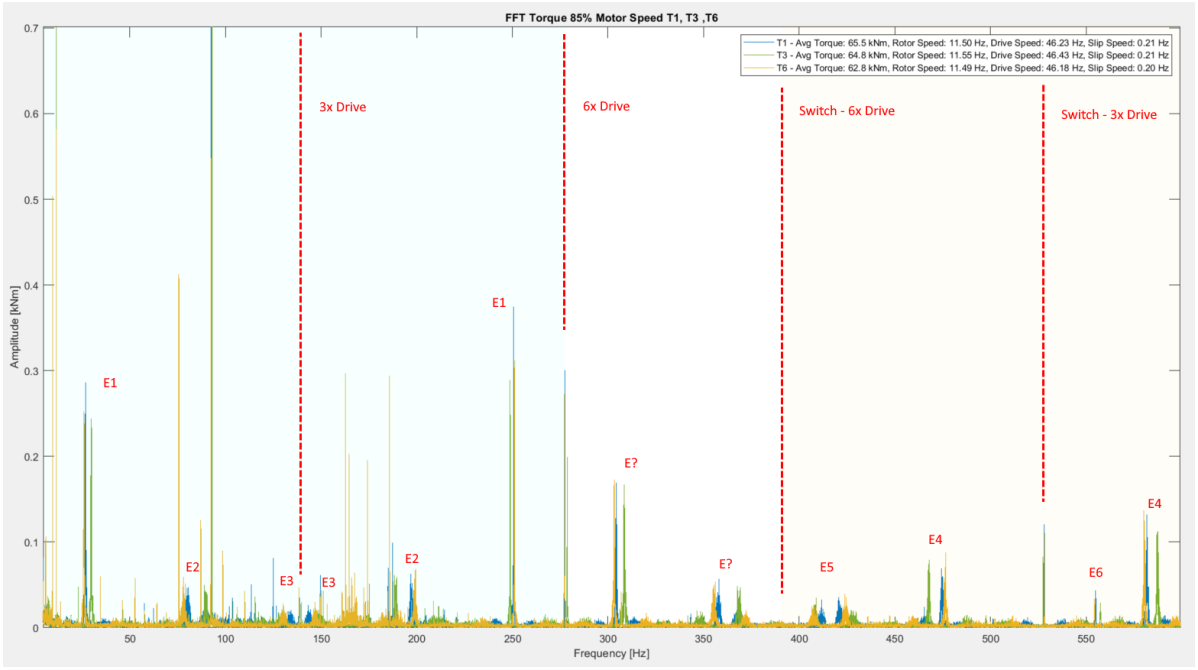

Figure G.1: Torque FFT T1, T3 and T6 with highlighted symmetry on drive and switching frequencies. Fs = 20 kHz, sample time = 50 s

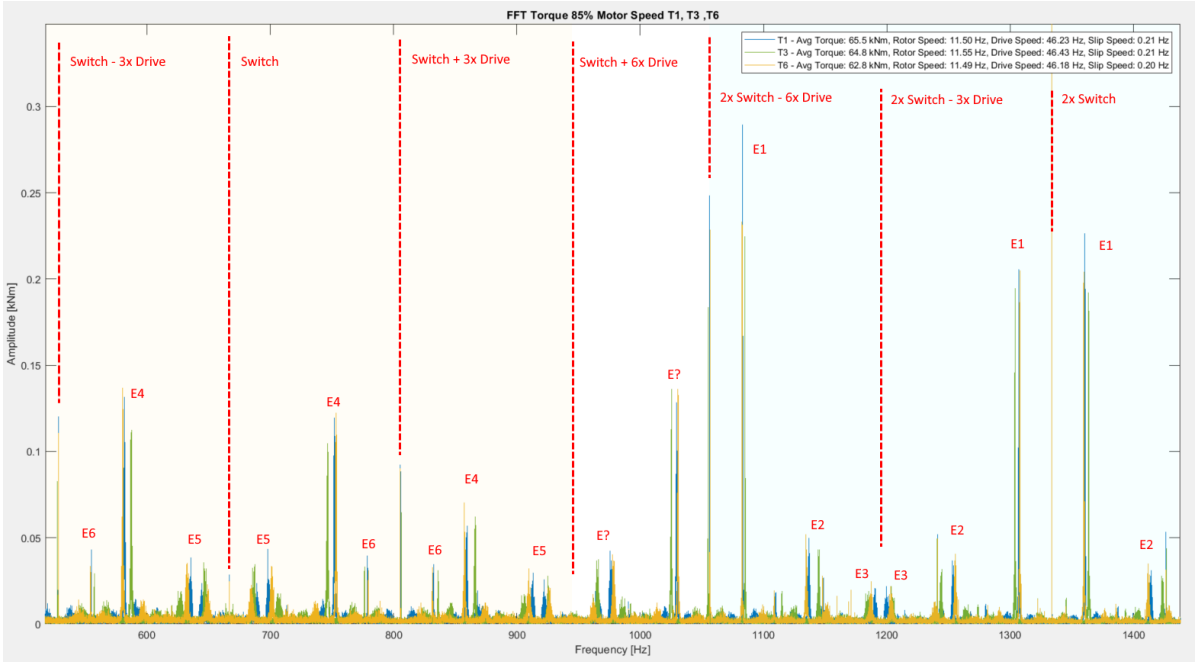

Figure G.2: Torque FFT T1, T3 and T6 with highlighted symmetry on drive and switching frequencies. Fs = 20 kHz, sample time = 50 s

D1 peak

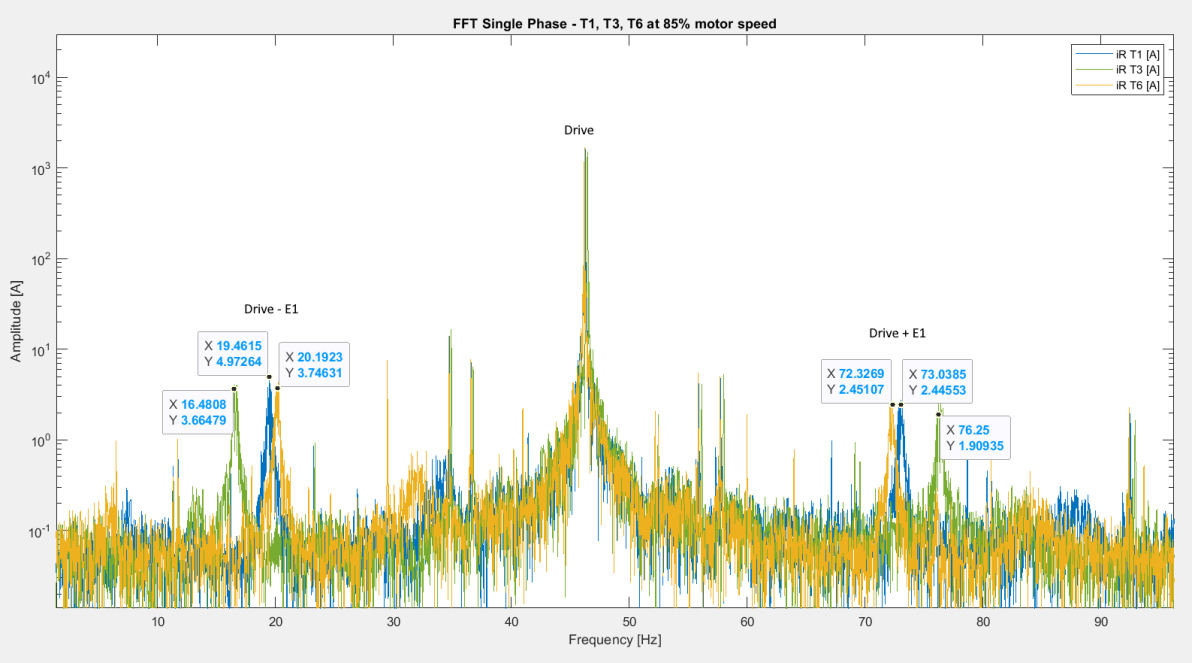

Figure G.3: Single Phase Current FFT T1, T3 and T6. Fs = 20 kHz, sample time = 50 s

A final interesting and unidentified peak appears in all demodulated spectra at exactly 6.0 Hz, regardless of the motor speed. This is especially visible in Figure F.13. This means the frequency is unrelated to the motor speed, which makes it very unlikely that this oscillation is of a mechanical nature. However, the amplitude does seem to increase for higher speeds and torques, meaning it might still be somehow related to the motor speed, drive speed, or motor torque in this way. Up until this point, unfortunately no explanation for the appearance of this oscillation has been found.

H Literature Review

Literature Assignment

Multi-Machine Engineering

Motor Current Signature Analysis for Predictive Maintenance of Medium Voltage Induction Motor Assemblies in the Maritime Industry

Authors:
Koen Kruimer (4469887)

Supervisors:
Dr. Ir. H. Polinder
Dr. A. Coraddu

September 13, 2022

Abstract This literature review analyses the best possibilities for implementation of a Motor Current Signature Analysis approach for predictive maintenance in the maritime industry. It does this by first highlighting the requirements of a predictive maintenance strategy in general, after which the current maintenance strategies and the use of induction motors in the maritime industry are explored. Then, the different methods and techniques of Motor Current Signature Analysis are examined, including a comparison with Vibration Analysis. Finally, an advice is presented for the experimental implementation of Motor Current Signature Analysis on a marine vessel.

Keywords - Predictive Maintenance, Motor Current Signature Analysis, Electrical Signature Analysis, Vibration Analysis, Induction Motor, Maritime Industry

TU Delft

Allseas

Preface

At the time I started the literature assignment, I had no idea what direction it would take. As I have a great interest in Predictive Maintenance, the only certainty was that this would be part of it. When starting the combined graduation assignment at Allseas Engineering BV. and Motor Current Signature Analysis came up as a topic, I was immediately enthusiastic on the technique and started the research. However, in the end I had great difficulty coming to a decent structure for this assignment including Predictive Maintenance, MCSA, and the maritime industry, while also trying to keep the assignment scientific and relevant. Eventually, more than five different versions of this assignment were started and abandoned, each containing different information, lots of which didn't make the final cut. Looking back, I think the main reason for this is the fact that Predictive Maintenance, MCSA and the maritime industry create a very broad base of research. With this I mean the following: On all three subjects alone it would be certainly possible to write individual literature assignments. However, despite this pity complaining and despite the fact that writing this review took longer than expected, mostly due to the fact that I had to align my schedule with the schedule of the Pioneering Spirit for the overall graduation project, I am very content with the result! Most importantly, I think I have all the tools and information necessary to finish the graduation assignment.

Lastly, I want to thank a few people for making the writing of this assignment possible. First and foremost my colleagues at the office of Allseas Engineering BV., of which Maarten Langelaar deserves special praise for the endless 'sparren'. Also, the mechanics, engineers and electricians on board the Pioneering Spirit who assisted me with the entire project. Especially Edo, for he will be the reason I finally 'grow some resilience'. Then, my TU Delft supervisors Henk Polinder and Andrea Coraddu for their advice, enthusiasm in the project and nudges in the right direction. Of course, Deesje and Bassie deserve praise for the never ending mental support as well as their unconditional faith in my education, even though it's taking some time already now. And last but not least: Jelmar, thanks for cooking me a nutritious meal every night.

List of Acronyms

AC	Alternating Current
ANFIS	Adaptive Neuro Fuzzy Inference System
ANN	Artificial Neural Network
CM	Condition Monitoring
CNN	Convolutional Neural Network
CWT	Continuous Wavelet Transform
DAQ	Data Acquisition
DNN	Deep Neural Network
DP	Dynamic Positioning
DT	Digital Twin
EKF	Extended Kalman Filter
EMD	Empirical Mode Decomposition
EPVA	Extended Park Vector Approach
ESA	Electrical Signature Analysis
FFT	Fast Fourier Transform
FMM	Fuzzy Min-Max (Neural Network)
FNN	Fuzzy Neural Network
GAN	Generative Adversarial Network
IM	Induction Motor
IMF	Intrinsic Mode Function
IPS	Instantaneous Power Spectrum
IPSA	Instantaneous Power Signature Analysis
kNN	k-Nearest Neighbour
LDA	Linear Discriminant Analysis
MCC	Motor Control Cabinet
MCSA	Motor Current Signature Analysis
ML	Machine Learning
MV	Medium Voltage
MVCSA	Motor Voltage and Current Signature Analysis
NB	Naive Bayes
PCA	Principal Component Analysis
PDA	Partial Discharge Analysis
PdM	Predictive Maintenance
PF	Particle Filter
PMSM	Permanent Magnet Synchronous Machine
PSD	Power Spectral Density
PVA	Park Vector Approach
PWM	Pulse Width Modulation
QDA	Quadratic Discriminant Analysis
RCM	Reliability Centered Maintenance
RF	Random Forests
RUL	Remaining Useful Life
SFFT	Short-time Fast Fourier Transform
SVM	Support Vector Machine
VA	Vibration Analysis
VFD	Variable Frequency Drive
WPT	Wavelet Packet Transform
WT	Wavelet Transform

Contents

1. Introduction

The Induction Motor (IM) is often seen as the workhorse of the industry, as it is responsible of over 60% of the global industrial electrical power consumption and more than 85% of motors used in industrial appliances are IMs. The main reasons for this are the low cost, robustness, low maintenance requirements and capability to operate in extreme working conditions of IMs [1]–[3]. Considering this crucial role the IM has in almost every industry, e.g. production plants, wind energy, and the rail, maritime and automotive industry, the reliability of these machines is of high importance in both safety and economical perspectives. Especially in the case of large and costly Medium Voltage (MV) or High Voltage (HV) machines, unexpected downtime of an IM could lead to an entire production process shutting down, often resulting in high revenue loss [4].

Logically, a proper maintenance strategy should be implemented in IM applications to prevent unnecessary downtime and its consequences. Currently, the maintenance strategy that is seen as most advanced is Predictive Maintenance (PdM), in which the conditions of the operating equipment are monitored in order to predict possible failures and correct this at an optimal time. The reasoning for this is that in 99% of the cases of equipment failure, the failure is preceded by certain signs, conditions or indications that a failure is going to occur [5]. However, a correct implementation of a PdM can be much more than using vibration analysis or thermal imaging to catch possible signs of failure beforehand. PdM is sometimes seen as a philosophy that can improve productivity, product quality, and overall effectiveness of a manufacturing plant by using the operating condition of the plants' equipment to optimize the total operation of the plant [6].

In the maritime industry seagoing vessels will often have hundreds of IMs running simultaneously, most noticeably a ship's thrusters in the case of diesel-electric propulsion systems. These assemblies of MV IMs and thrusters are tailor-made and highly expensive. Also, performing maintenance on them would halt the operations of the entire ship, causing a considerable revenue loss. Therefore, the implementation of a proper condition based PdM strategy for these thruster assemblies will likely increase a vessel's overall efficiency. However, the current industry standard for these machines is a planned maintenance strategy combined with Vibration Analysis (VA). One of the main downsides of this type of monitoring for thruster assemblies is its intrusiveness: Vibration sensors located in the underwater part of a thruster often can't be reached without removing the thruster assembly from the vessel. This makes the question arise whether other condition monitoring techniques might be better suited for designing a PdM strategy for these types of machines.

Another type of Condition Monitoring (CM) much similar to VA is Motor Current Signature Analysis (MCSA), a technique especially developed for the unintrusive monitoring of IMs [7], but not widely implemented in the maritime industry. This technique could potentially be more effective in setting up a PdM strategy for IMs in the maritime industry. This means investigating how this technique can best be implemented in order to reach this goal and how MCSA weighs up to VA in this industry can be useful research. Therefore, the main research question and the subquestions of this literature review are:

- *'How can Motor Current Signature Analysis be best implemented to create a predictive maintenance strategy for mechanical failures in induction motor assemblies in the maritime industry?'*
  - *'How is a predictive maintenance strategy ideally set up?'*
  - *'What are the common mechanical failures of an induction motor?'*
  - *'What sets the maritime industry, its maintenance strategies and its use of induction motors apart?'*
  - *'How are current maintenance strategies that make use of Vibration Analysis set up?'*
  - *'What different methods exist to use Motor Current Signature Analysis as a means for condition monitoring in induction motors?'*

These questions will be addressed by examining relevant literature on these subjects. Finally, the structure of this review will be the following: Firstly, the concept of PdM is explained in Chapter 2. Then, the failure behaviour of IMs is discussed in Chapter 3. Afterwards, the requirements for a possible MCSA based maintenance strategy are investigated by examining the maritime industry in Chapter 4. Furthermore, to explain the industry standard the process of VM is highlighted in Chapter 5 and the possibilities of MCSA are discussed in Chapter 6. Lastly, after a discussion in Chapter 7 a conclusion is drawn in Chapter 8 to answer the research question.

2. Predictive Maintenance

This chapter serves as background information on PdM and maintenance strategies in general. It is necessary information in order to be able to successfully implement MCSA into a PdM strategy that can outperform the current maintenance strategies used in IM assemblies in the maritime industry.

2.1 Maintenance Strategies

The strategies used for maintaining industrial machinery are traditionally subdivided into three basic categories, which are shown in Table 2.1 [8]. Firstly, Reactive or Corrective Maintenance is a strategy where a piece of equipment is operated until breakdown, after which it gets replaced or repaired. This a low effort method, where almost no costs are made in the monitoring of the equipment. However, failure of the equipment is inevitable, which causes downtime and generates costs for the replacement of components.

The second basic strategy is a time-based strategy called Preventive Maintenance. Within this strategy maintenance or inspections are carried out at regular intervals to prevent machines from failing completely and to keep them running for as long as possible. The scheduling of these intervals could be calendar based or calculated with the running hours of the machine.

The most advanced maintenance strategy is referred to as Predictive Maintenance (PdM). This is a condition-based maintenance approach, in which the operating conditions of the equipment, such as temperatures or vibrations, are monitored either continuously or at set intervals to assess the health of the machine and plan the maintenance of the components to be just-in-time [9]. This type of maintenance strategy is often difficult and expensive to set up, but will in the long term most likely ensure the optimum use of the machinery, causing the highest equipment availability and lowest maintenance costs. Commonly, most heavy and expensive equipment, such as HV or MV IMs, are maintained by using a combination of Preventive and Predictive Maintenance strategies, considering that any type of failure for this type of equipment will most likely result in long downtime and high costs, as these expensive machines are often critical for the functioning of a plant or other industrial site and have little spares.

This policy, in which multiple types of maintenance strategies might be combined to create the highest reliability of a machine or system is in literature also referred to as Reliability Centered Maintenance [10]. In essence, this strategy includes all forms of maintenance and is focused on ensuring the lowest amount of downtime of the entire facility. This is done by prioritizing the individual machines and their maintenance, and categorizing them in how crucial they are for the operations of the facility. Therefore, small machines that don't impede the production of a facility might be run until failure, as this will be cheaper than upholding a preventive or predictive maintenance strategy for these components. While large and expensive machinery might be maintained by both preventive and predictive strategies in order to prevent downtime. RCM is generally seen as one of the most cost-effective methods of maintenance, as it encompassed the most cost-effective method of maintenance for all individual components in a facility [11].

Method	Theory/principle	Data required	Data analysis	Decision process
Corrective maintenance	• Fail and fix • Reactive-based • Unscheduled	–	–	–
Preventive maintenance	• Prevent strategy • Time-based • At regular intervals	Event/failure user/time-based data	Reliability theory based on bathtub curve assumptions	Determining the maintenance interval that optimizes the criteria of interest (cost, availability, reliability and so on).
Predictive maintenance	• Predict & prevent strategy • Condition-based • Just-in-time	Measurements that provide information about mechanical or performance condition of equipment	Monitoring the equipment degradation	Performing continuous condition monitoring for health assessment, prognostics, and diagnostics.

Table 2.1: The three common maintenance strategies [8]

2.2 Predictive Maintenance

A PdM strategy can include many different techniques and approaches, but can generally be subdivided into five basic steps. A flowchart of these steps is shown in Figure 2.1 and explained in the list below:

1. **Data acquisition** - Essential to the functioning of a PdM strategy is the monitoring of the operating equipment. This can be done in multiple ways. Firstly, it is important to keep track of the operating state of a machine, such as its running hours at different capacities. Secondly, the performance of the machine in each state can be monitored, such as the consumed power or delivered torque. When using data-driven approaches, usually many types of condition monitoring techniques are being used and data is collected by various types of sensors, such as vibration sensors, current sensors or temperature sensors. Also, visual or audible signs of wear of a machine noticed by expert personnel, for example during inspections, can be seen as data collection [6].

2. **Information processing** - Depending on the type of acquired data, the information should be processed in order to use it for PdM purposes. This could be as simple as plotting the states and performances of a machine, but for more complex measurements more tools are needed to acquire a useful insight. Examples of this are filtering of vibration signals, transforming and spectral analysis, or to extract features from signals that can be implemented in ML algorithms [12].

3. **Diagnostics** - The following key feature of a PdM strategy is the diagnostics. The collected information is interpreted to decide whether components in the machine are showing failure behaviour or not. Diagnostics firstly detects anomalies in the gathered information that possibly indicate failures. The next step is diagnosis, in which faults are classified and quantified, to finally assess the current health of the machine or system [13].

4. **Prognostics** - After assessing failure behaviour and the current health of the systems, predictions can be made about the development of the failure behaviour and deterioration of the machine. In essence, the future health of the machine is predicted. An essential part of this is the Remaining Useful Life (RUL) estimation of the component [14]. Since, a worn-out component will often still be usable for some time until it either completely breaks and shuts down the machine, or deteriorates to a state in which the machines' performance is no longer sufficient. By estimating the RUL of a component it becomes possible to plan a maintenance interval at the optimum time before failure.

5. **Corrective action** - Once a fault has been detected and the RUL of a component has been estimated, the final step in the PdM process is to perform a corrective action to ensure the operation of the machine will be able to continue in the long term. Depending on the type of machinery, the criticality of the predicted failure and the cost and effort of the repair, this corrective action could range from an immediate replacement to waiting for the next scheduled maintenance interval to make a minor adjustment.

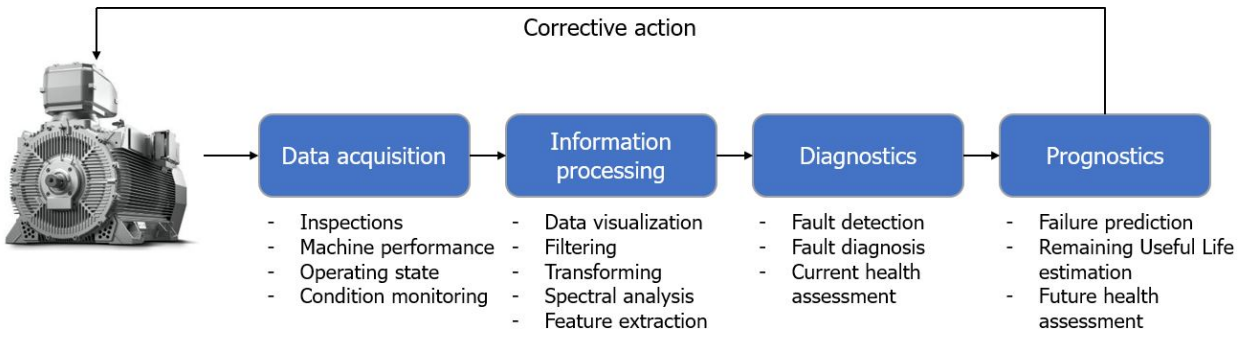

Figure 2.1: Flowchart of a generic Predictive Maintenance strategy [9], [12], [13], [15]

Historically, PdM techniques used to be mostly based on experience and statistics. By looking at historical failure data of machines, working conditions, inspections and by relying on expert knowledge health, failure behaviour could be predicted and prevented. This is sometimes referred to as a knowledge-based approach of PdM [16]. Another of PdM approach is the physics model-based approach. In this case a model of a system based on physics is created and used for the diagnostics and prognostics [13]. An example of this is to make a model containing all known frequencies of vibrations in a system in order to detect any deviant vibrations. A

more recent development in terms of model-based PdM is a Digital Twin (DT), which is a digital replica of a machine or system that can simulate the machines current state and performance in real time in order to make predictions on its current health and RUL, or even to simulate possible future operating scenarios [17].

The most recent development in terms of PdM is the data-driven approach, in which the diagnostics and prognostics of the PdM model are covered by data analytic algorithms such as Machine Learning (ML) algorithms [13]. This PdM approach goes hand-in-hand with the rise of Industry 4.0 or Smart Industry, as data is becoming more abundant and easier to process. This new phase of PdM is sometimes referred to as PdM 4.0 [18].

When examining recent literature in the field of PdM, it becomes clear that Industry 4.0 and data-driven approaches have sparked a new and growing interest in PdM: Looking specifically at research into implementing different types of ML algorithms in PdM models, Carvalho et al have identified 36 research papers published between 2009 and 2018 covering these techniques. Also, they noticed that the amount of papers published in this field seems to be exponentially growing [19]. Furthermore, Zonta et all identified 47 research papers covering PdM methods, architectures and technological developments in the Industry 4.0 published between 2014 and 2018. The vast majority of this research covered data-driven approaches to PdM, while only a few covered either physical model-based approaches or knowledge-based approaches. Also, some research papers were identified covering hybrid approaches, which is a combination of two or three of the discussed approaches [20]. Finally, when looking specifically at IMs, the interest in data-driven approaches based on ML algorithms have risen as well. A good overview of this can be seen in a recent paper by Kumar and Hati, who have published a review of a variety of ML algorithms for fault detection in IMs. This paper serves as an introduction into the most popular ML algorithms for fault detection, including the Artificial Neural Network (ANN) and Support Vector Machine (SVM), as well as a summary of their use and potential in IM fault detection [21].

3. Induction Motor Assemblies

As stated in the Introduction, the IM plays a key role in the global industry, causing them to be a popular topic in maintenance research papers. This becomes visible in [22], in which the authors have identified 80 research papers covering CM, a crucial part of most physics model-based and data driven approaches for PdM, for fault diagnosis in IMs between 2010 and 2020 [22]. To create a context for this research and to be able to implement MCSA as a viable CM method to setup a PdM strategy for IMs in the maritime industry, in this chapter the possible faults in IM assemblies are explained.

3.1 Common Induction Motor Failures

Depending on the use of an IM and the thermal, electrical, mechanical and environmental stresses it experiences in its operations, there are multiple types of failures that could arise in the machine. An overview the components of a common IM is shown in Figure 3.1 and an overview of the distribution of failures for three-phase squirrel cage IMs with a power of 100 HP or higher is shown in Figure 3.2 [23]. It becomes visible that the majority of all failures occurs in the bearings. Also, stator failures are common and occur mostly due to grounding errors. The smallest percentage of failures occurs in the rotor. This share of failures is mostly comprised of broken rotor bars. In the next subsections the most common failures and their causes will be described in detail.

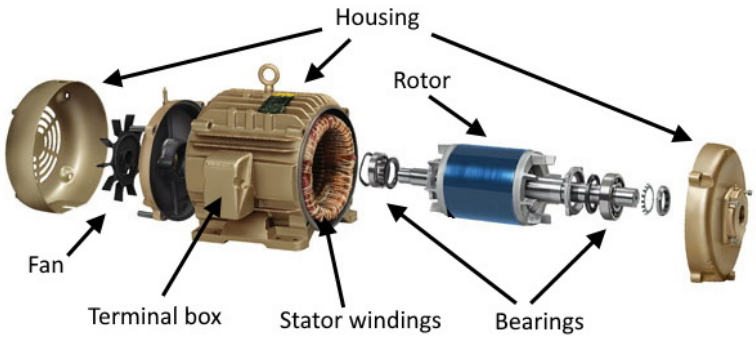

Figure 3.1: Exploded view of an IM (source: continental fan)

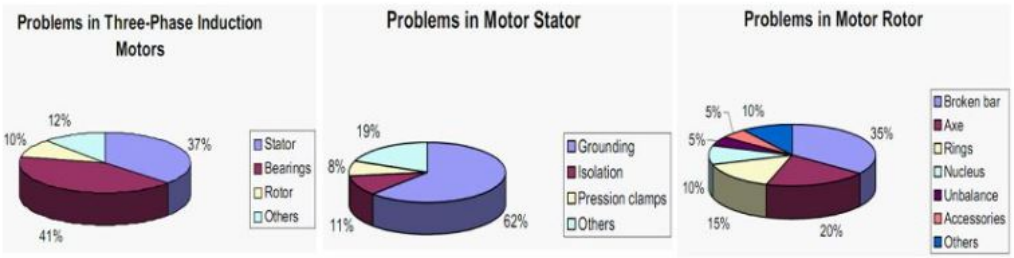

Figure 3.2: Distribution of failures in IMs [23]

Bearing Failures

As stated before, the most common type of IM failure is a bearing fault. These faults can originate from different failure mechanisms. For the use of ball bearings in general, fatigue failure would be the first failure mechanism to arise under normal operating conditions, causing small cracks under the surface of rolling elements and raceways that will propagate to the surface over time. These cracks will create detectable vibrations when the machine is in operation. Once fragments of the material start to break loose, which is known as flaking or spalling, the affected local area's of the raceways and rollers will rapidly expand, causing the lubrication to get contaminated with metal particles and the vibrations to worsen [24].

There are some operational factors that can accelerate the decay of the bearing elements. When looking at the applied load to the IM, successive overloads, pulsating loads, repeated departures (i.e. repeated switching on and off of the machine) and vibrations propagated through the drivetrain can all cause the condition of a bearing to deteriorate [23]. Secondly, environmental contamination by dirt or corrosion by water and acids can cause pitting and abrasive wear. Lastly, improper or careless installation can sometimes cause 'brinelling', which is the creation of surface dents by static overload, and 'false brinelling', which describes the same dents, only now created by vibrations of smaller loads, for example during transport [24].

Another type of failure which is seen in bearings specifically used inside IMs is caused by bearing currents. These currents are caused by magnetic asymmetries in a machine that create a current loop passing through the bearings. When this phenomenon occurs, arc currents can cause the metal of the raceway to melt locally, creating small craters. These pittings will be flattened out again by rolling of the elements, which will in time produce a trail on the raceway. Often, when the pittings are not flattened out perfectly, but the balls are forced to jump over the elevations, the dents in the raceway become worse, creating a hill-and-valley pattern. This failure mechanism, called fluting, dramatically deteriorates the surface of the raceway [25].

As described above, the deterioration or failure of bearings will result in increasing vibrations. This will eventually result in either the damaging of other components of the IM assembly, causing the machine to shut down, or the bearing itself breaking, also causing a shut-down. Two examples of heavily damaged bearings are shown in Figure 3.3.

Figure 3.3: Heavy spalling on the inner raceways of a bearing in a marine vessel thruster assembly [26]

Stator Failures

As seen in Figure 3.2, most failures in the stator are grounding and insulation damages. The most frequent causes for this are overheating, contamination and imbalance in phase voltages. Any kind of damaged insulation can cause shorted turns or shorted coils, which will further imbalance the machine [23], [27]. However, the main focus of this research is mechanical failures. Therefore, stator failures will not be discussed in further detail.

Rotor Failures

Rotor failures account for a small fraction of IM failures. The most common rotor failure is a broken rotor bar. This failure mode can be the result of many different conditions and stresses, which include: Thermal stress, torsional vibration, residual forces from production, magnetic force, centrifugal force and axial forces caused by skewing of the rotor bar. An overload of the consecutive appearance of these phenomena will most likely be the cause of a broken rotor bar [27].

A second common type of rotor failure is eccentricity, which is the phenomenon where the distance of the air gap between the stator and rotor is not uniform over the circumference of the shaft. Or in other words: the rotor is not exactly in the center of the stator, resulting in an area of maximum and minimum air gap. In the case of static eccentricity the rotor will rotate fixed in this non-concentric position, which can be caused by an overload on the shaft or misalignment. In the case of dynamic eccentricity, the areas of minimum and maximum air gap will move around while the rotor is rotating. This type of eccentricity is most likely caused by the outer

diameter of the rotor being non-concentric, a thermally bent rotor, bearing issues or an imbalance in the load. The two types of eccentricity can also occur simultaneously. this phenomenon is called mixed eccentricity. Any type of eccentricity will cause a further unbalance in the IM assembly [21], [23].

Load Failures

Failures can occur throughout an entire IM assembly. Generally, an IM assembly can be seen as the motor, transmission system and an attached load. In the case of an IM driven trhuster of a marine vessel. The transmission system will consist of a driveshaft connecting the engine to some gearbox, from which an outgoing shaft will drive propeller. Any failure in this system can affect the performance of the IM and might therefore be measurable in the condition of the IM. As different types of transmission systems, as well as different types of attached loads, such as compressors or centrifugal pumps, all have their own specific type of failure behaviour, it is beyond the scope of this literature review to list all failures and their causes. The important note is, however, that failure behaviour occurring in the transmission or attached load could be transduced throughout the system and might be detected by monitoring the IM [23].

Soft foot

A last type of failure, not just for IM assemblies, but for any kind of rotating equipment, is called a soft foot. In this type of failure one of the connection points of the equipment housing to the foundation is not rigidly connected, causing the machine to vibrate while operating, which can cause the machines' connection points to loosen up even further or even cause damage. A soft foot can originate from different sources, including a not-tightened bolt, a bent flange or an uneven foundation surface [28].

4. Maritime Industry

To be able to design a PdM strategy for IMs used in the maritime industry, the requirements of these machines in this specific industry need to investigated. Therefore, this chapter will highlight the industry standard in terms of maintenance for the maritime industry in general and discuss the use of the IMs in this industry.

4.1 Predictive Maintenance in the Maritime Industry

Maritime vessels are designed differently based on their intended use. For example, military vessels, cargo vessels, cruise ships or off-shore construction vessels are all operationally and thus technically different [29]. All these vessels consist of a collection of multiple different systems, which can categorized as the ship's hull, the propulsion system (e.g. engines driveshafts and propellers), crew equipment systems (e.g. fresh water, air conditioning, sewage), navigational of communication equipment (e.g. radar systems) and vessel specific equipment. Especially this last type of equipment will differ majorly between individual vessels. For example, a pipe-laying vessel will be entirely built around an on-board pipe-laying factory, while a naval vessel might be fully equipped with weaponry. [30]. Furthermore, the degradation of all these systems depends on the specific operations and the operational environment of the individual vessels or the classes of vessels. For example, the engines of a cargo vessel, which will be sailing at high speed most of the time, will wear faster than the engines of a heavy-lift vessel, which will be stationary on Dynamic Positioning (DP) most of the time [31]. DP refers to a method used by some vessels to position themselves, in which a control system drives the electric thrusters to automatically keep the ship stationary or remain in a certain speed and heading.

Since vessels are collections of systems and individual equipment, multiple maintenance strategies are used on board depending on specific systems and components. It is common that small easily replaceable parts are run until failure and then replaced, thus making only use of corrective maintenance. For larger and more critical machines preventive maintenance at regular intervals is the norm, in order to ensure the long term reliability of these machines. Also, this is mostly accompanied by some form of CM. Furthermore, all marine vessels have to comply to the rules and regulations set by Lloyd's Register. This is maritime institute that ensures the safety of vessels, employees on board an the marine environment. Logically, many of these rules and regulations concern the maintenance of marine vessels and dictate the periodical replacement or inspection of critical components. For example, under normal conditions a thruster needs to be visually inspected and thus removed from the ship every 5 years. However, when implementing further measures such as a proper CM strategy for a thruster, these intervals might be extended [32].

Overall, the maintenance strategy fitting most closely to the maintenance philosophy of the entire vessel is RCM, i.e. the maintenance actions on the vessel are prioritized in order to ensure the continuing operation of the entire vessel in the most cost-effective manner, incorporating different kinds of maintenance strategies for individual components. Currently, a shift from more preventive based strategies towards CM based maintenance is being observed in the maritime industry. However, this is still in line with the philosophy of RCM [30].

4.2 Induction Motors in the Maritime Industry

A single seagoing vessel can often contain hundreds of IMs, which are continuously used to fulfill key roles on the ship. The majority of these motors are used to power pumps for: cooling water, fresh water, sewage water, ballast water, bilge, fuel, hydraulic oil, lubrication, but compressors, air conditioning fans or exhaust systems are also powered by these motors. Furthermore, most types of cranes or winches on board a vessel will make use of one or more IMs as well. The size of these motors varies and is proportional to their use. For example, ballast water pumps will mostly be relatively large and powerful, and can even be MV, while individual lubrication pumps for an engine will be much smaller. The majority of these machines is controlled by Variable Frequency Drives (VFD), which is also called 'inverter driven' in literature. This is done in order to accurately control their speed and torque, as most of these motors have ever changing operational conditions. For example, fresh water pumps must accommodate both daily periods of high use and low use, and heating and ventilation fans must accommodate different climates. As stated in the previous section, the specific use of a vessel also dictates the need of VFD driven IMs: The highly varying engine load of a DP vessel will create a greater need for variable speed IMs then the continuous engine loads of a cargo vessel will. Also, recent research has shown that by

implementing VFD powered motors a considerable gain in energy saving can be made on board marine vessels [33]. Furthermore, most IMs will have some form of redundancy and for smaller IMs often spares are on board. Maintenance or replacement of the bigger pumps and IMs deep inside the hull of the ship, such as ballast water pumps, can be hard, since the pumps and motors have to be transported through different decks of the vessel to get them to shore.

However, the most critical and powerful IMs found in the maritime industry are those powering the thrusters of diesel-electric powered vessels. In this type of system one or more diesel motors will drive individual generators, which produce electrical power to be used by electric motors, usually a MV IM, which in turn power the thrusters. This type of propulsion system has many advantages, some of which being reduced fuel consumption, more flexibility in component placement and its ability to quickly adapt thrust levels. This last reason makes it the most popular propulsion type for DP vessels, like construction vessels [34]. This is because these vessels need to accurately position themselves during their work on heavy lifts, pipe laying, dredging, etc.

An example of DP vessel using inverter driven MV IMs is the Pioneering Spirit, operated by Allseas Engineering B.V., which drives its thrusters making use of twelve IMs, each capable of delivering 6.5 MW of power [35]. These thruster assemblies and their IMs can be regarded as some of the most critical on board, since a failure in one of these systems might halt the operations of the entire vessel. Also, as these IMs are not only the largest electric motors, but are also part of the most complex IM assemblies, their purchase costs and maintenance costs are the highest of all IMs on board. Therefore, when designing a PdM strategy to be used for IM assemblies in the maritime industry, the thruster assemblies of diesel-electric DP vessels are an interesting design topic.

Some considerations need to be made when researching possibilities for a PdM strategy for these IMs, however. Firstly, a VFD driven IM will be used at an entire range of motor speeds and torques. This makes CM for these systems hard, as there are countless setpoints for a specific speed and torque at which different machine behaviour might be considered healthy or faulty. Compared to a direct online machine, which will often have only one setpoint for speed and torque at which the machine condition must be considered, the diagnostics of a variable speed machine will be more complex [22]. Secondly, the thruster assemblies of a vessel will be partly submerged in water, containing a 'dry' part inside the hull and a sealed underwater part. This complicates CM for these assemblies even more, as any type of sensors connected in the underwater part of the thruster can't be maintained and the underwater part itself can't be otherwise inspected as long as the thruster is installed on the ship. This is only possible whenever the thruster is removed from the vessel, which is a highly expensive operation.

An industry making similar use of IMs and other electric machines is the wind energy industry. Wind turbines will be used at different rotational speeds, as wind speed is not constant. This means they will have similar properties in terms of multiple setpoints of healthy and unhealthy machine behaviour, depending on the generator speed and torque. Also, CM and maintenance in general is complex for wind turbines, as their entire mechanical drive system is elevated high in the air. In this case, a non-intrusive CM system could also prove useful.

5. Vibration Analysis

Currently, Vibration Analysis (VA) is the industry standard CM method for maintenance strategies for MV IMs in the maritime industry. In order to set up a PdM strategy based on MCSA that has the potential to outperform the industry standard, the working principles of VA are introduced in this chapter. By doing this, a comparison can be made between MCSA and VA.

5.1 Introduction

VA is one of the best known CM and, by extension, PdM techniques. It is even considered the industry standard in terms of CM for any type of rotating equipment. VA works by the principle that all rotating equipment will show vibrating motion while in operation, which depends on the characteristics of the specific machine and the rotational velocity. When a fault starts to occur in rotating machinery, the vibration levels often increase. Again, this increase depends on the type of machinery, type of failure and shaft speed. When the vibration behaviour of a 'healthy' machine is known, any deviation of this behaviour detected by VA might indicate a mechanical fault in a machine.

A mechanical system is often comprised of many different components, including a motor, gearbox, bearings, an attached load, etc. Each individual component will show its own specific vibrational behaviour. Therefore, when a mechanical system is equipped with multiple vibration sensors, a fault in an individual component can be deduced from aberrant vibration levels from one or multiple sensors. Some examples of machinery faults that cause elevated vibrations levels are: unbalance of any rotating part, misalignment, worn or damaged gears, worn or damaged bearings and looseness [36].

5.2 General Approach

The different steps of PdM as explained in Chapter 2 in the case of VA are [36]:

Data acquisition

Different types of sensors can be used to detect machine vibrations. These can be roughly divided into three categories: acceleration transducers, velocity transducers and displacement transducers. It depends on the frequency of vibrations as to which one will be most useful. In the case of high frequencies (>1kHz) the acceleration will be the most effective parameter, in the case of low frequencies (<10Hz), the displacement will be the most effective parameter and in the middle range of frequencies (10 Hz - 1kHz) the velocity will be the most effective parameter. Also, a combination of different types of sensors can be used to get a full picture of the vibrations in a machine. As the vibration frequencies generated by rotating equipment are most often in the middle range, a velocity transducer will almost always be one of the sensors used.

Mechanical vibrations can occur in different directions. When looking at rotating equipment, three general degrees of freedom can be identified in which vibrations can be conducted. Axially or parallel to the shaft rotation, radially or perpendicular to the shaft rotation and torsionally, which refers to rotational vibration around the axis of rotation of a shaft. It is important to line up the primary axis of any type of vibration transducer in the direction in which a machine vibration is occurring. Therefore, to get the full picture of vibrations in a system, multiple sensors should be placed in multiple directions in a machine assembly.

The sensor will be able to transduce a mechanical vibration signal into an electrical signal that is sent to a Data Acquisition (DAQ) device, where the signal is further processed. The further analysis of the signal will be done on a computer attached to this DAQ device. An important note about a measuring set-up, is that the DAQ device as well as the transducers need to have a sufficient sampling rate. The Nyquist theorem states that the lowest sampling frequency needed to accurately represent a signal is twice that of the highest frequency present in the signal [37]. However, in practice the optimal sampling rate to accurately represent a signal is ten times the highest frequency. For this reason, the maximum sampling frequency used for vibration analysis is often in the range of 10 - 20 kHz for acceleration based measurements.

Information processing

Often the initial parameter to be looked at in a VA is the overall amplitude of the vibrations. This is used as a rough indication of the state of the machine and determines whether more detailed analysis will be necessary to check for failure behaviour. As stated before, the vibration frequencies generated by rotating equipment are most often in the middle range. Therefore, the overall amplitude of velocity is an easy parameter to check and see if further investigation is necessary. [38]

The first and foremost information processing tool for vibration analysis is the Fast Fourier Transform (FFT). This transform maps the amplitude of individual frequencies present in a vibration signal. This way it is possible to check whether frequencies belonging to certain mechanical defects, such as a worn out rolling element of a bearing, are present in the machine in heightened levels. If an FFT proves ineffective for the specific purpose, there are more information processing and signal analysis techniques that can be used to extract useful information out of the vibration signal. Some of these techniques have a similar use for MCSA and will therefore be explained in Chapter 6. Other VA specific techniques are considered not relevant for the purpose of this paper and will not be investigated further.

Diagnostics and Prognostics

Diagnostics for VA mostly include searching for certain fault frequencies present in heightened values in a machine. For the different types of detectable faults, the related frequencies can either be calculated using the specific component dimensions and the rotational frequency of the shaft, or they can be detectable by heightened noise levels over a whole range of frequencies. These frequencies are component specific and can be deduced by using shaft speeds and component geometry [39].

There are generally two ways of performing diagnostics and prognostics for VA. The first is a physics-based approach, in which all healthy and unhealthy machine frequencies are calculated before the analysis. Then, the analysis is performed by either an expert checking the data for aberrant behaviour, or by an automatic computer model working with thresholds for healthy and unhealthy behaviour. The second and more modern approach is called the data-driven approach, in which some sort of ML or AI algorithm is used in order to learn to detect faulty behaviour from healthy behaviour over time, by feeding it plenty of machine data.

Prognostics for VA can often only be performed when plenty of historical data of a specific machine is available. The reason for this is that the development of faults is highly dependent on the specific machine and of its use. This means that often only when a fault is being noticed, for example early stage bearing wear, and this same failure for this specific failure has occurred before, an accurate prediction can be made on the RUL of the machine or component.

6. Motor Current Signature Analysis

Motor Current Signature Analysis is a type of CM approach that is comparable to VA. However, in this case the IM itself is used as vibration sensor. In this chapter the concept of MCSA is explained for both a physics model-based and data-driven approach of PdM. Also, the most recent research into data-driven MCSA for detecting mechanical faults is highlighted.

6.1 Introduction

The concept of MCSA was first proposed in the 1970s as a maintenance tool to be used in nuclear power plants, as these contain many inaccessible motors or motors placed in hazardous areas and MCSA is a specifically unintrusive monitoring technique [7]. Since then the application has slowly been developed and commercialized. MCSA falls in a larger category of Electrical Signature Analysis (ESA). ESA is an umbrella term for different kinds of CM based analysis types for electrical machines such as generators, motors or transformers. Examples of other ESA methods are: Instantaneous Power Signature Analysis (IPSA), Park's Vector Approach (PVA) and Partial Discharge Analysis (PDA) [23]. As some of these techniques can be seen as variations on MCSA, as they make use of the stator currents, they will be introduced in more detail in this chapter as well.

Since the concept of MCSA has existed for over 60 years, there have been many books and articles published about the concept and workings of MCSA [7], [23], [24], [40]–[44]. In the next sections, firstly, a comparison is made between MCSA and VA. Secondly, the necessary steps in the PdM process, as explained in Chapter 2, for MCSA are explained. Afterwards, a distinction is made between physics model-based approaches and data-driven approaches, for which the information processing techniques and diagnostics are somewhat different. Finally, recent research for conducting prognostics in MCSA is highlighted and two companies which have commercialized the technique of MCSA are introduced.

6.2 Comparison to Vibration Analysis

The concept of MCSA works much similar to vibration analysis: When a failure of a mechanical nature (and some of an electrical nature as well) starts to arise in a motor, this failure will have an influence on the current signature of the machine. When the stator current of a motor is then measured and analysed, patterns can be spotted that indicate a specific failure. The reason for this is that each type of failure will have its own specific frequency of vibration that it will add to the normal 'healthy' current signal of the machine. In Table 6.1 the failures detectable by MCSA are shown.

Rotor	Mechanical imbalance Misalignment Broken rotor bar Air gap eccentricity
Stator	Electrical imbalance Shorts
Other mechanical faults	Bearing faults Load faults Transmission faults Coupling faults Looseness Soft foot

Table 6.1: Detectable faults by MCSA [7], [23], [45]–[47]

As can be seen, the use of VA and MCSA have some overlapping functionalities. When comparing the two, MCSA knows some benefits. Firstly, MCSA can detect electrical faults as well as mechanical faults. Also, the sensors used for MCSA can usually be installed in the MCC (Motor Control Cabinet), which is a safe and easily

reachable place. There is no need for placing many different sensors throughout the entire assembly, as would be the case for VA, which makes MCSA an unintrusive CM technique. Finally, the vibration sensors on a machine are susceptible for vibrations and noise orignating from other machinery in the same room, while MCSA does not have this problem.

However, there are some downsides to MCSA as well. First of all, by only using one set of sensor in one location, there is also a lot of information on vibrations further away in the system that will be missed. This can be due to dampening in long drivetrains. In this case local vibration sensors might be better suited to detect vibrations, while for smaller drivetrains MCSA can be similarly accurate to VA [47]. Also, the information processing for MCSA tends to be harder. This has two reasons: Firstly, the current signature contains much more information and noise generated by all electrical components in the system when comparing it to the signal of a single vibration sensor. Secondly, an important distinction between MCSA and VA is the fact that the mechanical vibrations of interest are superpositioned on a carrier wave in the case of MCSA. This carrier wave is the line frequency, or fundamental frequency of the supply current. This means the mechanical frequencies and their harmonics will appear as sidebands of the line frequency at $|F_{supply} \pm n * F_{vibration}|$, whereas a mechanical vibration signal will capture these vibrations and their harmonics in their own frequency $|n * F_{vibration}|$ [48]. Retrieving the useful information out of this modulated signal can sometimes prove difficult. An example of the characteristic frequencies for both VA and MCSA is shown in Table 6.2.

Furthermore, the fact that VA can make use of multiple vibration sensors placed throughout a mechanical assembly means that not only more data can be gathered at different locations in the assembly, there are also multiple directions and degrees of freedom in which vibrations can be detected. This direction depends on the direction in which a vibration sensor in placed. In the case of MCSA there is only one direction in which vibrations can be detected. Namely, the torsional direction of the motor shaft, as this is the direction in which the motor is driven. It is possible for MCSA to detect lateral vibrations as well, but this is only possible when there is a significant relative displacement between rotor and stator [38].

Another advantage of VA is its ability to capture some mechanical failures in earlier stages than MCSA can. For example, in the first stages of bearing wear, no characteristic fault frequencies can be spotted yet. In fact, only the high frequency 'ringing' effect of the bearing components in their eigenfrequency can be encountered, which is only possible through VA. Also, there are some specific methods for VA making use of these high frequencies, such as the shock-pulse method [48]. In fact, the ability to catch mechanical failures, such as bearing faults, at these early stages through VA, makes it possible to classify a bearing fault in different severity stages. This provides useful information on fault diagnostics that cannot yet be equaled by MCSA [38].

Fault	Frequency
Rotor eccentricity	$k.f_r$
Bearing inner race	$k.f_r \frac{m}{2}\left(1+\frac{bd}{pd}\cos\beta\right)$
Bearing outer race	$k.f_r \frac{m}{2}\left(1-\frac{bd}{pd}\cos\beta\right)$
Bearing cage	$k.f_r \frac{1}{2}\left(1-\frac{bd}{pd}\cos\beta\right)$
Bearing ball	$k.f_r \frac{pd}{2.bd}\left(1-\left[\frac{bd}{pd}\cos\beta\right]^2\right)$

Fault	Frequency
Stator winding shortcut	$v.f_1 \pm k.f_r$
Broken rotor bar	$f_1 \pm 2.k.s.f_1$
Static rotor eccentricity	$v.f_1 \pm k.RS.f_r$
Dynamic rotor eccentricity	$v.f_1 \pm (k.RS \pm n).f_r$
Mixed rotor eccentricity	$f_1 \pm k.f_r$
Bearing inner race	$f_1 \pm k.f_r \frac{m}{2}\left(1+\frac{bd}{pd}\cos\beta\right)$
Bearing outer race	$f_1 \pm k.f_r \frac{m}{2}\left(1-\frac{bd}{pd}\cos\beta\right)$
Bearing cage	$f_1 \pm k.f_r \frac{1}{2}\left(1-\frac{bd}{pd}\cos\beta\right)$
Bearing ball	$f_1 \pm k.f_r \frac{pd}{2.bd}\left(1-\left[\frac{bd}{pd}\cos\beta\right]^2\right)$

Table 6.2: Overview of some characteristic frequencies for both VA and MCSA [38]

6.3 General Approach

Data acquisition

The frequencies of interest for MCSA are in the range of 0 - 5000 Hz. The mechanical and electrical fault frequencies of interest will usually be lower than 2000 Hz. However, in certain situations it can occur that harmonics of these frequencies can reach higher this level. Sometimes, it is even possible for a machine fault to only be detectable in its higher harmonic frequencies and not in its fundamental frequency. As explained in Chapter 5: The optimal sampling frequency to accurately map a signal is 10 times the frequency of the signal to be captured. In practice this means that sampling frequencies of between 10 and 20 kHz are used for MCSA, similar as for VA. Using higher sampling rates might prove inefficient, has the density of the data gets higher, while the chance of identifying faults at these high frequencies becomes lower [7].

Different types of current sensors can be used for MCSA, but there are some requirements to the sensors in order to make the process work. Firstly, the sensors must be able to accurately capture the entire range of frequencies of interest. In practice this means that a sensor needs to be able to work perfectly for frequencies from 0 - 20 kHz. An example of a sensor that will not work due to this fact is the Rogowski coil. This is a popular sensor type in industry, as it offers a high resolution and is easily attachable and thus unintrusive, but it is unable to accurately measure frequencies below 20 Hz, making it unusable for MCSA. This is because many mechanical frequencies of interest will be in this low frequency range. Secondly, the resolution of a sensor can influence the accuracy of MCSA. Evidently, a low resolution and inaccurate sensor will make frequency analysis hard. Therefore, a popular type of sensor used for MCSA are closed-loop Hall sensors. The most accurate of this type of sensors is the recently developed Fluxgate or Zero-flux variant. These sensors currently offer the best resolution, lowest response time and smallest phase error of all current sensor types used in industry [49].

Similar to VA, the sensors will be connected to a DAQ device, which is attached to a computer for further analysis.

Information processing

Usually the first information processing method applied to in MCSA is the FFT, similar as for VA. This transform can often make differences in fault frequencies easily visible over time. However, most research in the field of MCSA has been in the different information processing techniques used to extract usable information from the raw data, or in the field of diagnostics. Therefore, many methods for this purpose have arisen over the last years. The research into these different methods will be explained in Section 6.4 for methods that do not make use of ML techniques, and in Section 6.5 for methods that are based on ML techniques.

Diagnostics and Prognostics

The diagnostics and prognostics for MCSA are dependant on the type of information processing techniques that are used. So, as the information processing techniques have developed over the last years, the diagnostics and prognostics techniques have evolved with them. Therefore, more information on the different techniques can be found in Section 6.4 and 6.5 as well.

In general, diagnostics for MCSA works by the detection of certain fault frequencies that can be related to faults developing in a machine, which is again similar to VA. In the case of a physics-based diagnostics model, these frequencies and their amplitudes are known. In the case of a data-driven model, the healthy signature of the machine is learned by the model over time, so that unhealthy behaviour can be detected when it arises. As different types of faults all have their own specific frequencies, faults can not only be detected, but also classified. Also, by checking the severity of the vibrations, as well as the development of the vibrations over time, an estimation can be made on the RUL of a machine or component. However, in practise this is very complex, since the degradation of the components is dependent on many different factors. This means that accurate prognostics are usually only possible when a specific machine has been monitored for a long time and much historical data is available [38].

6.4 Physics-based Approaches

As stated in the previous section, a physics-based MCSA strategy will rely on a physics-based model of a machine containing all known healthy vibration frequencies and amplitudes, as well as the 'unhealthy' frequencies that can be expected if a fault is present in the system. Logically, the first step in setting up a physics-based MCSA strategy, is creating this physics-based model. This is an extensive effort, as there are multiple fault frequencies related to every single component inside an IM assembly. After setting up the model, a CM program is run in order to detect failure behaviour.

A physics-based MCSA approach can be seen as the historical way of performing MCSA, as this was the only possibility at the time MCSA was introduced. Therefore, the first papers describing the process date back well into the previous century. One of the oldest, much cited paper on the subject was published in 1989 and explains the implementation of MCSA in nuclear power plants, meaning it was already a defined concept at the time [50]. After this, many more descriptive papers were published, each more advanced then the previous one. The most popular descriptive papers over the years have been 'Methods of Motor Current Signature Analysis' (Kliman and Stein, 1992) [41], which has been cited over 400 times, 'Motor Bearing Damage Detection Using Stator Current Monitoring' (Schoen et all, 1995) [24], which has been cited over 1000 times and 'A Review of Induction Motors Signature Analysis as a Medium for Faults Detection' (Benbouzid, 2000) [40], which has been cited over 1900 times. One of the most elaborate descriptions on the subject is 'Predictive Maintenance by Electrical Signature Analysis' (Bonaldi et all, 2012) [23], describing not only the process of MCSA in detail, but also introducing other types of ESA. The most recent description of MCSA is 'Brief Review of Motor Current Signature Analysis' (Miljkovic, 2014) [7] and is therefore one of the most useful sources in understanding the use of MCSA.

6.4.1 Methods of Information Processing and Diagnostics

As stated before, most research into physics model-based approaches has been in terms of trying out new information processing techniques in order to be able to make a better analysis of the current data. However, it is important to note that many of these techniques can also be partly implemented in data-driven approaches, so they will appear in Section 6.5 as well.

Fast Fourier Transform

The first and most common type of analysis tool to be used on motor current data is the FFT. This transform portraits a signal from the time domain into the frequency domain and an analysis can then be performed into what specific frequencies are present at what amplitude in a system, in order to deduce the presence of a fault in the system. Since this is the first, easiest and most common type of analysis, research into this dates well back into the previous century. In the first extensive explanatory research paper from 1992 by Kliman and Stein [41] the FFT was the only used information processing and fault detection method, together with the demodulated spectrum. For machines in steady operating states the FFT can be used to detect many different types of failures, as long as the specific fault frequency is transferred sufficiently to the current spectrum to be noticeable above noise or other phenomena causing vibrations in the same frequency ranges.

A drawback of the FFT is the fact that it is unsuited for transient machine behaviour, as the FFT spectrum will only show what frequencies are present at what magnitudes, but not at what time. For this reason the short-time FFT (SFFT) or windowed FFT is most often used. In this case an FFT is made for a shorter time frame using a window function. However, the drawback of this is that a trade-off has to be made for high precision in time or high precision in resolution. An FFT sampled over a short time will have a low resolution, but due to the short time sample it is well known when the certain vibrations have taken place in time. Comparing this to a longer time sample, the information about when a certain frequency was present will be lost. Also, when the machine vibrations are transient and an overly long time sample is taken, the frequencies change so much that they start to overlap, creating an FFT from which no clear peaks can be deduced [40]. Still, the SFFT is not the best use for analysing transient machine behaviour. A better solution is the Wavelet Transform (WT), which will be discussed later in this section.

In theory, all detectable faults by MCSA can be made visible in an FFT, such as broken rotor bars (Figure 6.1) [51]. However, due to noise or transient machine behaviour this can sometimes be hard or impossible in a specific case. In these instances, more advanced information processing techniques can be used, which are introduced in the following subsections [7], [41].

A technique providing a similar current spectrum as the FFT in which faults might be detectable is the Power Spectral Density (PSD). This is a spectrum in which the power of vibration mapped per frequency over an entire range of frequencies. Even though it is comparable to the FFT, it is much less frequently used for the purpose of MCSA in literature. One clear example in which the PSD is used on stator current of a wind turbine in order to detect gearbox faults is shown in [52].

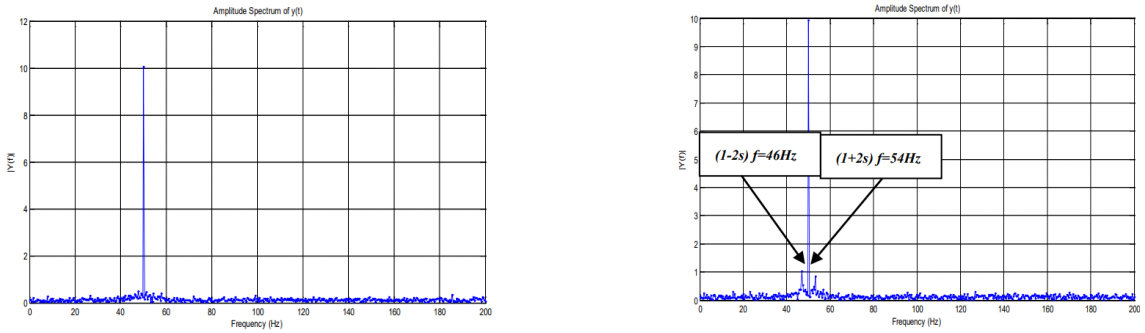

Figure 6.1: FFT of a healthy IM (left) and an IM with a broken rotor bar (right) [51]

Instantaneous Power Spectrum

A more elaborate type of analysis is the Instantaneous Power Spectrum (IPS). This type of analysis used both motor current and voltage data and is therefore sometimes seen as a different CM technique than MCSA. It might be better described under the umbrella term Motor Voltage and Current Signature Analysis (MVCSA) or simply ESA. However, the process works very similar to an FFT containing just the motor current signal, but in this case there is more information on the machine available. Therefore, it can offer more reliable analysis into the state of the machine [40]. The downside of this method is that it does not work well at this point for VFD driven e-motors [7]. This is because the AC voltage in a VFD is created by Pulse Width Modulation (PWM), which is a technique that creates short voltage pulses in a high frequency, the switching frequency, which in turn creates an alternating current. However, this means that the voltage wave itself will never be a sine waveform, but rather a square waveform of varying width. To accurately measure this, a high sampling rate is needed, many times higher than the switching frequency. As switching frequencies are often in range of 4 kHz to 20kHz range [53], it proves difficult to accurately capture this in practice. However, a VFD for a large MV IM will sometimes have a switching frequency below 1 kHz. In this case, the IPS might still be a useful tool.

The IPS can also be used for non-stationary or varying load conditions for induction motors. In the case of varying load conditions, the IPS will outperform the current spectrum analysis in fault detection [54]. In this case, both IPS and the current spectrum where being used for fault detection of gear faults under varying load conditions. The IPS proved accurate under these conditions whereas an FFT of the current signature alone proved unreliable. Fault detection can even be made more accurate by using a technique called Smoothed Instantaneous Power Spectrum [55]. This technique combines the IPS with a current spectogram approach, which enabled the dampening of high frequency oscillations in the IPS, causing more accurate gear fault detection [55].

Demodulation

In the field of VA, modulation is used in order to make fault frequencies better visible in the vibration spectrum. This works as follows: The time signal of the vibration will first be modulated by creating an envelope over its peaks, as shown in Figure 6.2. Then a spectral analysis, for example by using an FFT, will be performed on this new modulated signal. This spectrum is called the envelope spectrum. The benefit of this method is that the expected fault frequencies, for example when a bearing fault is present, will be elevated in this spectrum. The reason for this is that the ringing effect, which is the eigenfrequency vibration of the bearing caused by the bearing fault, will elevate the fault frequency in the modulated spectrum, instead of showing up in the high frequency ranges by itself in the FFT of the original vibration signal. This makes the envelope spectrum especially useful in applications with high random noise and vibrations or with low speeds and frequencies [56].

In the case of MCSA demodulation is sometimes used instead of modulation. Opposed to the vibration signature of a machine, which does not have a fundamental carrier frequency, the current signature of a machine has a carrier frequency which is equal to the fundamental frequency of the supplied current. This means that in

any FFT or current spectrum this carrier frequency will have a much higher amplitude than most fault frequencies that might be present in the signal, causing the carrier frequency to overshadow other useful information. Therefore, in the field of MCSA demodulation refers to the removal of the carrier frequency out of the current signature before performing an FFT. Together with the FFT, demodulation has been one the first information processing techniques used for MCSA and is therefore well known [41], [57], [58].

There are some different techniques used for demodulation in MCSA. One the easiest ways to demodulate a signal is by implementing a notch filter that can accurately filter the signal at only the carrier frequency. [59]. Also, multiple easy mathematical algorithms can be used on the current signature to demodulate it [58], or a Hilbert transform can be used [60]–[62]. Furthermore, there are two more novel ways to demodulate a current signal. Firstly, by using the three phase currents to calculate a magnetic-torque vector, which automatically demodulates the carrier frequency [63]. And secondly, by creating a 'synchronous reference frame' for capturing the stator currents. This reference frame rotates at the supply frequency and is therefore able to filter out this frequency [59]. All these methods have proven successful in making fault frequencies easier to detect and can therefore improve fault detection. An example of a current spectrum and its demodulated current spectrum are shown in Figure 6.3.

In [64] the authors reviewed five different demodulation techniques to compare their usefulness. These techniques included: the synchronous demodulator, the Hilbert transform, the Teager energy operator, the Concordia transform and the Principal Component Analysis (PCA). As the approach for these techniques is quite different, with some using a single stator current signal and some combining all three, the applicability of techniques differ as well. In short: The synchronous demodulator, Hilbert transform and Concordia transform are somewhat easier to implement methods, but offer a smaller domain of validity. While the Teager energy operator and PCA have a larger domain of validity, but tend to be more susceptible to noise. Also, the PCA is actually considered a data-driven technique and will therefore be further discussed in Section 6.5.

A final recently proposed technique is the combined use of the vibration envelope and the demodulated current spectrum. In this case, the acceleration envelope was first used to accurately determine specific fault frequencies for a machine, after which the demodulated current spectrum was used over a longer period of time to monitor the presence of these fault frequencies and thus to detect developing faults. This technique proved useful as the current spectrum itself can be very complex and the acceleration envelope can aid in with the initial characterization of the current spectrum [60].

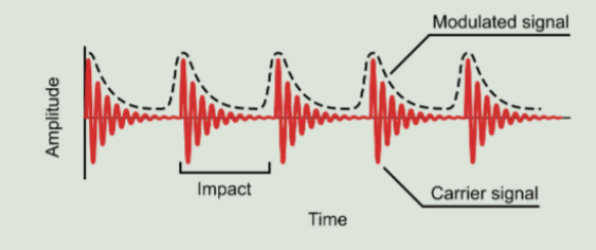

Figure 6.2: Carrier vibration signal and its modulated signal [56]

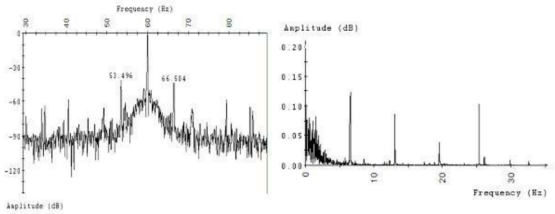

Figure 6.3: Current spectrum (left) and demodulated current spectrum (right) [7]

Wavelet Analysis

Another popular and well researched information processing technique is the Wavelet Transform (WT), which is known for being able to capture transient vibration behaviour, as the WT is much better suited to create a high precision local time analysis of a signal than an FFT or SFFT. A WT will either refer to a Continuous Wavelet Transform (CWT) or a Discrete Wavelet Transform (DWT). Both types of analysis consist of decomposing a signal into specific wavelets, that are finite in length and irregular in shape, by shifting and scaling them over the length of the signal. There are multiple shapes of wavelets, called mother wavelets, that can be used for decomposing a signal. One mother wavelet that is often used for signal analysis is the Morlet wavelet, of which a picture is shown in Figure 6.4.

By using a CWT, a time-frequency representation of a signal can be made, showing what frequencies are present in the signal at what magnitude and at what certain time. It is then possible to pinpoint an event and see what frequencies of interest it was comprised of. An example of this representation, resembling a heat map

or a spectogram, can be seen in Figure 6.5. Consequently, a second use of the CWT can be to then reproduce the signal with only the frequencies of interest. [40], [65], [66]

A DWT works slightly different, but to the same result. By using discrete steps of finer representations of a mother wavelet, it represents multiple levels of high-pass and low-pass filters, which are able to denoise and compress a signal, while retaining the useful information. Also, similar to the CWT, a time-frequency representation of a signal can be made using DWT [67].

The different types of WT have been widely used in research for information processing and fault detection in MCSA. For example, a Wavelet Packet Transform (WPT), which is a special kind of DWT, is used in [68] to detect bearing faults and assess their severity in an IM. Furthermore, in [69] a DWT was successfully implemented to detect broken rotor bars in transient start-ups of IMs, without the need for information such as the motor speed and load. Also, an extensive research into CM of IMs with gear failures has shown that a correct combination of a DWT and an FFT can be accurately used to detect gear failures. The need of a DWT arises in this case, because the broken gears will cause large load fluctuations in the system. [70].

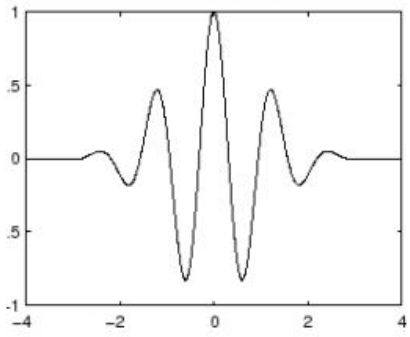

Figure 6.4: Morlet Wavelet [7]

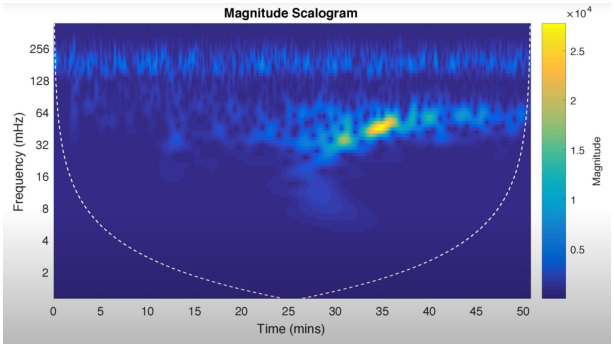

Figure 6.5: CWT of an earthquake vibration signal [71]

Park's Vector Approach

A further information processing technique that can be performed by using the stator currents of an IM is the Park's Vector Approach (PVA). In this analysis all three stator currents will be measured and used to calculate the Park's Vector. Under ideal and healthy operating conditions, the Park's Vector will appear graphically as a perfect circle centered around the origin, when plotted in two dimensions. In the case of a mechanical or an electrical failure, this perfect circle will be distorted. Therefore, monitoring the Park's Vector of an IM can be used as a means of fault detection. Since PVA requires all three stator currents, it is by definition more information dense than the analysis of a single phase stator current and can be used to detect failures only detectable by measuring all three phase currents, such as voltage imbalance. Also, a property of PVA is that it automatically demodulates the current signature: The fundamental component of the supply frequency is removed in the calculation of Park's Vector. An example of mechanical failures that are easily detectable by PVA are bearing faults [72], [73]. This is shown in Figure 6.6.

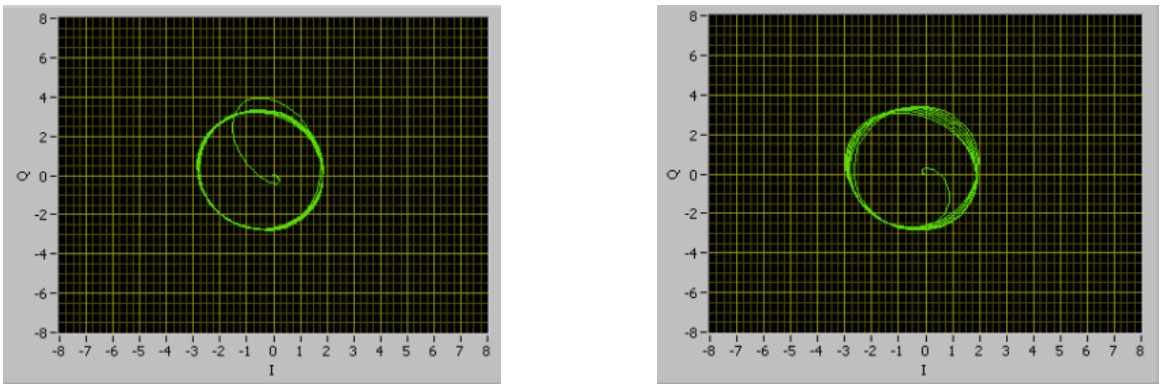

Figure 6.6: Park's Vector of healthy IM (left) and IM with an artificially broken bearing (right) [73]

PVA can also be used for a more thorough analysis called the Enhanced Park's Vector Approach or Extended Park's Vector Approach (EPVA). In this case, the Park's Vector is not only monitored by plotting it in 2D, but is also used to create an FFT containing the frequency information of all three phases simultaneously. An example of a failure that can be monitored through this method is stator winding unbalance, by not only detecting the failure, but also being able to assess its severity [23], [74].

Cepstrum Analysis

Cepstrum Analysis is a type of analysis especially useful for modulated signals, as it can be used to clearly indicate the presence of sideband frequencies and harmonics in a signal. The Cepstrum is obtained from a time signal by: 1. Performing a fourier analysis on the time signal. 2. Calculating the logarithm of the absolute magnitude of the fourier series. 3. Performing an inverse fourier transform on the resulting series. The resulting 'spectrum' is called the 'cepstrum'. The independent variable of this analysis is called the 'quefrency'. This terminology is similar for some other properties that can be analysed. For example, filtering is called 'liftering' and 'harmonic' is called 'rahmonic' when discussing a cepstrum [75].

The main use of cepstrum analysis is that of speech recognition. However, historically some research has been performed in VA and fault detection as well. Its best known use is the detection of individual gear faults in gearboxes through VA. As stated before, the frequencies of interest in VA are usually not sideband frequencies. However, in the case of gear faults, the effect of sideband frequencies modulated on top of a carrier frequency will occur in mechanical vibration monitoring as well. The cepstrum analysis can be used to detect these sidebands indicating gear failures [76].

More recent research has shown that the cepstrum analysis can be used for condition monitoring and detection of bearing faults as well. The cepstrum even appeared to show changes in machine behaviour clearer than the spectrum analysis, providing earlier fault detection [77]. Also, in recent research the cepstrum analysed was used for bearing and gear fault diagnosis in variable speed (VFD driven) machines, which clearly showed the different manifestation of gear faults and bearing faults at variable speeds [78]. Finally, cepstrum analysis has been proven to be useful in detecting broken gas turbine blades. This might be less relevant for research in IM fault detection, but it shows a very clear example of the potential of the cepstrum analysis, as can be seen in Figure 6.7 [79].

Let it be clear that the above-mentioned research on cepstrum analysis for mechanical fault diagnosis was all applied to VA as CM technique. There was only one example found of cepstrum analysis performed on stator current data for mechanical fault detection. This paper, which dates back to 2002, states that cepstrum analysis could not efficiently be used for bearing fault detection, since the fault related quefrencies are multiplied by a cosine function of the supply frequency and the rahmonic, making them less visible in the cepstrum [80]. However, as this is the only clear mention of cepstrum analysis for MCSA in literature, it can be stated that the full potential of cepstrum analysis for MCSA has not yet been tested and it could prove relevant to further develop this for use on MCSA. A specific reason for this is the fact that almost all fault frequencies for MCSA will be modulated on top of a carrier signal and thus appear as sidebands in a spectrum, for which cepstrum analysis seems highly effective.

Figure 6.7: Power spectra (left) and cepstra (right) of gas turbine with and without broken blades [79]

Fuzzy Logic

A fault diagnosis and classification technique that is sometimes used for MCSA is fuzzy logic. The reasoning for this is that a machine condition is never 100% broken or 100% healthy. Rather, there exists a whole range of machine behaviour in which its condition can be considered as healthy, which also holds true for unhealthy machine behaviour. Furthermore, machine data and information is frequently vague and inconclusive, which means that fuzzy logic could help in classifying a machine and its components in either a healthy or damaged condition [81], [82]. A block diagram of this process is shown in Figure 6.8.

Fuzzy logic as fault diagnosis has thus far been primarily used for stator faults, such as short circuits [83] and voltage unbalance [81], but also for broken rotor bars [84], [85]. The research in terms of mechanical fault diagnosis by fuzzy logic has been less common. There are some examples for bearing fault diagnosis by fuzzy logic for vibration analysis [86] and multisensory CM using both vibration signals and stator currents [87]. All this research shows that fuzzy logic based classification systems can be viable for fault diagnosis in IM assemblies.

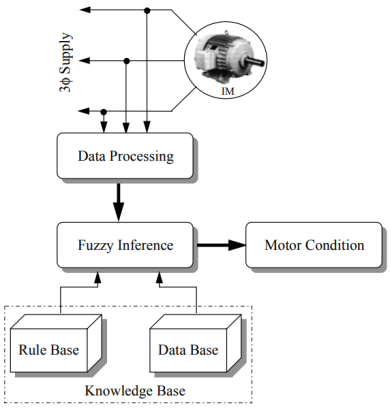

Figure 6.8: Block diagram of IM condition monitoring system using fuzzy logic [81]

Sparse Signal Processing

As stated before, the fault frequencies of interest for MCSA can be up to 5 kHz, but are usually below 2 kHZ. For this reason a common sampling rate for sensors and datalogging devices used for MCSA will be in the range of 10 - 20 kHz. When equipment with these specifications is not available, there can still be an opportunity to perform MCSA by using the principle of sparse signal processing. This signal analysis technique makes it possible to acquire and reconstruct signals at lower frequencies and still retrieve useful information out of it. Research has shown that sparse signal processing can effectively be used for fault detection of broken rotor bars, bearing faults and eccentricity at sample rates of roughly 100 Hz, which is 20 times lower than the Nyquist rate for the experiments [88].

However, when designing a set-up to test the potential of MCSA the problem of a low sampling rate can be immediately eliminated by choosing equipment with an appropriate sampling rate. Therefore, sparse signal processing is not a tool likely to be used in research that is meant to test the potential of MCSA. It can prove more useful in the case that MCSA has proven useful, but the existing or built-in sensor and DAQ equipment is not able to reach these high sampling rates.

6.5 Data-driven Approaches

With the rise of industry 4.0 and the progress in the field of ML a new data-driven approach has seen a growing interest over the last years. With this approach it is no longer necessary to calculate and determine all possible faulty and healthy frequencies in the system. Rather, in this case the ML algorithm would learn to detect unhealthy behaviour from healthy behaviour by feeding it with enough training data. Again, this entire process is very similar as for VA. In this case however, the data will originate from feature extraction from the current signal. Examples of features that can be extracted from a current signal are shown in Table 6.3, in which I_1, I_2, I_3 are the stator currents of the three phases of an IM.

RMS value of I_1, I_2, I_3	Auto correlation coefficient of I_1, I_2, I_3
Max value of I_1, I_2, I_3	Auto regression coefficient of I_1, I_2, I_3
Min value of I_1, I_2, I_3	Energy at different frequency components of I_1, I_2, I_3
Mean value of I_1, I_2, I_3	Amplitude at different frequency components of I_1, I_2, I_3
Standard deviation of I_1, I_2, I_3	Kurtosis of frequency signal of I_1, I_2, I_3

Table 6.3: Some examples of features that can be extracted from a current signal [89]

The extracted features can be implemented in different types of ML algorithms in order to classify and detect faulty machine behaviour or other information processing purposes, such as dimensionality reduction and regression. Many different types of ML algorithms can be used for this purpose. In fact, most research into MCSA in the last decade has been into what types of ML algorithms are useful for fault diagnosis in MCSA and how these are best implemented.

6.5.1 Methods of Information Processing and Diagnostics

Research into data-driven approaches mostly concerns the different fault identification and classifying approaches, based on different kinds of ML techniques. Also, some ML techniques offer other kinds of purposes and fit more in the category of information processing. The research into these techniques will be highlighted in this chapter.

Support Vector Machine

Support Vector Machine (SVM) is a supervised learning algorithm that is more and more used for machine fault diagnosis. It works as follows: Datapoints are plotted in an n-dimensional space, with extracted features as the coordinates. By feeding labeled training data the SVM will create a hyperplane to separate the different labeled sets by a margin as large as possible. This way, when a new unlabeled datapoint is added into the space, the SVM can predict to which set it belongs. In 2D a hyperplane will be represented by a single line. An example of this can be seen in Figure 6.9.

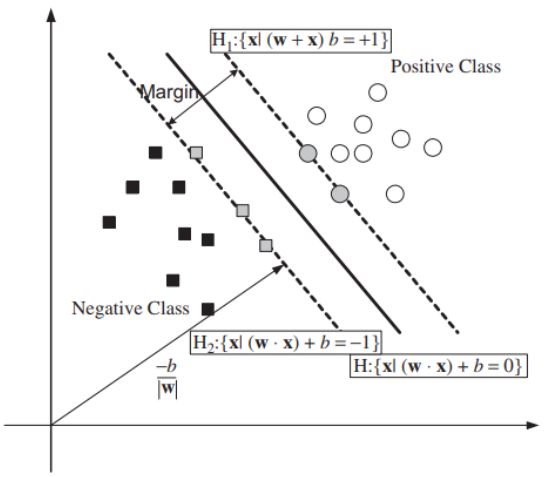

Figure 6.9: Classification of two classes using SVM [90]

In the case of machine fault diagnosis the SVM can be used to classify machine condition. This can be either healthy behaviour, or a certain type of fault can be pinpointed. The extracted features can originate from different kinds of measurements, such as vibrations or stator currents. Ever since the introduction of SVM to machine fault diagnosis, it has been thoroughly tested in combination with MCSA [90]. SVM in combination with MCSA can be successfully used to classify and diagnose multiple types of faults by extracting different kinds of features from current measurements. For example, Pandarakone et all used feature extraction of different frequency components directly from a stator current FFT to classify bearing faults in IMs. Their method proved able to successfully classify different severities of bearing faults under varying load and speed conditions, which means they were able to not only detect faults, but also assess the health of the machine [91].

Other examples of implementation of SVM in MCSA for fault diagnosis are detection of broken rotor bars [92], detection of short-circuits [93] and multifault diagnosis [94]. In the last example, the authors were able to use wavelet packet decomposition for their feature extraction, which enabled them to succesfully classify broken rotor bars, bearing faults, coupling misalignment and healthy machine behaviour.

Principal Component Analysis

The Principal Component Analysis (PCA) is a type of unsupervised learning analysis that is useful for dimensionality reduction in complex datasets that contain many different variables. It works by creating new variables as a linear combination of the original variables, which will capture as much of the original variance as possible. The new variable containing the most variance will be the 1st principal component, the new variable containing the most remaining variance will be the 2nd principal component, and so on. By performing this analysis the amount of variables can be reduced while maintaining the variance.

As stated before, PCA can be succesfully used as a demodulation technique for MCSA [64]. A second interesting PCA approach for MCSA is to use the three stator currents as inputs and reduce the output into a 2D set of variables, as done in [95]. The reasoning of the authors in this case is that the 3 individual stator currents are highly correlated and this analysis would leave them with variables only containing their differences. Eventually they were able to use this analysis as a preprocessing step in a larger algorithm that was able to successfully classify IMs with cracked rotors, rotors with out-of-tolerance geometry and backlash, which is type of fault caused by play or too large clearances in rotating machines.

In theory, PCA seems a good fit as a data processing technique for fault diagnosis in MCSA, as the current signatures of a machine contain much information that is irrelevant in deciding whether a machine shows faulty behaviour or not. By performing a PCA on the extracted features of a current signature containing both healthy and faulty behaviour, a smaller set of variables can be created that might be better suited to classify the behaviour in either healthy or faulty. However, this approach was not successful for the purpose of classifying different artificial bearing faults in [89]. In this case, the authors were not able to obtain a lower dimensional representation of the machine data that enabled them to classify bearing faults.

In practice, PCA has been more successful for MCSA based fault diagnosis in cooperation with other data processing techniques. This includes the above-mentioned demodulation and preprocessing techniques [64], [95], but another example is [96], in which the authors used PCA in cooperation with a multi-scale entropy algorithm to detect gear tooth pitting. Finally, PCA can be successfully used to detect broken rotor bars in transient start-up behaviour, in cooperation with both Wavelet Analysis and Hidden Markov Modeling [97].

Artificial Neural Network

One of the most popular and versatile types of ML algorithms is the Artificial Neural Network (ANN). Over the last two decades countless different types of ANNs have been developed for all different kinds of purposes, such as clustering, filtering, classification, compression, regression analysis and much more. It is therefore a technique applicable to different fields of study, not only data processing. In short, the concept of an ANN is loosely based on the network of neurons in a biological brain: It contains a layer of artificial neurons as inputs, which are nothing more than weighted variables. The neurons in this layer are all connected with weights and biases to the neurons in the next 'hidden' layer, which are in turn all connected to the neurons in the output layer. A specific input of variables or features will be translated to a certain output, which can be a prediction, classification, or anything else. So, by self-learning in the form of adjusting the weights and biases of its neurons and connections, an ANN can be trained to reach a certain output for a specific input. This learning can be both supervised and unsupervised. A visualisation of the structure of an ANN is shown in Figure 6.10. In this

example from [98] the input of the ANN originates from Intrinsic Mode Functions (IMF) of the stator current, which are created in a preprocessing step called Empirical Mode Decomposition (EMD). However, a complete explanation of this process is deemed out of scope of this literature review.

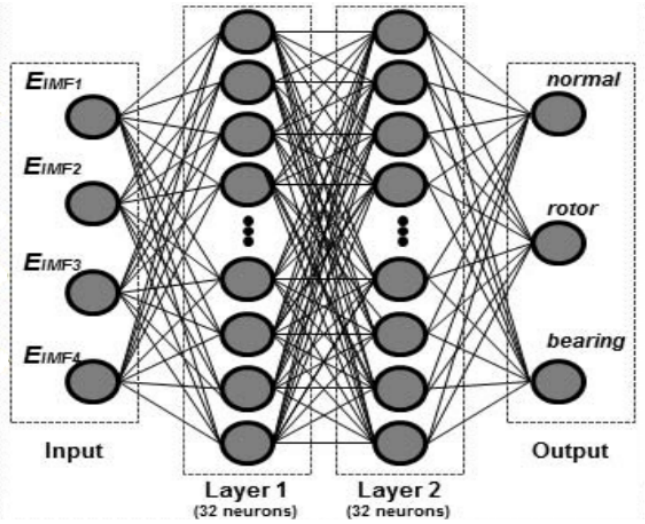

Figure 6.10: Structure of ANN, more specifically a Deep Neural Network, used in [98]

In the case of MCSA this offers functionalities as well. By using features extracted from stator currents as inputs, an ANN can diagnose healthy or faulty machine behaviour as output. This type of researched has been performed continuously over the last years, using different types of ANNs for different kinds of purposes. An example of this is [99], in which the authors try three different types of Deep Neural Networks (DNN), a type of ANN with multiple hidden layers, with different methods of feature extraction and data preprocessing to diagnose bearing faults. Their results show that the feature extraction and preprocessing steps are an important factor in the reliability of the algorithms, while the 'deep' part of the ANN, namely the hidden layers, doesn't necessarily improve the accuracy.

Furthermore, the DNN has proven to be a reliable fault detection method for both bearing faults and broken rotor bars in [98]. In this research the authors implemented other information processing techniques on stator current analysis for data balancing as well, which will be highlighted in the next section. A different approach to fault diagnosis by a DNN is performed in [89]. In this case, the authors succesfully used a DNN as an unsupervised dimensionality reduction tool in order to make a representation of a bearings degradation state, which ultimately leads to a bearing fault diagnosis system. For this purpose, the DNN outperformed both a single hidden layer ANN and a PCA.

Some kinds of ANN are a combination of different information processing techniques with an ANN, thus creating a 'hybrid' method making use of both techniques advantages. A popular type of these methods in machine fault diagnosis is an ANN in combination with fuzzy logic. The advantage of fuzzy logic is that it can provide a heuristic reasoning on the fault detection process, while the advantage of the ANN is that it can provide exact answers [100]. In this research, the Adaptive Neuro Fuzzy Inference System (ANFIS) is used for detecting stator insulation faults and bearing faults. ANFIS proved to be an accurate fault detection system for these faults. However, the motor speed, stator winding temperature and bearing temperature were used as features next to the stator current as well. A similar hybrid method is the Fuzzy Min-Max (FMM) neural network, which was succesfully used for fault detection and classification of stator winding faults and eccentricity [101]. Also, in [102] the authors were able to design a Fuzzy Neural Network (FNN) for fault detection and classification of bearing faults, broken rotor bars and stator faults under varying load conditions.

A final type of ANN is the Convolutional Neural Network (CNN), which makes use of a mathemical convolution of weights and neurons instead of a multiplication in at least one of the layers. The CNN is mostly used in image recognition algorithms, but can be succesfully used for machine fault diagnosis as well. This is done in [103], in which the CNN is succesfully used to detect stator winding faults, localize the fault and assess its severity, while being only fed raw stator current data. This is can prove interesting for mechanical fault diagnosis as well, as no complex preprocessing steps or feature extraction were necessary in this case.

Other Techniques

Next to SVM, PCA and ANN, there are many more ML algorithms that have been implemented in MCSA in scientific literature. As stated before, these algorithms can fulfill different purposes, such as classification, regression, clustering and dimensionality reduction. Also, sometimes multiple ML algorithms or other information processing techniques are combined in order to create 'hybrid models', which can be better suited to fulfill a specific purpose. Some examples of these hybrid models have already been highlighted in previous sections, such as [97], in which the authors make use of Wavelet Analysis, PCA and Hidden Markov Modeling for fault detection. As the number of ML algorithms experimented with for MCSA is high and their purpose is often advanced and specific, it is beyond the scope of this research to explain and list them all individually. Rather, a selection has been made of interesting methods and uses.

Firstly, for fault detection and classification there is a variety of ML algorithms that show potential. The Random Forests (RF) algorithm has been able to successfully classify multiple IM faults, such as misalignment, broken rotor bars, bearing faults and unbalance with a high (>98%) accuracy, both in a hybrid model and on its own [104]. This was done using both vibration and stator current signals. Similarly, another clustering algorithm called k-Nearest Neighbors (kNN) has been proven to be able to accurately classify both electrical and mechanical faults in IMs by using stator currents as well as a combination of stator currents and vibration signals [105], [106]. The Naive Bayes (NB) classifier also shows promise in accurately classifying different kinds of IM bearing faults, which was done in combination with a multiwavelet transform in [107]. However, in this case only vibration signals were used.

Furthermore, there are multiple ML available for dimensionality reduction of the gathered electrical current data. An example of one of these is Linear Discriminant Analysis (LDA). In [108] this method is used for evaluating the extracted features of a current signal, after which a NB classifier is used for fault diagnosis of bearing faults in a Permanent Magnet Synchronous Machine (PMSM). Evidently, this is a type of electric motor or generator with vastly different working principles compared to an IM, but it still shows the potential of this specific ML algorithm for stator current evaluation. A method much similar to LDA is Quadratic Discriminant Analysis (QDA). In [109] both LDA and QDA are used as a method of feature evaluation before fault detection and classification of bearing faults and eccentricity. In this case QDA proved to create a more reliable feature evaluation before the fault detection and classification by SVM.

Another interesting implementation for certain ML algorithms in MCSA is data balancing. A common difficulty in using ML algorithms for fault diagnosis is the unbalance in machine data sets. This is because for the majority of its lifetime a machine will be healthy and thus show healthy behaviour in its current signature. At some point faulty behaviour starts to occur, which will be followed by either a machine failure or a maintenance action. Therefore, the amount of healthy machine data will be much higher than the amount of data in which faults can actually be detected. When training a fault diagnosis algorithm, the data set can be first balanced by creating artificial data, for which other (data-driven) techniques can be used. This is done in [98], in which three different methods are compared for data balancing before fault diagnosis, namely SMOTE, ADASYN and the Generative Adversarial Network (GAN). The extracted features of the balanced datasets were first evaluated using a technique called Empirical Mode Decompisition (EMD) before the fault diagnosis was done by a DNN. For this purpose, the GAN proved to be the most reliable data balancing technique.

6.6 Prognostics

In order to set up an effective PdM strategy for IMs, an accurate prediction needs to be made on the RUL of a machine. Without this functionality, it is not possible to define an ideal time for a maintenance action, even though faulty behaviour in the machine might already have been detected. In other words: Without the possibility to perform prognostics, a CM strategy cannot be transformed into successful PdM strategy. Therefore, this section will discuss the possibilities for prognostics in MCSA.

As shown in the previous sections, there has been plenty of research conducted in the field of diagnostics for IM by MCSA to state that MCSA can be successfully implemented in many different ways to: detect mechanical as well as electrical faults, classify faults and sometimes even assess fault severity. Also, this can be done under continuous operating conditions, varying loads, varying speeds and transient machine behaviour. However, the research on successfully performing prognostics by means of MCSA is scarce. A reason for this is that creating an accurate fault diagnostics model for a specific machine can already be complex. To create a reliable CM system, the relationship between mechanical faults and fault components in the current spectrum is crucial, but this can be different for each individual IM assembly [39]. In order to expand this CM strategy into an accurate prognostics strategy, often even more operational machine data is necessary, mostly including faulty machine data. Of course, this type of data is rare, as machines will mostly be quickly repaired after showing faulty behaviour.

However, there has been some research conducted in the field of prognostics and RUL estimation using MCSA. Meaning, there are some experimental methods that can be used instead of just collecting enormous amounts of individual machine data. Firstly, in [110] the authors handpicked the most obvious degradation features of an IM and used them as an input for a PCA. The first principal component was then chosen as an estimator for the degradation of a broken rotor bar fault in an exponential degradation algorithm. This approach showed promising results. However, this entire method has been conducted in a Simulink simulation and wasn't based on actual operational machine data. Also, it contained more features then only stator current. Therefore, the method shows an interesting approach to prognostics for IMs, but doesn't prove that it would work on a real machine and by only using electrical data.

Another method that can be used for RUL estimation is an Extended Kalmar Filter (EKF). A Kalman filter in general is an algorithm that uses both a physical model as well as actual measurements to predict the state of a system. In [111] the authors used an EKF to successfully design a RUL prediction algorithm for insulation faults in inverter driven IMs based on a low sampling rate and without the use for expensive measuring equipment. A similar technique would likely be more difficult for the prognostics of mechanical failures in MV IMs, as insulation fault degradation is a relatively easy measurement to perform compared to the analysis needed for detection of mechanical failures. However, EKF might be an interesting method for RUL prediction of mechanical failures.

Furthermore, in [112] the authors were able to design a RUL prediction algorithm for stator winding faults. In this case, multiple physical based fault indicators were used assessing the severity level of the fault, after which a Particle Filter (PF) algorithm was implemented to predict the RUL. A PF is a type of algorithm used for prediction which is containing a probability distribution based on pre-knowledge of the problem and measurements. This way, the most likely state a system will be in can be predicted. Again, this type of electrical fault analysis is relatively easy compared to analysis needed for mechanical fault diagnostics, but the technique might also prove interesting.

In other industries similar research is starting to be conducted. For example, [52] shows a promising technique for RUL prediction in wind turbine gearboxes by solely using current signal analysis. An ANFIS algorithm was used to learn fault features of a machine, after which a PF algorithm predicted the RUL of the gearbox. This method was verified using a run-to-failure test on a wind-turbine gearbox, in which the actual time of failure was accurately predicted after only 32.7% of the gearbox's lifetime. As the wind energy industry shows much similarity to the large variable speed IMs used in the maritime industry, and as this research successfully performed the RUL prediction of actual, i.e. not simulated, mechanical failures, this technique shows much promise to be used for the MV IMs in the maritime industry.

Finally, an intelligent Digital Twin (DT) is starting to become more common for prognostics and RUL prediction accross multiple industries. This means by creating an accurate DT of a machine based on a either a physical or data-driven model of multiple machine variables, a prognostics analysis can be based and a RUL might be calculated out of the measured variables of the machine and the calculated degradation of the DT. An example of health monitoring and prognostics using a DT for an electric vehicle driven by a PMSM is shown in [113], in which a DT is created out of an ANN with the goal to extend the lifetime of the electric vehicle.

The input variables for this ANN range from average motor speed to winding temperature. Even though the method proved effective, it is unsure whether a similar technique for IMs would work when focusing on stator currents as input variables.

6.7 Companies Specialized in MCSA

At this point there are two companies which have commercialized the technique of MCSA. These are Artesis [46] and Samotics [47]. As both companies use all three phase currents as well as the phase voltages, it is better to refer to this technique as MVCSA or ESA. Artesis and Samotics have brought products to the market with similar capabilities. Namely, to detect the failures in IM assemblies stated in Table 6.1 and to then perform diagnostics and prognostics for these assemblies. However, the two companies use slightly different techniques in their products to do this.

Artesis was founded in 1999 after 15 years of research by its founders. It produces three different ESA devices. One of which is the Artesis AMT-Pro, a testing device to be installed in the MCC for rotating LV and MV equipment. This device works by means of Model-Based MVCSA. However, this is a different type of physical model as for the model-based MCSA described in Section 6.4. The model-based system of Artesis works by measuring both the phase currents and the phase voltages at a sampling rate of 2500 Hz. It then analyses these six signals to create a 'residual', which is defined as the variations in current signature that aren't produced by variations in the voltage signature. For example, this technique eliminates the dominant supply frequency in the current spectrum in order to only retain fault frequencies. For this type of physical model, it is not necessary to have prior knowledge of the assembly, making it easy to implement [46].

Samotics also makes use of MVCSA, but with a different approach. The company was founded in 2015 and has brought one product to the market thus far, called SAM4. This device is installed in the MCC and measures all three phase currents and voltages, similar to the Artesis AMT-Pro. However, unlike the device Artesis AMT-Pro, the SAM4 uses data-driven methods, or ML algorithms, to distinguish unhealthy from healthy machine behaviour. In a matter of months the device gathers enough data of a specific machine to familiarize itself with healthy vibrations, in order to detect unhealthy ones. In the case that aberrant data starts to be detected, SAM4 will automatically alert a Samotics Reliability Engineer that will manually look at the data and advice a course of action. SAM4 proves to be very effective, making Samotics a fast growing company that already implements their product in many different industries, such as production plants, chemical plants, waste water treatment systems and wind energy [47].

However, both companies are not yet able to apply their products in VFD driven MV IM assemblies as used in the maritime industry. This has multiple reasons. Firstly, the VFD drive will create harmonic vibrations at high frequencies that contaminate the current and voltage signature and make the signal harder to analyse. Secondly, the function of a VFD is to generate a variable AC frequency for the e-motor to be driven at different speeds. This means that there is no single frequency at which the devices of Artesis and Samotics can calibrate and create setpoints and thresholds for healthy and unhealthy machine vibrations. Rather, there is an entire range of healthy and unhealthy machine vibrations at different drive frequencies. Furthermore, both companies require large data transfer at the site of measurement. This is because the high frequency measurements create a lot of data that needs to be processed elsewhere. In the case of the maritime industry this proves difficult, as most vessels at sea don't have the appropriate internet connection requirements to smoothly facilitate this. And finally, neither company currently uses sensor packages appropriate for use on MV or HV electrical systems. Due to these difficulties, the automated devices of Artesis and Samotics are currently unable to perform their analysis to large VFD driven MV IM assemblies in the maritime industry.

7. Discussion

The research presented in this paper has solely been sourced from scientific and educational literature. However, obtaining information and knowledge out of a single type of source might give a twisted view of reality. Therefore, this chapter includes the views on the research topic gained by working within the maintenance department of a maritime company, namely Allseas Engineering BV [35]. As well as by conversations with an industry expert on both MCSA and VA, namely Bram Corne, author of [38], [39].

First of all, it has been proven countless times that MCSA can serve as a means of fault diagnostics for mechanical failures in IMs. However, this is not used to great extent in the industry. One reason for this is that, even though it is possible, it is still a complex process and it is not uncommon that MCSA cannot give the expected results. In fact, often a research paper is only published on MCSA when the technique proved to function correctly. Meaning, whenever it doesn't work as expected, no research paper is published and there will be no record of it. This can give a corrupted view on the technique.

Secondly, the majority of the research in fault diagnostics with MCSA has been on IMs in laboratory or test bench set-ups. These set-ups can lack the complexity of actual IM assemblies used in the industry. Also, the faults present in these tests were mostly artificially created, for example by drilling holes in bearings. This type of damage is not a good reflection of an actual worn and damaged bearing and can be easier to detect in frequency spectra than a bearing containing early signs of actual damage would.

Furthermore, both MCSA and VA have their different functionalities. Some types of failure are easier to detect by and MCSA and others by VA. When looking at the actual maintenance plan of a critical asset, it is wise to first conduct a Failure Mode Effects and Criticality Analysis (FMECA). This should be done in order to identify what types of failures should be prioritized over others in setting up a maintenance strategy. Therefore, a FMECA can give a clear image in what both MCSA and VA could accomplish in the specific maintenance for one machine and what option might be a better solution to implement, in the case one has to be chosen.

Still, MCSA is an interesting unintrusive method to be tested on an actual maritime vessel. When designing a test set-up for this type of work, it is wise to not only implement stator current measurements, but also voltage measurements. This is relatively little extra effort, but will provide double the information for analysis and enables the use of more data processing methods than MCSA on its own would. An example of this is the IPS, but also the measuring of motor torque would become possible, which could be promising, but is not well represented in scientific research. In this case it is more accurate to continue referring to the research methods as Electrical Signature Analysis (ESA) instead of Motor Current Signature Analysis (MCSA).

Finally, in literature the converter-driven IMs and VFD's are often seen as an added complexity. Since, the variable speed and variable torque will create an entire range of setpoints at which healthy and faulty machine behaviour can occur, but also because the fact that VFD's can create added noise and harmonic vibrations to the electrical signature. However, a VFD knows some benefits in ESA as well. Firstly, when faults are present in a system, their behaviour might be analysed at different speeds and torques in order to gain more information. Also, because of the high switching frequency of a VFD, it can be used to perform electrical measurements such as a PDA without the need for added measuring equipment.

8. Conclusion

Out of the information presented in this literature review, along with the added views of the discussion, multiple conclusions can be drawn. These conclusions are listed below.

A - Firstly, MCSA is proven to have functionalities that other CM techniques, such as VA, do not have and is proven to be able to detect mechanical failures in IM assemblies. Therefore, it would be interesting further research to try and develop this method in the maritime industry on an actual marine IM assembly, instead of solely researching the method in a test-bench setup.

B - Secondly, when setting up this type of research, it is of added value to include voltage measurements next to stator current measurements. This way, more information is gathered for analysis. The method would then be more accurately called ESA instead of MCSA.

C - Continuing, one of the most appealing assets in the maritime industry on which a PdM strategy based on ESA might be interesting to develop would be the IM driven thruster assemblies of marine vessels. These heavy and costly machines with complex maintenance requirements offer the most possible gain of a successful PdM strategy in terms of overall expenses and preventing unexpected maintenance. Also, these partially submerged assemblies are a good subject for unintrusive CM techniques.

D - The first attempts at information processing should be the easiest and most conventional ones, such as manually analysing the frequency spectrum and the demodulated spectrum. Depending on the effectiveness of this, more complex techniques can be implemented to improve the fault diagnostics process, work towards a prognostics approach or enable fault detection in the first place, in the case that the FFT is not able to distinctly show fault behaviour. This more complex techniques can be both physical model-based or data-driven. It depends on the type of data obtained to judge what will be most useful, but there are plenty of data processing tools that have proven successful.

E - Ultimately, a WT approach might be best suited for an actual PdM strategy based on ESA for DP thruster assemblies. This is because a vessel on DP will constantly change its motor torque and speed to remain in the same geographical position. Therefore, the motor speed and load will always be transient, for which the WT offers the best analysis.

F - Also, some techniques that show promise to be used for MCSA, but have not been widely implemented are: Cepstrum analysis, as it is effective in the analysis of sidebands, and the CNN, as it required no data pre-processing and feature evaluation for it to be successfully used for diagnostics.

G - Finally, to be able to set up a PdM strategy based on MCSA, the prognostics will be the most difficult part to set up. This is because either an extensive amount of machine data including failure data has to be available or a novel prognostics technique has to be used, which are currently being researched, but cannot yet be called proven concepts.

Bibliography

[1] C. Reza, D. Islam, and S Mekhilef, "A review of reliable and energy efficient direct torque controlled induction motor drives," *Elsevier*, 2014.

[2] S. Kumar and e.a., "A comprehensive review of condition based prognostic maintenance (cbpm) for induction motor," *IEEEAccess*, 2019.

[3] I. Alsofyani and N. Idris, "A review on sensorless techniques for sustainable reliablity and efficient variable frequency drives of induction motors," *Elsevier*, 2013.

[4] R. Wellens, "Semiotic labs: Predictive maintenance system for ac motors and rotating equipment," Company Power Point, 2020.

[5] H. Bloch and F. Geitner, *Machinery Failure Analysis and Troubleshooting - Volume 2*, ser. Practical Machinery Management for Process Plants. Gulf Prosessional Publishing, 1999, ISBN: 978-0-88415-662-8.

[6] R. Keith Mobley, *An Introduction to Predictive Maintenance, Second Edition*. Butterworth Heinemann, 2002, ISBN: 0-7506-7531-4.

[7] D. Miljkovic, "Brief review of motor current signature analysis," 2014.

[8] M. Tahan, E. Tsoutsanis, M. Muhammad, and Z. Abdul Karim, "Performance-based health monitoring, diagnostics and prognostics for condition-based maintenance of gas turbines: A review," *Elsevier*, 2017.

[9] M. Tahan, M. Muhammad, and Z. Abdul Karim, "A framework for intelligent condition-based maintenance of rotating equipment using mechanical condition monitoring," *MATEC Web of Conferences*, 2014.

[10] M. Bevilacqua and M. Braglia, "The analytic hierarchy process applied to maintenance strategy selection," *Elsevier*, 2000.

[11] A. Mokashi, J. Wang, and A. Vermar, "A study of reliability-centered maintenance in maritime operations," *Elsevier Marine Policy*, 2002.

[12] M. Carmen Canero, "An evaluation system of the setting up of predictive maintenance programmes," *Elsevier*, 2005.

[13] W. Tiddens, J. Braaksma, and T. Tinga, "Exploring predictive maintenance applications in industry," *Journal of Quality in Maintenance Engineering*, 2020.

[14] J. Sikorska, M. Hodkiewicz, and L. Ma, "Prognostic modelling options for remaining useful life estimation by industry," *Elsevier*, 2010.

[15] Siemens, *Simotics hv c flameproof*, 2022. [Online]. Available: `https://new.siemens.com/nl/nl/products/aandrijftechniek/electric-motors/high-voltage-motors/simotics-hv-c-flameproof.html`.

[16] D. Edwards, G. Holt, and F. Harris, "Predictive maintenance techniques and their relevance to construction plant," *Journal of Quality in Maintenance Engineering*, 1998.

[17] R. Abbate, M. Caterino, M. Fera, and F. Caputo, "Maintenance digital twin using vibration data," *Elsevier*, 2022.

[18] PWC and Mainnovation, "Predictive maintenance 4.0 - predict the unpredictable," 2017.

[19] T. P. Carvalho and et all, "A sytematic literature review of machine learning methods applied to predictive maintenance," *Elsevier*, 2019.

[20] T. Zonta, C. A. da Costa, R. da Rosa Righi, M. J. de Lima, E. S. de Trindade, and G. P. Li, "Predictive maintenance in the industry 4.0: A systematic literature review," *Elsevier*, 2020.

[21] P. Kumar and A. S. Hati, "Review on machine learning algorithm based fault detection in induction motors," *CIMNE*, 2020.

[22] S. K. Gundewar and P. V. Kane, "Condition monitoring and fault diagnosis of induction motor," *Springer*, 2020.

[23] E. L. Bonaldi, L. E. de Lacerda de Oliveira, J. G. B. da Silva, G. Lambert-Torresm, and L. E. B. da Silva, "Predictive maintenance by electrical signature analysis to induction motors," *IntechOpen*, 2012.

[24] R. R. Schoen, T. G. Habetler, F. Kamran, and R. G. Bartheld, "Motor bearing damage detection using stator current monitoring," *IEEE*, 1995.

[25] A. Muetze, "Bearing currents in inverter-fed ac-motors," *Technischen Universitaet Darmstadt*, 2004.

[26] M. van Emmerik, "Pioneering spirit technical & functional description (tfd)," ALLSEAS Engineering BV, Delft, Nederland, ISO PI-10110-023-N-F-001, 2022.

[27] A. H. Bonnet and G. C. Soukup, "Cause and analysis of stator and rotor failures in three-phase squirrel-cage induction motors," *IEEE*, 1992.

[28] B. Case. "Soft foot - what is it and how to minimize it." (), [Online]. Available: `https://acoem.us/blog/shaft-alignment/soft-foot-what-it-is-and-how-to-minimize-it/`.

[29] D. Eyres and G. J. Bruce, "Development of ship types, in: Ship construction," *Elsevier*, 2012.

[30] A. Eruguz, T. Tan, and G. van Houtum, "A survey of maintenance and service logistics management: Classification and research agenda from maritime sector perspective," *Elsevier*, 2017.

[31] R. Dekker and et all, "On the use of installed base information for spare parts logistics: A review of ideas and indsustry practice," *Elsevier*, 2011.

[32] L. R. G. Limited, "Rules and regulations for the classification of ships july 2022," 2022.

[33] C.-L. Su, W.-L. Chung, and K.-T. Yu, "An energy-savings evaluation method for variable-frequency-drive applications on ship central cooling systems," *IEEE*, 2014.

[34] A Adnanes, "Maritime electrical installations and diesel electric propulsion," *ABB Technical Brochure*, 2003.

[35] Allseas, *Pioneering spirit*, 2022. [Online]. Available: `https://allseas.com/equipment/pioneering-spirit/`.

[36] C. Scheffer and P. Girdhar, *Practical Machinery Vibration Analysis and Predictive Maintenance*. Elsevier, 2004, ISBN: 0-7506-6275-1.

[37] Wikipedia. "Nyquist-shannon sampling theorem." (), [Online]. Available: `https://en.wikipedia.org/wiki/Nyquist-Shannon_sampling_theorem`.

[38] B. Corne, B. Vervisch, C. Debruyne, J. Knockaert, and J. Desmet, "Comparing mcsa with vibration analysis in order to detect bearing faults - a case study," *Ghent University*, 2015.

[39] B. Corne, C. DeBruyne, P. de Baets, and J. Desmet, "Stator current measurements as a condition monitoring technology - the-state-of-the-art," *Ghent University*, 2014.

[40] M. E. H. Benbouzi, "A review of induction motors signature analysis as a medium for faults detection," *IEEE*, 2000.

[41] G. B. Kliman and J. Stein, "Methods of motor current signature analysis," *Electric Machines and Power Systems, 20:5, 463-474*, 1992.

[42] W. T. Thomson and M. Fenger, "Current signature analysis to detect induction motor faults," *IEEE*, 2001.

[43] E. L. Bonaldi, L. L. Oliveira, and G. Lambert-Torres, "Proposing a procedure for the application of motor current signature analysis on predictive maintenance for induction motors," *Comadem 07 conference*, 2007.

[44] N. Mehala and R. Dahiya, "Motor current signature analysis and its applications in induction motor fault diagnosis," *International Journal of Systems Applications, Engineering Development*, 2007.

[45] M. Messaoudi and L. Sbita, "Multiple faults diagnosis in induction motor using the mcsa method," *International Journal of Signal and Image Processing*, 2010.

[46] Artesis. "How does artesis technology work." (), [Online]. Available: `https://www.artesis.com/how-does-artesis-technology-work/`.

[47] Samotics. "Meet sam4." (), [Online]. Available: `https://www.samotics.com/solution`.

[48] M. Institute, "Vibration analysis training manual - category ii," 2016.

[49] LEM. "Innovations." (), [Online]. Available: `https://www.lem.com/en/innovations`.

[50] R. C. Kryter and H. D. Haynes, "Condition monitoring of machinery using motor current signature analysis," *Seventh Power Plant Dynamics, Control and Testing Symposium, Knoxville, Tennessee*, 1989.

[51] K. Gaeid, "Fault diagnosis of induction motor using mcsa and fft," *Academia*, 2012.

[52] F. Cheng and et all, "Fault prognosis and remaining useful life prediction of wind turbine gearboxes using current signal analysis," *IEEE*, 2017.

[53] BearingNews. "Vfd switching frequency bearing current." (), [Online]. Available: `https://www.bearing-news.com/vfd-switching-frequency-bearing-current/`.

[54] N. Baydar and A. Ball, "Detection of gear deterioration under varying load conditions by using the instantenous power spectrum," *Academic Press*, 1999.

[55] I. Yesilyurt, "Fault detection and location in gears by the smoothed instantaneous power spectrum distribution," *Elsevier*, 2003.

[56] A. Fernandez. "Demodulation or envelope analysis." (), [Online]. Available: `https://power-mi.com/content/demodulation-or-envelope-analysis`.

[57] D. Fossum. "Identifying mechanical faults with motor current signature analysis." (), [Online]. Available: `https://www.reliableplant.com/Read/28633/motor-current-signature-analysis`.

[58] P.Pillay and Z. Xu, "Motor current signature analysis," *IEEE*, 1996.

[59] E. L. Bonaldi, L. E. L. Oliveira, L. E. B. da Silva, and G. L. Torres, "Removing the fundamental component in mcsa using the synchronous referance frame approach," *IEEE*, 2013.

[60] I. A. dos Santos Areias and et all, "Evaluation of current signature in bearing defects by envelope analysis of the vibration in induction motors," *Energies*, 2019.

[61] I. Jaksch and P. Fuchs, "Rotor cage faults detection in induction motors by motor current demodulation analysis," *IEEE*, 2007.

[62] R. Puche-Panadero and et all, "Improved resolution of the mcsa method via hilbert transform, enabling the diagnosis of rotor asymmetries at very low slip," *IEEE*, 2009.

[63] N. Q. Hu and et all, "A novel transform demodulation algorithm for motor incipient fault detection," *IEEE*, 2011.

[64] E. H. E. Bouchikhi and et all, "Stator current demodulation for induction machine rotor faults diagnosis," *IEEE*, 2014.

[65] C. Torrence and G. P. Compo, "A practical guide to wavelet analysis," *American Meteorological Society*, 2016.

[66] K. M. Lau and H. Weng, "Climate signal detection using wavelet transform: How to make a time series sing," *Bulletin of the American Meteorological Society*, 1995.

[67] Wikipedia. "Discrete wavelet transform." (), [Online]. Available: `https://en.wikipedia.org/wiki/Discrete_wavelet_transform`.

[68] E. C. C. Lau and H. W. Ngan, "Detection of motor bearing outer raceway defect by wavelet packet transformed motor current signature analysis," *IEEE Transactions on Industry Applications*, 2004.

[69] H. Douglas and et all, "A new algorithm for transient motor current signature analysis using wavelets," *IEEE Transactions on Industry Applications*, 2004.

[70] C. Kar and A. Mohanty, "Monitoring gear vibrations through motor current signature analysis and wavelet transform," *Elsevier*, 2006.

[71] Mathworks. "Understanding wavelets, part 4: An example application of continuous wavelet transform." (), [Online]. Available: `https://www.youtube.com/watch?v=GV34hKXDw_c&ab_channel=MATLAB`.

[72] I. Onel and M. Benbouzid, "Induction motors bearing failures detection and diagnosis: Park and concordia transform approaches comparative study," *IEEE*, 2007.

[73] N. Mehala and R. Dahiya, "Detection of bearing faults of induction motor using park's vector approach," *International Journal of Engineering and Technology*, 2010.

[74] S. M. A. Cruz and A. J. M. Cardoso, "Stator winding fault diagnosis in three-phase synchronous and asynchronous motors, by the extended park's vector approach," *IEEE*, 2001.

[75] R. B. Randall, "A history of cepstrum analysis and its application to mechanical problems," *Elsevier*, 2016.

[76] R. Randall, "Cepstrum analysis and gearbox fault diagnosis," *Bruel Kjaer Precision Instruments*, 1981.

[77] M. E. Morsy and G. Achtenova, "Bearing condition monitoring approaches - envelope and cepstrum analyses," *Int. J. Vehicle Noise and Vibration*, 2017.

[78] R. Randall and W. Smith, "New cepstral methods for the diagnosis of gear and bearing faults under variable speed conditions," *International Congress on Sound Vibration*, 2016.

[79] G. Sapy, "Une application du traitement numérique des signaux au diagnostic vibratoire de panne : La détection des ruptures d'aubes mobiles de turbines," *Automatisme*, 1975.

[80] B. Raison and G. Rostating, "Investigations of algorithms for bearing fault detection in induction drives," *IEEE*, 2002.

[81] M. Zeraoulia, A. Mamoune, H. Mangel, and M. Benbouzid, "A simple fuzzy logic approach for induction motors stator condition monitoring," *Journal of electrical systems*, 2005.

[82] N. Mehja and R. Dahiya, "An approach of condition monitoring of induction motors using mcsa," *International Journal of Systems Applications*, 2007.

[83] L. A. Pereir and D. da Silva Gazzana, "Motor current signature analasys and fuzzy logic applied to the diagnosis of short-circuit faults in induction motors," *IEEE*, 2005.

[84] M. Akar and I. Cankaya, "Broken rotor bar fault detection in inverter-fed squirrel cage induction motors using stator current analysis and fuzzy logic," *Turkish Journal of Electrical Engineering and Computer Sciences*, 2012.

[85] S. Shukla, M. Jha, and M. Qureshi, "Motor current signature analysis for fault diagnosis and condition monitoring of induction motors using interval type-2 fuzzy logic," *International Journal of Innovative Science, Engineering and Technology*, 2014.

[86] F. Gougam and et all, "Bearing faults classification under various operation modes using time domain features, singular value decomposition and fuzzy logic system," *IEEE*, 2020.

[87] E. Pazouki and S. Choi, "Fault diagnosis and condition monitoring of bearing using multisensory approach based fuzzy-logic clustering," *IEEE*, 2015.

[88] A. Naha, A. K. Samanta, and A. Routray, "Low complexity motor current signature analysis using sub-nyquist strategy with reduced data length," *IEEE*, 2017.

[89] F. cipollini, L. Oneto, A. Coraddu, S. Savio, and D. Anguita, "Unintrusive monitoring of induction motors bearings via deep learning on stator currents," *Elsevier*, 2018.

[90] A. Widodo and B.-S. Yang, "Support vector machine in machine condition monitoring and fault diagnosis," *Elsevier*, 2007.

[91] S. E. P. et all, "Distinct fault analysis of induction motor bearing using frequency spectrum determination and support vector machine," *IEEE*, 2017.

[92] M. Armaki and R. Roshanfekr, "A new approach for fault detection of broken rotor bars in induction motor based on support vector machine," *IEEE*, 2010.

[93] S. Bensaoucha and et all, "Induction machine stator short-circuit fault detection using support vector machine," *COMPEL*, 2020.

[94] H. Guo and M.-K. Liu, "Induction motor faults diagnosis using support vector machine to the motor current signature," *IEEE*, 2018.

[95] A. Giantomassi and et al, "Electric motor fault detection and diagnosis by kernel density estimation and kullback-leibler divergence based on stator current measurements," *IEEE*, 2015.

[96] S. Aouabdi and et all, "Using multi-scale entropy and principal component analysis to monitor gears degradation via the motor current signature analysis," *Elsevier*, 2017.

[97] G. Georgoulas and et all, "Principal component analysis of the start-up transient and hidden markov modleing for broken rotor bar fault diagnosis in asynchronous machines," *IEEE*, 2015.

[98] Y. O. Lee, J. Jo, and J. Hwang, "Application of deep neural network and generative adversarial network to industrial maintenance: A case study of induction motor fault detection," *IEEE*, 2017.

[99] Z. Chen and et all, "Deep neural networks-based rolling bearing fault diagnosis," *Elsevier*, 2017.

[100] M. Ballal and et all, "Adaptive neural fuzzy inference system for the detection of inter-turn insulation and bearing wear faults in induction motor," *IEEE*, 2007.

[101] M. Seera and et all, "Application of the fuzzy min–max neural network to fault detection and diagnosis of induction motors," *Springer*, 2012.

[102] Z. Wang and et all, "Online fault detection of induction motors using independent component analysis and fuzzy neural network," *Singapore University*, 2009.

[103] M. Skowron and et all, "Convolutional neural network-based stator current data-driven incipient stator fault diagnosis of inverter-fed induction motor," *Energies*, 2020.

[104] B.-S. Yang, X. Di, and T. Han, "Random faults classifier for machine fault diagnosis," *Springer*, 2008.

[105] S. Samanta, J. N. Bera, and G. Sarkar, "Knn based fault diagnosis system for induction motor," *CIEC*, 2016.

[106] M. Z. Ali and et all, "Machine learning-based fault diagnosis for single- and multi-faults in induction motors using measured stator currents and vibration signals," *IEEE*, 2019.

[107] M. K. Saini and A. Aggarwal, "Detection and diagnosis of induction motor bearing faults using multi-wavelet transform and naive bayes classifier," *Wiley*, 2017.

[108] C. P. Mbo'o and K. Hameyer, "Fault diagnosis of bearing damage by means of the linear discriminant analysis of stator current features from the frequency selection," *IEEE*, 2016.

[109] E. T. Esfahani, S. Wang, and V. Sundararajan, "Multisensor wireless system for eccentricity and bearing fault detection in induction motors," *IEEE*, 2014.

[110] I. Bejaoui, D. Bruneo, and M. G. Xibilia, "A data-driven prognostics technique and rul prediction of rotating machines using an exponential degradation model," *IEEE*, 2020.

[111] W. R. Jensen and et all, "A method for online stator insulation prognosis for inverter-driven machines," *IEEE*, 2018.

[112] H. Nguyen and et all, "Model-based diagnosis and rul estimation of induction machines under interturn fault," *IEEE*, 2017.

[113] S. Venkatesan and et all, "Health monitoring and prognosis of electric vehicle motor using intelligent-digital twin," *IET*, 2019.